University of Alberta

PRIONS AND REGULATION OF PRION VARIANTS IN *SACCHAROMYCES CEREVISIAE*

by

David Lee Lancaster

A thesis submitted to the Faculty of Graduate Studies and Research in partial fulfillment of the requirements for the degree of

Doctor of Philosophy

Department of Cell Biology

Spring 2013
Edmonton, Alberta

ABSTRACT

Prions are infectious proteins. In their prion conformation, they catalyze the transformation of non-prion isomers into prions. Another characteristic common to currently identified prions is that they form amyloid aggregates. They occur in several mammals and multiple species of yeast, acting in a variety of biological processes, and their numbers continue to grow. Prions can adopt different infectious conformations known as "strains" in mammals or "variants" in yeast, each with distinct, epigenetically inheritable phenotypes. Mechanisms by which prion variants are determined remain unclear.

In this thesis, I describe the characterization of a potential novel prion in *Saccharomyces cerevisiae*, Riq1p. I show that Riq1p can form SDS/heat-resistant aggregates and is sufficient to maintain a reversibly curable, nonsense-suppression phenotype when it is used to replace Sup35p's prion determining domain. These findings are significant because, unlike the majority of previously identified prion proteins, Riq1p is richer in glutamine (Q) than asparagine (N) and its prion-like behavior cannot be isolated to its Q/N rich domain. In this way, Riq1p provides an important exception to amino-acid composition trends proposed to govern prion behavior and suggests that such theories require revision.

I also report the results of a targeted screen for genes affecting early stages of *de novo* conversion of the prion protein Sup35p into its [*PSI*$^+$] conformation. From this screen, I identify several chaperone genes that affect the variant of the *S. cerevisiae* prion Rnq1p/[*PIN*$^+$]. I show that the deletion of specific chaperone genes alters [*PIN*$^+$] variant phenotypes, including [*PSI*$^+$] induction efficiency, Rnq1p aggregate morphology/size,

and variant dominance. Genetic analysis demonstrated that the deletion-induced phenotypic changes are stably inherited in a non-Mendelian manner even after restoration of the deleted gene, confirming that they are due to a *bona fide* change in the [*PIN*$^{+}$] variant. Taken together, these results not only show that it is possible to alter an established prion variant *in vivo*, but also that molecular chaperones may play an important part in this mechanism for regulating prion variants.

ACKNOWLEDGEMENTS

I could not have accomplished any of this without the support, both financial and scientific, of my supervisor Dr. Richard Rachubinski. I have striven to take every piece of advice that he has given to heart. The freedom he has allowed me to decide my own research path has given me a great deal of self-confidence and his scientific standards and integrity are an inspiration.

I am grateful to all of my colleagues in the lab and the department, both past and present, especially C. Melissa Dobson, Andrei Fagarasanu, Monica Fagarasanu, Robert Tower, Erin Brown, Jinlan Chang, Chris Tam, Barbara Knoblach, Richard Poirier, Hanna Kroliczak, Dwayne Weber, and Elena Savidov. They have helped me with experimental trouble shooting, interpreting results, and composing manuscripts. They have been my friends and role models. I wish them all the best.

I would like to express my appreciation for the members of my supervisory committee, Dr. Paul Melançon and Dr. Christopher Power, for their support and guidance. I would also like to thank Dr. Paul LaPointe for theoretical discussions about the implications of my results.

I would also like to thank the Department of Cell Biology and all support staff, the Faculty of Medicine and Dentistry, the Faculty of Graduate Studies and Research, the Graduate Students' Association and the Canadian Institutes of Health Research for the financial support provided during my studies.

I would like to thank my family, my parents and brothers and most of all my wife, Vanessa, who have supported me in good times and bad and will be almost as happy to see me graduate as I am. The best way that I can thank them is not to make them read it.

TABLE OF CONTENTS

LIST OF TABLES

LIST OF FIGURES

LIST OF SYMBOLS AND ABBREVIATIONS

[*PRION*$^{+}$]^{variant}	the conformational designation of a given prion protein. Upper-case text in the brackets with a superscripted "+" signifies that the protein is in the prion conformation and that the cell displays a prion phenotype. Lower-case text with a superscripted "-" signifies that the prion protein is in the native, non-prion conformation. The superscripted text outside of the brackets signifies the specific prion variant.
200KgP	pellet obtained from centrifugation at 200,000 × *g*
200KgS	supernatant obtained from centrifugation at 200,000 × *g*
aa	amino acid
bp	base pair
BSA	bovine serum albumin
Da	dalton
dNTP	deoxyribonucleoside triphosphate
ddH_2O	distilled, deionized water
ECL	enhanced chemi-luminescence
ER	endoplasmic reticulum
g	gram
g	gravitational acceleration
GFP	green fluorescent protein
GuHCl	guanidine hydrochloride
h	hour
HA	amino acid tag derived from human influenza hemagglutinin (YPYDVPDYA)
HRP	horse radish peroxidase
IgG	immunoglobulin G
IPTG	isopropyl β-D-thiogalactoside
N	asparagine
NMR	nuclear magnetic resonance
OD	optical density
PAGE	polyacrylamide gel electrophoresis

PCR	polymerase chain reaction
PrD	prion determining domain
Q	glutamine
S. cerevisiae	*Saccharomyces cerevisiae*
SDD-AGE	Semi-denaturing detergent agarose gel electrophoresis
ThioT	thioflavin T
TSE	transmissible spongiform encephalopathy

CHAPTER ONE: INTRODUCTION

1.1 The discovery of prions

1.1.1 How sheep challenged classical genetics

In the early twentieth century, the scientific community's understanding of genetics was in its infancy. The principles of Mendelian genetics were widely accepted but what precisely comprised the hereditary material remained unknown. Debate focused on two candidates: 1) nucleic acids (DNA, RNA), and 2) amino acids (protein). Those in the protein camp cited greater chemical and structural diversity of protein compared to nucleic acids as qualities one would expect in something capable of encoding all the complexities of life. As such, it came as a surprise when a series of landmark experiments demonstrated that nucleic acids and not proteins were the hereditary material (Avery et al., 1944; Griffith, 1928; Hershey and Chase, 1952). Through continued research, this understanding evolved to become a generally accepted principle of biology: first DNA is transcribed to make RNA, then RNA is translated to make specific proteins, and then those proteins go on to perform their functions within the cell. Still, the unique pathology of a fatal disease observed in sheep led to questions about whether DNA was the sole means of genetic inheritance.

Named for the tendency of infected animals to scrape against fences to alleviate an apparent itching, scrapie has been a recognized disease for over 200 years (McGowan, 1922). It presents with symptoms including behavioral changes, lethargy, weight loss, anorexia, ataxia, and eventual death with postmortem examination of infected animal brains revealing spongiform encephalopathy. Several other fatal neurological diseases observed in humans, as well as other mammals, displayed similar symptoms (reviewed in Collinge, 2001; Mastrianni and Brown, 2010). These comprise a family of diseases now

known as Transmissible Spongiform Encephalopathies (TSEs). TSEs can arise spontaneously but also are genetically inheritable. It was accidently found that TSEs could be infectious when a formalin extract derived from a scrapie-infected sheep was used to inoculate a healthy flock against a common virus. Over the next two years 10% of the flock had developed scrapie (Gordon, 1946). Subsequent investigations not only reproduced scrapie infectivity but demonstrated that it was transmissible across species barriers to goats and mice (Cullie and Chelle, 1939; Chandler, 1961). This was not a unique quality of scrapie as the human TSEs, kuru and Creutzfeldt-Jakob disease, were also demonstrated to be transmissible across species (Gajdusek et al., 1966; Gibbs et al., 1968).

The infectious agent responsible for scrapie and other TSEs remained unknown. Cell free filtrates of scrapie infected animals could infect other animals, suggesting that it may be a virus, as opposed to a bacterial infection (Andrewes, 1964). The particularly long incubation period between the first exposure to the infectious material and the onset of scrapie symptoms led to the suggestion that a "slow virus" capable of long-term incubation was the culprit (Cho, 1976). Experiments showed that whatever the infectious agent was, it was significantly smaller than any known virus (Alper et al., 1966). Some suggested that a virino, a tightly packed protein coat surrounding a small amount of nucleic acid, could explain the unique characteristics of scrapie infection (Kimberlin, 1982), but more and more evidence was amassing that suggested that nucleic acids, in fact, played no part in scrapie at all.

1.1.2 The protein-only hypothesis

Tikvah Alper and colleagues were the first to suggest the protein-only hypothesis, proposing that scrapie's infectious agent may be a protein lacking any nucleic acid. This was based upon their results that showed that it was smaller than known viruses and resistant to levels of UV radiation that normally destroyed nucleic acids (Alper et al. 1967; 1966). Even so, their findings provided no direct evidence and suggested no specific mechanism. The mathematician John Stanley Griffith suggested multiple mechanisms whereby a protein could theoretically replicate itself in the absence of DNA or RNA (1967). One mechanism postulated that a protein capable of multiple conformations, but unable to efficiently adopt the second conformation without the catalytic presence of that very same conformation, could be the infectious agent (Fig. 1-1). If this were the case, he suggested that the agent would be "a protein or a set of proteins which the animal is genetically equipped to make, but which… it does not make in that form" (Griffith, 1967). In spite of the controversy surrounding the protein-only hypothesis (Chesebro, 1998; Mestel, 1996) and although Griffith did not personally follow up any of his own hypotheses, this is the mechanism that was eventually proven fundamentally correct.

1.1.3 Prions and PrP

It was Stanley Prusiner who coined the term "prion", a loose contraction of proteinacious infectious particle, to describe the infectious agent responsible for scrapie (1982), and it was his research group that performed the crucial experiments that legitimized the protein-only hypothesis. In an attempt to purify scrapie infectious agent from a sucrose gradient fraction scrapie-infected hamster brain homogenate, they

Figure 1-1: Theoretical mechanism of protein-only infection. It was proposed that a protein in an infectious state could interact with a protein of the same type, but in the normal, non-infectious state, and thereby catalyze the transformation of the normal protein, to the infectious state. The exact nature of the interaction was unknown, but dimerization was suggested. (Adapted from Griffith, 1967).


Normal protein
Infectious protein

discovered a proteinase resistant protein massing 27-30 kDa whose concentration had a direct relationship to scrapie infectivity (Prusiner et al., 1984; 1982). This protein was named PrP 27-30 (Prion Protein), and although it was resistant to proteinase K, if it was digested for extended periods it would eventually degrade, at which point they found that scrapie infectivity also decreased, supporting the hypothesis that PrP 27-30 had a role in infection (McKinley et al., 1983).

Later, Chesebro and colleagues were able to generate a cDNA sequence based upon protein sequence analysis of PrP 27-30 to identify endogenous PrP-specific mRNA (1985). PrP 27-30 mRNA was detected in both scrapie-infected and healthy hamsters suggesting that PrP 27-30 may be a normal component of animal brain. Bruno Oesch and his collaborators detected a single PrP encoding gene in the human and mouse genome, *Prnp* (1985). They also used PrP-specific anti-sera (Bessen and Marsh, 1992) to demonstrate that like PrP mRNA, the protein was not only present in scrapie infected brains, but also in uninfected animals, albeit at much lower levels. They were designated PrP^{Sc} (Scrapie) and PrP^{C} (Cellular) respectively (Meyer et al., 1986; Barry et al., 1986).

The importance of PrP to scrapie and other TSEs has been supported by a number of experiments. It was observed that *Prnp* frequently carries mutations in patients suffering from familial TSEs, with specific mutations common to specific TSEs (reviewed in Collinge, 2001; Prusiner, 1998). This suggested that mutations in the PrP gene could increase the likelihood of PrP^{C} adopting the PrP^{Sc} isoform, which then could act as an infectious agent. Hsiao and colleagues tested this hypothesis and found that by overexpressing mutant forms of *Prnp*, they were able to induce an infectious form of TSE in previously healthy animals (1990; 1994). It was also found that mice with the PrP gene

knocked-out were resistant to infection by PrP^{Sc} and did not develop scrapie-related symptoms although the PrP^{Sc} used to infect them persisted in their brain (Büeler et al., 1993). The KO mice were otherwise healthy and even heterozygous knock-outs displayed a degree of scrapie resistance (Büeler et al., 1992; 1994). This showed that endogenous PrP was an essential part of scrapie infection.

Even so, the protein-only hypothesis remained controversial. Infectious material had always been derived through purification from sick animals allowing for the possibility that PrP, while crucial, was not the only mediator of infection. Some groups were able to detect small amounts of nucleic acids in infectious samples, allowing for the possibility of a virino or other nucleic acid-based disease vector (reviewed in Chesebro, 1998; Narang, 2002). What was required to put doubts to rest and close the book on the "slow virus" hypothesis was a demonstration of infectiousness of prions generated *in vitro* in a system free of any potential prion-related nucleic acids. Prusiner's group addressed this question by using *E. coli* to express a shortened version of PrP, which they allowed to adopt an infectious state through incubation in an optimized folding buffer and then used to infect *Prnp* KO mice expressing the same shortened version of PrP (Legname et al., 2004). Claudio Soto's group took a different approach, using a protocol for the amplification of infectious PrP called Protein Misfolding Cyclic Amplification (PCMA) (Castilla et al., 2005). They used a small amount of PrP^{Sc} to convert PrP^{C} into PrP^{Sc} in a cell free system, diluted that sample, and repeated the process until the original PrP^{Sc} sample was diluted to a concentration of 10^{-55}. To put that in perspective, mathematical estimates suggested that the original sample, and by extension any non-PrP scrapie-related contaminants, should have been diluted out at a concentration of 10^{-14}.

They then successfully induced scrapie in previously healthy animals. Together, these findings had demonstrated that PrP was both necessary and sufficient to act as scrapie's infectious agent. The obvious next question was: how?

1.1.4 Distinguishing features of PrP^{C} and PrP^{Sc}

Another principle of biology that prions challenged was the concept that a given primary structure of an amino acid chain will fold into a single biologically active conformation (Anfinsen, 1973). It was known that PrP^{C} and PrP^{Sc} were encoded by the same gene and translated from a single exon (Basler et al., 1986). Examination of their primary structures by mass spectrometry and Edman sequencing revealed them to be identical. And yet, multiple biochemical and physiochemical differences exist between to two isoforms of PrP. PrP^{Sc} is resistant to proteinase K digestion, difficult to solubilize, resistant to denaturation, and highly prone to aggregation; while PrP^{C} is susceptible to proteinase K, easily soluble, and does not form detectable polymers (Oesch et al., 1985; Meyer et al., 1986; Prusiner et al., 1983). It was suggested that these properties were due to "posttranslational events" (Basler et al., 1986), which fit with the model proposed by Griffith in which the prion protein can adopt multiple isoforms, of which one or more may be able to catalyze the transformation of the other isoforms into itself (1967).

PrP^{C} has 253 amino acid residues that are reduced to 219 after glycosylation and proteolytic removal of a 22 amino acid, amino-terminal signal peptide and a 23 amino acid, carboxy-terminal peptide (De Fea et al., 1994; Stahl et al., 1990). No difference in posttranslational modification was detected in PrP^{Sc} when compared to PrP^{C}, suggesting that the differences may lie in conformation of the protein (Stahl et al., 1993). PrP is synthesized on the ER and is targeted to the Golgi apparatus to eventually localize to the

external membrane of the cell, tethered by a glycosylphosphatidylinositol (GPI) anchor (reviewed in Harris, 2003). Some PrP is released from the membrane to external medium by cleavage of the GPI tether. Nuclear Magnetic Resonance (NMR) structural studies of PrP^{C} have shown that it's N-terminus domain is disordered up to residue 128 and that it has a globular C-terminal domain, a structure which is highly conserved across species (Riek et al., 1996; Zahn et al., 2000; López García et al., 2000; Gossert et al., 2005; Calzolai et al., 2005; Lysek et al., 2005). These studies showed that the globular domain of PrP^{C} is composed of three α-helices and two short β-sheet regions (Fig.1-2). Additionally, Antonyuk and colleagues (2009) generated an X-ray crystal structure of antibody-associated PrP^{C} which contained the same structural features, supporting the NMR results.

PrP^{Sc}, unlike PrP^{C}, was found to be in an amyloid state as will be described below. Amyloid is a term first used by the German physician Rudolph Virchow to describe macroscopic abnormalities in brain tissue, which he believed to be comprised of cellulose or starch. Since then, amyloids have been characterized as highly ordered filamentous protein aggregates rich in β-sheets (reviewed in Sipe and Cohen, 2000; Chiti and Dobson, 2006). Evidence that PrP^{Sc} was an amyloid protein was first obtained when purified PrP^{Sc} was examined by electron microscopy. It was found to aggregate into rod shapes, which "ultrastructurally resembled purified amyloid" (Prusiner et al., 1983). The same study employed polarization microscopy to show that, like amyloid, PrP^{Sc} aggregates displayed a green birefringence when stained with Congo red dye. Using anti-sera raised against purified PrP^{Sc}, researchers were able to detect plaques of accumulated PrP^{Sc} in TSE-infected brain (Bendheim et al., 1984) and demonstrate that PrP^{Sc} in those

Figure 1-2: PrP structure. (A) Cartoon of the three-dimensional structure of the intact human prion protein, hPrP(23–230). The helices are orange, the β-strands cyan, the segments with nonregular secondary structure within the C-terminal domain yellow, and the flexibly disordered "tail" of residues 23–121 is represented by yellow dots. (B) Stereoview of an all-heavy atom presentation of the globular domain, with residues 125–228, in hPrP(23–230) in the same orientation as in (A). The backbone is shown as a gray spline function through the Cα positions, hydrophobic side chains are yellow, and polar and charged side chains are orange. (Reproduced from Zahn et al. 2000).

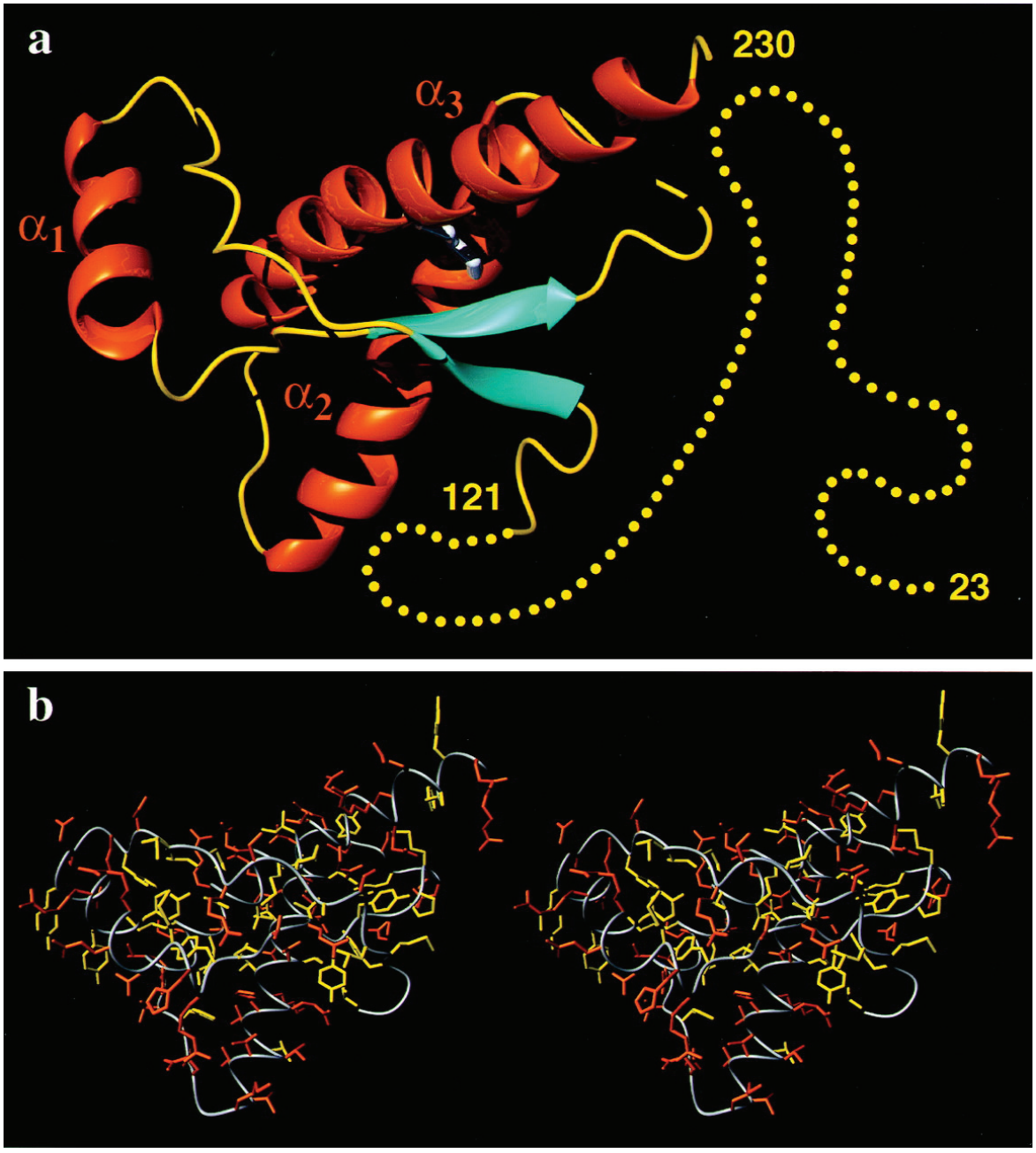
a
230
α3
α1
α2
121
23
b

plaques was in an amyloid state (DeArmond et al., 1985; Kitamoto et al., 1986). Additionally, methods such as Fournier-transform infrared (FTIR) spectroscopy and circular dichroism measurements were able to demonstrate that the secondary structures of PrP^{C} (42% α-helices, 3% β-sheets) were not conserved in $PrP^{Sc,}$, which contained increased β-sheets (54%) and decreased α-helices (21%) (Caughey et al., 1991; Gasset et al., 1993; Pan et al., 1993). As β-sheet polymers are a major characteristic of amyloids (Glenner et al., 1974), this also suggested that PrP^{Sc} is organized into an amyloid aggregate. It should be noted at this point that while amyloid plaques can accrue in the brain matter of individuals who suffer from prion diseases over extended periods, most prion-infected brains do not present with high levels of amyloid (reviewed in Ghetti et al., 1996). This implies that high levels of amyloid are not necessary for pathologically significant effects.

Intrinsic physical characteristics of amyloids, such as their large size, particulate nature, and inability to form crystals, make it difficult to obtain high-resolution structures by methods such as x-ray crystallography or solution NMR (reviewed in Shewmaker et al., 2011). To overcome this obstacle, Peretz et al. generated a library of antibodies raised against unique epitopes of PrP (1997). Using this library, they were able to show that amino acid residues 90-120 were accessible in PrP^{C} but not PrP^{Sc}. This suggested that this region may comprise the core of the proposed prion amyloid. Electron crystallography and computational modeling of PrP 27-30 and a "mini-prion" composed of 106 discontinuous PrP amino acid residues provided further insight into PrP^{Sc} prion structure (Wille et al., 2002; Govaerts et al., 2004; Wille et al., 2009). 2D crystals of these proteins were observed by negative-stain electron microscopy and, with image

processing, provided a structure to a 7-Å resolution. The only computational model that could account for the structure of the crystals, the previously observed high β-sheet content, and the known glycosylation sites, included β-sheets arranged in trimeric, left-handed β-helices (Fig 1-3). As more is understood about PrP^{Sc} structure, it will become easier to understand how PrP^{C} transitions to its prion state.

1.1.5 Mechanisms of prion infection and inheritance

The precise mechanism of prion propagation remains unclear, even so multiple theories have been proposed to explain how PrP^{C} changes into PrP^{Sc}. Central to each is Griffith's concept that PrP^{Sc} acts directly upon PrP^{C} and catalyzes the transformation (Griffith, 1967). Evidence suggesting that they interact was provided by a transgenetic study (Prusiner et al., 1990). Wild type mice infected with prions obtained from either mice ($MoPrP^{Sc}$) or hamsters ($HaPrP^{Sc}$) only contracted prion disease from $MoPrP^{Sc}$. When mice expressing both mouse and hamster versions of PrP were similarly infected, both species of prion were found to be infectious and all the mice became sick. Strikingly, when the aggregated PrP^{Sc} levels were measured by enzyme-linked immunosorbent assay (ELISA), researchers discovered that transgenic mice infected with $HaPrP^{Sc}$ or $MoPrP^{Sc}$ had the PrP^{C} of the same species converted to PrP^{Sc} while PrP^{C} of the other species was not converted. The design of these experiments controlled for other cellular factors, only manipulating the infecting species of prion. As such, their results suggest that PrP^{Sc} catalyzes PrP^{C}'s transformation directly and will preferentially convert PrP^{C} that matches it best. These conclusions were supported by other studies also demonstrating primary amino acid sequence specificity in prion infection and, of course,

Figure 1-3: Projection map of PrP 27–30 and statistically significant differences from PrPSc106. (A) Projection map of PrP 27–30 obtained by processing and averaging three independent 2D crystals of PrP 27–30. (B) Statistically significant differences between PrP 27–30 and PrPSc106 overlaid onto the projection map of PrP 27–30. The differences attributed to the internal deletion of PrPSc106 (residues 141–176) are shown in red; the differences in glycosylation between PrP 27–30 and PrPSc106 are shown in blue. (C) Superimposition of the trimeric left-handed model onto the EM maps. The trimeric left-handed β-helical model of PrP 27–30 is superimposed on a 1:1 scale (bar = 50 Å) with the electron crystallographic maps of PrP 27–30. For the sugars linked to N180 and N196 shown as blue space-filling spheres, only the conserved core region (two N-acetylglucosamine and three mannose molecules) is depicted. Sensible side chain dihedral angles for the asparagines and oligosaccharides were selected to optimize the fit with the EM maps. (D) The scaled trimeric model was copied onto the neighboring units of the crystals (bar = 50 Å) to show the crystallographic packing suggested by the model. (Reproduced from Govaerts, 2004)

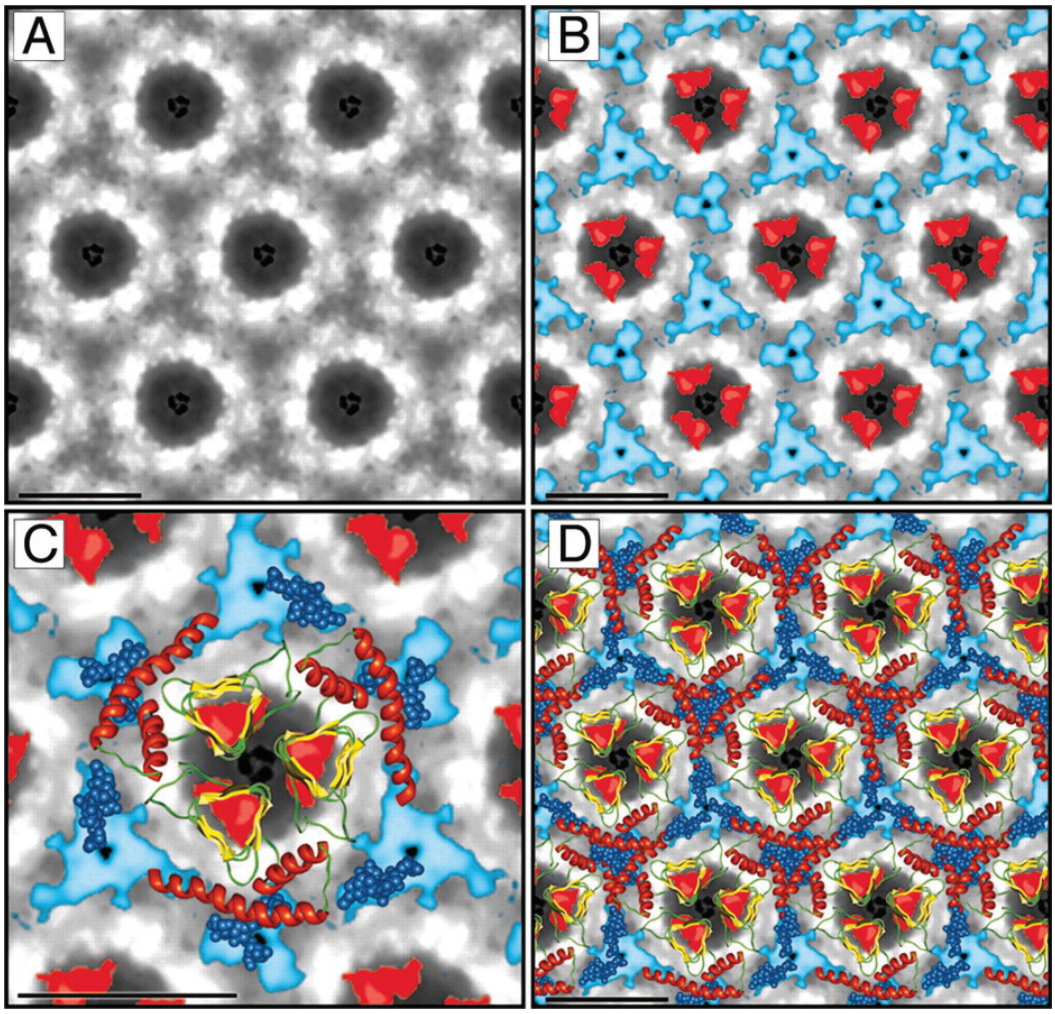
A
B
C
D

in vitro generation of prions by mixing purified PrP^{C} and PrP^{Sc} (Horiuchi et al., 2000; Kocisko et al., 1994; 1995).

An early theory suggested that PrP^{Sc} and PrP^{C} bound together in a heterodimer, which, after causing a conformational change, separated and allowed the liberated PrP^{Sc} molecules to catalyze further transformations (Fig. 1-4). This theory assumed that the PrP^{Sc} monomer was the infectious agent, but that so much PrP^{Sc} incorporates into amyloid makes this seem impractical. Additionally, in an analysis of the kinetics of prion infection, Manfred Eigen argued that the heterodimer model required PrP^{Sc} to be an extraordinarily effective catalyst to match observed infectiousness, which would predict a rate of spontaneous prion-linked disease 10^{15} times higher than that observed in reality (1996). It was clear that a more sophisticated model was required.

Jon Come and his collaborators suggested a variety of nucleation polymerization models that incorporated PrP^{Sc} amyloid characteristics (Fig 1-4) (Come et al., 1993; Caughey, 2001). They suggested that the rate-limiting step of PrP^{C}'s conversion to PrP^{Sc} was the formation of a stable PrP^{Sc} oligomer. PrP^{C} was proposed to either spontaneously convert to an unstable PrP^{Sc} state that could only be stabilized by the PrP^{Sc} oligomer, or that PrP^{C} is converted into PrP^{Sc} autocatalytically by the oligomer. In both cases, the oligomer serves as the infectious agent as opposed to a monomer.

Further genetic studies performed by the Prusiner research group suggested that other cellular factors beyond PrP may act in prion propagation (Telling et al., 1994; 1995) (Fig. 1-4). They found that introduction of PrP^{Sc} purified from CJD patients post-mortem ($HuPrP^{Sc}$) to transgenic mice expressing both $MoPrP^{C}$ and human PrP ($HuPrP^{C}$) did not give rise to prion disease in the mice. But, when the mouse *Prnp* gene was knocked out,

Figure 1-4: Proposed mechanisms of PrP^{C} conversion to PrP^{Sc}. (A) Conversion through heterodimerization. PrP^{C} forms a heterodimer with PrP^{Sc} catalyzing its conversion into PrP^{Sc}, at which point the dimer dissociates, freeing the new PrP^{Sc} to catalyze further PrP^{C} molecules. (B) Conversion through nucleation. Only PrP^{Sc} polymers are capable of efficiently converting PrP^{C}. Breakage of the growing amyloid can provide multiple polymers to convert PrP^{C}. (C) Conversion through Protein X-assisted nucleation. PrP^{C} spontaneously converts to unstable PrP*, which can be stabilized into PrP^{Sc} by Protein X, allowing it to be incorporated into the PrP^{Sc} polymer as in (B). (Adapted from Soto, 2006)

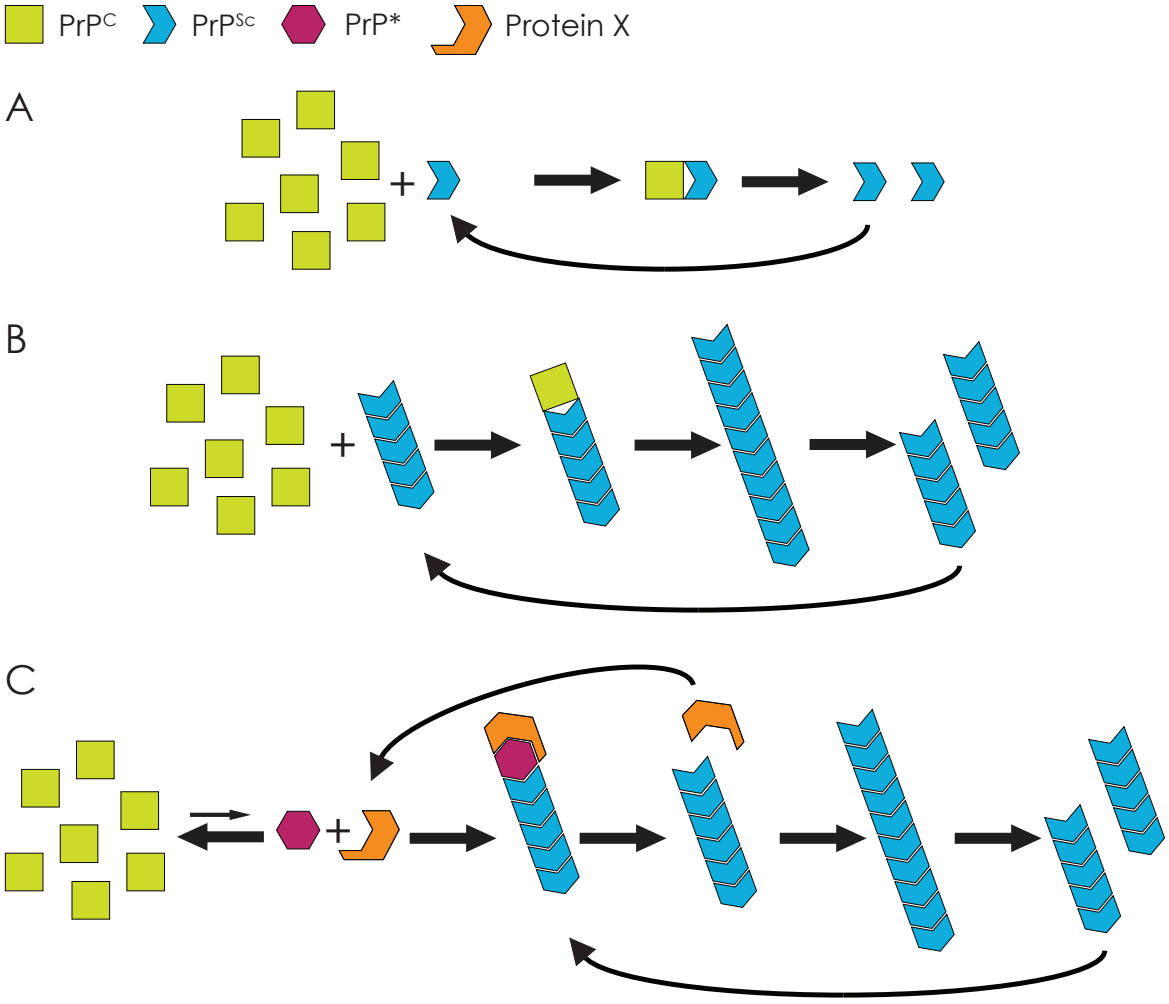
PrP^C
PrP^Sc
PrP*
Protein X
A
B
C

the mice became susceptible to infection with human prions. Additionally, the animals became sick when a transgenic combination of human and mouse PrP was expressed (MHu2M) in the presence or absence of $MoPrP^{C}$. This suggested that some other factor, required for prion propagation, preferentially bound $MoPrP^{C}$ over $HuPrP^{C}$, and was only free to aid in the prion conversion of $HuPrP^{C}$ when $MoPrP^{C}$ was depleted from the cell or when mouse and human PrP where combined, as was the case for MHu2M. This factor, assumed to be a protein, has been designated protein X. To explain its mechanism Cohen and Prusiner proposed a "template-assisted" model (1998). They suggested that PrP^{Sc} is more thermodynamically stable than PrP^{C}, but that there is a significant energetic barrier to overcome in order to make the transition. They also proposed that an intermediate PrP conformation, PrP^{*}, which exists in equilibrium with PrP^{C}. PrP^{*} can be made to adopt the PrP^{Sc} conformation with the assistance of Protein X. By facilitating the association of PrP^{*} with PrP^{Sc} oligomers, Protein X allows PrP^{Sc} to act as a template. The resulting PrP^{Sc} homomultimer is then released from protein X and is free to break into smaller fragments, which can also act as prion templates with the assistance of protein X. In this manner, the preferential binding of Protein X can dictate which species of prions will be the most infectious. Although recent studies on PrP folding using single-molecule force spectroscopy failed to demonstrate a PrP* intermediate in the same folding pathway as PrP^{C}, they did show at least two unstable off-pathway conformations that could conceivably be PrP* (Yu et al., 2012). As for Protein X, its identity remains uncertain. Molecular chaperones have been suggested as candidates but, with no conclusive evidence indicating any endogenous factor(s), it remains a matter of speculation.

1.1.6 More than a one-trick pony: prion strains

Even before PrP was identified as the infectious agent for scrapie, researchers observed a variety of distinct strains, each with unique symptoms and pathogenesis (Dickinson and Meikle, 1969; Fraser and Dickinson, 1973). These "strains", as they were called, could be faithfully transmitted, maintaining the same characteristics. At the time, when scrapie was still considered to be a disease arising from viral infection, it was assumed that the strains arose from genetic variation of the viral genome. As such, when PrP was suggested as the infectious agent, the strain phenomenon became a strong argument against the protein-only hypothesis (Chesebro, 1998). How could one protein give rise to so many strains?

One answer to that question was that mutations in *Prnp* could give rise to changes in PrP^{Sc}'s prion conformation. Supporting this idea is a significant correlation between specific genetic polymorphisms and specific familial prion diseases in the human population (reviewed in Collinge, 2001). Also, it was found that specific mutations in *Prnp* could dramatically affect the incubation period of PrP^{Sc} in mice (Westaway et al., 1987). It was clear that the primary sequence of PrP could affect prion strains, but this did not fully address all observations.

The fact remained that a variety of distinct strains could be maintained in genetically identical backgrounds (Dickinson and Meikle, 1969; Fraser and Dickinson, 1973). If no genetic differences were present, how did diversity persist? Glenn Telling and his colleagues used PrP^{Sc} purified post-mortem from patients who died from different prion diseases (FFI, fCJD, and sCJD) to infect mice expressing transgenic human mouse PrP chimera proteins (MHu2M) (1996). They observed that, although the endogenous

MHu2M was identical in all infected animals, the prion characteristics of the infected animals matched those of the strain of prion used to infect them. They proposed that the differences between strains arose from “distinct secondary and tertiary structures”. Or in other words, that the PrP could adopt different prion amyloid conformations which gave rise to the different disease pathologies.

A growing body of biochemical evidence supports this theory. Richard Bessen and Richard March treated two different strains of a mink TSE (Hyper and Drowsy) with proteinase K and found that the amino acid residues included in the proteinase resistant region were different, suggesting that the composition of the amyloid core of the two strains differed. Similar findings were published regarding sporadic and new variant CJD (Collinge et al., 1996). It has been found that hamster strains have strain-specific conformational stabilities (Peretz et al., 2001). Taken together, these findings provide convincing arguments that strains arise due to conformational differences between prions.

In all, prion strains and exactly how they occur remain only basically understood, but that prions can exist in multiple infectious states suggests a greater level of complexity than suspected when the protein-only hypothesis was originally proposed. If different conformations are linked to different phenotypes, it is possible that some strains, as yet unidentified, may have positive effects. That prions may have a function beyond disease agents is a subject of great interest, and, while no “good” prions have been found in mammals as of yet, investigations of prion and prion-like proteins in a wide variety of other organisms have uncovered a growing number of self-propagating amyloids with positive functions.

1.2 Prions in yeast

1.2.1 Why yeast?

Prions are not limited to PrP. Many have been identified in the budding yeast *Saccharomyces cerevisiae*. The ability to characterize prions and their behaviors in yeast has been a great boon to prion research as a whole. *S. cerevisiae* provides many advantages over more complex systems such as mice and humans. Its genome is fully sequenced, highly annotated, and easily manipulated for experimental purposes. Culture protocols are relatively simple, ideal for high-throughput studies with large n-numbers. This allows for valuable statistical analysis. Genetic analysis is a simple matter as mating experiments can be performed quickly and on a large scale. These strengths as well as others make yeast a powerful tool for understanding prions, with discoveries in yeast often predicting findings in mammals. In this section, what is known about several yeast prions will be outlined[1], as well as how these prions have expanded the understanding of prions over all.

1.2.2 How yeast caught "scrapie"

While controversy and debate continued in the field of mammalian prions, the concept of protein as a mechanism for epigenetic inheritance held the promise of explaining strange patterns of trait inheritance observed by yeast biologists. In 1965, Brian Cox observed a nonsense-suppression trait that he designated as ψ, or [PSI^+] (1965). [PSI^+] was inherited in a non-Mendelian manner with a 4:0 ratio, rather than in a

[1] Before discussing the known yeast prions, it is important to understand a few nomenclature conventions. Originally, the names linked to prions ([*URE3*][*PSI*]) described only the observed trait, but after it was confirmed that prions were the root cause of the traits, these names came to signify not only the phenotype, but also the prion state of the protein itself. With some exceptions, a protein in the non-prion state is designated [$prion^-$] (*e.g.* [psi^-]) and one in the prion state is designated [$PRION^+$] (*e.g.* [PSI^+]). The specific prion strains, or "variants" as they are called in yeast, can be added to the prion designation after the closed square bracket (*e.g.* [PSI^+]^{weak}).

2:2 ratio predicted if it were due to a classical genetic determinant. Specifically, strains with the nonsense-suppression trait, mated with strains lacking that trait, produced offspring that all had a nonsense-suppression phenotype. Later, in 1971, a trait designated [*URE3*$^{+}$], regulating ureidosuccicic acid uptake, with the same strange inheritance pattern was also reported (Lacroute, 1971). Both of these phenotypes were observed to be metastable – generally inherited from mother to daughter cell, but easily lost when the cells were grown in rich medium containing low concentrations of the protein denaturant guanidine hydrochloride (3-5 mM GuHCl). This process is called "curing" but was reversible as the phenotype could be regained at a low spontaneous frequencies (Tuite et al., 1981; Chernoff et al., 1993; Wickner, 1994).

Their non-Mendelian pattern of inheritance suggested that an extrachromosomal factor was responsible for the observed phenotype. Even so, inheritance could not be correlated to previously characterized cytoplasmic genetic elements such as plasmids, viruses, or mitochondrial DNA (Leibowitz and Wickner, 1978; Tuite et al., 1982; Young and Cox, 1972). It was not until decades later that Reed Wickner provided the first evidence that the [*URE3*$^{+}$] trait may be due to a prion, specifically, a prion state adopted by the endogenous protein Ure2p (1994). They showed that [*URE3*$^{+}$] required Ure2p and while the *ure2*Δ phenotype was similar to that of [*URE3*$^{+}$], it was inherited in a recessive, Mendelian manner. They also found that [*URE3*$^{+}$] was reversibly curable, which would not be expected if it was due to a virus or other cytoplasmic inheritance factor. Also, [*URE3*$^{+}$] was inducible with transient overexpression of *URE2*. Newly induced [*URE3*$^{+}$] phenotypes were inherited in the same non-Mendelian dominant manner as previously observed. The most important aspect of this paper was explaining all of these phenomena

by suggesting that Ure2p was a prion protein and that other strange phenotypes such as [*PSI*$^+$] may also be due to other, as yet unidentified, prions. With this landmark hypothesis, a new era in prion research began and general understanding of prions and their possible roles continues to expand to this day.

1.2.3 Identification of yeast prions

1.2.3.1 The double life of Sup35p, the [*PSI*$^+$] determinant

While [*URE3*$^+$] was the first of an expanding family of yeast prions, [*PSI*$^+$] is one of the best characterized. It bestows a nonsense-suppression phenotype, allowing a higher frequency of STOP codon read-through (Cox, 1965). It is often detected by introducing nonsense mutations into auxotrophic or fluorescent markers. One of the most common reporters is *ADE1-14 UGA*, which only allows growth on medium lacking adenine (ADE) for [*PSI*$^+$] strains. Additionally, the build-up of a red-pigmented secondary metabolite in [*psi*$^-$] strains carrying *ADE1-14 UGA* is decreased or eliminated in [*PSI*$^+$] strains, leading to pale pink or white colonies on rich medium as opposed to red colonies observed in [*psi*$^-$] strains (Fig 1-5).

Although it was Wickner who first suggested that the [*PSI*$^+$] phenotype was caused by an unidentified prion (1994), other researchers would eventually identify [*PSI*$^+$]'s determining factor. Before a prion was suggested, and studies into genetic determinants of [*PSI*$^+$] were underway, it was reported that mutations in the *SUP35* gene could mimic the [*PSI*$^+$] phenotype (Liebman and Cavenagh, 1980). *SUP35* mutations alone could not be responsible for [*PSI*$^+$] as mutation phenotypes were recessive and segregated with a 2:2 ratio upon meiosis. Still, when [*PSI*$^+$] was suggested to be a prion, Sup35p seemed a likely suspect and was subjected to extensive scrutiny. Overexpression

Figure 1-5: [*PSI*$^+$]-mediated nonsense-suppression. In its [*psi*$^-$] conformation, Sup35p acts together with Sup45p to facilitate translation termination at the stop codon. When Sup35p is in its [*PSI*$^+$] conformation, the ribosome reads through stop codons more frequently. Stop codon read-through can be measured by introducing a nonsense mutation into the *ADE1* gene. [*psi*$^-$] strains cannot grow on -ADE medium and accumulate a red-pigmented secondary metabolite usually consumed by the adenine metabolism. On the other hand, without soluble Sup35p in [*PSI*$^+$] strains, the ribosome reads-through the *ADE1* nonsense mutation, allowing growth on -ADE medium and npreventing pigment build-up.

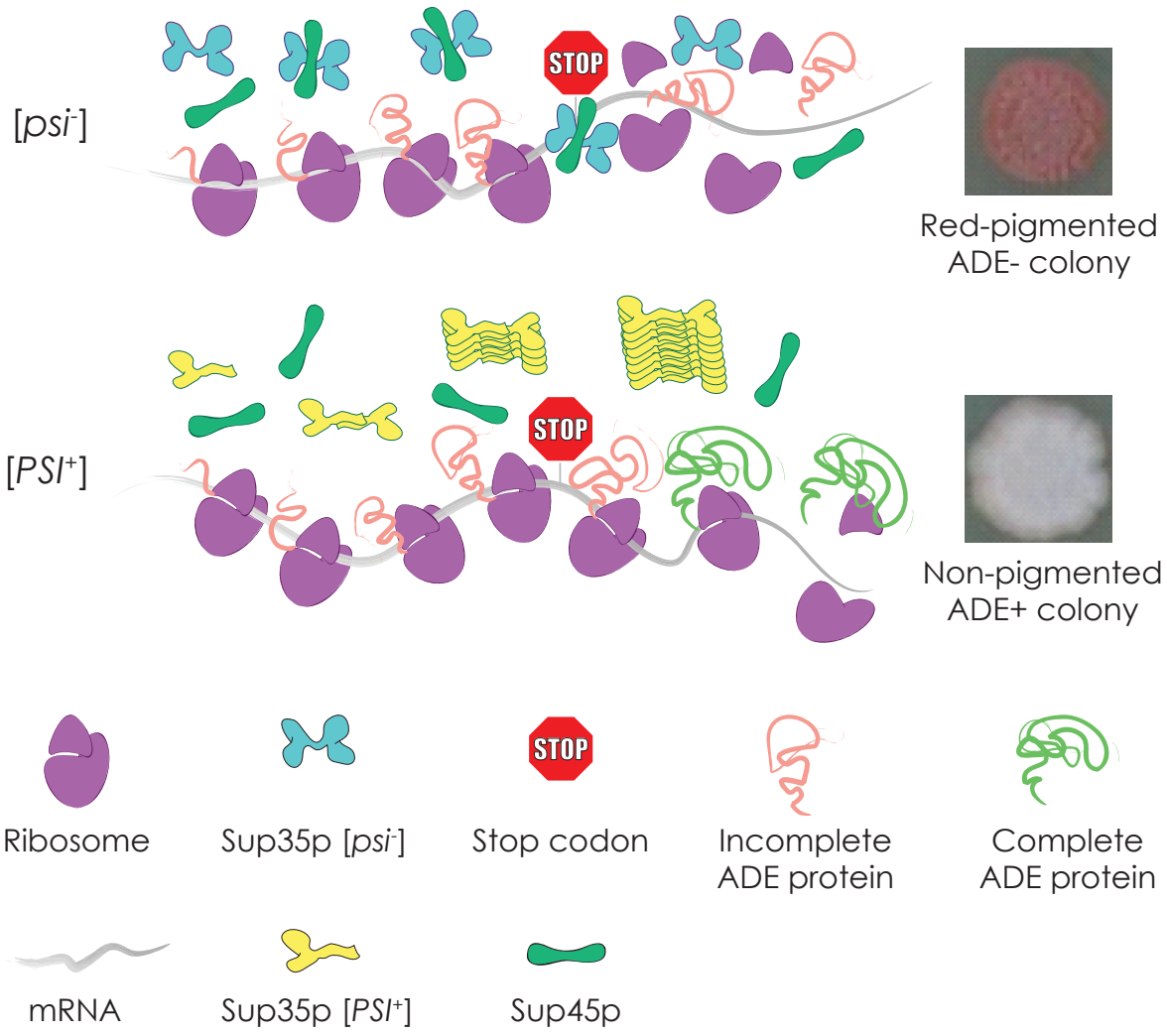
[psi-]
STOP
Red-pigmented
ADE- colony
[PSI+]
STOP
Non-pigmented
ADE+ colony
Ribosome
Sup35p [psi-]
Stop codon
STOP
Incomplete
ADE protein
Complete
ADE protein
mRNA
Sup35p [PSI+]
Sup45p

of *SUP35* was found to cause nonsense suppression (Chernoff et al., 1988). *SUP35* is essential for cell viability (Cottrelle et al., 1985; Wilson and Culbertson, 1988), prompting Michael Ter-Avanesyan and colleagues to perform a series of truncation experiments in order to characterize how different domains of Sup35p affect [*PSI*$^{+}$] and cell viability (1993; 1994). They localized the prion domain to the N-terminal domain of Sup35p (amino acid residues 1-114; Sup35N) finding that it was necessary to maintain the [*PSI*$^{+}$] phenotype and that overexpression of the Sup35N alone was sufficient to increase nonsense suppression similar to the full length protein (Chernoff et al., 1988; 1993; Derkatch et al., 1996). Sup35N has also been implicated in interactions with poly-A-binding protein, thereby influencing mRNA stability (Hosoda et al., 2003). Meanwhile, they also showed that the C-terminal region (amino acid residues 254-685; Sup35C) is required for cell viability and that exogenous expression of Sup35C alone had an anti-nonsense-suppression effect. When a strain deleted for *SUP35N*, expressing only *SUP35C*, was mated with a wild type [*PSI*$^{+}$] strain, they found that Sup35C's anti-suppressor effect was dominant over [*PSI*$^{+}$] in the diploid but the [*PSI*$^{+}$] determinant returned in wild type haploids after meiosis. Taken together, these findings suggested that the Sup35N and Sup35C had different functions, with the N-terminal acting as the prion-determining domain (PrD) facilitating nonsense suppression and the C-terminal antagonizing it. The middle region (Sup35M) is enriched in charged residues and is proposed to have a role in maintaining the equilibrium of Sup35p in prion and non-prion conformations, potentially through interactions with chaperone proteins important to prion propagation that will be discussed in greater depth further on in this literature review (Liu et al., 2002; Helsen and Glover, 2012).

Differential centrifugation of Sup35p along with immuno-EM and fluorescence microscopy of GFP-tagged Sup35p demonstrated that it formed large aggregates in [*PSI*$^+$] but not [*psi*$^-$] cells (Patino et al., 1996; Paushkin et al., 1996; Kawai-Noma et al., 2010). These aggregates pelleted upon high-speed centrifugation, while both [*psi*$^-$] Sup35p and Sup35C were found to be soluble. Shortly before these studies, it was shown that Sup35p, in cooperation with Sup45p, normally acts in translation termination, assisting in removing ribosomes from mRNA upon encountering a STOP codon (Frolova et al., 1994; Stansfield et al., 1995). Sup35C specifically was found to be sufficient to act in translation termination. Paushkin and colleagues explained their results in context of Sup35p's normal function as follows, "Similarly to mammalian prions, in [*PSI*$^+$] cells Sup35p forms high molecular weight aggregates, accumulating most of this protein. The aggregation inhibits Sup35p activity leading to a [*PSI*$^+$] nonsense-suppressor phenotype. N-terminally altered Sup35p molecules are unable to interact with the [*PSI*$^+$] Sup35p isoform, remain soluble and improve the translation termination in [*PSI*$^+$] strains, thus causing an antisuppressor phenotype" (1996). In brief, they interpreted the data to conclude that the [*PSI*$^+$] phenotype arises due to a loss of Sup35p function when it is incorporated into aggregates.

Evidence that Sup35p was the prion determinant responsible for [*PSI*$^+$] continued to mount. It was shown that excess Sup35 protein and not DNA or mRNA was required to induce the [*PSI*$^+$] phenotype in [*psi*$^-$] strains (Derkatch et al., 1996). Sup35p was found to form aggregates *in vitro* that could catalyze the non-aggregated Sup35p to aggregate as well (Paushkin et al., 1997). These aggregates were found to be amyloids, as will be discussed below in section 1.3.1.

All of these observations strongly suggested that Sup35p is a prion. Still, the core prediction of the prion hypothesis, that only prion protein is necessary to faithfully inherit the prion phenotype, had not been tested. In an effort to do so, one study reported that purified truncations of Sup35p prion determining domain (amino acid residues 1-254; Sup35NM) could be made to form aggregates *in vitro* and that these aggregates induced the [*PSI*$^{+}$] state when introduced by lipid droplets into [*psi*$^{-}$] strains (Sparrer et al., 2000). The frequency of conversion observed in that study were quite low (1-2% of transformed cells) and did not exclude the possibility that the observed change was simply due to the increased amount of Sup35p in the cell increasing the likelihood of spontaneous conversion to [*PSI*$^{+}$] (Soto, 2006). In 2004, *Nature* published two letters that described the successful generation of [*PSI*$^{+}$] seeds from recombinant Sup35NM and the subsequent infection of [*psi*$^{-}$] strains with the [*PSI*$^{+}$] seeds (King and Diaz-Avalos, 2004; Tanaka et al., 2004). Efficiency of infection was much higher that previous findings, ranging from 16% to 50%. Together, all of these data confirmed Sup35p to be a prion protein responsible for the [*PSI*$^{+}$] phenotype. The methods used for its characterization became the gold standard for identification of novel prions, which was a good thing as [*URE3*$^{+}$] and [*PSI*$^{+}$] were about to get a lot more company.

1.2.3.2 Rnq1p, a prion's prion

Unlike Sup35p and Ure2p before it, Rnq1p was not first identified based on investigation of a non-Mendelian phenotype. Instead it was found in a screen of the *S. cerevisiae* proteome for proteins sharing physical traits similar to known prions (Sondheimer and Lindquist, 2000). The PrDs for both of the Sup35p and Ure2p had been identified through truncation studies (Ter-Avanesyan et al., 1994; Masison and Wickner,

1995; Patino et al., 1996). Comparison of these domains did not show any marked sequence homology, but did reveal them both to be rich in the amino acid residues asparagine (N) and glutamine (Q). Using high N/Q content as the primary criterion of their search, Neal Sondheimer and Susan Lindquist performed a BLAST (Basic Local Alignment Search Tool) search (Altschul et al., 1990; 1997) of the yeast proteome that yielded several prion candidates including the open reading frame *YCL028c* (2000). The protein product of *YCL028c*, which they named Rnq1p (for Rich in N and Q), also showed no sequence homology to other prions but did contain an N/Q-rich domain at the C-terminal end of the protein (amino acid residues 153-405). Overexpressed GFP-tagged Rnq1p mostly localizes diffusely throughout the cytoplasm, but occasionally is found in bright foci. The bright Rnq1-GFP foci phenotype proved to be inheritable in a non-Mendelian pattern. Additionally, recombinant Rnq1p purified from bacteria was observed to form long filamentous aggregates by EM that took up the amyloid-specific dye, thioflavin T. These data both supported Rnq1p as a prion. Deletion of *RNQ1* did not provide an easily detectable loss-of-function phenotype so Sondheimer and Lindquist replaced Sup35p's prion domain with the putative prion domain of Rnq1p to generate the fusion protein RMC. This construct proved to be able to rescue Sup35p prion behavior, causing a nonsense-suppression phenotype that was reversibly curable just like normal [*PSI*$^{+}$] and inherited in a non-Mendelian manner. In this way Rnq1p was identified as a novel prion without having any particular idea about what its cellular function may be.

Serendipitously, Susan Liebman's group had begun to characterize a novel prion phenotype, [*PIN*$^{+}$], given its name because it bestowed a [*PSI*$^{+}$]-inducing phenotype. It had been observed that after curing [*PSI*$^{+}$] strains by treatment with GuHCl, the resulting

[*psi*$^-$] strains could be divided into two categories, those that could be readily induced to become [*PSI*$^+$] *de novo* upon overexpression of Sup35p, and those that could not (Derkatch et al., 1997). This trait was observed to be inheritable in a non-Mendelian manner and was first proposed to represent two different [*psi*$^-$] isoforms of Sup35p one prone to becoming [*PSI*$^+$], [*psi*$^-$]$^{PIN+}$, and the other not, [*psi*$^-$]$^{pin-}$. Further tests showed that [*PIN*$^+$] was only required for induction and not propagation of [*PSI*$^+$] and [*PSI*$^+$]-related phenotypes were not affected by [*PIN*$^+$]/[*pin*$^-$]. It also showed that [*PIN*$^+$] was reversibly curable, making it more likely that [*PIN*$^+$] was a unique non-[*PSI*$^+$] prion (Derkatch et al., 2000). The prion protein responsible for the [*PIN*$^+$] phenotype remained unidentified until a study performed by Irena Derkatch and colleagues showed that prion isoform of Rnq1p gave cells the [*PIN*$^+$] phenotype (Derkatch et al., 2001). In this study it was demonstrated that [*PIN*$^+$] could be lost through deletion of *RNQ1*, that overexpression of other Q/N rich proteins could overcome Sup35p's need for [*PIN*$^+$] to be induced *de novo*, and that other prions, specifically [*URE3*$^+$], could also serve as [*PIN*$^+$] factors. Even so, as Ure2p already had [*URE3*$^+$] as a prion designation and Rnq1p had none, it was given [*PIN*$^+$] [2]. Incidentally, it was later found that while existing prions facilitated the induction of other prions, they antagonized each other's stable propagation from mother to daughter (Schwimmer and Masison, 2002). The final proof that Rnq1p was the prion determinant for [*PIN*$^+$] came when recombinant Rnq1p PrD was purified from *E. coli*, made to form amyloid aggregates *in vitro*, which were then used to successfully transform a [*pin*$^-$] strain into [*PIN*$^+$] (Patel and Liebman, 2007; Vitrenko et al., 2007b).

[2] While it is true that multiple prion proteins can be responsible for the [*PIN*$^+$] phenotype of efficient [*PSI*$^+$] induction, and some experts have taken to referring the Rnq1p's prion isoform as [*RNQ*$^+$] to differentiate it from [*URE3*$^+$]-related [*PIN*$^+$], it will be referred to only as [*PIN*$^+$] throughout this thesis in order to agree with terminology employed in most of the published literature.

Even though Rnq1p's cellular function in its non-prion conformation remains unknown, a great deal of research has contributed to understanding how its [*PIN*$^+$] prion conformation helps Sup35p become [*PSI*$^+$]. Derkatch *et al.* presented two models (Fig. 1-6) (2001). The first, the titration model, proposed the existence of an inhibitory factor that prevents the formation of [*PSI*$^+$] prions and that the [*PIN*$^+$] prion amyloid sequestered this factor so that it could no longer perform that function, freeing Sup35p to become [*PSI*$^+$]. An obvious candidate for inhibitory factor was Rnq1p itself, as its sequestration is a fundamental requirement for the [*PIN*$^+$] amyloid. This was quickly ruled out because *rnq1*Δ strains displayed a phenotype similar to [*pin*$^-$] instead of [*PIN*$^+$] (Derkatch et al., 2001; Osherovich and Weissman, 2001). Further genetic screens failed to identify any [*PIN*$^+$]-dependent [*PSI*$^+$] inhibitory factor (Derkatch et al., 2001; Osherovich and Weissman, 2002).

On the other hand, the seeding model, which suggested that [*PIN*$^+$] prion aggregates act as an early template for the conversion of Sup35p to its prion state, continues to accumulate support. Rnq1p amyloid aggregates generated *in vitro* have a positive effect on the formation of Sup35p amyloid *in vitro* (Derkatch et al., 2004; Vitrenko et al., 2007a). That Rnq1p can have this effect in the absence of any theoretical inhibitory factor endogenous to yeast is strong evidence for the seeding model, but this does not mean that the same thing occurs *in vivo*. To address this concern, Choe *et al.* used an interesting *in vivo* approach (2009). According to the rationale that it is through association with [*PIN*$^+$] Rnq1p that Sup35p converts to its prion state *de novo* and that increased likelihood of association would increase *de novo* Sup35p conversion, they generated a fusion protein of the PrD of Sup35p, Sup35NM, with full-length Rnq1p. By

Figure 1-6: Titration and Seeding models of [*PIN*$^+$] mechanism. (A) The Titration model proposes that [*PIN*$^+$] aggregates sequester a [*PSI*$^+$]-inhibitory factor that prevents *de novo* formation in [*pin*$^-$] strains. (B) The Seeding model proposes that the [*PIN*$^+$] aggregate is necessary to act as a template for Sup35p to convert into its [*PSI*$^+$] conformation. (Adapted from Derkatch et al., 2001)

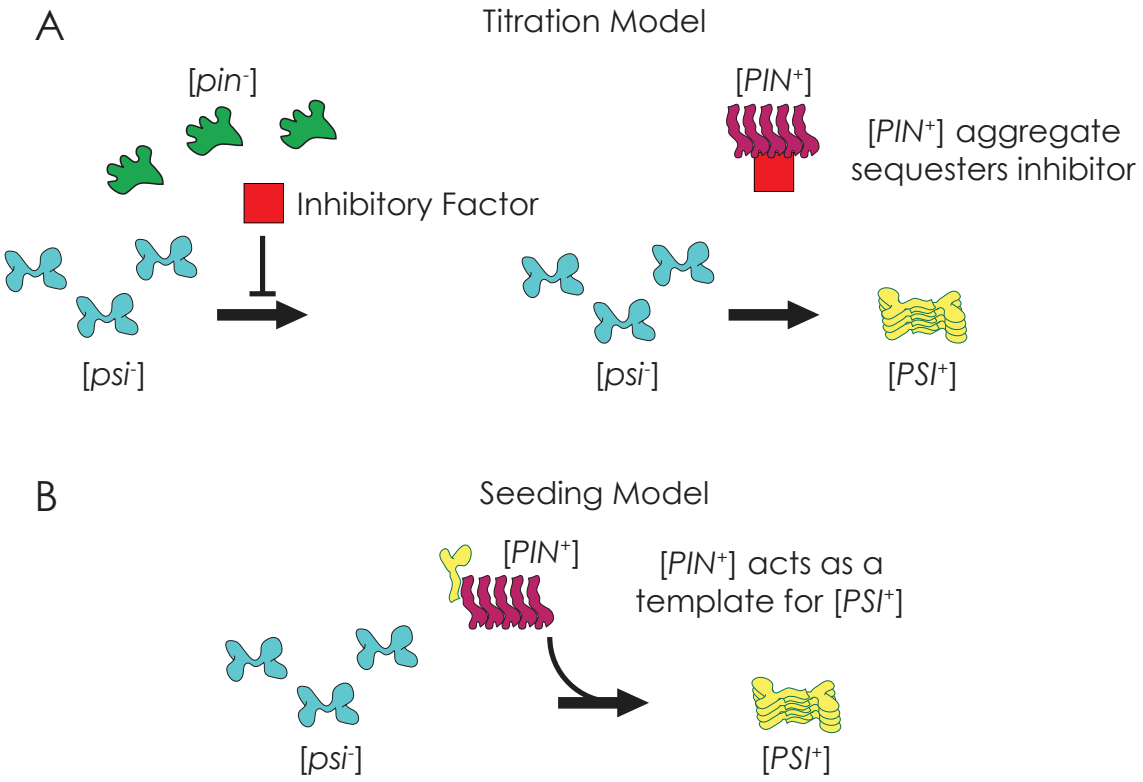
A
Titration Model
[pin-]
[PIN+]
[PIN+] aggregate sequesters inhibitor
Inhibitory Factor
[psi-]
[psi-]
[PSI+]
B
Seeding Model
[PIN+]
[PIN+] acts as a template for [PSI+]
[psi-]
[PSI+]

fusing the two proteins they increased the chances of Sup35NM coming into close association with Rnq1p in its prion state. When this construct was expressed in a [*PIN*$^+$] background, [*PSI*$^+$] induction was observed to be much higher than Sup35NM expressed on its own, but, like wild type, no induction was observed in a [*pin*$^-$] background.

Mutational analysis of *RNQ1* showed that mutation of specific amino acid residues in the Rnq1p's PrD strongly impair [*PSI*$^+$] induction (Bardill and True, 2009). Interestingly, the Rnq1p's N-terminal non-prion domain has been implicated in [*PSI*$^+$] induction as well. Expression of a truncated version of Rnq1p with its first 100 amino acid residues removed (Rnq1Δ100) in a wild type background inhibits the propagation of both [*PSI*$^+$] and [*URE3*$^+$] (Kurahashi et al., 2008). Point mutations in Rnq1p's non-PrD with similar [*PSI*$^+$] inhibitory effects were shown to lead to an increase in the size of Sup35p aggregates (Kurahashi et al., 2011). Strangely, when expressed without full-length Rnq1p, Rnq1Δ100 can facilitate the induction of [*PSI*$^+$] and does not strongly inhibit its propagation. In fact, [*RNQΔ100*$^+$] is often eliminated by the presence of [*PSI*$^+$] (Kurahashi et al., 2009). Other mutations in the non-PrD destabilize [*PIN*$^+$], thereby inhibiting [*PSI*$^+$] formation, further suggesting that Rnq1p's function and prion behavior are more complicated that simply containing an amyloidgenic prion domain (Shibata et al., 2009).

1.2.3.3 The expanding prion family

Just as the castaway astronauts of the classic film *Planet of the Apes* were encouraged upon finding the first green plant in a barren landscape because "where there is one, there is another, and another, and another" (Schaffner, 1968), so too was the yeast prion research community encouraged by the discovery of the three prions

Ure2p/[*URE3*], Sup35p/[*PSI*$^+$], and Rnq1p/[*PIN*$^+$]. If there could be three yeast prions, why couldn't there be more? The study of these three prion proteins suggested a set of common characteristics (Crow and Li, 2011). All three proteins contain PrDs, without which the prion cannot form *de novo* or propagate effectively (Masison and Wickner, 1995; Derkatch et al., 1996; Sondheimer and Lindquist, 2000). The PrDs are all rich in N and Q residues and, like the mammalian prion PrP and other proteins linked to amyloidgenic diseases in humans, they are capable of forming β-sheet-rich amyloids. Aggregation can often be detected by a shift of the protein from a soluble to an insoluble state (Patino et al., 1996; Edskes et al., 1999; Sondheimer and Lindquist, 2000). Prion proteins also form bright puncta *in vivo* when labeled with GFP and overexpressed in [*PRION*$^+$] cells. PrDs can be exchanged or added to fusion proteins and retain their amyloid nature (Sondheimer and Lindquist, 2000). All of these prions can be inherited in a dominant, non-Mendelian manner and are reversibly curable, so that if the prion characteristic was lost spontaneously, or through treatment with GuHCl, it can be regained in the same cell (Wickner et al., 1999). A good way to induce the prion state is to overproduce the prion protein, presumably because a larger amount of the protein increases the odds of one misfolding into its prion conformation (Chernoff et al., 1993; Wickner, 1994; Sondheimer and Lindquist, 2000). Loss of endogenous prion protein leads to a curing of the prion, although frequently the phenotype of a strain deleted for the prion-encoding gene is very similar to that of the [*PRION*$^+$] strain.

Using these characteristics as a guide, many more prion-like proteins have been identified and characterized (Table 1-1). Some were identified by phenotype, such as [*SWI*$^+$], [*ISP*$^+$], and [*NSI*$^+$], and later linked to prion determinants (Du et al., 2008;

Table 1-1: Known Prions of *Saccharomyces cerevisiae* [a]

Prion/Protein	Native Function	Citation
[*OCT*$^+$]/Cyc8p	Transcriptional regulation	(Patel et al., 2009)
[*MCA*$^+$]/Mca1p	Metacaspase homolog	(Erhardt et al., 2010; Nemecek et al., 2009)
[*MOD*$^+$]/Mod5p	t-RNA modification	(Suzuki et al., 2012)
[*MOT3*$^+$]/Mot3p	Transcriptional regulation	(Alberti et al., 2009)
[*PIN*$^+$]/Rnq1p	*De novo* prion formation Unknown function in non-prion state	(Sondheimer and Lindquist, 2000)
[*ISP*$^+$]/Sfp1p	Transcription factor	(Rogoza et al., 2010)
[*PSI*$^+$]/Sup35p	Translational termination	(King and Diaz-Avalos, 2004; Tanaka et al., 2004)
[*SWI*$^+$]/Swi1p	Chromatin remodeling	(Du et al., 2008)
[*URE3*$^+$]/Ure2p	Nitrogen metabolism	(Wickner, 1994)
[*NSI*$^+$]/unknown	Unknown	(Saifitdinova et al., 2010)

[a] Putative prion proteins whose prion characteristics have not been fully confirmed include: Asm4p, Cbk1p, Gln3p, Gpr1p, Gst1p, Hrp1p, Ksp1p, Lsm4p, Mrn1p, New1p, Ngr1p, Nrp1p, Nsp1p, Pab1p, Pdr1p, Psd1p, Puf2p, Rbs1p, Rlm1p, Sap30, Ybr016wp, Ybr022cp, Ybl081wp (Santoso et al., 2000; Sondheimer and Lindquist, 2000; Alberti et al., 2009).

Rogoza et al., 2010; Saifitdinova et al., 2010). Others were identified like Rnq1p, by screening for proteins sharing characteristics of known prions. Cyc8p/[*OCT*$^+$] and Mod5p/[*MOD*$^+$] were first brought to the attention of the scientific community as epigenetic factors that promoted [*PSI*$^+$] formation, similar to [*PIN*$^+$] and [*URE3*$^+$] (Patel et al., 2009; Suzuki et al., 2012). Mca1p/[*MCA*$^+$] was found by testing its ability to replace the PrD of Sup35p and rescue prion-linked nonsense suppression (Nemecek et al., 2009; Erhardt et al., 2010). Simon Alberti and colleagues from the Lindquist laboratory published one of the most comprehensive screens for novel prions to date (2009). In their report, they identified 100 candidate PrDs in the yeast proteome based upon N/Q content and hydrophobicity. They then tested these PrDs for a variety of prion characteristics,

including *in vivo* and *in vitro* aggregate/amyloid formation, their ability to rescue [*PSI*$^{+}$] nonsense suppression when they are used to replace Sup35p's own PrD, and their non-Mendelian inheritance. Overall they identified 19 putative prion proteins. One in particular, Mot3p/[*MOT3*$^{+}$], was investigated more thoroughly. It was shown that recombinant Mot3p could form aggregates *in vivo* which could transform [*mot3*$^{-}$] cells into [*MOT3*$^{+}$], confirming it to be a *bona fide* prion. This "systematic survey" also brought to light a tendency for PrDs rich in N to be more likely to form functional prion amyloid than those rich in Q. A follow up study reported that replacing N residues with Q residues had a cytotoxic effect and decreased prion activity of the PrD dramatically (Halfmann et al., 2011).

It is important to note that not all prions identified are rich in N/Q residues, suggesting that it may not be a physical requirement. For example, the fungus *Podospora anserina* has an endogenous prion protein, [Het-S] that is not N/Q-rich but can propagate as an amyloidgenic prion, even when expressed in *S. cerevisiae* (Coustou et al., 1997; Maddelein et al., 2002; Taneja et al., 2007). Additionally, [*MOD*$^{+}$] has been found to be the prion amyloid conformation of Mod5p, an *S. cerevisiae* protein that does not contain N/Q-rich domains (Suzuki et al., 2012).

The only confirmed prion in humans is PrP, linked to deadly neurodegenerative diseases. Even so, as more prions are identified it has led some to suggest that prions may be a common cellular mechanism of affecting phenotype, with potentially beneficial roles. Orb2 and CPEB are proteins whose prion-like conformations have been implicated in formation of long-term memory in fruit-flies and snails (Si et al., 2003; 2010; Mastushita-Sakai et al., 2010; Majumdar et al., 2012). In yeast it has been suggested that

prions can increase adaptive fitness (True and Lindquist, 2000). For example, it has been shown that environmental stress increases the *de novo* appearance of [*PSI*$^{+}$] (Tyedmers et al., 2008), suggesting it to have a role in evolvability (Lancaster et al., 2010). Some have suggested that prions may be rare diseases, only made common in the laboratory, but with little representation in the wild (Nakayashiki et al., 2005; Wickner et al., 2011; McGlinchey et al., 2011). On the other hand, both [*PSI*$^{+}$] and [*MOT3*$^{+}$] were recently found to occur frequently in a sample of 700 different wild strains of yeast (Halfmann et al., 2012), while [*PIN*$^{+}$] also occurs in natural and industrial strains (Resende et al., 2003). If prions do prove to occur even at a low frequency in the wild, it may be that they act as "bet-hedging devices", which can increase the adaptability of the cell and the population independently of genomic mutations (Halfmann et al., 2010).

1.2.3.4 Prion vs. Prionoid

Some debate has arisen in the scientific community as to what specifically constitutes a prion (Aguzzi and Rajendran, 2009). There are many amyloidogenic proteins in mammals and yeast that are structurally very similar to PrP in its amyloid state, can be made to be self-propagating *in vitro*, and can have limited degree of infectivity between cells, but are not infectious between individuals or populations. Due to these important differences, it has been proposed that only *bona fide* prions such as PrP should be called prions and other self-propagating amyloidogenic proteins with limited infectivity should be designated prionoids. For the purposes of this thesis, the term prion will be used to refer to infectious amyloid proteins in *S. cerevisiae*, but the distinction should be noted.

1.3 The physical and structural basis of prion-linked phenotypes

1.3.1 Yeast prions are amyloids

Similar to mammalian PrP, yeast prions form β-sheet-rich amyloid aggregates. Negative staining and examination by electron microscopy of prion aggregates generated *in vitro* has shown them to form long filamentous aggregates that could be stained by amyloid reactive dyes Congo Red and Thioflavin T (Glover et al., 1997; King et al., 1997; Schlumpberger et al., 2000; Sondheimer and Lindquist, 2000; Vitrenko et al., 2007a; Wickner et al., 2008a). Recent advances in electron microscopy techniques have confirmed that fluorescent Sup35-GFP foci observed *in vivo* are composed of amyloid fibrils (Tyedmers et al., 2010). The prion domains of these proteins have been found to form the amyloid core with non-prion domains able to extend outwards from the core (Baxa et al., 2003; 2005; 2011; Diaz-Avalos et al., 2005; Kryndushkin et al., 2011). The non-prion functional domains of Sup35p and Ure2p appear to retain their tertiary folding structure even though the PrD is incorporated into the amyloid core (Baxa et al., 2004; Bai et al., 2004; Krzewska et al., 2007). This suggests that the loss-of-function phenotypes typically associated with prions are not due to denaturing of their functional domains, but instead possibly due to sequestration of the protein in a cellular locale non-conducive to performing their function efficiently (Baxa et al., 2011).

There are two models that might explain the multi-molecular structure of the amyloid core. The first proposes that the adjacent prion molecules interact through parallel in-register β-sheets, while the second suggests a β-helix conformation (Fig. 1-7). Characterization of the amyloid *in vitro* has shown Sup35p and Ure2p fibrils to be arranged in such a way as to contain one molecule per 4.7 Å as predicted for parallel in-

Figure 1-7: Structural models of yeast prion amyloid. (A) Model of parallel in-register beta-sheet structure. The ribbon represents the prion domain (blue) along with some of the non-prion domain (red). Residue i of chain n is opposite residue i of the next polypeptide (blue spheres) (Adapted from Shewmaker et al., 2009). (B) Model of beta-helix structure. Head residues (red) in one prion domain are in close proximity to Head residues of their neighbours; the same is true for the Tail residues (green). Central Core residues (blue) are sequestered from intermolecular interactions. (Adapted from Krishman et al., 2005).

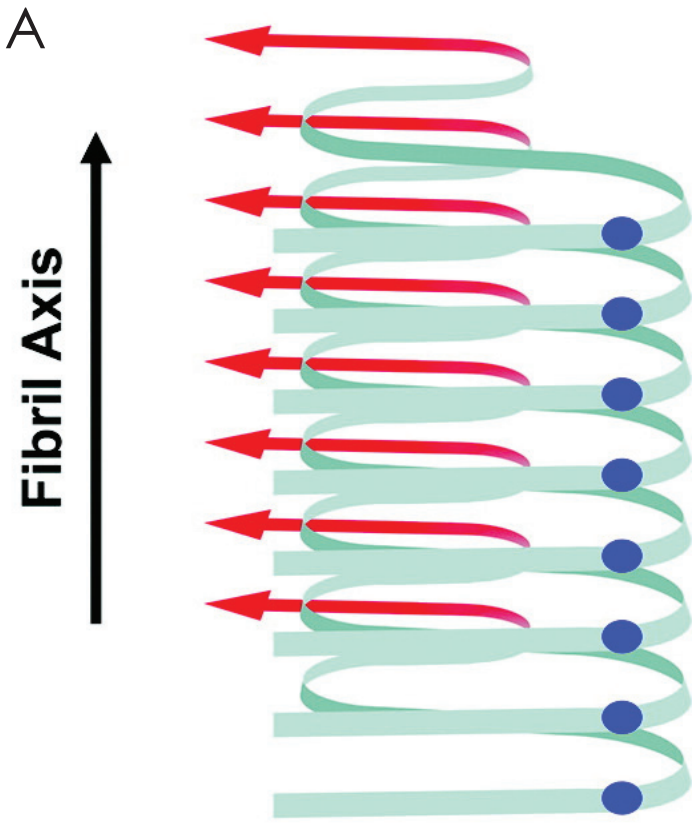
A
Fibril Axis

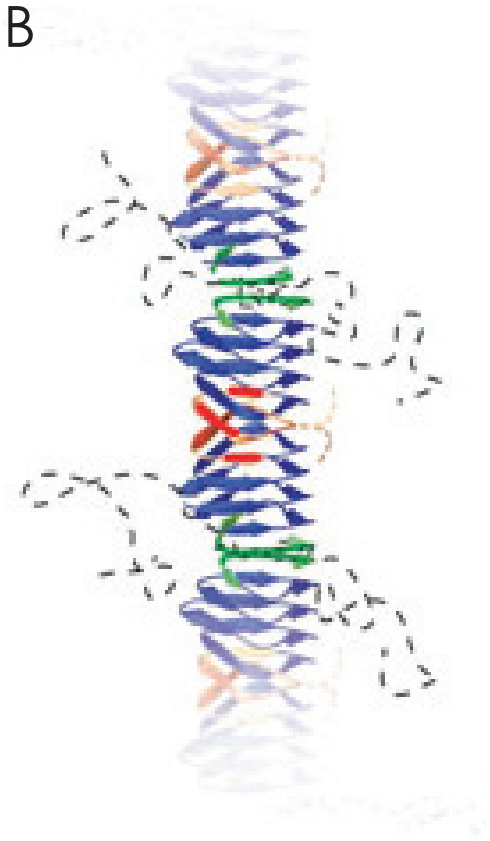
B

register β-sheets (Baxa et al., 2003; 2011; Diaz-Avalos et al., 2005; Chen et al., 2009). In further support of this model, when specific amino acid species were labeled with ^{13}C and analyzed by solid-state NMR to determine the relative distances between labeled residues, many were found to be 4.7 Å from the same residue in other prion molecules, the same distance separating β-sheets, but more distant than would be observed for intramolecular interactions (Chan et al., 2005; Fayard et al., 2006; Baxa et al., 2007; Shewmaker et al., 2008; 2009; Wickner et al., 2008a; b; Chen et al., 2009). A recent study provided evidence that the Ure2p amyloid also adopts an in-register β-sheet configuration (Ngo et al., 2012). This model explains how amino acid sequence of Sup35p and Ure2p PrDs can be shuffled (rearranged while preserving content) and the resulting mutant prions can still form amyloids and generate heritable traits (Ross et al., 2004; 2005; Toombs et al., 2010). If the β-sheets interact in an in-register parallel fashion, then the order of the amino acid residues should not inhibit amyloid formation. On the other hand, the Lindquist group used the introduction of cysteine residues labeled with fluorescent dyes to investigate which regions of Sup35p's PrD were most protected from the external environment and found the core regions to be shorter than those predicted by the parallel in-register model (Kishimoto et al., 2004; Krishnan and Lindquist, 2005). Based upon these findings, they suggested a β-helix model that proposes that intermolecular interactions only occur at the "head" and "tail" of a β-helix with the central domain of the PrD more exposed to interaction with the solvent. Further study will be required to clarify prion amyloid structure.

1.3.2 Multiple prion conformations give rise to prion variants

While the precise structure of each prion amyloid remains uncertain, it is believed that most yeast prion proteins are capable of adopting multiple unique amyloid conformations that, like mammalian prion strains, give rise to prion phenotypes with differing levels of severity. Irena Derkatch and colleagues first reported this phenomenon when they observed that overexpressing identical Sup35p in identical genetic backgrounds led to the induction of multiple types of [*PSI*$^{+}$] colonies (1996). In yeast, these phenotypes are referred to as "variants" instead of strains to differentiate them from genetically distinct strains of yeast. They classified the variant with lighter colonies and better growth on –ADE medium, reflecting stronger nonsense suppression, as [*PSI*$^{+}$]^{strong}, and the pink colour variant with weaker growth, typical of weaker nonsense suppression, as [*PSI*$^{+}$]^{weak}. Further characterization of [*PSI*$^{+}$] variants determined that a higher proportion of Sup35p is in the non-soluble, prion conformation in [*PSI*$^{+}$]^{strong} than [*PSI*$^{+}$]^{weak}, presumably causing its increased nonsense suppression (Zhou et al., 1999; Uptain et al., 2001). Additionally, it was found that [*PSI*$^{+}$]^{strong} aggregates are smaller and less stable than those of [*PSI*$^{+}$]^{weak} (Toyama et al., 2007). Interestingly, when [*PSI*$^{+}$]^{strong} and [*PSI*$^{+}$]^{weak} haploid strains were mated together, [*PSI*$^{+}$]^{strong} was found to be dominant over [*PSI*$^{+}$]^{weak} and, when the diploid was sporulated, the resulting tetrad cells that were stably [*PSI*$^{+}$]^{strong} as well (Derkatch et al., 1999; King, 2001). Once variants are established they tend to be stably inherited (Derkatch et al., 1996; Kochneva-Pervukhova et al., 2001), although specific [*PSI*$^{+}$] variants can be selected using antagonistic drugs (Shorter, 2010). Also, it has recently been shown that variants may be undetermined or unstable shortly after *de novo* induction of the prion (Sharma and Liebman, 2012). Since

their first characterization in [*PSI*$^{+}$], variants have been identified for both [*URE3*$^{+}$] and [*PIN*$^{+}$] (Schlumpberger et al., 2001; Sondheimer et al., 2001; Bradley et al., 2002).

Variants can be caused by the introduction of a variety of mutations in *SUP35* or by generating recombinant Sup35p amyloid *in vitro* at different incubation temperatures (4°C and 37°C) (King, 2001; Tanaka et al., 2004; Derkatch et al., 1999; DiSalvo et al., 2011; Verges et al., 2011). As different amino acid compositions and thermodynamic stabilities could potentially affect the structure of the prion amyloid, this supported the theory that structural differences were the underlying cause of prion variants in yeast. Research was directed to understand these differences. It was found that the size and compositions of the protease resistant amyloid core differ from variant to variant (Tanaka et al., 2005; Krishnan and Lindquist, 2005; Toyama et al., 2007).

Motomasa Tanaka along with the Weissman group proposed an abundance model to explain how differences in the amyloid core could lead to variant phenotypes (2006). According to this model, [*PSI*$^{+}$] variants compete for a limited pool of soluble Sup35p to incorporate into the prion aggregate and the variant that can do this most efficiently will out-compete the others and over time become the sole variant conformation present in the cell. The equilibrium between soluble and insoluble protein determines the severity of the prion phenotype as the amount of soluble prion protein will determine how effectively it can perform its normal non-prion function. In support of this theory, they presented data showing that while the dominant [*PSI*$^{+}$]^{strong} filaments do grow more slowly than those of [*PSI*$^{+}$]^{weak}; their filaments fragment more readily, thereby exposing more growing ends and allowing for faster incorporation of soluble Sup35p. The greater nonsense

suppression phenotype of [*PSI*$^{+}$]^{strong} is therefore due to there being less soluble Sup35p in the cell.

As a refinement of the abundance model, a research group led by Tricia Serio has suggested a sized-based model in which a subpopulation of prion aggregates of a specific size are responsible for establishing and propagating the prion state *in vivo* and different variants differ in their accumulation of this subpopulation (Sindi and Serio, 2009; Derdowski et al., 2010). They performed an *in silico* simulation of [*PSI*$^{+}$]^{strong} and [*PSI*$^{+}$]^{weak} variants for both the abundance and size-based models. Their simulation showed that only the size model was able to recapitulate all of the [*PSI*$^{+}$] variants observed characteristics. They went further and provided several experimental validations of their model. They found that daughter cells contained fewer and smaller Sup35p aggregates relative to mother cells regardless of [*PSI*$^{+}$] variant. Aggregates in daughter cells grow in size and number until reaching variant specific equilibrium after a number of cell divisions. They demonstrate that nonsense suppression gets stronger as the cell ages and they showed that the transfer of Sup35p from daughter to mother and vice versa is aggregate size dependent. They went on to suggest that size equilibrium for the different variants is a function of the cellular environment, with chaperone proteins, which will be discussed further in section 1.4, responsible for fragmenting the different aggregates with different efficiencies. Overall, the evidence that prion variants may have abundance and/or size-dependent components is compelling, but will require further investigation amongst a variety of prions and their variants to determine if they are common mechanisms of variant differentiation or if others exist as well.

1.3.3 [*PIN*$^+$] variants

Variants have also been characterized for the Rnq1p prion, [*PIN*$^+$]. The first evidence that Rnq1p was capable of propagating multiple phenotypic variants was reported not long after its discovery (Sondheimer et al., 2001). It was found that a mutation in the gene encoding the chaperone Sis1p altered the solubility of purified Rnq1p and its *in vivo* aggregation patterns while allowing it to remain in a [*PRION*$^+$] state. Later, after Rnq1p had been linked to [*PIN*$^+$], Michael Bradley and the Liebman group characterized four unique variants: [*PIN*$^+$]^{low}, [*PIN*$^+$]^{medium}, [*PIN*$^+$]^{high}, and [*PIN*$^+$]$^{very\ high}$ (2002). These variants were named for their respective abilities to facilitate the induction of [*PSI*$^+$]. The Liebman group went on to characterize several other phenotypes that served to distinguish these variants (Bradley et al., 2002; Bradley and Liebman, 2003; Liebman et al., 2006). By testing the solubility of Rnq1p in the different backgrounds, they determined that the highest proportion of Rnq1p was insoluble in [*PIN*$^+$]^{high}, followed by [*PIN*$^+$]^{medium}, [*PIN*$^+$]^{low}, and finally [*PIN*$^+$]$^{very\ high}$. By overexpressing Rnq1-GFP *in vivo* they found that in [*PIN*$^+$]^{low}, [*PIN*$^+$]^{medium}, and [*PIN*$^+$]$^{very\ high}$ backgrounds, Rnq1-GFP localized mostly to a single dots in the cell while it localized to multiple dots in [*PIN*$^+$]^{high} variants. This is interesting as the *SIS1* mutation mentioned above led to an increase in the number of Rnq1-GFP foci per cell (Sondheimer et al., 2001). Examination of aggregate size by semi-denaturing detergent-agarose gel electrophoresis (SDD-AGE) showed that aggregates in variants with predominantly a single Rnq1-GFP focus per cell ranged in size between 750 and over 3000 kDa, while the size range of variants with multiple foci included aggregates both smaller (~200 kDa) and larger than single focus variants. The single dot variants were shown to destabilize

[*PSI*$^{+}$]^{weak} when strains carrying those variants were mated. They also characterized the [*PSI*$^{+}$] variants that arose when [*PSI*$^{+}$] was induced *de novo* in the presence of the different [*PIN*$^{+}$] variants. [*PSI*$^{+}$] colonies derived from [*PIN*$^{+}$]^{low} were a mixture of [*PSI*$^{+}$]^{strong} and an unstable [*PSI*$^{+}$] variant. [*PIN*$^{+}$]^{medium} strains produced those variants as well as [*PIN*$^{+}$]^{weak} and also often became [*pin*$^{-}$]. [*PIN*$^{+}$]^{high} strains produced [*PSI*$^{+}$]^{strong} and [*PSI*$^{+}$]^{weak}, and [*PIN*$^{+}$]$^{very\ high}$ strains produced [*PSI*$^{+}$]^{strong} and a variant of [*PSI*$^{+}$]^{weak} that often spontaneously converted to [*PSI*$^{+}$]^{strong}. Finally, by mating the different [*PIN*$^{+}$] variants one with another, they determined that [*PIN*$^{+}$]^{high} was dominant over [*PIN*$^{+}$]^{medium}, which in turn was dominant over [*PIN*$^{+}$]^{low}, which was dominant over [*PIN*$^{+}$]$^{very\ high}$. At this point the physical or structural reasons why one [*PIN*$^{+}$] variant is dominant over another are not known. Together these phenotypic differences allowed for the putative identification of [*PIN*$^{+}$] variants, but also raised questions of how the different observed biochemical properties contributed to [*PIN*$^{+}$]-dependent [*PSI*$^{+}$] induction efficiency.

In an effort to better understand these variants, a study was performed to characterize variants of Rnq1p generated *in vitro* at different temperatures using strains expressing a chimera prion protein called RRP, comprised of Rnq1p's PrD and Sup35MC, as a reporter (Kalastavadi and True, 2010). They found that RRP in a [*PIN*$^{+}$]^{high} background displays strong nonsense suppression similar to [*PSI*$^{+}$]^{strong} while in a [*PIN*$^{+}$]^{low} and [*PIN*$^{+}$]^{medium} it is a weaker nonsense suppressor. Transformation of [*pin*$^{-}$] strains with Rnq1p amyloid generated *in vitro* at 18, 25 and 37°C gave rise to mixture of RRP variants called weak, medium, and strong based on their nonsense suppression. Prion seeds generated at 18°C were more likely to be strong or medium; 25°C, were a

mixture of all variants; and 37°C, were mostly weak or medium. They measured Rnq1p solubility in strains carrying these variants and found that in RRP strong it is the least soluble, RRP medium is more soluble, and RRP weak is the most soluble. When their respective abilities to induce [*PSI*$^{+}$] were tested it was found that RRP weak and strong induced at equally high levels, while medium induced [*PSI*$^{+}$] 2-3 fold less efficiently. The most interesting aspect of this study was the examination of the *in vitro* generated Rnq1p prion seeds. They found that aggregates formed faster if seeded with 25°C aggregates than with 37°C aggregates and that aggregates formed at higher temperatures were more resistant to denaturation by heating. Additionally, Rnq1p aggregates are detected by EM as short curly fibrils when formed at 18°C, long and curly at 25°C, and long and bundled at 37°C, suggesting that the fundamental structure of the amyloid differs when formed at different temperatures.

From these findings it is difficult to conclude if the RRP variants match with classical [*PIN*$^{+}$] variants. Even if they do not correlate, the biochemical and physical characteristics of the *in vitro* generated seeds may suggest how Rnq1p's different amyloid conformations could be responsible for its multiple phenotypes. Fitting with what has been observed for [*PSI*$^{+}$] variants, their results suggest that for Rnq1p the smaller the size of the variant's aggregate, the stronger the prion phenotype and the more stably it is propagated. Accordingly, RRP weak was found to be the least stable, while RRP strong was the most. The only inconsistency with this finding is that RRP weak was equally effective at inducing [*PSI*$^{+}$] as RRP strong, suggesting that induction of [*PSI*$^{+}$] is dependent on factors other than aggregate size and stability. What those factors may be remains unclear.

How the structures of Rnq1p's variants differ also remains uncertain. The structure of Rnq1p's PrD in an amyloid state has been investigated, although without specific attention paid to the variant (Wickner et al., 2008a). By labeling various amino acid residues throughout the primary sequence of Rnq1p's PrD with ^{13}C and performing solid-state NMR based experiments, Reed Wickner and colleagues were able to determine that Rnq1p's PrD can form parallel in-register β-sheets when incubated *in vitro* and identify several amino acid residues likely to be incorporated into the amyloid core. Investigations of Rnq1p's PrD have shown it to contain four discrete Q/N-rich domains that are individually dispensable for [*PIN*$^+$] activity (Fig 1-8) (Vitrenko et al., 2007b; Kadnar et al., 2010). QN-2, QN-3, and QN-4 can form amyloid fibrils *in vitro* but only QN-2 and QN-4 amyloid efficiently infect [*pin*$^-$] cells to become [*PIN*$^+$], if admittedly, a [*PIN*$^+$] variant significantly less effective for [*PSI*$^+$] induction. In fact, several combinations of the QN-regions proved capable of transmitting the [*PIN*$^+$] state, so long as they included either QN-2 or QN-4. Constructs with more than one QN domain proved more efficient at facilitating [*PSI*$^+$] induction. Transmission barriers, that is to say inefficient inheritance, arose in these truncated versions of [*PIN*$^+$] when mated with strains carrying the wild type *RNQ1* gene, suggesting that the prion conformations of the truncated Rnq1p were not compatible with wild type Rnq1p. Interestingly, deletion of QN-3 has been shown to destabilize the [*PIN*$^+$]^{high} variant specifically while increasing the effectiveness of [*PSI*$^+$] induction in a [*PIN*$^+$]^{low} background (Bardill and True, 2009). Together, these findings raise the attractive possibility that the putative variant conformations of the [*PIN*$^+$] variants arise through different Q/N-rich regions being

Figure 1-8: Schematic diagram of non-Q/N-rich and Q/N-rich regions in the Rnq1 protein. The frequency of QN residues was calculated from every 10-aa interval. Q/N-rich subregions are indicated in red roman numerals (Adapted from Kurahashi et al., 2008).

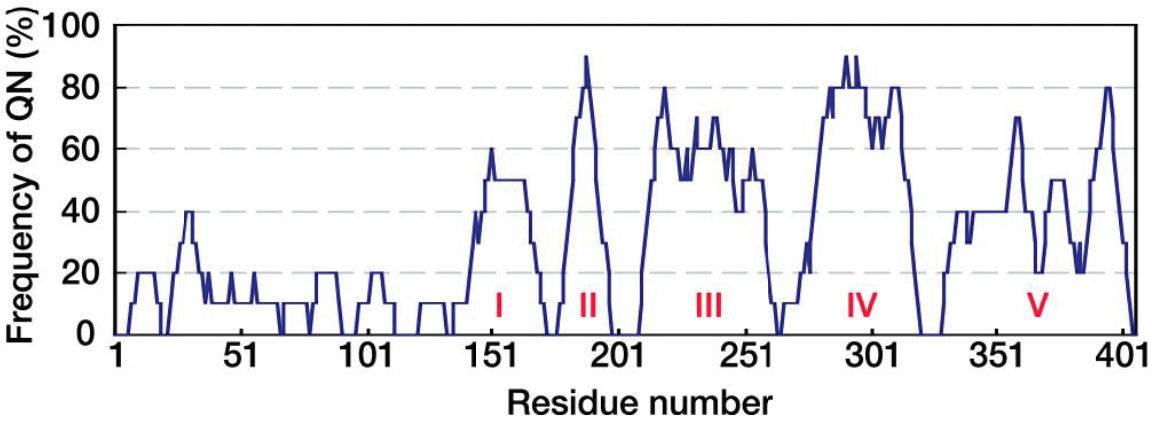
Frequency of QN (%)
100
80
60
40
20
0
1
51
101
151
201
251
301
351
401
Residue number
I
II
III
IV
V

included in that parallel β-sheets. In any case, questions surrounding [*PIN*$^+$] variants will require significantly more study before answers can be confirmed.

1.4 Role of chaperone proteins in prion propagation

It is one of the central contentions of the protein-only hypothesis that prion seeds alone are all that is required to inherit the prion phenotype. Both mammalian and yeast prions can form infectious prion seeds *in vitro* that are sufficient to infect other cells. That said, it was found that successful propagation of yeast prions *in vivo* is strongly affected by a variety of chaperone proteins.

Chaperone proteins are a class of protein that help other proteins to fold correctly, and failing that, aid in the disposal of misfolding protein aggregates (reviewed in Morano et al., 2012). In *S. cerevisiae*, chaperone proteins include Hsp104p as well as the Hsp90, Hsp70, Hsp40 and Hsp110 chaperone families. As the prion phenomenon arises from a prion protein's propensity to adopt self-propagating amyloid conformation, it is not surprising that proteins dedicated to regulating protein conformations have an effect. How chaperones modulate prion behavior will be reviewed in this section in addition to how these findings have shaped the current understanding of prion propagation mechanisms.

1.4.1 GuHCl and the prion "Propagon"

Guanidine hydrochloride (GuHCl) is a protein denaturant that was shown to cure prion phenotypes even before their protein determinants were identified, but its mechanism was uncertain (Tuite et al., 1981; Wickner, 1994). [*PRION*$^+$] strains grown on medium containing millimolar concentrations of GuHCl become [*prion*$^-$] at a high rate (reviewed in Cox et al., 2007; Halfmann and Lindquist, 2010). It was hypothesized that

GuHCl denatured the amyloid aggregate, but as curing occurred at millimolar concentrations significantly lower than the molar levels normally required for protein denaturation *in vitro*, this seemed unlikely (Tuite et al., 1981). Also, it has been found that GuHCl does not inhibit aggregate formation or growth, but instead blocks aggregate fragmentation *in vivo*, making it more unlikely that its protein denaturing properties mediate prion curing (Eaglestone et al., 2000; Ferreira et al., 2001; Ness et al., 2002; Cox et al., 2003; Byrne et al., 2009; Palmer et al., 2011). It was eventually shown that GuHCl inhibits the chaperone Hsp104p's ATPase activity *in vivo* (Ferreira et al., 2001; Jung and Masison, 2001; Grimminger et al., 2004). Although prions such as [*ISP*$^+$] can be cured by GuHCl treatment independent of Hsp104p (Volkov et al., 2002; Rogoza et al., 2010), it is thought that most of GuHCl's curing effect is mediated through Hsp104p, the role of which will be discussed further in Section 1.4.2.2.

Researchers took advantage of GuHCl prion curing properties to investigate the minimum infectious unit required for prion propagation (Cox et al., 2003). This unit is called a prion seed, or a propagon. They tracked the loss of [*PSI*$^+$] when cells were grown in the presence of GuHCl and from this estimated the number of propagons present in the cell prior to the beginning of curing. While the exact number of propagons varied dramatically, the results of this study demonstrated that [*PSI*$^+$] and presumably other prions are transmitted by propagons that are finite in number. Estimates of the number of propagons in the cell range from 20 to 1000 (Eaglestone et al., 2000; Cox et al., 2003), making it unlikely that a single Sup35p molecules can act as a prion seed as they number in the order of 10^4 molecules per cell (Didichenko et al., 1991). As purified prion seeds generated *in vitro* can infect [*prion*$^-$] cells, this suggested that the propagon was in fact an

aggregate of prion proteins (Cox et al., 2003). In support of this, *in vitro* generated prion amyloids grow steadily in an unidirectional fashion from their exposed end into large filaments with low infectivity (Inoue et al., 2001; Fay et al., 2003; Collins et al., 2004). Fragmentation of these filaments by sonication or other mechanical forces increases both infectivity of the aggregates and the rate conversion of native protein to the prion state, consistent with the propagon being a smaller prion oligomer and not the larger aggregates (DePace et al., 1998; Kushnirov and Ter-Avanesyan, 1998; Collins et al., 2004).

Several kinetic studies show that if curing is not carried to completion, propagon number and stable propagation of [*PSI*$^+$] are quickly restored (Eaglestone et al., 2000; Ferreira et al., 2001; Ness et al., 2002; Byrne et al., 2007; Palmer et al., 2011). The eventual curing of [*PSI*$^+$] over generations of cell divisions was consistent with random segregation of prion seeds, although there is some evidence to suggest that there is a bias towards retention of prion seeds in the mother cell (Cox et al., 2003; Sindi and Serio, 2009; Derdowski et al., 2010). Taken together, these findings suggest that the propagon is lost by dilution and the inability to replicate as opposed to an active destructive process.

1.4.2 General function of Hsp104p

Hsp104p is a hexameric AAA$^+$ (ATPase associated with diverse activities) protein-disaggregase that is important under a variety of stress conditions, increasing survival more than 10,000 fold (Sanchez and Lindquist, 1990; Sanchez et al., 1992). A WU-BLAST of the RCSB Protein Data Bank (Bernstein et al., 1977) shows that Hsp104 does not have any close homologues in humans but does in bacteria (SGD-Project). Unlike other chaperone proteins, Hsp104p has the capacity to re-solubilize misfolded protein aggregates and promote their re-folding into an active conformation (Glover and

Lindquist, 1998; Cashikar et al., 2005; Haslbeck et al., 2005; Doyle et al., 2007). It does so by threading unfolded proteins through the central pore of a hexameric ring in an ATP-dependent manner (Wendler et al., 2007; 2009; Wendler and Saibil, 2010). GuHCl inhibits its ATPase activity (Grimminger et al., 2004). Hsp104p requires a variety of chaperones in order to efficiently recognize and refold misfolded proteins (Parsell et al., 1994). For example, it cooperates with the Hsp70, Ssa1p as well as the Hsp40, Ydj1p to refold misfolded luciferase (Glover and Lindquist, 1998).

1.4.3 Hsp104p is essential for prion propagation

Although prions can be generated and propagated *in vitro* in the absence of other cofactors, deletion of *HSP104* or inhibition of Hsp104p activity has been shown to cure many of the known yeast prions (Chernoff et al., 1995; Patino et al., 1996; Sondheimer and Lindquist, 2000; Moriyama et al., 2000; Du et al., 2008; Patel et al., 2009; Alberti et al., 2009; Suzuki et al., 2012). The only exception to date is [*ISP*$^+$] (Rogoza et al., 2010). Overproduction of Hsp104p was also shown to cure [*PSI*$^+$] and [*MCA*$^+$], although no similar curing effects have been observed in other prion strains (Chernoff et al., 1995; Nemecek et al., 2009). In keeping with these results, high levels of Hsp104p *in vitro*, eliminates [*PSI*$^+$] infectivity of Sup35p while only decreasing [*URE3*$^+$] infectivity of Ure2p (Shorter and Lindquist, 2006). In the case of a [*PSI*$^+$] variant with uncommonly large aggregates, higher levels of Hsp104p increased the stability of [*PSI*$^+$] propagation (Borchsenius et al., 2006). *In vivo* studies of the loss of [*PSI*$^+$] upon depletion/inhibition of Hsp104p mirrored those of GuHCl curing, showing that Sup35p aggregates gradually increased in size in mother and daughter cells were less likely to be [*PSI*$^+$] (Wegrzyn et

al., 2001; Kryndushkin et al., 2003; Satpute-Krishnan and Serio, 2005; Satpute-Krishnan et al., 2007).

Taken together with observation of GuHCl and Hsp104p related effects, these data contributed to the current fragmentation model of prion propagation (reviewed in Liebman and Chernoff, 2012). According to this model, the infectious prion seed is not a monomer prion of Sup35p or the large aggregates, but instead a smaller aggregate, although the precise size and conformation of the amyloidogenic prion oligomer remains unclear. By binding and helping to refold monomer subunits in the midst of the prion polymer into their native state, it is believed that Hsp104p fragments the larger prion aggregates and increases the incidence of effective prion seeds (Paushkin et al., 1996; Kushnirov and Ter-Avanesyan, 1998). Without Hsp104p, the prion aggregates are not efficiently fragmented, leading to less prion seeds and less growing ends at which prion conversion can occur. This both increases the likelihood that daughter cells will not inherit sufficient prion seeds and decreases the rate at which native proteins are converted to their prion conformation. In the case of [*PSI*$^{+}$], it is possible that overproduction of Hsp104p leads to extreme fragmentation of the prion aggregate such that only native Sup35p and non-amyloidogenic aggregates remain, effectively curing the cell (Kryndushkin et al., 2003). Recent findings suggest that [*PSI*$^{+}$] curing through high levels of Hsp104p is more complicated than simple disaggregation as overexpression of an Hsp104p mutant deleted for its N-terminal domain, which is not essential for protein disaggregation, could not cure [*PSI*$^{+}$] (Hung and Masison, 2006). Why Hsp104p overexpression does not cure all prions is not clear but it could be due to Hsp104p having a special affinity for Sup35p that allows this unique behavior.

1.4.4 General function of Hsp70, Hsp40, and nucleotide exchange factors

Members of the Hsp70 chaperone family in yeast are active participants in all stages of the protein lifecycle and have been identified in the endoplasmic reticulum, mitochondria, and cytosol (reviewed in Frydman, 2001; Morano et al., 2012). They have been shown to act in protecting nascent proteins; translocation; refolding of misfolded proteins; and/or targeting misfolded proteins for ubiquitination and degradation. The Hsp70s most often implicated in prion biology are found in the cytosol. Ssa3p and Ssa4p are induced under stress conditions while Ssa1p and Ssa2p are constitutively expressed and are responsible for the bulk of Hsp70 activity under non-stress conditions (Werner-Washburne et al., 1987). Ssb1p and Ssb2p are specialized to work with ribosomes in folding nascent proteins with Ssz1p modulating their activity (Nelson et al., 1992; Gautschi et al., 2002; Hundley et al., 2002). Hsp70 chaperones, with the exception of Ssz1p, have a functional ATPase region localized to their N-terminus and a substrate/client-binding region localized in their C-terminus (Zhu et al., 1996; Osipiuk et al., 1999; Vogel et al., 2006a; b; Li et al., 2006). Hsp70s mostly bind to regions of hydrophobic amino acid residues exposed in misfolded proteins (Flynn et al., 1991; Blond-Elguindi et al., 1993; Rüdiger et al., 1997). When Hsp70s bind ATP, they bind and release client proteins relatively quickly, but the rate of binding and release decreases 2-3 orders of magnitude when they are bound to ADP (Schmid et al., 1994; Gisler et al., 1998; Mayer et al., 2000). Client binding increases ATP-hydrolysis and induces conformational changes that stabilize the chaperone complex (Jiang et al., 2005). Even so, Hsp70s cannot perform their functions independently. Their intrinsic ATPase activity is very slow, which prevents efficient binding of clients, and their client binding is

promiscuous, which impairs specificity. They overcome these limitations with the help of Hsp40 and nucleotide exchange factors.

The Hsp40 family of cochaperones is larger and more diverse than the core Hsp70s (reviewed in Qiu et al., 2006; Kampinga and Craig, 2010). Hsp40 chaperones identified in *S. cerevisiae* include Ydj1p, Xdj1p, Apj1p, Sis1p, Djp1p, Zuo1p, Swa2p, Jjj1p, Jjj2p and Jjj3p (Caplan and Douglas, 1991; Schwarz et al., 1994; Luke et al., 1991; Lu and Cyr, 1998b; Hettema et al., 1998; Yan et al., 1998; Huang et al., 2008; Pishvaee et al., 2000; Walsh et al., 2004). These Hsp40s vary greatly in size and composition, but the one structural characteristic that they all have in common is a J domain, leading them to sometimes be referred to as J proteins. First characterized in the *E. coli* chaperone DnaJ, the J domain, normally located in the N-terminal region of the J protein, is a sequence of ~70 amino acid residues that contains a histidine-proline-aspartic acid tripeptide flanked by alpha helices (Pellecchia et al., 1996). This domain increases the ATPase activity of Hsp70 chaperones (Szabo et al., 1994; McCarty et al., 1995; Laufen et al., 1999). One of Hsp40's primary roles is to facilitate Hsp70 chaperone activity by increasing their intrinsic ATPase activity so that they can better hang on to their client proteins (Cyr et al., 1992). Hsp40s do this best when present at lower concentrations that Hsp70s, presumably because at higher concentrations Hsp70 ATPase rates are increased to the point that clients are either not bound by Hsp70 because it is stuck in a closed conformation, or because clients are not efficiently released (Diamant and Goloubinoff, 1998).

Hsp40 function extends beyond increasing Hsp70 ATPase activity. As stated above, Hsp40 structures vary greatly aside from the conserved J domain. Many yeast Hsp40s have their own client-binding and dimerization domains that allow them to

independently recruit client proteins and present them to Hsp70s for refolding or eventual degradation (Lu and Cyr, 1998a; Fan et al., 2005; Kampinga and Craig, 2010). While Hsp70 chaperones are promiscuous, their interactions with structurally diverse Hsp40s give them specificity and allow them to perform a wide variety of functions throughout the cell (Holstein et al., 1996; Yan et al., 1998; Lu and Cyr, 1998b; Fan et al., 2005; Ramos et al., 2008). Researchers have observed a degree of functional redundancy between yeast Hsp40s but some have proven to have unique functions that cannot be replaced by overexpression of other Hsp40s (Sahi and Craig, 2007).

The other essential class of proteins that Hsp70 requires to efficiently perform its chaperone function is nucleotide exchange factors (NEF) (reviewed in Kampinga and Craig, 2010; Morano et al., 2012). In *S. cerevisiae* these include proteins such as Fes1p and the Hsp70-like Hsp110 family members Sse1p and Sse2p (Easton et al., 2000; Kabani et al., 2002; Shaner and Morano, 2007). These proteins interact with Hsp70 ATPase domains to promote the release of ADP and thereby facilitate the release of the Hsp70 client, allowing it a chance to refold (Mukai et al., 1993; Dragovic et al., 2006; Raviol et al., 2006; Shaner et al., 2006; Polier et al., 2008). Although Hsp110s lack a functional ATP-dependent client-binding release cycle, they can bind misfolded proteins and act as "holdases", protecting denatured clients under times of stress (Oh et al., 1997).

1.4.5 The role of Hsp70s in prion biology

A large body of work has provided ample evidence of the important role Hsp70 and their related chaperones play in prion biology (reviewed in Summers et al., 2009a; Masison et al., 2009). While it has been shown that excess Ssa1p or depletion of Ssa2p can cure the [*URE3*$^{+}$] prion (Schwimmer and Masison, 2002), [*PSI*$^{+}$] has served as the

primary model prion to study the roles of Hsp70p in prion propagation. Both Ssa and Ssb chaperones have been co-purified with Sup35p prion aggregate with the closely related Ssa1/2 chaperones found in a 1:2 ratio with Sup35p and Ssb1p found at lower levels (Bagriantsev et al., 2008). This shows that Hsp70-related chaperones can associate physically with Sup35p in the prion state, indeed, members of the Ssa family as well as Hsp40s such as Ydj1p and Sis1p have been found to bind preferentially to prion proteins when in their prion conformation, while Ssb family members associate with either prion or non-prion Sup35p (Sondheimer et al., 2001; Allen et al., 2005; Bagriantsev et al., 2008; Shorter and Lindquist, 2008). Interestingly, members of the Ssa and Ssb subfamilies of Hsp70 have opposite effects upon [*PSI*$^{+}$]. Overproduction of Ssa chaperones increases nonsense suppression, promotes [*PSI*$^{+}$] *de novo* formation, and mitigates curing via increased levels of Hsp104p (Chernoff et al., 1999; Newnam et al., 1999; Allen et al., 2005). Overproduction of Ssa's can also cure some variants of [*PSI*$^{+}$] that propagate more efficiently with increased Hsp104p (Kushnirov et al., 2000; Borchsenius et al., 2001; 2006). Mutation of *SSA1* leads to curing of [*PSI*$^{+}$]^{weak}, with mutant cells showing decreased propagons and increased aggregates size, similar to Hsp104p depletion curing (Jung et al., 2000). On the other hand, Ssb overproduction increases the curing rate due to Hsp104p overproduction, while deletion of *SSB1* and *SSB2* decreases it (Chernoff et al., 1999; Chacinska et al., 2001). *SSB* gene deletion, like Ssa overproduction, increases stop codon read-through and [*PSI*$^{+}$] induction efficiency. Dissection of Ssa and Ssb proteins eventually determined that the domains responsible for their differing behavior were their respective peptide binding domains, suggesting that

it is by binding different motifs in the Sup35p amyloid that the two subfamilies can exert different effects.

Based on these findings, it is hypothesized that Hsp70 chaperones regulate prion propagation primarily by affecting how Hsp104p fragments the prion amyloid (Shorter and Lindquist, 2008; Sweeny and Shorter, 2008). According to this theory, Ssa binding to the Sup35p aggregate predisposes Hsp104p to fragment it in such a way as to create viable propagons, stabilizing prion propagation. Ssb affects Hsp104p so that it fragments the Sup35p aggregate into non-templating species, thereby destabilizing the prion. How they might alter Hsp104p activity has not been characterized.

Generally, the Hsp40 Sis1p promotes prion propagation while another Hsp40, Ydj1p, inhibits it (Summers et al., 2009a). Sis1p has been shown to be essential for propagation of [*PSI*$^{+}$], [*URE3*$^{+}$], and some variants of [*PIN*$^{+}$] (Sondheimer et al., 2001; Higurashi et al., 2008; Bardill et al., 2009). Increased Sis1p levels increased efficiency of curing of [*PSI*$^{+}$] with excess Hsp104p and increased the proportion of Rnq1p incorporated into [*PIN*$^{+}$] aggregates (Douglas et al., 2008; Kirkland et al., 2011). Conversely, Ydj1p overproduction can inhibit Ure2p fibril formation and cure [*PSI*$^{+}$]^{weak} as well as some [*PIN*$^{+}$] variants such as [*PIN*$^{+}$]^{medium} (Kushnirov et al., 2000; Bradley et al., 2002; Lian et al., 2007; Savistchenko et al., 2008). Strangely, although Ydj1p seems to antagonize several prion species, it is required for propagation of [*SWI*$^{+}$], suggesting that its function is more complex (Hines et al., 2011).

How exactly Sis1p or Ydj1p act upon prion proteins is not fully understood. As stated above, Sis1p and Ydj1p can both be co-precipitated *ex vivo* with Sup35p prion aggregates (Bagriantsev et al., 2008). Additionally, both preferentially associate with

Rnq1p in its prion conformation, with Sis1p binding a short, hydrophobic region in Rnq1p's non-prion domain at a 1:1 ratio, and Ydj1p binding the N/Q-rich PrD at sub-stoichiometric levels (Sondheimer et al., 2001; Lopez et al., 2003; Douglas et al., 2008; Summers et al., 2009b). It may be that binding different domains is what leads to their different effects, but as binding domains in other prions are not characterized, this is uncertain and it could be that these differences arise instead through the different ways that Ydj1p and Sis1p act upon Hsp70s (Lu and Cyr, 1998b). It has been suggested that Sis1p's role may be to promote the fragmentation of prion aggregates into infectious propagons by presenting prions to Hsp70 and Hsp104 chaperone complexes (Summers et al., 2009a). In support of this, Sis1p has been shown to be crucial to Hsp104p binding of Sup35p (Tipton et al., 2008). Ydj1p is thought to antagonize prions by binding N/Q-rich growing ends of prion amyloids and/or directing prion protein in an intermediate conformation away from the aggregate for refolding (Summers et al., 2009a). It seems unlikely that Ydj1p acts only by blocking aggregate growth at the ends as overproduction of Ydj1p has been shown to lead to poly-Q aggregates of increased size (Gokhale et al., 2005). Directing intermediates for refolding seems more likely because Ydj1p-mediated curing requires Hsp70s, suggesting that it delivers the prion protein to Hsp70 for refolding or disposal (Sharma et al., 2009).

As stated above, it is the peptide binding domains of Hsp70s that dictate their effects on various prions. This, combined with demonstrated physical association, suggests that prion proteins can be Hsp70 clients. Further support of this conclusion is found through the investigation of how NEFs, essential for Hsp70 nucleotide exchange, also affect prions. Deletion of either *SSE1* or *FES1* can weaken the propagation of [*PSI*$^{+}$],

[*URE3*$^+$], and [*SWI*$^+$]. Overproduction of Fes1p has been shown to improve [*PSI*$^+$] propagation but excess Sse1p cures [*URE3*$^+$] and [*SWI*$^+$], while inhibiting Hsp104-mediated [*PSI*$^+$] curing (Jones et al., 2004; Kryndushkin and Wickner, 2007; Sadlish et al., 2008; Hines et al., 2011). Qing Fan and colleagues showed that depleting or overproducing Sse1p has a direct correlation with [*PSI*$^+$] induction efficiency through Sup35NM overexpression (Fan et al., 2007). They also found that [*PSI*$^+$] variants arising in *Sse1*Δ strains were limited to weak and unstable variants, as opposed to stronger variants that can arise in wild type strains. Interestingly, an *in vitro* study showed that Sse1p + ATP, in the absence of Hsp70, can increase the rate of Sup35NM assembly into amyloid, suggesting that it may have an NEF-independent activity (Sadlish et al., 2008). Nevertheless, mutational analysis of Sse1p demonstrated that mutations that impair its NEF activity also lead to [*SWI*$^+$] curing, supporting the common belief that NEFs affect prions by regulating Hsp70 chaperone activity (Hines et al., 2011).

1.4.6 General function of Hsp90-related chaperones

The final family of chaperone proteins to be discussed in this introductory chapter is the Hsp90 family (reviewed in Taipale et al., 2010; Krukenberg et al., 2011). *S. cerevisiae* has two closely related Hsp90 isoforms: Hsc82p and Hsp82p. The proteins can comprise as much as 1-2% of the cells total protein and at least one must be present to maintain cell viability (Borkovich et al., 1989). *HSC82* is constitutively expressed and both *HSC82* and *HSP82* are upregulated under conditions of stress. Although Hsp90 is important during stress response, its role extends beyond the refolding or disposal of misfolded proteins and includes aiding in the maturation of proteins. Indeed, some proteins require Hsp90 to adopt their active conformations (reviewed in Nathan et al.,

1999; Picard, 2002; Burnie et al., 2006). The full-length structure of Hsp90 has been determined by x-ray crystallography. It is comprised of a highly conserved N-terminal domain (NTD) with weak intrinsic ATPase activity, a middle domain (MD), and a C-terminal domain (CTD) that mediates dimerization of two Hsp90 monomers (Nadeau et al., 1993; Minami et al., 1994; Prodromou et al., 1997a; b; Harris et al., 2004; Hainzl et al., 2009; Tsutsumi et al., 2009). Hsp90 functions as a dimer. The Hsp90 dimer captures client proteins that have a degree of secondary structure. All domains of Hsp90 affect client binding and processing (Jakob et al., 1995; Vaughan et al., 2006; Richter and Buchner, 2011; Street et al., 2011). In yeast, open and closed conformations of the Hsp90 dimer exist in an equilibrium affected by its nucleotide bound state, with ATP-bound Hsp90 correlated with more closed dimers and ADP-bound Hsp90 with more open (Csermely et al., 1993; Grenert et al., 1997; Sullivan et al., 1997; Prodromou et al., 2000; Southworth and Agard, 2008). Data from a series of biochemical studies has contributed to a model for Hsp90 kinetics (McLaughlin et al., 2006; Phillips et al., 2007; Hessling et al., 2009; Graf et al., 2009). In brief, it is thought that when Hsp90 binds ATP, it stimulates a slow transition to a closed state where the two NTDs can interact. This has been shown to promote ATPase activity (Cunningham et al., 2008). Upon ATP-hydrolysis, the dimer adopts another, ambiguous state that is not yet fully characterized. Finally, upon ADP release, the open configuration of the dimer is restored.

The ATPase activity of Hsp90 is extremely weak, impairing its chaperone activity. NTD interactions, client binding, and a variety of Hsp90 cochaperones can increase Hsp90's intrinsic ATPase activity, allowing it to bind and release clients more efficiently. Hsp90 has several cochaperones that modulate its activity and influence client

binding. These cochaperones can compete for shared binding sites and can also bind to Hsp90 at different conformation stages of the Hsp90 cycle (Siligardi et al., 2004; Harst et al., 2005). Some of these cochaperones interact with Hsp90 via tetratricopeptide repeat (TPR) domains that bind a conserved MEEVD sequence located in Hsp90's CTD (Owens-Grillo et al., 1995; D'Andrea and Regan, 2003; Wandinger et al., 2008). Hsp90 cochaperones investigated in this study include Sti1p, Aha1p, Cpr6p, Cpr7p, Sba1p, and Tah1p.

Sti1p contains multiple TPR domains and preferentially binds nucleotide-free Hsp90, leading to inhibition of Hsp90 ATPase activity (Prodromou et al., 1999; Richter et al., 2003). It also contains multiple TPR domains, through which it has been shown to bind both Hsp70 and Hsp90 simultaneously (Smith et al., 1993; Cintron and Toft, 2006) It is believed that Sti1p facilitates transfer of client proteins from Hsp70 complexes to empty Hsp90.

Another TPR domain containing cochaperone is Tah1p. It binds specifically to Hsp90's CTD and, on its own, weakly stimulates ATPase activity (Millson et al., 2008). Tah1p is also a member of the Rvb1-Rvb2-Tah1-Pih1 (R2TP) complex that has been implicated in small nucleolar ribonucleoprotein biogenesis (reviewed in Kakihara and Houry, 2012). When it binds Hsp90 along with Pih1p, the two proteins together inhibit Hsp90 ATPase activity (Eckert et al., 2010).

Cpr6p and Cpr7p are two more Hsp90 cochaperones that associate with Hsp90 via their TPR domains with Cpr7p also able to interact with the C-terminus of Hsp104p (Marsh et al., 1998; Abbas-Terki et al., 2001; Li et al., 2011). Cpr6 has been shown to weakly stimulate Hsp90 ATPase activity with some evidence suggesting that it requires

Cpr7 to displace Sti1p from the CTD in order to bind (Prodromou et al., 1999; Zuehlke and Johnson, 2012; Li et al., 2013). In addition to modulating Hsp90, both Cpr6p and Cpr7p are cyclophilins with Hsp90-independent prolyl isomerase activity (Duina et al., 1996a; b; Mayr et al., 2000).

Neither Aha1p nor Sba1p bind Hsp90 at its CTD. Instead, Aha1p binds across the MD and NTD during the early stages of Hsp90's ATP driven conformational changes, thus increasing ATP hydrolysis (Panaretou et al., 2002; Meyer et al., 2004; Hessling et al., 2009; Retzlaff et al., 2010). Sba1p, on the other hand, binds the NTD while the Hsp90 dimer is in a more closed configuration, thereby reducing its flexibility and keeping it closed (Young and Hartl, 2000; Freeman et al., 2000). In this way Sba1p inhibits ATPase activity while stimulating ATP binding, stabilizing the Hsp90-client complex, and giving the client time to mature (McLaughlin et al., 2006).

1.4.7 Do Hsp90 chaperones affect prions?

Unlike Hsp104 and Hsp70/40 chaperone systems, Hsp90 does not appear to play a central role in prion regulation. It was shown that Hsp82p could hamper Ure2p aggregation to a degree *in vitro* (Savistchenko et al., 2008). Also, chemical inhibition of Hsp90 ATPase activity or deletion of either *HSC82* or *HSP82* reduced [*PSI*$^{+}$] curing rates due to *HSP104* overexpression, although it is possible that this effect is indirect as decreased Hsp90 activity has been linked to increased levels of Ssa1p (Reidy and Masison, 2010).

That being said, both Sti1p and Cpr7p cochaperones have demonstrated reguation of [*PSI*$^{+}$]. Depletion of Sti1p or Cpr7p inhibits [*PSI*$^{+}$] curing by Hsp104p overproduction as well as curing due to mutations in *HSP104* that lead to decreased ATPase activity and

client release, but had no effect on GuHCl curing (Moosavi et al., 2010). Overexpression of *STI1* can cure a hybrid [*PSI*$^{+}$] prion composed of the *S. cerevisiae* catalytic domain and the yeast *Pichia methanolica* prion domain (Kryndushkin et al., 2002). These effects could be mediated through Hsp90 but, as both Sti1p and Cpr7p can interact with multiple chaperone complexes and/or have intrinsic chaperone abilities, it remains uncertain (Marsh et al., 1998; Mayr et al., 2000; Abbas-Terki et al., 2001; Wegele et al., 2003; Jones et al., 2004). Some evidence was found later that suggested that these cochaperones may act through Hsp70 and not Hsp90, when it was shown that deletion of *STI1* or *CPR7* could impair curing due to a mutation in *SSA1* that causes enhanced substrate binding (*SSA1-21*), while mutation of the Hsp90 domains essential for interaction with Sti1p or Cpr7p had no effect (Jones et al., 2004; Reidy and Masison, 2010). In all, it seems that Hsp90 does not have an important role in propagation of [*PSI*$^{+}$], but further studies may yet show that it is important to other prions or to other aspect of prion biology, such as variant determination.

1.4.5 Chaperones in collaboration

The primary role of chaperones in the cell is to ensure correct protein folding, even under conditions of increased stress. While chaperones can act independently, they often work together to refold client proteins. Hsp40s, Hsp70s, Hsp90s and Hsp104 can all recognize and bind clients, but can also have clients presented to them by other chaperones. Thus, it is not surprising that the specific equilibrium of chaperones and cochaperones can strongly affect their activities. This is very clearly demonstrated in yeast prions where altered expression levels or mutations for a given chaperone that normally disrupt propagation can be compensated for by altering the levels of or mutating

other chaperones. This degree of interconnectivity, balanced with their own intrinsic chaperone activities, makes it difficult to fully understand exactly how they all act together, but it is an attractive theory that chaperones generally promote propagation by maintaining a balance between prion amyloid growth and fragmentation in such a way as to allow sufficient inheritance of propagons by daughter cells. Any other roles they may have, such as Sis1p's effect upon [*PIN*$^+$] variant, are poorly understood and may yet add another layer of chaperone-mediated regulation of prions and prion phenotypes.

1.5 Focus of this Thesis

1.5.1 Specific Aim 1: Identification of novel prion proteins in *S. cerevisiae*

Hypothesis: Of the currently identified prions in *S. cerevisiae*, most are rich in the amino acid residues asparagine (N) and glutamine (Q). In this study, I hypothesized that other N/Q rich proteins may also have prion-like characteristics and be able to act as self-propagating amyloidogenic proteins.

In chapter three, I describe the screening of the yeast proteome for proteins rich in N and/or Q and the characterizing of several of these proteins for prion-like qualities using a variety of methods. This screen for novel prion proteins remains incomplete at this time, but I report the identification of a novel putative prion of unknown function, Riq1p/[*RIQ*$^+$] and describe its prion-like characteristics including aggregate formation and the ability to maintain a reversibly curable phenotype. This finding adds another possible member to *S. cerevisiae*'s growing cadre of prion proteins and suggests that the current view of the different effects of N and Q residues have on prion formation may require a reexamination.

1.5.2 Specific Aim 2: Identification of factors regulating [*PIN*$^+$] variants

Hypothesis: Subscribing to the theory that prions have an adaptive role in *S. cerevisiae* and perform a positive function, I hypothesized that the cell would have mechanisms in place for modulating prion-linked phenotypes through modulation of the prevailing prion variants.

In chapter four, I describe the screening of a limited set of strains deleted for potential candidate prion-cofactor encoding genes for strains that affected morphological features of Sup35p aggregates upon [*PSI*$^+$] induction *in vivo*. Strains deleted for a variety of chaperone genes linked to Hsp90 chaperone activity were shown to have a strong effect in this screen. As chaperones have been heavily implicated in the stable propagation of yeast prions, it seemed likely that they could have a role in regulating prion variants. Through further characterization of these deletion strains, I demonstrate stable shifts in [*PIN*$^+$] variants from the original variant present prior to gene deletion to another variant afterwards. These findings suggest that the cell can potentially regulate its prion-linked phenotype through modulation of its chaperone network and how those chaperones affect prion variants.

CHAPTER TWO: MATERIALS AND METHODS

2.1 Materials

Table 2-1. Chemicals and reagents employed in this study

Reagent	Source
2-mercaptoethanol	BioShop
acrylamide	Roche
agar	Difco
agarose, UltraPure	Invitrogen
albumin, bovine serum (BSA)	Roche
α-factor	Sigma-Aldrich
ampicillin	Sigma-Aldrich
ammonium bicarbonite (NH_4HCO_3)	Sigma-Aldrich
anhydrous ethyl alcohol	Commercial Alcohols
boric acid	EM Science
bromophenol blue	BDH
calcium chloride	BDH
chloroform	Fisher
complete protease inhibitor cocktail (EDTA free)	Roche
complete supplement mixture (CSM)	BIO 101
coomassie brilliant blue R-250	ICN
cyclosporin A	Cell Signaling
D-(+)-glucose	EM Science
deoxyribonucleotide triphosphate mixture (dNTPs)	Invitrogen
dithiothreitol (DTT)	Fisher
dry ice (solid state CO_2)	Biochemistry stores
ethidium bromide	Sigma-Aldrich
ethylenedinitrilo-tetraacetic acid (EDTA)	EM Science
formaldehyde, 37% (v/v)	Biochemicals
FM4-64	Molecular Probes
galactose	EMD
geldanamycin	Sigma-Aldrich
glacial acetic acid (17.4 M)	Fisher
glass beads (acid washed)	Sigma-Aldrich
glycerol	EM Science
glycine	Roche
guanidine hydrochloride	Sigma-Aldrich
hydrocholic acid	Fisher
imidozole	Sigma-Aldrich
isoamyl alcohol	Fisher
isopropyl β-D-thiogalactopyranoside (IPTG)	Roche
L-histidine	Sigma-Aldrich
lithium acetate	Sigma-Aldrich
L-leucine	Sigma-Aldrich
L-lysine	Sigma-Aldrich
magnesium sulfate ($MgSO_4$)	Sigma-Aldrich
methanol	Fisher
N,*N*,*N*',*N*'-tetramethylethylenediamine (TEMED)	EM Science
N,*N*'-dimethyl 73ormamide (DMF)	BDH
N,*N*'-methylene bisacrylamide	Sigma-Aldrich
NVP-AUY-922	Active Biochem
peptone	Difco
phenol, buffer saturated	Invitrogen
phenylmethylsulphonylfluoride (PMSF)	Roche

poly *L*-lysine	Sigma-Aldrich
polyethylene glycol, M.W. 3350 (PEG)	Sigma-Aldrich
ponceau S	Sigma-Aldrich
potassium phosphate, dibasic (K_2HPO_4)	EM Science
raffinose	EMD
salmon sperm DNA, sonicated	Sigma-Aldrich
sephadex G25	Amersham
skim milk powder	Carnation
sodium acetate	EM Science
sodium azide	Sigma-Aldrich
sodium chloride (NaCl)	EM Science
sodium dodecyl sulfate (SDS)	Bio-Rad
sorbitol	EM Science
TALON Superflow Metal Affinity Resin	Clontech
thiamine-HCl	Sigma-Aldrich
thioflavin T	Sigma-Aldrich
trichloroacetic acid (TCA)	EM Science
Tris-2(carboxyethy)phosphine (TCEP)	Roche
tris(hydroxymethyl)aminomethane (Tris)	Roche
triton X-100	VWR
trypan blue	Gibco
tryptone	Difco
tween 20	Sigma-Aldrich
uracil	Sigma-Aldrich
xylene cyanol FF	Sigma-Aldrich
yeast extract	Difco
yeast nitrogen base without amino acids (YNB)	Difco

Table 2-2. Enzymes

Enzyme	Source
CIP (calf intestinal alkaline phosphatase)	NEB
Easy-A high-fidelity DNA polymerase	Stratagene
Phusion High Fidelity DNA polymerase	NEB
restriction endonucleases	NEB
Quick T4 DNA ligase	NEB
RNase A (ribonuclease A), bovine pancreas	Sigma-Aldrich
T4 DNA ligase	NEB
Zymolyase 20T	ICN
Zymolyase 100T	ICN

Table 2-3. Molecular size standards

Molecular Size Standard	Source
1 kb DNA ladder (500-10,000 bp)	NEB
prestained protein marker, broad range (6-175 kDa)	NEB

Table 2-4. Multicomponent systems

Multicomponent System	Source
BigDye Terminator Cycle Sequencing Ready Reaction Kit	Applied Biosystems
Matchmaker Two-Hybrid System	Clontech
QIAprep Spin Miniprep Kit	Qiagen
QIAquick Gel Extraction Kit	Qiagen
QIAquick PCR Purification Kit	Qiagen
Ready-To-Go PCR Beads	Amersham Biosciences

Table 2-5. Primary antibodies

Specificity	Type	Name	Dilution[a]	Reference
S. cerevisiae Sup35p	guinea pig	RU6	1:10,000	This study
S. cerevisiae Sup35NMp	guinea pig	R-25-final	1:10,000	This study
S. cerevisiae Rnq1p	rabbit	αRnq1p	1:10,000	(Sondheimer and Lindquist, 2000)
S. cerevisiae Riq1p	guinea pig	PU7-4°	1:5000	This study
GFP	rabbit	P34-final	1:5000	This study
HA	mouse	F-7 Sc7392	1:500	Santa Cruz
penta-HIS	mouse	34660	1:1000	QIAGEN
S. cerevisiae G6PDH	rabbit	A9521	1:10,000	Sigma-Aldrich
S. cerevisiae Ubiquitin	mouse	P4D1	1:1000	Cell Signalling

[a]Dilutions are for use in immnunoblotting.

Table 2-6. Secondary antibodies

Specificity	Type	Dilution	Source
horseradish peroxidase (HRP)-conjugated anti-rabbit IgG	donkey	1:10,000	GE Healthcare UK Limited
HRP-conjugated anti-mouse IgG	sheep	1:10,000	GE Healthcare UK Limited
HRP-conjugated anti-guinea pig IgG	goat	1:30,000	Sigma-Aldrich
rhodamine-conjugated anti-guinea pig IgG	donkey	1:250	Jackson Immunoresearch Laboratories

Table 2-7. Common solutions

Solution	Composition	Reference
1 × TBST	20 mM Tris-HCl, pH 7.5, 150 mM NaCl, 0.05% (w/v) Tween 20	(Glover and Hames, 1995)
1 × Transfer buffer	20 mM Tris-HCl, 150 mM glycine, 20% (v/v) methanol	(Towbin et al., 1979; Burnette, 1981)
5 × SDS-PAGE running buffer	0.25 M Tris-HCl, pH 8.8, 2 M glycine, 0.5% SDS	(Ausubel et al., 1993)
10 × TBE	0.89 M Tris-borate, 0.89 M boric acid, 0.02 M EDTA	(Maniatis et al., 1982)
2× protein sample buffer	20% (v/v) glycerol, 167 mM Tris-HCl, pH 6.8, 2% SDS, 0.005% bromophenol blue	(Ausubel et al., 1993)
6 × DNA loading dye	0.25% bromophenol blue, 0.25% xylene cyanol, 30% (v/v) glycerol	(Maniatis et al., 1982)
Breakage buffer	2% (v/v) Triton X-100, 1% SDS, 100 mM NaCl, 10 mM Tris-HCl, pH 8.0, 1 mM EDTA, pH 8.0	(Ausubel et al., 1993)
Ponceau stain	0.1% Ponceau S, 1% TCA	(Szilard and Rachubinski, 2000)
1 × TE	10 mM Tris-HCl, pH 7.0-8.0 (as needed), 1 mM EDTA	(Maniatis et al., 1982)
1 × TAE	40 mM Tris-HCl, pH 7.4, 20 mM Glacial Acetic Acid, 1 mM EDTA	(Ogden and Adams, 1987)
1 × TBS	50 mM Tris-HCl, pH 7.4, 150 mM NaCl	(Ogden and Adams, 1987)
Lysis Buffer (yeast)	25mM Tris-HCl, pH 7.4, 100 mM NaCl, 1 mM DTT, 2 × Complete EDTA free protease inhibitor	(Halfmann and Lindquist, 2008)

2.2 Microorganisms and culture conditions

2.2.1 Bacterial strains and culture conditions

The *Escherichia coli* strains and culture media used in this study are described in Tables 2-8 and 2-9, respectively. Bacteria were grown at 37°C. Cultures of 5 ml or less were grown in culture tubes in a rotary shaker at 200 rpm. Cultures greater than 5 ml were grown in flasks in a rotary shaker at 200 rpm. Culture volumes were approximately 20% of flask volumes.

Table 2-8. Bacterial strains

Strain	Genotype	Source
DH5α	F^-, Φ80d*lac*ZΔM15, Δ(*lac*ZY A-*arg*F), U169, *rec*A1, *end*A1, *hsd*R17(r_k^-, m_k^+), *pho*A, *sup*E44, λ^-, *thi*-1, *gyr*A96, *rel*A1	Invitrogen
BL21(DE3)	F^-, *omp*T, *hsd*SB(r_B^- m_B^-] *gal*, *dcm* (DE3)	Novagen

Table 2-9. Bacterial culture media

Meidum	Composition	Reference
LB	1% tryptone, 0.5% yeast extract, 1% NaCl	(Maniatis et al., 1982)
LB Amp	1% tryptone, 0.5% yeast extract, 1% NaCl, Ampicillin 100 μg/ml	(Maniatis et al., 1982)

2.2.2 Yeast strains and culture conditions

The *Saccharomyces cerevisiae* strains used and media employed in culturing them in this study are listed in Tables 2-10 and 2-11 respectively. Yeast was cultured at 30°C. Cultures of 10 ml or less were grown in 16 × 150-mm glass tubes in a rotating wheel. Cultures greater than 10 ml were grown in flasks in a rotary shaker at 250 rpm. Culture volumes were approximately 20% of flask volumes.

Table 2-10. *S. cerevisiae* strains

Strain	Genotype	Reference
BY4742	*MATα, his3Δ1, leu2Δ0, lys2Δ0, ura3Δ0*	(Giaever et al., 2002)
BY4741/BY4742 gene knockout library strains	All gene knock outs in these parental strains were generated using the *KanMX4* cassette to replace the ORF of interest	(Giaever et al., 2002)
GFP library strains	*MATa, his3Δ1, leu2Δ0, met15Δ0, ura3Δ0,* All ORFs were C-terminally tagged with *GFP* using the *HIS3MX6* cassette as a selective marker.	(Huh et al., 2003) Invitrogen
GT17[a]	*MATa, ade1-14UGA, his3-200, leu2-3, 112 trp1-289UAG, ura3-52*	(Bailleul et al., 1999)
GT17 knock out strains[a]	All gene knock outs in this parental strain were generated using the *HIS3* cassette to replace the ORF of interest	This study
GT17 Sup35MC	*MATa, ade1-14UGA, his3-200, leu2-3, 112 trp1-289UAG, ura3-52, SUP35Δ2-369*	This study
GT17 Riq1-Sup35MC[b]	*MATa, ade1-14UGA, his3-200, leu2-3, 112 trp1-289UAG, ura3-52, SUP35Δ1-369::RIQ1*	This study
GT17 Riq1-Sup35MC knock out strains[b]	All gene knock outs in this parental strain were generated using the *HIS3* cassette to replace the ORF of interest	This study
GT17 RiqNQ-Sup35MC	*MATa, ade1-14UGA, his3-200, leu2-3, 112 trp1-289UAG, ura3-52, SUP35Δ1-369::RIQ1 1-690*	This study
GT17 RiqQ-Sup35MC	*MATa, ade1-14UGA, his3-200, leu2-3, 112 trp1-289UAG, ura3-52, SUP35Δ2-369::RIQ1 301-690*	This study
GT17 RiqC-Sup35MC	*MATa, ade1-14UGA, his3-200, leu2-3, 112 trp1-289UAG, ura3-52, SUP35Δ2-369::RIQ1 691-1884*	This study
GT17 Def1-Sup35MC	*MATa, ade1-14UGA, his3-200, leu2-3, 112 trp1-289UAG, ura3-52, SUP35Δ1-369::DEF1*	This study
GT17 Ent2-Sup35MC	*MATa, ade1-14UGA, his3-200, leu2-3, 112 trp1-289UAG, ura3-52, SUP35Δ1-369::ENT2*	This study
GT17 Taf12-Sup35MC	*MATa, ade1-14UGA, his3-200, leu2-3, 112 trp1-289UAG, ura3-52, SUP35Δ1-369::TAF12*	This study
GT234[a]	*MATα, ade1-14 UGA, his3-delta200, leu2-3, 112 trp1-289UAG, ura3-52, lys2*	(Wegrzyn et al., 2001)
GT234 Riq1-Sup35MC[b]	*MATα, ade1-14 UGA, his3-delta200, leu2-3, 112 trp1-289UAG, ura3-52, lys2, SUP35Δ1-369::RIQ1*	This study
GT234 RiqNQ-Sup35MC	*MATα, ade1-14 UGA, his3-delta200, leu2-3, 112 trp1-289UAG, ura3-52, lys2, SUP35Δ1-369::RIQ1 1-690*	This study

GT234 RiqQ-Sup35MC	*MATα, ade1-14 UGA, his3-delta200, leu2-3, 112 trp1-289UAG, ura3-52, lys2, SUP35Δ2-369::RIQ1 301-690*	This study
GT234 RiqC-Sup35MC	*MATα, ade1-14 UGA, his3-delta200, leu2-3, 112 trp1-289UAG, ura3-52, lys2, SUP35Δ2-369::RIQ1 691-1884*	This study
L1943	*MATa, ade1-14, ura3-52, leu2-3, 112, trp1-289, his3-200* [*psi*$^-$][*PIN*$^+$]^{low}	(Bradley et al., 2003)
L1943 alpha	*MATα, ade1-14, ura3-52, leu2-3, 112, trp1-289, his3-200* [*psi*$^-$][*PIN*$^+$]^{low}	This study
L1943 knock out strains	*MATa, ade1-14, ura3-52, leu2-3, 112, trp1-289, his3-200 chaperone gene*::*HIS3* [*psi*$^-$]	This study
L1945	*MATa, ade1-14, ura3-52, leu2-3, 112, trp1-289, his3-200* [*psi*$^-$][*PIN*$^+$]^{medium}	(Bradley et al., 2003)
L1945 alpha	*MATα, ade1-14, ura3-52, leu2-3, 112, trp1-289, his3-200* [*psi*$^-$][*PIN*$^+$]^{medium}	This study
L1945 knock out strains	*MATa, ade1-14, ura3-52, leu2-3, 112, trp1-289, his3-200 chaperone gene*::*HIS3* [*psi*$^-$]	This study
L1749	*MATa, ade1-14, ura3-52, leu2-3, 112, trp1-289, his3-200* [*psi*$^-$][*PIN*$^+$]^{high}	(Bradley et al., 2003)
L1749 alpha	*MATα, ade1-14, ura3-52, leu2-3, 112, trp1-289, his3-200* [*psi*$^-$][*PIN*$^+$]^{high}	This study
L1749 knock out strains	*MATa, ade1-14, ura3-52, leu2-3, 112, trp1-289, his3-200 chaperone gene*::*HIS3* [*psi*$^-$]	This study
L1991	*MATα, SUQ5, ade2-1, lys1-1, his3-11,15, leu1, kar1-1,* [*RHO*$^+$][*psi*$^-$][*PIN*$^+$]^{low}	(Bradley et al., 2003)
L1992	*MATα, SUQ5, ade2-1, lys1-1, his3-11,15, leu1, kar1-1,* [*RHO*$^+$][*psi*$^-$][*PIN*$^+$]^{medium}	(Bradley et al., 2003)
L1998	*MATα, SUQ5, ade2-1, lys1-1, his3-11,15, leu1, kar1-1,* [*RHO*$^+$][*psi*$^-$][*PIN*$^+$]^{high}	(Bradley et al., 2003)
HF7c	*MATa, ura3-52, his3-200, lys2-801, ade2-101, trp1-901, leu2-3, 112, gal4-542, gal80-538, LYS2::GAL-HIS3, URA3::(GAL4 17-mers)*$_3$*-CYC1-lacZ*	Clontech
2081	*MATα, sst2Δ, ste2Δ, ura3-52, his3-200, lys2-801, ade2-101, trp1-901, leu2-3*	Wozniak Lab
2082	*MATa, bar1Δ, ura3-52, his3-200, lys2-801, ade2-101, trp1-901, leu2-3*	Wozniak Lab

[a] These strains were maintained with the following prion states: [*PSI*$^+$][*PIN*$^+$], [*psi*$^-$] [*PIN*$^+$], and [*psi*$^-$][*pin*$^-$].
[b] These strains were maintained with the following prion states: [*RIQ1*$^+$] or [*riq1*$^-$].

Table 2-11. Yeast culture media

Medium	Composition[a]	Reference
CSM (Complete Supplement Mixture)	1 × Yeast Nitrogen Base w/o amino acids, 1 × CSM-amino acid mixture[b], 2% glucose[c]	(Rose et al., 1990)
Sporulation Media	1% potassium acetate, 0.1% yeast extract, 0.05% glucose	(Rose et al., 1990)
YEPD	1% yeast extract, 2% peptone, 2% glucose[c]	(Rose et al., 1990)
5-FOA	0.1% 5-FOA[d], 1.2 % uracil[d], 0.17% yeast nitrogen base, 0.07% CSM-URA amino acid mixture, 2% glucose[d]	(Boeke et al., 1987)

[a] For solid media, agar was added to 2%.
[b] The addition of amino acid to CSM lacked specific amino acids so as to act as an auxotrophic selective marker.
[c] In cases where overexpression of GAL promoter driven genes, 2% galactose was added *in lieu* of glucose. Both were added after autoclaving.
[d] These ingredients were mixed in half the solution volume, filter sterilized and added after autoclaving.

2.2.3 Mating, sporulation and tetrad dissection of *S. cerevisiae*

Haploid *S. cerevisiae* strains were mated following the method employed by Rose and colleagues (1990). Briefly, haploids were streaked in straight lines onto separate YEPD agar plates (Table 2-11) and incubated overnight. These plates were then replica plated onto fresh YEPD plates in such a manner as the streaked lines are oriented perpendicular to one another and incubated overnight. Cells from intersecting points were streaked out on CSM minimal media supplemented for the auxotrophic requirements of the diploid strain and incubated overnight.

Sporulation and tetrad dissection of diploid strains were also performed according to Rose *et al*. (1990) with modifications. A single diploid colony was grown overnight in 5 ml of YEPD medium. Cells were harvested by centrifugation, washed twice in 10 ml ddH_2O, and resuspended in approximately 60 µl of ddH_2O. 5 µl of this suspension was used to inoculate 3 ml of sporulation medium (Table 2-11), which was then incubated for 3 to 7 days. Formation of tetrads was assessed by light microscopy. When at least 10%

of cells had formed tetrads, 1 ml of cells was transferred to a microcentrifuge tube and washed twice with ddH_2O. The pellet was then resuspended in 1 ml ddH_2O and 10 µl of this suspension was transferred to 990 µl of ddH_2O containing 3 to 5 µg of zymolase 20T and incubated at 30°C in a rotating wheel for 15 minutes. 20 µl of the spheroplasted cells were then streaked out on a thinly poured YEPD agar plate in a single line. Tetrads were dissected using a Zeiss Axioskop 40 microscope equipped with a Tetrad Manipulator System (Carl Zeiss). Isolated spores were incubated for 2-3 days at 30°C before further analysis.

2.2.4 *De novo* induction of prions

Strains to be induced were transformed with a galactose inducible plasmid expressing a GFP-tagged copy of the gene encoding the prion of interest i.e. pYES2.0-Sup35NM-GFP for [*PSI*$^+$] and pYES2.0-Riq1-GFP for [*RIQ*$^+$] (see Table 2-12). Transformations were done according to the methods outlined in Section 2.3.2. Transformed strains were grown overnight in CSM-URA 2% glucose liquid medium then subcultured in CSM-URA 2% galactose for 2-3 days, at which point they were plated onto plates of the desired medium either for single colonies or as dilution series as described in Section 2.2.5. Some were also observed for aggregate formation *in vivo* following the protocols for fluorescence microscopy outlined in Section 2.9.

2.2.5 Assay for nonsense-suppression

In order to quantify the effective induction of prions with a nonsense-suppression phenotype, dilution series were spotted onto CSM plates and the nonsense-suppression selective medium, CSM-ADE. The strains of interest were grown up in liquid culture and then prepared into serial dilutions in ddH_2O in microcentrifuge tubes at OD_{600} 1.0,

0.1, 0.01, 0.001, 0.0001, and 0.00001. 5 µl of each dilution was then spotted onto each of the plates to be tested and the spots were allowed to dry. The plates were incubated at 30°C until the desired level of growth was reached (2-6 days). At this point colony forming units (cfu) were counted for two or three dilutions and averaged. The prion induction efficiency was calculated as [cfu (CSM-ADE)/ cfu (CSM)] × 100.

2.2.6 Prion curing protocol

[*PRION*$^{+}$] strains were converted to a [*prion*$^{-}$] state by culturing them in either liquid YEPD or on YEPD plates that included 3 mM guanidine hydrochloride (GuHCl). They were allowed to grow under these conditions for 3 days and then streaked for single colonies on YEPD plates lacking GuHCl. For [*PSI*$^{+}$] and Sup35MC-chimeric prions, cells were selected for red-pigment and tested to see if they had lost ADE-competence by streaking on CSM-ADE medium. For [*PIN*$^{+}$], they were tested for [*PSI*$^{+}$] induction by the *de novo* induction protocol described above.

2.3 Introduction of DNA into microorganisms

2.3.1 Chemical transformation of *E. coli*

DH5α *E. coli* was transformed following standard protocols (Hanahan, 1983). Basically, *E. coli* was grown in 200 ml LB liquid medium to an OD_{600} ~0.35 at which point cells were harvested through centrifugation at 4ºC and subsequent removal of the supernatant. The pellet was resuspended in 100 ml of ice-cold, sterile 100 mM $CaCl_2$ and incubated on ice for 30 minutes. The cells were harvested again by the same steps and resuspended in 5 ml of ice-cold, sterile 100 mM $CaCl_2$ + 20% glycerol. 50 µl aliquots of this suspension were prepared and flash frozen using dry ice and ethanol. The aliquots were stored at -80ºC until needed.

A typical transformation involved thawing 50 µl aliquots of competent cells on ice and then adding 1-2 µl of plasmid DNA, mixing it gently with the pipette tip. When transforming cells with ligation reaction mixtures, 5-10 µl of ligation was added. The cell-DNA mixture was incubated on ice for 30 minutes and then heat-shocked at 42ºC for 2 minutes. 500 µl of LB was immediately added to the transformation mixture, which was then incubated for 1 hour at 37ºC in a shaking water bath. 20-50 µl of the transformation mix was plated onto LB plates containing the appropriate antibiotic supplement (*e.g.* Ampicillin). When transforming with ligation products, 200 µl of the transformation mixture was plated to maximize the odds of success.

2.3.2 Chemical transformation of the yeast *Saccharomyces cerevisiae*

Plasmid DNA was transformed into *S. cerevisiae* according to standard protocol (Gietz and Woods, 2002). Briefly, 25 µl of cells from the desired yeast strain were scraped off of plate with a sterile pipette tip and suspended in 1 ml of ddH_2O. Cells were then pelleted through centrifugation, resuspended in 500 µl of 100 mM lithium acetate (Li-Ac), and incubated at 30ºC for 5 minutes in order to induce permeability and allow DNA cross the cell membrane (Brzobohatý and Kovác, 1986). Cells were again harvested by centrifugation, and the following solutions were added to the pellet in this order: 64 µl ddH_2O, 32 µl 1M Li-Ac (at this point the cells were resuspended as resuspension was difficult after the addition of 50% w/v polyethylene glycol (PEG)), 240 µl 50% w/v PEG, 10 µl boiled, sheared salmon sperm DNA, 2-3 µl purified plasmid DNA. The role of PEG is to protect the cell from the detrimental effects of the permeability induced by high concentrations of Li-Ac, as well as to help trap plasmid DNA near the cell by inducing cell clumping (Chen et al., 2008). The role of Salmon sperm DNA is to bind to the cell

wall and reduce the amount of plasmid DNA that is bound there, allowing more to be taken up into the cell. The mixture was vortexed for 1-3 minutes and then heat shocked at 42ºC for 20 minutes. The cells were then harvested again through centrifugation, resuspending in 150 µl ddH_2O, and plated on CSM plates lacking the appropriate amino acid supplement(s). Plates were incubated for 2-4 days at 30ºC before single colonies were picked for further experimentation.

2.3.3 Electroporation of the yeast *Saccharomyces cerevisiae*

Cells were transformed following a protocol adapted from Thompson *et al*. (1998). Cells were grown overnight in 5 ml of YEPD, and then 1 ml of primary culture was used to inoculate 9 ml of fresh YEPD. The secondary culture was allowed to grow at 30ºC for ~5 hours or until reaching an OD_{600} of ~1.0. Cells were harvested at 2,500 × *g*, resuspended in 10 ml LTE solution (9 ml TE buffer, 1 ml 1 M lithium acetate, 200 µl 1 M DTT), and incubated for 30 minutes at 30ºC. Cells were again harvested at 2,500 × *g*, washed once with room-temperature ddH_2O, once with ice-cold ddH_2O, and once with ice-cold 1 M sorbitol. The excess sorbitol was discarded and the pellet was resuspended in a minimal volume of ice-cold 1 M sorbitol. 50 µl of cell suspension was mixed with 1 µl of plasmid DNA or 3-5 µl of purified DNA fragment. This mixture was placed between the anode and cathode of an ice-cold electroporation chamber (Bio-Rad) and submitted to an electrical pulse of 250 V (amplified to 1.6 kV) at a capacitance of 2 µF and a resistance of 4 kΩ using a Bio-Rad MicroPulser. Cells were immediately resuspended in 100 µl of ice-cold sorbitol and plated onto the appropriate selective plates. Plates were incubated for 3-5 days at 30ºC for colony formation.

2.3.4 Plasmid retention assay

Strains to be tested for plasmid retention were plated for single colonies on CSM plates. These where then replica plated onto CSM plates and CSM plates lacking the appropriate amino acid using sterilized velvet. I then quantified the number of colonies that retained the plasmid as those that grew on both media and the number of colonies that lost it as those that only grew on CSM plates. I calculated retention as the percentage of plasmid retaining colonies: [cfu (CSM-URA)/cfu (CSM)] × 100.

2.3.5 Mating type switch protocol

Mating type of *S. cerevisiae* haploid strains was switched using standard protocols (Herskowitz and Jensen, 1991). In brief, the strain of interest was transformed with YCpGAL::HO using the chemical transformation method outlined in section 2.3.2. A transformed colony was then selected and grown in CSM-URA 2% raffinose until its cell density was 0.5 – 1.0 OD_{600}, at which point galactose was added to a concentration of 2%. This culture was then grown for another 3-4 hours at which point it was plated for single colonies on YEPD. It is important not to induce the YCpGAL::HO vector with galactose for longer because it could lead to double strand break and once the cell mating types have switched, the cells in culture may begin to mate and form diploids.

Single colonies were tested for mating type by plating on lawns of tester strains 2081 or 2082. Colonies that generate halos in the 2081 tester strain lawn are *MATa* while those that do so in the 2082 lawns are *MAT*α.

2.4 DNA isolation from microorganisms

2.4.1 Isolation of plasmid DNA from *E. coli*

Single colonies of *E. coli* were inoculated into 2 ml of LB containing 1 μM ampicillin and incubated overnight at 37ºC. Cells were then harvested by centrifugation for 5 minutes at 18,000 × *g* and the plasmid DNA was isolated using the QIAprep Spin Miniprep Kit according to manufacturer's instructions (Qiagen). This method is based upon alkaline lysis of bacterial cells, followed by the adsorption of DNA onto a silica column in the presence of high salt and elution of the DNA in a low salt buffer. Plasmid DNA was eluted in 50 μl of the supplied elution buffer or ddH_2O.

2.4.2 Isolation of chromosomal DNA from *S. cerevisiae*

Yeast genomic DNA was prepared as recommended (Ausubel et al., 1993). Cultures were grown overnight in 5 ml of YEPD, harvested by centrifugation for 5 minutes at 2,500 × *g*, washed once in 5 ml ddH_2O, resuspended in 200 μl of breakage buffer (Table 2-7), and transferred to a 1.6 ml microcentrifuge tube. 200 μl of acid-washed glass beads were added to the suspension along with 300 μl phenol/chloroform/isoamyl alcohol (25:24:1). The mixture was vortexed for 5 minutes at room temperature then 200 μl of TE buffer pH 8.0 (Table 2-7) was added. The organic and aqueous phases were then separated by centrifugation at 16,000 × *g* for 5 minutes at room temperature. The aqueous phase (top layer) was transferred to a fresh microcentrifuge tube and subjected to another round of extraction with an equal volume of phenol/chloroform/isoamyl alcohol as described above. The aqueous layer was once again recovered and the DNA was precipitated by the addition of 2.5 volumes of anhydrous ethanol and incubation at 4ºC for 30 minutes to an hour. The DNA was

pelleted by centrifugation at 16,000 × *g* for 5 minutes at room temperature and washed once with 1 ml of 70% v/v ethanol. The pellet was dried in a rotary vacuum desiccator, resuspended in 50 µl TE buffer pH 8.0 containing 100 µg RNase A/ml, and incubated at 37ºC for 1 to 2 hours in order to allow for digestion of RNA.

2.4.3 Isolation of plasmid DNA from *S. cerevisiae*

Plasmids were isolated from *S. cerevisiae* by an adapting the manufacturer's recommended protocol for the QIAprep Spin Miniprep Kit (QIAGEN). Buffers and columns are provided in the kit. Cultures were grown overnight in 5 ml YEPD, harvested by centrifugation for 5 minutes at 2,500 × *g*, washed once in 5 ml ddH_2O, and resuspended in 250 µl of buffer. 200 µl of acid-washed beads were added and the mixture was vortexed for 5 minutes at room temperature. 250 µl of buffer P2 was added and mixed by inversion. Next, 350 µl of buffer N3 was added and mixed by inversion. The mixture was incubated on ice for 10 minutes and then subjected to centrifugation for 10 minutes at 18,000 × *g* at room temperature. The supernatant was then transferred to the column. From this point on, the manufacturer's instructions were followed without deviation.

2.5 DNA manipulations and analysis

Unless otherwise indicated, reactions were carried out in 1.5 ml microcentrifuge tubes and microcentrifugation was performed in an Eppendorf microcentrifuge at 18,000 × *g*.

2.5.1 Amplification of DNA by polymerase chain reaction (PCR)

PCR was used to amplify specific DNA sequences from chromosomal or plasmid DNA and to introduce modifications in the amplified sequence, such as the introduction

of a DNA restriction endonuclease recognition site. Primer design, reaction components and cycling were conformed to standard protocols (Innis and Gelfland, 1990; Saiki et al., 1988). A typical reaction contained 0.1-0.5 µg of chromosomal DNA or 0.1-0.2 µg of plasmid DNA to act as template for the reaction. There was also 20 pmol of each primer, 0.25 mM of each dNTP, 1 mM Mg_2SO_4, 1.25 U of EasyA high-fidelity polymerase (Stratagene) or Phusion high-fidelity polymerase (Finnzymes). Reactions were performed in either 0.6-ml microfuge tubes in a Robocycler 40 with Hot Top attachment (Stratagene) or in 0.2-ml microfuge tubes in a 2720 Thermocycler (Applied Biosystems). When high fidelity was not important, Ready-to-Go PCR Beads were used as recommended by the manufacturer (Amersham Biosciences).

2.5.2 Digestion of DNA by restriction endonucleases

A typical digestion required 1-2 µg of plasmid/purified DNA, 1 µl of the desired restriction endonuclease(s), and a 1 × final concentration of the manufacturer's recommended buffer(s) (NEB). Digestions were carried out over ~2 hours at the recommended temperature (*e.g.* 37ºC) and, in the case of plasmid DNA, was simultaneously treated with 10U of Calf Intestinal Phosphatase (CIP)(NEB) for the final hour of incubation in order to dephosphorylate the 5′ ends of the DNA. This was done to prevent intramolecular ligations. Digestion and dephosphorylation reactions were terminated immediately by agarose gel electrophoresis.

2.5.3 Separation of DNA fragments by agarose gel electrophoresis

DNA fragments in solution were mixed with 0.2 volume of 6 × DNA loading dye (Table 2-7) and separated by electrophoresis in 1% agarose gels in 1 × TBE (Table 2-7) containing 0.5 µg of ethidium bromide/ml TBE. The ethidium bromide binds to the DNA

strands and fluoresces upon exposure to UV light. Gels were subjected to electrophoresis at ~10 V/cm of gel in 1xTBE. DNA fragments were subsequently visualized on an ultraviolet transilluminator (Photodyne, Model 3-3006).

2.5.4 Purification of DNA fragments from agarose gel

When a DNA fragment required purification, it was run on an agarose gel as described above and the desired band was excised. The DNA was purified from the agarose slice using the QIAquick Gel Extraction Kit according to the manufacturer's instructions (Qiagen). Similar to the method employed to purify plasmid DNA from *E. coli*, this protocol is based upon the dissolution of agarose gel and adsorption of DNA to the silica membrane in high salt concentrations, followed by washing and elution of DNA in the presence of low salt. DNA was eluted in 30 µl of the supplied elution buffer or ddH_2O.

2.5.5 Purification of DNA from solution

Contaminants (small oligonuclueotides, salts, enzymes, etc.) were removed from a DNA solution using the QIAquick PCR purification Kit according to the manufacturer's directions (Qiagen). Again, the principle of this method is the adsorption of DNA to a silica column in the presence of high salt and, after washing, elution of the DNA in low salt solution. DNA was eluted in 30 to 50 µl of the supplied elution buffer of ddH_2O.

2.5.6 Ligation of DNA fragments

DNA fragments treated with restriction endonucleases and purified as described in Section 2.5.4 were ligated using 1 µl of T4 DNA ligase in the buffer supplied by the manufacturer (NEB). Reactions were typically conducted in a volume of 5 µl, with the

molar ratio of the plasmid to insert being between 1:3 and 1:10, and incubated overnight at 16ºC.

2.5.7 Fusion of DNA fragments by PCR

Two or more domains of DNA from various original sources can be joined by PCR. This method is based upon "two-sided splicing by overlap extension" (Horton et al., 1989). Basically, primers were designed for the DNA fragments to be included in the fusion construct with homogenous tail regions (~20bp) engineered into the primers to allow for overlap between the PCR products. Phusion high-fidelity polymerase was used in these PCRs. The first round of PCR amplifies each desired fragment independently of the others, while the second round of PCR uses the first rounds PCR products as the primers. Subsequent rounds of PCR can add further DNA domains to the construct as desired.

2.5.8 DNA sequencing

DNA sequencing was performed using the BigDye Terminator v1.1/3.1 Cycle Sequencing Ready Reaction Kit as described by the manufacturer (Applied Biosystems). This method is based on the method of Sanger *et al*. (1977) and involves the random incorporation of fluorescent dideoxy terminators during the elongation of DNA sequences with a modified version of *Taq* DNA polymerase. Essentially, a reaction contained 3 µl of plasmid DNA, 3.2 pmol of primer, 3 µl of Terminator Ready Reaction Mix (TRR), and 2.5 µl of the supplied 5 × buffer in a total volume of 20 µl. The reaction was subjected to cycle sequencing using the Robocycler 40 with a Hot Top attachment and the following conditions: 1 cycle 96°C for 2 minutes; 25 cycles at 96°C for 46 seconds, 50°C for 51 seconds, and 60°C for 4 minutes; 1 cycle at 6°C to hold until ready

to purify. Reaction products were precipitated with 80 µl of 75% isopropanol for 30 min at room temperature, subjected to micro-centrifugation at 16,000 × *g* for 20 min, washed once with 250 µl 75% isopropanol, dried in a rotary vacuum desiccator and resuspended in 15 µl of Hi-Di Formamide. They were then heated at 95°C for 2 min and immediately cooled on ice. Finally, they were separated by capillary electrophoresis, and fluorescence was detected and recorded by ABI 310 Genetic Analyzer (Applied Biosystems).

2.6 Generation of plasmids

All the plasmids employed in this study are listed in Table 2-12. Those that were generated for this study were constructed by one of three methods. The first method uses restriction endonuclease digest to insert cloned regions of DNA inserted into empty plasmid backbones and is described in Section 2.6.1. The second method is a variation of the first, where the inserted DNA region is a hybridization of various DNA sequences assembled through PCR. This method is described in Section 2.6.2. The last method used homologous recombination instead of restriction endonuclease methods to insert the DNA into the plasmid and is described in Section 2.6.3. All plasmids were verified through sequencing (Section 2.5.8).

2.6.1 Restriction endonuclease based plasmid assembly

When assembling plasmids using only restriction endonucleases, I first amplified the desired DNA region for insertion using specific primers each with an endonuclease recognition site added to the primer tail (Table 2-13). The endonuclease recognition sites were selected based upon 3 criteria: first, that they were unique and not present in the main body of the cloned DNA; second, that they allow the cloned DNA to be inserted in-frame and in the correct orientation into similarly digested plasmid backbones relative to

important plasmid features (*e.g.* promoters or tags); and lastly, that they perform effectively in double digests. Once the DNA region was amplified, it was digested with the appropriate restriction endonucleases, as was the empty plasmid backbone as described in Section 2.5.2. The digestion products were then purified by electrophoresis in an agarose gel and ligated (Sections 2.5.3, 2.5.4, and 2.5.6). The ligation was then transformed into *E. coli* to select for successful ligation (Section 2.3.1).

Of the plasmids listed in Table 2-12, all the plasmids assembled using only two primers were assembled by this method. Additionally, pYES2.0-Sup35-GFP, pYES2.0-Sup35NM-GFP, and YIplac211-Sup35prom-Sup35MC were assembled by this method with the only variation being that multiple separate PCR fragments were ligated into the plasmid backbone at the same time.

2.6.2 PCR based plasmid assembly

When plasmids involved the assembly of more than one different DNA region were assembled, a PCR based method was employed. In brief, primers were designed to fuse the different DNA fragments as described in Section 2.5.7 and listed in Table 2-13. Once all fragments were successfully assembled, the final product was digested and ligated into empty plasmid backbone as described in Section 2.6.1.

Of the plasmids listed in Table 2-12, all the plasmids with more than two primers used in their generation were assembled by this method with the exception of the plasmids mentioned in Section 2.6.1.

2.6.3 Homologous recombination based plasmid assembly

Plasmids with pGREG-derived backbones were assembled by the Drag & Drop method (Jansen et al., 2005). DNA sequence homologous to sequence found in the

plasmid was added onto the DNA to be inserted by PCR. The forward primer had GAATTCGATATCAAGCTT ATCGATACCGTCGACA added to its 5′ end and the reverse primer had GCGTGACATAACTAATTACATGACTCGAGGTCGA added to its 5′ end. The resulting PCR product was co-transformed with *Sal*1 digested pGREG vector into a *S. cerevisiae* strain where the endogenous DNA repair mechanisms facilitated homologous recombination between the insert and the pGREG vector. Successful transformants were selected by auxotrophic marker, after which plasmids were purified as described in Section 2.4.3.

Table 2-12. Plasmids

Plasmid [a]	Description	Primers	Markers	Source
pJC45	***E. coli* T7 RNA polymerase dependent expression vector with 10xHIS tag derived from pJC40**	**NA**	**Amp^r**	(Clos and Brandau, 1994)
pJC45-Sup35	Used for Sup35p expression and purification	2372 2372	Amp^r	This study
pJC45-Riq1	Used for Riq1p expression and purification	2145 2146	Amp^r	This study
pJC45-RiqNQ	Used for RiqNQp expression and purification	2145 2226	Amp^r	This study
pJC45-RiqQ	Used for RiqQp expression and purification	2228 2226	Amp^r	This study
pJC45-RiqC	Used for RiqCp expression and purification	2934 2146	Amp^r	This study
pYES2.0	**Galactose inducible yeast expression vector**	**NA**	**Amp^r, *URA3***	**Invitrogen**
pYES2.0-GFP	Used to observe localization of overexpressed GFP *in vivo*	0850 0851	Amp^r, *URA3*	This study
pYES2.0-New1-GFP	Used to observe localization of overexpressed GFP-tagged *NEW1 in vivo*	0994 0851	Amp^r, *URA3*	This study
pYES2.0-*RIQ1*-GFP	Used to observe localization of overexpressed GFP-tagged *YLR177w in vivo*	1073 0851	Amp^r, *URA3*	This study

pYES2.0-*RIQNQ*-GFP	Used to observe localization of overexpressed GFP-tagged *YLR177w in vivo*	1073 3968 3967 0851	Amp^r, *URA3*	This study
pYES2.0-*RIQQ*-GFP	Used to observe localization of overexpressed GFP-tagged *YLR177w in vivo*	3571 3968 3967 0851	Amp^r, *URA3*	This study
pYES2.0-*RIQC*-GFP	Used to observe localization of overexpressed GFP-tagged *YLR177w in vivo*	3572 0851	Amp^r, *URA3*	This study
pYES2.0-Rnq1-GFP	Used to observe localization of overexpressed GFP-tagged *RNQ1 in vivo*	0993 0851	Amp^r, *URA3*	This study
pYES2.0-Sup35-GFP	Used to observe localization of overexpressed GFP-tagged *SUP35 in vivo*	0850 0851 0852 0853	Amp^r, *URA3*	This study
pYES2.0-Sup35NM-GFP	Used to observe localization of overexpressed GFP-tagged *SUP35* PrD *in vivo*	0850 0851 0852 0854	Amp^r, *URA3*	This study
pYES2.0-Ure2-GFP	Used to observe localization of overexpressed GFP-tagged *URE2 in vivo*	0994 0851	Amp^r, *URA3*	This study
pYES2.0-Ybr016w-GFP	Used to observe localization of overexpressed GFP-tagged *YBR016w in vivo*	0971 0851	Amp^r, *URA3*	This study
pYES2.0-Ybr059c-GFP	Used to observe localization of overexpressed GFP-tagged *YBR059c in vivo*	1234 1043	Amp^r, *URA3*	This study
pYES2.0-Ybr112c-GFP	Used to observe localization of overexpressed GFP-tagged *YBR112c in vivo*	1251 0851	Amp^r, *URA3*	This study
pYES2.0-Ybr150c-GFP	Used to observe localization of overexpressed GFP-tagged *YBR150c in vivo*	1229 1043	Amp^r, *URA3*	This study
pYES2.0-Ycr093w-GFP	Used to observe localization of overexpressed GFP-tagged *YCR093c in vivo*	1046 1045	Amp^r, *URA3*	This study
pYES2.0-Ydl005c-GFP	Used to observe localization of overexpressed GFP-tagged *YDL005c in vivo*	1216 0851	Amp^r, *URA3*	This study
pYES2.0-Ydl012c-GFP	Used to observe localization of overexpressed GFP-tagged *YDL012c in vivo*	1243 1043	Amp^r, *URA3*	This study
pYES2.0-Ydl017w-GFP	Used to observe localization of overexpressed GFP-tagged *YDL017w in vivo*	1079 0851	Amp^r, *URA3*	This study
pYES2.0-Ydl161w-GFP	Used to observe localization of overexpressed GFP-tagged *YDL161w in vivo*	1220 0851	Amp^r, *URA3*	This study

pYES2.0-Ydr081c-GFP	Used to observe localization of overexpressed GFP-tagged *YDR081c in vivo*	1250 1043	Amp^r, *URA3*	This study
pYES2.0-Ydr145w-GFP	Used to observe localization of overexpressed GFP-tagged *YDR145w in vivo*	1050 1045	Amp^r, *URA3*	This study
pYES2.0-Ydr228c-GFP	Used to observe localization of overexpressed GFP-tagged *YDR228c in vivo*	1075 0851	Amp^r, *URA3*	This study
pYES2.0-Ydr378c-GFP	Used to observe localization of overexpressed GFP-tagged *YDR378c in vivo*	1608 1045	Amp^r, *URA3*	This study
pYES2.0-Ydr505c-GFP	Used to observe localization of overexpressed GFP-tagged *YDR505c in vivo*	1620 0851	Amp^r, *URA3*	This study
pYES2.0-Ydr515w-GFP	Used to observe localization of overexpressed GFP-tagged *YDR515w in vivo*	1223 0851	Amp^r, *URA3*	This study
pYES2.0-Yer049w-GFP	Used to observe localization of overexpressed GFP-tagged *YER049w in vivo*	1074 1045	Amp^r, *URA3*	This study
pYES2.0-Yer111c-GFP	Used to observe localization of overexpressed GFP-tagged *YER111c in vivo*	1230 1043	Amp^r, *URA3*	This study
pYES2.0-Yer112c-GFP	Used to observe localization of overexpressed GFP-tagged *YER112c in vivo*	1242 0851	Amp^r, *URA3*	This study
pYES2.0-Ygl013c-GFP	Used to observe localization of overexpressed GFP-tagged *YGL013c in vivo*	1239 0851	Amp^r, *URA3*	This study
pYES2.0-Ygr214w-GFP	Used to observe localization of overexpressed GFP-tagged *YGR214c in vivo*	1222 0851	Amp^r, *URA3*	This study
pYES2.0-Ygr233c-GFP	Used to observe localization of overexpressed GFP-tagged *YGR233c in vivo*	1146 1043	Amp^r, *URA3*	This study
pYES2.0-Yhr082c-GFP	Used to observe localization of overexpressed GFP-tagged *YHR082c in vivo*	1244 1045	Amp^r, *URA3*	This study
pYES2.0-Yhr129c-GFP	Used to observe localization of overexpressed GFP-tagged *YHR129c in vivo*	1236 0851	Amp^r, *URA3*	This study
pYES2.0-Yhr161c-GFP	Used to observe localization of overexpressed GFP-tagged *YHR161c in vivo*	1078 1045	Amp^r, *URA3*	This study
pYES2.0-Yil056w-GFP	Used to observe localization of overexpressed GFP-tagged *YIL056w in vivo*	1076 0851	Amp^r, *URA3*	This study
pYES2.0-Yil119c-GFP	Used to observe localization of overexpressed GFP-tagged *YIL119c in vivo*	1219 0851	Amp^r, *URA3*	This study
pYES2.0-Yjl127c-GFP	Used to observe localization of overexpressed GFP-tagged *YJL127c in vivo*	1077 1043	Amp^r, *URA3*	This study
pYES2.0-Yjr091c-GFP	Used to observe localization of overexpressed GFP-tagged *YJR091c in vivo*	1223 0851	Amp^r, *URA3*	This study

pYES2.0-Ykl032c-GFP	Used to observe localization of overexpressed GFP-tagged *YKL032c in vivo*	1136 0851	Amp^r, *URA3*	This study
pYES2.0-Ykl054c-GFP	Used to observe localization of overexpressed GFP-tagged *YKL054c in vivo*	1150 0851	Amp^r, *URA3*	This study
pYES2.0-Ykl074c-GFP	Used to observe localization of overexpressed GFP-tagged *YKL074c in vivo*	1051 0851	Amp^r, *URA3*	This study
pYES2.0-Ykr096w-GFP	Used to observe localization of overexpressed GFP-tagged *YKR096w in vivo*	1147 1043	Amp^r, *URA3*	This study
pYES2.0-Ylr206w-GFP	Used to observe localization of overexpressed GFP-tagged *YLR206w in vivo*	1135 0851	Amp^r, *URA3*	This study
pYES2.0-Ylr278c-GFP	Used to observe localization of overexpressed GFP-tagged *YLR278c in vivo*	1145 1043	Amp^r, *URA3*	This study
pYES2.0-Ylr373c-GFP	Used to observe localization of overexpressed GFP-tagged *YLR373c in vivo*	1842 1045	Amp^r, *URA3*	This study
pYES2.0-Ylr430w-GFP	Used to observe localization of overexpressed GFP-tagged *YLR430w in vivo*	1044 1045	Amp^r, *URA3*	This study
pYES2.0-Yml017w-GFP	Used to observe localization of overexpressed GFP-tagged *YML017w in vivo*	1138 0851	Amp^r, *URA3*	This study
pYES2.0-Ymr043w-GFP	Used to observe localization of overexpressed GFP-tagged *YMR043w in vivo*	1238 0851	Amp^r, *URA3*	This study
pYES2.0-Ymr070w-GFP	Used to observe localization of overexpressed GFP-tagged *YMR070w in vivo*	1140 0851	Amp^r, *URA3*	This study
pYES2.0-Ymr173w-GFP	Used to observe localization of overexpressed GFP-tagged *YMR173w in vivo*	1221 0851	Amp^r, *URA3*	This study
pYES2.0-YNL016w-GFP	Used to observe localization of overexpressed GFP-tagged *YNL016w in vivo*	1217 0851	Amp^r, *URA3*	This study
pYES2.0-Ynr052c-GFP	Used to observe localization of overexpressed GFP-tagged *YNR052c in vivo*	1218 0851	Amp^r, *URA3*	This study
pYES2.0-Yol004w-GFP	Used to observe localization of overexpressed GFP-tagged *YOL004w in vivo*	1047 1043	Amp^r, *URA3*	This study
pYES2.0-Yol148c-GFP	Used to observe localization of overexpressed GFP-tagged *YOL148c in vivo*	1134 0851	Amp^r, *URA3*	This study
pYES2.0-Yor290c-GFP	Used to observe localization of overexpressed GFP-tagged *YOR290c in vivo*	1048 1045	Amp^r, *URA3*	This study
pYES2.0-Ypl016w-GFP	Used to observe localization of overexpressed GFP-tagged *YPL016w in vivo*	1148 0851	Amp^r, *URA3*	This study
pYES2.0-Ypl026c-GFP	Used to observe localization of overexpressed GFP-tagged *YPL026c in vivo*	1080 0851	Amp^r, *URA3*	This study

pYES2.0-Ypl119c-GFP	Used to observe localization of overexpressed GFP-tagged *YPL119c in vivo*	1137 0851	Amp^r, *URA3*	This study
pYES2.0-Ypr022c-GFP	Used to observe localization of overexpressed GFP-tagged *YPR022c in vivo*	1228 0851	Amp^r, *URA3*	This study
pYES2.0-Ypr185w-GFP	Used to observe localization of overexpressed GFP-tagged *YPR185w in vivo*	1151 0851	Amp^r, *URA3*	This study
pGREG505	**Galactose inducible vectors used in drag & drop recombinant cloning**	**NA**	**Amp^r, kanMX, *LEU2***	(Jansen et al., 2005)
pGREG505-Sup35NM-GFP	Used to observe localization of overexpressed GFP-tagged gene *in vivo*	2729 2728	Amp^r, kanMX, *LEU2*	This study
pGREG505-Rnq1-GFP	Used to observe localization of overexpressed GFP-tagged gene *in vivo*	3988 2728	Amp^r, kanMX, *LEU2*	This study
pGREG535	**Galactose inducible vectors used in drag & drop recombinant cloning with N-terminal 7xHA tag**	**NA**	**Amp^r, kanMX, *LEU2***	(Jansen et al., 2005)
pGREG535-Rnq1	Used for SDD-AGE	3988 3989	Amp^r, kanMX, *LEU2*	This study
pGREG535-Riq1	Used for SDD-AGE	4044 4045	Amp^r, kanMX, *LEU2*	This study
pGREG535-RiqNQ	Used for SDD-AGE	4044 4245	Amp^r, kanMX, *LEU2*	This study
pGREG535-RiqQ	Used for SDD-AGE	4246 4245	Amp^r, kanMX, *LEU2*	This study
pGREG535-RiqC	Used for SDD-AGE	4247 4045	Amp^r, kanMX, *LEU2*	This study
YIplac211	***E. coli* shuttle vector used for replacement of *S. cerevisiae* genes**	**NA**	**Amp^r, *URA3***	(Gietz and Sugino, 1988)
YIplac211-Sup35prom-Sup35MC	Used to remove *SUP35* PrD	1170 1172 1174 1176	Amp^r, *URA3*	This study

YIplac211-Sup35prom-Riq1-Sup35MC	Used to replace *SUP35* PrD with *RIQ1*	1270 1276 1277 1278 1279 1275	Amp^r, *URA3*	This study
YIplac211-Sup35prom-RiqNQ-Sup35MC	Used to replace *SUP35* PrD with *RIQNQ*	1270 1276 1277 2055 2056 1275	Amp^r, *URA3*	This study
YIplac211-Sup35prom-RiqQ-Sup35MC	Used to replace *SUP35* PrD with *RIQQ*	1270 2059 2060 2055 2056 1275	Amp^r, *URA3*	This study
YIplac211-Sup35prom-RiqC-Sup35MC	Used to replace *SUP35* PrD with *RIQC*	1270 2057 2058 1278 1279 1275	Amp^r, *URA3*	This study
YIplac211-Sup35prom-Def1-Sup35MC	Used to replace *SUP35* PrD with *DEF1*	1270 1286 1287 1288 1289 1275	Amp^r, *URA3*	This study
YIplac211-Sup35prom-Ent2-Sup35MC	Used to replace *SUP35* PrD with *ENT2*	1280 1281 1282 1283 1284 1285	Amp^r, *URA3*	This study
YIplac211-Sup35prom-Taf12-Sup35MC	Used to replace *SUP35* PrD with *TAF12*	1270 1271 1272 1273 1274 1275	Amp^r, *URA3*	This study
pGAD424	**Yeast two-hybrid strain for generating GAL4 activation domain hybrids**	**NA**	**Amp^r, *LEU2***	**Clontech**
pGAD424-Aha1	Used in yeast two-hybrid	3647 3620	Amp^r, *LEU2*	This study

pGAD424-Cpr6	Used in yeast two-hybrid	3649 3624	Amp^r, *LEU2*	This study
pGAD424-Cpr7	Used in yeast two-hybrid	3650 3626	Amp^r, *LEU2*	This study
pGAD424-Hch1	Used in yeast two-hybrid	3648 3622	Amp^r, *LEU2*	This study
pGAD424-Hsc82	Used in yeast two-hybrid	3646 3618	Amp^r, *LEU2*	This study
pGAD424-Hsp104	Used in yeast two-hybrid	3156 3157	Amp^r, *LEU2*	This study
pGAD424-Hsp82	Used in yeast two-hybrid	3645 3615	Amp^r, *LEU2*	This study
pGAD424-Rnq1	Used in yeast two-hybrid	3150 3151	Amp^r, *LEU2*	This study
pGAD424-Sba1	Used in yeast two-hybrid	3144 3145	Amp^r, *LEU2*	This study
pGAD424-Ssa2	Used in yeast two-hybrid	3655 3636	Amp^r, *LEU2*	This study
pGAD424-Ssa3	Used in yeast two-hybrid	3656 3638	Amp^r, *LEU2*	This study
pGAD424-Sse1	Used in yeast two-hybrid	3651 3628	Amp^r, *LEU2*	This study
pGAD424-Sse2	Used in yeast two-hybrid	3652 3630	Amp^r, *LEU2*	This study
pGAD424-Sti1	Used in yeast two-hybrid	3653 3632	Amp^r, *LEU2*	This study
pGAD424-Sup35	Used in yeast two-hybrid	3159 3160	Amp^r, *LEU2*	This study
pGAD424-Tah1	Used in yeast two-hybrid	3654 3634	Amp^r, *LEU2*	This study
pGAD424-Ydj1	Used in yeast two-hybrid	3657 3642	Amp^r, *LEU2*	This study
pGAD424-Riq1	Used in yeast two-hybrid	3162 3163	Amp^r, *LEU2*	This study
pGBT9	**Yeast two-hybrid strain for generating GAL4 DNA-binding domain hybrids**	**NA**	**Amp^r, *TRP1***	**Clontech**
pGBT9-Aha1	Used in yeast two-hybrid	3647 3620	Amp^r *TRP1*	This study

pGBT9-Cpr6	Used in yeast two-hybrid	3649 3624	Amp^r, *TRP1*	This study
pGBT9-Cpr7	Used in yeast two-hybrid	3650 3626	Amp^r, *TRP1*	This study
pGBT9-Hch1	Used in yeast two-hybrid	3648 3622	Amp^r, *TRP1*	This study
pGBT9-Hsc82	Used in yeast two-hybrid	3646 3618	Amp^r, *TRP1*	This study
pGBT9-Hsp104	Used in yeast two-hybrid	3156 3157	Amp^r, *TRP1*	This study
pGBT9-Hsp82	Used in yeast two-hybrid	3645 3615	Amp^r, *TRP1*	This study
pGBT9-Rnq1	Used in yeast two-hybrid	3150 3151	Amp^r, *TRP1*	This study
pGBT9-Sba1	Used in yeast two-hybrid	3144 3145	Amp^r, *TRP1*	This study
pGBT9-Ssa2	Used in yeast two-hybrid	3655 3636	Amp^r, *TRP1*	This study
pGBT9-Ssa3	Used in yeast two-hybrid	3656 3638	Amp^r, *TRP1*	This study
pGBT9-Sse1	Used in yeast two-hybrid	3651 3628	Amp^r, *TRP1*	This study
pGBT9-Sse2	Used in yeast two-hybrid	3652 3630	Amp^r, *TRP1*	This study
pGBT9-Sti1	Used in yeast two-hybrid	3653 3632	Amp^r, *TRP1*	This study
pGBT9-Sup35	Used in yeast two-hybrid	3159 3160	Amp^r, *TRP1*	This study
pGBT9-Tah1	Used in yeast two-hybrid	3654 3634	Amp^r, *TRP1*	This study
pGBT9-Ydj1	Used in yeast two-hybrid	3657 3642	Amp^r, *TRP1*	This study
pGBT9-Riq1	Used in yeast two-hybrid	3162 3163	Amp^r, *TRP1*	This study
pLAM5	Yeast two-hybrid control vector	NA	Amp^r, *TRP1*	Clontech
pTD1	Yeast two-hybrid negative control vector (with pLAM5)	NA	Amp^r, *LEU2*	Clontech

pVA3	Yeast two-hybrid positive control vector (with pLAM5)	NA	Amp^r, *LEU2*	Clontech
YCpGAL::HO	Galactose inducible vector for switching haploid yeast mating type	NA	Amp^r, *URA3*	(Rine et al., 1981)

[a] Vectors used as backbones in plasmid construction are in **BOLD**.

Table 2-13. Oligonucleotides employed in the generation of plasmids

Name	Sequence [a,b,c]	Application
AA0655-T7-26	GTAATACGACTCACTATAGGGCGAAT	Sequencing pJC45 and pYES2.0 based vector constructs
2372-DL-Sup35-Nde1-f	TAACATATGATGTCGGATTCAAACCAAGG	Generation of pJC45-SUP35
2373-DL-Sup35-BamHI-r	TAAGGATCCTTACTCGGCAATTTTAACAA	Generation of pJC45-SUP35
2145-DL-YLR177w-NdeI-f	TAACATATGATGGAGCTGCCTTCAATAAATAGC	Generation of pJC45-Riq1 and pJC45-RiqNQ
2146-DL-YLR177w-BamHI-r	TAAGGATCCTTAGCCGAACAAAACCTTCA	Generation of pJC45-Riq1 and pJC45-RiqC
2226-DL-YLR177(1-690)-BamHI-r	TAAGGATCCTTAATTGAAGGGTGACGAGT	Generation of pJC45-RiqNQ and pJC45-RiqQ
2228-DL-YLR177(301-690)-NdeI-f	TAACATATGATGAACGGGAAGAGCCCTAATTTGTCT	Generation of pJC45-RiqQ
2934-DL-Ylr177-691-Nde1-f	TAACATATGATGGCTAGGCGCAACACCCAG	Generation of pJC45-RiqC
0850-MD-GFP-NotI-f	ATTGCGGCCGCGATGGCTAGCAAAGGAGAAGAAC	Generation of pYES2.0-GFP, pYES2.0-Sup35-GFP, and pYES2.0-Sup35NM-GFP
0851-MD-GFP-XbaI-r	ATTTCTAGATTATTTGTAGAGCTCATCCAT	Generation of pYES2.0-*GENE-X*-GFP vectors
1043-DL-GFP-NotI-r	ATTGCGGCCGCTTATTTGTAGAGCTCATCCATGCCATG	Generation of pYES2.0-*GENE-X*-GFP vectors
1045-DL-GFP-SphI-r	ATTGCATGCTTATTTGTAGAGCTCATCCATGCCATG	Generation of pYES2.0-*GENE-X*-GFP vectors
0852-MD-sup35-EcoRI-f	ATTGAATTCATGTCGGATTCAAACCAAGGCAAC	Generation of pYES2.0-Sup35-GFP and pYES2.0-Sup35NM-GFP

0853-MD-sup35fl-NotI-r	ATTGCGGCCGCCTCGGCAATTTTAACAATT	Generation of pYES2.0-Sup35-GFP
0854-MD-sup35NM-NotI-r	ATTGCGGCCGCCATATCGTTAACAACTTCG	Generation of pYES2.0-Sup35NM-GFP
0995-DL-new1-Kpn1-f	ATTGGTACCAATGCCTCCAAAGAAGTTTAAGGATCTAAAC	Generation of pYES2.0-New1-GFP
1073-DL-YLR177-EcoRI-f	TAAGAATTCATGGAGCTGCCTTCAATAAATAGCACC	Generation of pYES2.0-Riq1-GFP and pYES2.0-RiqNQ-GFP
3967-DL-GFP-Ylr177w690-f	AGTACTCGTCACCCTTCAATAGTAAAGGAGAAGAACTTTT	Generation of pYES2.0-RiqNQ-GFP and pYES2.0-RiqQ
3968-DL-Ylr177w690-GFP-r	AAAAGTTCTTCTCCTTTACTATTGAAGGGTGACGAGTACT	Generation of pYES2.0-RiqNQ-GFP and pYES2.0-RiqQ
3571-DL-Ylr177(301)-BamHI-f	TAAGGATCCATGAACGGGAAGAGCCCTAATTTGTCTC	Generation of pYES2.0-RiqQ-GFP
3572-DL-Ylr177(691)-BamHI-f	TAAGGATCCATGGCTAGGCGCAACACCCAGCCAGTGC	Generation of pYES2.0-RiqC-GFP
0993-DL-rnq-NotI-f	ATTGCGGCCGCATGGATACGGATAAGTTAATCTCAGAGGC	Generation of pYES2.0-Rnq1-GFP
0994-DL-ure2-KpnI-f	ATTGGTACCATGATGAATAACAACGGCAACCAAGTGTCG	Generation of pYES2.0-Ure2-GFP
0971-MD-Ybr016w-EcoR1-f	ATTGAATTCATGTCTGCTAACGATTACTACGGC	Generation of pYES2.0-Ybr016w-GFP
1234-DL-YBR059c-EcoRI-f	TAAGAATTCATGTCGATCACGAATGGTACTTCTAGA	Generation of pYES2.0-Ybr059c-GFP
1251-DL-YBR112c-NotI-f	TAAGCGGCCGCATGAATCCGGGCGGTGAACAAACAATA	Generation of pYES2.0-Ybr112c-GFP
1229-DL-YBR150c-EcoRI-f	ATTGAATTCATGAATATGGATTCTGGTATTACAAGT	Generation of pYES2.0-Ybr150c-GFP
1046-DL-YCR093w-EcoRI-f	ATTGAATTCATGCTATCGGCCACATACCGTGATTTG	Generation of pYES2.0-Ycr093w-GFP
1216-DL-YDL005c-NotI-f	ATTGCGGCCGCATGGTAGTACAAAATAGCCCAGTTTCG	Generation of pYES2.0-Ycr093w-GFP
1243-DL-YDL012c-EcoRI-f	TAAGAATTCATGTCAGCTCAAGATTATTACGGAAAC	Generation of pYES2.0-Ydl012c-GFP

1079-DL-YDL017w-EcoRI-f	TAAGAATTCATGACAAGCAAAACG AAGAATATCGATG	Generation of pYES2.0-Ydl017w-GFP
1220-DL-YDL161w-NotI-f	ATTGCGGCCGCATGTCGAAACAAT TTGTTAGATCTGCG	Generation of pYES2.0-Ydl161w-GFP
1250-DL-YDR081c-KpnI-f	TAAGGTACCATGCTTTCCATTCAGC AAAGATATAAT	Generation of pYES2.0-Ydr081c-GFP
1050-DL-YDR145w-EcoRI-f	TAAGAATTCATGTCTTCCAATCCAG AAAATTCTGGTG	Generation of pYES2.0-Ydr145w-GFP
1075-DL-YDR228c-KpnI-f	TAAGGTACCATGGATCACGACACA GAAGTTATAGTC	Generation of pYES2.0-Ydr228c-GFP
1608-DL-YDR378c-NotI-f	TAAGCGGCCGCATGTCTGGTAAGA CTAGCTTTATCCAG	Generation of pYES2.0-Ydr378c-GFP
1620-DL-YDR505c-NotI-f	TAAGCGGCCGCATGCAACTTCAAA GAAGCAGTTCTGTCCCTT	Generation of pYES2.0-Ydr505c-GFP
1223-DL-YDR515w-NotI-f	ATTGCGGCCGCATGTCATCGCAAA ACCTCAATGATAAT	Generation of pYES2.0-Ydr515w-GFP
1074-DL-YER049w-EcoRI-f	TAAGAATTCATGAAGAGAAAAACT GCTGAAGTTAAAG	Generation of pYES2.0-Yer049w-GFP
1230-DL-YER111c-KpnI-f	ATTGGTACCATGCCATTTGATGTTT TGATATCAAACC	Generation of pYES2.0-Yer111c-GFP
1242-DL-YER112w-NotI-f	TAAGCGGCCGCATGCTACCTTTATA TCTTTTAACAAAT	Generation of pYES2.0-Yer112w-GFP
1239-DL-YGL013c-NotI-f	TAAGCGGCCGCATGCGAGGCTTGA CACCTAAGAACGGT	Generation of pYES2.0-Ygl013c-GFP
1222-DL-YGR214w-NotI-f	ATTGCGGCCGCATGTCCTTACCAGC TACTTTTGACTTG	Generation of pYES2.0-Ygr214w-GFP
1146-DL-YGR233c-KpnI-f	TAAGGTACCATGAAATTCGGCAAG TATTTGGAAGCC	Generation of pYES2.0-Ygr233c-GFP
1244-DL-YHR082c-NotI-f	TAAGCGGCCGCATGACTTTAGATT ACGAGATTTACAAA	Generation of pYES2.0-Yhr082c-GFP
1236-DL-YHR129c-NotI-f	TAAGCGGCCGCATGGACCAGCTAA GTGACAGCTATGCT	Generation of pYES2.0-Yhr129c-GFP
1078-DL-YHR161c-EcoRI-f	TAAGAATTCATGACAACATATTTC AAGTTGGTAAAAG	Generation of pYES2.0-Yhr161c-GFP
1076-DL-YIL056w-NotI-f	TAAGCGGCCGCATGAACGGTCCTC CAACATTCACTCAA	Generation of pYES2.0-Yil056w-GFP

1219-DL-YIL119c-NotI-f	ATTGCGGCCGCATGTACTTGGAATATCTTCAACCGAAG	Generation of pYES2.0-Yil119c-GFP
1077-DL-YJL127c-KpnI-f	TAAGGTACCATGCTAAATCAGCACACAAGTTCAGTAC	Generation of pYES2.0-Yjl127c-GFP
1233-DL-YJR091c-NotI-f	TAAGCGGCCGCATGGATAAAAGTAAGCAGATGAACATC	Generation of pYES2.0-Yjr091c-GFP
1136-DL-YKL032c-KpnI-f	TAAGGTACCATGAACACCGGTATCTCGCCCAAACAG	Generation of pYES2.0-Ykl032c-GFP
1150-DL-YKL054c-NotI-f	TAAGCGGCCGCAATGTCTACACAATTTAGGAAGTCTAA	Generation of pYES2.0-Ykl054c-GFP
1051-DL-YKL074c-NotI-f	TAAGCGGCCGCATGGCTGATGAAAAGAGACTGGAGGAT	Generation of pYES2.0-Ykl074c-GFP
1147-DL-YKR096w-KpnI-f	TAAGGTACCAATGCCAGAAACCTCTGTTCAGAATCC	Generation of pYES2.0-Ykr096w-GFP
1135-DL-YLR206w-KpnI-f	TAAGGTACCATGTCTAAGCAGTTTGTTCGTTCTGCA	Generation of pYES2.0-Ylr206w-GFP
1145-DL-YLR278c-KpnI-f	TAAGGTACCATGGGCCGTCCAAGGAAGAATGTTAGC	Generation of pYES2.0-Ylr278c-GFP
1842-DL-YLR373c-NotI-f	TAAGCGGCCGCATGAGAGCGATGGACACACA	Generation of pYES2.0-Ylr373c-GFP
1044-DL-YLR430w-NotI-f	ATTGCGGCCGCATGAATTCCAACAATCCTGATAATAAT	Generation of pYES2.0-Ylr430w-GFP
1138-DL-YML017w-NotI-f	TAAGCGGCCGCATGGGTATGTGCCTCGGTTTTTCTCATT	Generation of pYES2.0-Ymr043w-GFP
1238-DL-YMR043w-NotI-f	TAAGCGGCCGCATGTCAGACATCGAAGAAGGTACGCCT	Generation of pYES2.0-New1-GFP
1140-DL-YMR070w-EcoRI-f	TAAGAATTCATGAATGCGGACCATCACCTGCAACAG	Generation of pYES2.0-Ymr070w-GFP
1221-DL-YMR173w-NotI-f	ATTGCGGCCGCATGGGTTTATTTGATAAAGTGAAGCAA	Generation of pYES2.0-Ymr173w-GFP
1217-DL-YNL016w-NotI-f	ATTGCGGCCGCATGTCTGAAAATAACGAAGAACAACAT	Generation of pYES2.0-Ynl016w-GFP
1218-DL-YNR052c-NotI-f	ATTGCGGCCGCATGCAATCTATGAATGTACAACCGAGG	Generation of pYES2.0-Ynr052c-GFP
1047-DL-YOL004w-KpnI-f	ATTGGTACCATGTCACAGGTTTGGCATAATTCGAAT	Generation of pYES2.0-Yol004w-GFP

1134-DL-YOL148c-NotI-f	TAAGCGGCCGCATGAGTGCCAATAGCCCGACAGGAAAC	Generation of pYES2.0-Yol148c-GFP
1048-DL-YOR290c-Not1-f	ATTGCGGCCGCATGAACATACCACAGCGTCAATTTAGC	Generation of pYES2.0-Yor290c-GFP
1148-DL-YPL016w-NotI-f	TAAGCGGCCGCAATGGATTTCTTTAATTTGAATAATAA	Generation of pYES2.0-Ypl016w-GFP
1080-DL-YPL026c-EcoRI-f	TAAGAATTCATGCTGTCAGACTGCTTGCTGAACAAT	Generation of pYES2.0-Ypl026c-GFP
1137-DL-YPL119c-NotI-f	TAAGCGGCCGCATGGCAGACTTGCCACAGAAGGTATCTA	Generation of pYES2.0-Ypl119c-GFP
1228-DL-YPR022c-NotI-f	ATTGCGGCCGCATGCACGGCAAAGAGTTGGCTGGCAGG	Generation of pYES2.0-Ypr022c-GFP
1151-DL-YPR185w-NotI-f	TAAGCGGCCGCAATGGTTGCCGAAGAGGACATCGAGAA	Generation of pYES2.0-Ypr185w-GFP
3990-One4all-B-r	GCGTCCCAAAACCTTCTCAAGCAAG	Sequencing pGREG series constructs
2729-DL-Sup35-rec1-f	**GAATTCGATATCAAGCTTATCGATACCGTCGACA**ATGTCGGATTCAAACCAAGG	Generation of pGREG505-Sup35NM-GFP
2728-DL-GFP-rec2-r	**GCGTGACATAACTAATTACATGACTCGAGGTCGAC**TTTGTATAGTTCATCCATGC	Generation of pGREG505-Sup35NM-GFP and pGREG505-Rnq1-GFP
3988-Rnq1-rec1-f	**GAATTCGATATCAAGCTTATCGATACCGTCGACA**GATACGGATAAGTTAATCTC	Generation of pGREG505-Rnq1-GFP and pGREG535-Rnq1
3989-Rnq1-rec2-r	**GCGTGACATAACTAATTACATGACTCGAGGTCGAC**TCAGTAGCGGTTCTGGTTGC	Generation of pGREG535-Rnq1
4044-DL-Ylr177w-rec1-f	**GAATTCGATATCAAGCTTATCGATACCGTCGACA**ATGGAGCTGCCTTCAATAAA	Generation of pGREG535-Riq1 and pGREG535-RiqNQ
4045-DL-Ylr177w-rec2-r	**GCGTGACATAACTAATTACATGACTCGAGGTCGAC**TTAGCCGAACAAAACCTTCA	Generation of pGREG535-Riq1 and pGREG535-RiqC
4245-Ylr177w-690-rec2-r	**GCGTGACATAACTAATTACATGACTCGAGGTCGAC**TCAATTGAAGGGTGACGAGTACTGTT	Generation of pGREG535-Riq1NQ and pGREG535-RiqQ
4246--Ylr177w-301-rec1-f	**GAATTCGATATCAAGCTTATCGATACCGTCGACA**AACGGGAAGAGCCCTAATTT	Generation of pGREG535-RiqQ

4247--Ylr177w-691-rec1-f	**GAATTCGATATCAAGCTTATCGATACCGTCGACA**GCTAGGCGCAACACCCAG	Generation of pGREG535-RiqC
OUT73-M13Rev	CAGGAAACAGCTATGAC	Sequencing of Yipllac211 vector constructs
OUT74-M13Fwd	GTAAAACGACGGCCAGT	Sequencing of Yipllac211 vector constructs
1640-DL-Sup35prom-seq-f	TTGGTACATCTTCTCTTGAAAGACTCC	Sequencing of Yipllac211 vector constructs
1641-DL-Sup35MC-seq-r	CAACTTGATACCGGAACTGGAGACAAG	Sequencing of Yipllac211 vector constructs
2022-DL-Sup35MC-seq2	ACTGGTAACATTGGCATTGTTGG	Sequencing of Yipllac211 vector constructs
2023-DL-YLR177w-seq1	CACTAATGGCTTATAGAGCAAATG	Sequencing of Yipllac211 vector constructs
2024-DL-YLR177w-seq2	GACTTATATCTTGACTGCGGG	Sequencing of Yipllac211 vector constructs
2025-DL-YDR145w-seq1	GTGTGCAAGACACAATCCGG	Sequencing of Yipllac211 vector constructs
2026-DL-YDR145w-seq2	TTCCGATATGGGTATGGCAGG	Sequencing of Yipllac211 vector constructs
2027-DL-YKL054c-seq1	GGCGCAGTGACAAGATGGG	Sequencing of Yipllac211 vector constructs
2028-DL-YKL054c-seq2	GAGAGTCTTCAATGCTGGG	Sequencing of Yipllac211 vector constructs
2029-DL-YKL054c-seq3	CAACCAAAGAAAATGTCGTGGG	Sequencing of Yipllac211 vector constructs
2030-DL-YKL054c-seq4	TGGATGCTGTTGCTGTTGCTGAG	Sequencing of Yipllac211 vector constructs
1170-DL-Sup35prom-NotI-f	ATTGCGGCCGCTCAACCACACAAAAATCATACAACGAA	Construction of Yiplac211-Sup35prom-Sup35MC
1172-DL-Sup35prom-EcoRI-r	ATTGAATTCGTTGCTAGTGGGCAGATATAGATGTTA	Construction of Yiplac211-Sup35prom-Sup35MC
1174-DL-Sup35MC-EcoRI-f	ATTGAATTCATGTCTTTGAACGACTTTCAAAAGCAAC	Construction of Yiplac211-Sup35prom-Sup35MC
1176-DL-Sup35MC-NotI-r	ATTGCGGCCGCTTACTCGGCAATTTTAACAATTTTACC	Construction of Yiplac211-Sup35prom-Sup35MC

1270-DL-Sup35prom-EcoRI-f	TAAGAATTCCAACCACACAAAAATCATACAACGAAT	Construction of various Yiplac211-Sup35prom-*GENE X*-Sup35MC
1275-DL-Sup35MC-EcoRI-r	TAAGAATTCTTACTCGGCAATTTTAACAATTTTACC	Construction of various Yiplac211-Sup35prom-*GENE X*-Sup35MC
1276-DL-Sup35prom-177-r	TGAAGGCAGCTCCATTGTTGCTAGTGGGCAGATATAGATGTT	Construction of Yiplac211-Riq1/RiqNQ-Sup35prom-Sup35MC
1277-DL-YLR177w-Sup35-f	TGCCCACTAGCAACAATGGAGCTGCCTTCAATAAATAGCACC	Construction of Yiplac211-Riq1/RiqNQ-Sup35prom-Sup35MC
1278-DL-YLR177w-Sup35-r	GTCGTTCAAAGACATGCCGAACAAAACCTTCACCAATTCCAT	Construction of Yiplac211-Riq1/RiqC-Sup35prom-Sup35MC
1279-DL-Sup35MC-177-f	AAGGTTTTGTTCGGCATGTCTTTGAACGACTTTCAAAA	Construction of Yiplac211-Riq1/RiqC-Sup35prom-Sup35MC
2055-DL-YLR177w 690-MC-r	GTCGTTCAAAGACATATTGAAGGGTGACGAGTACT	Construction of Yiplac211-RiqNQ/RiqQ-Sup35prom-Sup35MC
2056-DL-Sup35MC-690-f	TCGTCACCCTTCAATATGTCTTTGAACGACTTTCAAAA	Construction of Yiplac211-RiqNQ/RiqQ-Sup35prom-Sup35MC
2059-DL-SP-177 301-690-r	GCTCTTCCCCGTTCATTGTTGCTAGTGGGCAGATAT	Construction of Yiplac211-RiqQ-Sup35prom-Sup35MC
2060-DL-YLR177w301-690-SP-f	TGCCCACTAGCAACAATGAACGGGAAGAGCCCTAATTTGTCT	Construction of Yiplac211-RiqQ-Sup35prom-Sup35MC
2057-DL-Sup35P-177C-r	GTTGCGCCTAGCCATTGTTGCTAGTGGGCAGATAT	Construction of Yiplac211-RiqC-Sup35prom-Sup35MC
2058-DL-YLR177wC-SP-f	TGCCCACTAGCGCAACAATGGCTAGGCGCAACACCCA	Construction of Yiplac211-RiqC-Sup35prom-Sup35MC
1286-DL-Sup35prom-054-r	AAATTGTGTAGACATTGTTGCTAGTGGGCAGATATAGATGTT	Construction of Yiplac211-Def1-Sup35prom-Sup35MC

1287-DL-YKL054c-Sup35-f	TGCCCACTAGCAACAATGTCTACACAA TTTAGGAAGTCTAAT	Construction of Yiplac211-Def1-Sup35prom-Sup35MC
1288-DL-YKL054c-Sup35-r	GTCGTTCAAAGACATGTAGAAACCTCT TGAATTTTTAGAATT	Construction of Yiplac211-Def1-Sup35prom-Sup35MC
1289-DL-Sup35MC-054-f	TCAAGAGGTTTCTACATGTCTTTGAACG ACTTTCAAAA	Construction of Yiplac211-Def1-Sup35prom-Sup35MC
1280-DL-Sup35prom-SacI-f	TAAGAGCTCCAACCACACAAAAAT CATACAACGAAT	Construction of Yiplac211-Ent2-Sup35prom-Sup35MC
1281-DL-Sup35prom-206-r	AAACTGCTTAGACATTGTTGCTAGTGG GCAGATATAGATGTT	Construction of Yiplac211-Ent2-Sup35prom-Sup35MC
1282-DL-YLR206w-Sup35-f	TGCCCACTAGCAACAATGTCTAAGCAG TTTGTTCGTTCTGCA	Construction of Yiplac211-Ent2-Sup35prom-Sup35MC
1283-DL-YLR206w-Sup35-r	GTCGTTCAAAGACATAAGATCAATTAA GCTTACACCTTGGTC	Construction of Yiplac211-Ent2-Sup35prom-Sup35MC
1284-DL-Sup35MC-206-f	AGCTTAATTGATCTTATGTCTTTGAACG ACTTTCAAAA	Construction of Yiplac211-Ent2-Sup35prom-Sup35MC
1285-DL-Sup35MC-SacI-r	TAAGAGCTCTTACTCGGCAATTTTA ACAATTTTACC	Construction of Yiplac211-Ent2-Sup35prom-Sup35MC
1271-DL-Sup35prom-145-r	TGGATTGGAAGACATTGTTGCTAGTGG GCAGATATAGATGTT	Construction of Yiplac211-Taf12-Sup35prom-Sup35MC
1272-DL-YDR145w-Sup35-f	TGCCCACTAGCAACAATGTCTTCCAATC CAGAAAATTCTGGT	Construction of Yiplac211-Taf12-Sup35prom-Sup35MC
1273-DL-YDR145w-Sup35-r	GTCGTTCAAAGACATTTTTTTTGTATTC AAGCTTGCAACATT	Construction of Yiplac211-Taf12-Sup35prom-Sup35MC
1274-DL-Sup35MC-145-f	TTGAATACAAAAAAAAATGTCTTTGAAC GACTTTCAAAA	Construction of Yiplac211-Taf12-Sup35prom-Sup35MC
0059-GAL4AD	TACCACTACAATGGATG	Sequencing pGAD424 vector constructs

0060-GAL4DNA-BD	TCATCGGAAGAGAGTAG	Sequencing pGBT9 vector constructs
3647-DL-Aha1-BamHI-f	TAAGGATCCGTATGGTCGTGAATAACCCAAA	Generation of Yeast Two-hybrid vector constructs
3620-DL-Aha1-SalI-r	TAAGTCGACTTATAATACGGCACCAAAGC	Generation of Yeast Two-hybrid vector constructs
3649-DL-Cpr6-BamHI-f	TAAGGATCCGTATGACTAGACCTAAAACTTTT	Generation of Yeast Two-hybrid vector constructs
3624-DL-Cpr6-SalI-r	TAAGTCGACTCAGGAGAACATCTTCGAAA	Generation of Yeast Two-hybrid vector constructs
3650-DL-Cpr7-BamHI-f	TAAGGATCCGTATGATTCAAGATCCCCTTGTA	Generation of Yeast Two-hybrid vector constructs
3626-DL-Cpr7-SalI-r	TAAGTCGACTTAGGAGAAAAACTTTGATA	Generation of Yeast Two-hybrid vector constructs
3648-DL-Hch1-BamHI-f	TAAGGATCCGTATGGTTGTCTTGAATCCAAA	Generation of Yeast Two-hybrid vector constructs
3622-DL-Hch1-SalI-r	TAAGTCGACTCAAACTTGTATATCCTTTG	Generation of Yeast Two-hybrid vector constructs
3646-DL-Hsc82-BamHI-f	TAAGGATCCGTATGGCTGGTGAAACTTTTGA	Generation of Yeast Two-hybrid vector constructs
3618-DL-Hsc82-SalI-r	TAAGTCGACTTAATCAACTTCTTCCATCT	Generation of Yeast Two-hybrid vector constructs
3156-DL-Hsp104 SmaI-f	TAACCCGGGGATGAACGACCAAACGCAATT	Generation of Yeast Two-hybrid vector constructs
3157-DL-Hsp104 SalI-r	TAAGTCGACTTAATCTAGGTCATCATCAATTTCC	Generation of Yeast Two-hybrid vector constructs
3645-DL-Hsp82-BamHI-f	TAAGGATCCGTATGGCTAGTGAAACTTTTGA	Generation of Yeast Two-hybrid vector constructs
3615-DL-Hsp82-SalI-r	TAAGTCGACCTAATCTACCTCTTCCATTT	Generation of Yeast Two-hybrid vector constructs
3150-DL-Rnq1 SmaI-f	TAACCCGGGGATGGATACGGATAAGTTAAT	Generation of Yeast Two-hybrid vector constructs
3151-DL-Rnq1 SalI-r	TAAGTCGACTCAGTAGCGGTTCTGGTTGC	Generation of Yeast Two-hybrid vector constructs
3144-DL-Sba1 EcoRI-f	TAAGAATTCATGTCCGATAAAGTTATTAA	Generation of Yeast Two-hybrid vector constructs

3145-DL-Sba1 BamHI-r	TAAGGATCCTTAAGCTTTCACTTCCGGCT	Generation of Yeast Two-hybrid vector constructs
3655-DL-Ssa2-BamHI-f	TAAGGATCCGTATGTCTAAAGCTGTCGGTAT	Generation of Yeast Two-hybrid vector constructs
3636-DL-Ssa2-PstI-r	TAACTGCAGTTAATCAACTTCTTCGACAG	Generation of Yeast Two-hybrid vector constructs
3656-DL-Ssa3-SmaI-f	TAACCCGGGGATGTCTAGAGCAGTTGGTAT	Generation of Yeast Two-hybrid vector constructs
3638-DL-Ssa3-SalI-r	TAAGTCGACTCAATCAACCTCTTCCACTG	Generation of Yeast Two-hybrid vector constructs
3651-DL-Sse1-BamHI-f	TAAGGATCCGTATGAGTACTCCATTTGGTTT	Generation of Yeast Two-hybrid vector constructs
3628-DL-Sse1-SalI-r	TAAGTCGACTTAGTCCATGTCAACATCAC	Generation of Yeast Two-hybrid vector constructs
3652-DL-Sse2-BamHI-f	TAAGGATCCGTATGAGCACTCCATTTGGCTTA	Generation of Yeast Two-hybrid vector constructs
3630-DL-Sse2-SalI-r	TAAGTCGACTTAATCAAGGTCCATGTTTT	Generation of Yeast Two-hybrid vector constructs
3653-DL-Sti1-BamHI-f	TAAGGATCCGTATGTCATTGACAGCCGATGA	Generation of Yeast Two-hybrid vector constructs
3632-DL-Sti1-SalI-r	TAAGTCGACTTAGCGGCCAGTCCGGATGA	Generation of Yeast Two-hybrid vector constructs
3159-DL-Sup35 EcoRI-f	TAAGAATTCATGTCGGATTCAAACCAAGG	Generation of Yeast Two-hybrid vector constructs
3160-DL-Sup35 BamHI-r	TAAGGATCCTTACTCGGCAATTTTAACAA	Generation of Yeast Two-hybrid vector constructs
3654-DL-Tah1-BamHI-f	TAAGGATCCGTATGAGCCAATTTGAAAAGCA	Generation of Yeast Two-hybrid vector constructs
3634-DL-Tah1-SalI-r	TAAGTCGACTCAGGACCGGTCGTATCCCT	Generation of Yeast Two-hybrid vector constructs
3657-DL-Ydj1-BamHI-f	TAAGGATCCGTATGGTTAAAGAAACTAAGTT	Generation of Yeast Two-hybrid vector constructs
3642-DL-Ydj1-SalI-r	TAAGTCGACTCATTGAGATGCACATTGAA	Generation of Yeast Two-hybrid vector constructs
3162-DL-ylr177w EcoRI-f	TAAGAATTCAATTTGGCACTATTTATAAA	Generation of Yeast Two-hybrid vector constructs

3163-DL-ylr177w BamHI-r	TAAGGATCCTATATCTACAACCGG TTCCA	Generation of Yeast Two-hybrid vector constructs

[a] Regions designed for homologous recombination are in **BOLD**.
[b] Endonuclease restriction sites are underlined.
[c] Regions designed for fusion by PCR are in SMALL FONT.

2.7 Integrative modification of *S. cerevisiae* genome

2.7.1 Integrative disruption of *S. cerevisiae* genes

S. cerevisiae genes were disrupted by site-directed homologous recombination of the *S. cerevisiae HIS3* gene at the locus of the gene of interest following the protocols outlined in Brachmann *et al.* (1998). Briefly, forward and reverse primers specific to the 1184 bp *HIS3* cassette were designed with 40-60 nucleotide 5′ tails specific for regions upstream of the start codon and downstream of the stop codon of the gene targeted for disruption (Table 2-14). These primers were used to amplify a targeted *HIS3* DNA fragment by PCR using pRS413 as template DNA. The DNA fragment was then introduced into the *S. cerevisiae* strain of interest by standard chemical or electroporation transformation methods outlined in Sections 2.3.2 and 2.3.3 then plated on CSM-HIS plates. Candidate colonies were screened by PCR using forward primers upstream of the site of integration and the reverse primers used in the amplification of the *HIS3* cassette. A PCR product of the expected size signified a successful disruption, while no PCR product signified an unsuccessful disruption.

2.7.2 Integrative replacement of Sup35p prion determining domain

YIplac211 based vectors described in 2.6 and listed in Table 2-12 were employed to replace the region of *SUP35* that encodes its PrD (bp 1-369) following a pop-in, pop-out protocol outlined in Rothstein *et al*. (Rothstein, 1991).

Table 2-14. Oligonucleotides employed in the generation of *S. cerevisiae* knockouts

Name	Sequence [a,b]	Application
2607-DL-Rnq1-pRS-f	CATTAAAAGAACGTACATATAGCGATACAA ACGTATAGCAAAGATCTGAAAGATTGTA CTGAGAGTGCAC	Deletion of *RNQ1*
2608-DL-Rnq1-pRS-r	TATATAAACAAATACGTAAACAAAGGATAG AAGGCGAACTGAATCATCGTCTGTGCGG TATTTCACACCG	Deletion of *RNQ1*; Confirmation of *RNQ1* deletion
2768-DL-Rnq1 KO chk-f	GTTCGAGCTCCAATTGTTGC	Confirmation of *RNQ1* deletion
2599-DL-Hsp104-pRS-f	AACAAAGAAAAAAGAAATCAACTACACGTA CCATAAAATATACAGAATATAGATTGTA CTGAGAGTGCAC	Deletion of *HSP104*
2600-DL-Hsp104-pRS-r	TATATTACTGATTCTTGTTCGAAAGTTTTTA AAAATCACACTATATTAAACTGTGCGGT ATTTCACACCG	Deletion of *HSP104*; Confirmation of *HSP104* deletion
2764-DL-Hsp104 KO chk-f	TTTCCAATCAGAGCAAGAGT	Confirmation of *HSP104* deletion
2956-DL-Hsp82-pRS-f	CCAACGTGCAAGCGTGTGATATATCACATTC CGGAGGGTGAGATTGTACTGAGAGTG CAC	Deletion of *HSP82*
2957-DL-Hsp82-pRS-r	CTGCAAGGTCTTATAGTCACTCGTCTCTGAG AGTTCTCGCTGTGCGGTATTTCACAC CG	Deletion of *HSP82*; Confirmation of *HSP82* deletion
2958-DL-Hsp82 KO chk-f	TAACACTTTCCTTACAAGTCGAA	Confirmation of *HSP82* deletion
3887-DL-Hsc82-pRS-f	CTTGTTTTCTTTTTCTTGAAACGCTACAGAA CCAATAGAAAAATAGAATCATTCTGAAATT GTGAGATTGTACTGAGAGTGCAC	Deletion of *HSC82*
3888-DL-Hsc82-pRS-r	TACATTAAGACCAACTTTTTTAAAGGCGCGT AAAGCAGAATCATTATTACAAATAGTAAAC TGTGCGGTATTTCACACCG	Deletion of *HSC82*; Confirmation of *HSC82* deletion
3889-DL-Hsc82 KO chk-f	ACAATTTTTCTCGTTTTCTC	Confirmation of *HSC82* deletion
2938-DL-Aha1-pRS-f	CAAGATGGATTCAAAATGCCTACTTACCGC ATTGTATGTGAGATTGTACTGAGAGT GCAC	Deletion of *AHA1*
4062-DL-Aha1-pRS-r	GCCAATAGTGGTATGTAAATATTTACGCATA CTTTTATTGAAACATGAGAACAATATATCC TGTGCGGTATTTCACACGCC	Deletion of *AHA1*; Confirmation of *AHA1* deletion

2940-DL-Aha1 KO chk-f	TAATCGTTAGCAAATGCTAGTGG	Confirmation of *AHA1* deletion
2941-DL-Hch1-pRS-f	GTGCAGTATTTGAGCGGCGCTCACGGAAAC AGCGACCCAGAGATTGTACTGAGAGT GCAC	Deletion of *HCH1*
4042-DL-Hch1-pRS-r	TAGCCATAATGTTTTTGGGTTTCCACATCTT CCACTCGGCCTGTGCGGTATTTCACA CCG	Deletion of *HCH1*; Confirmation of *HCH1* deletion
2943-DL-Hch1 KO chk-f	TAAATGCACATCCTATTGCCAGG	Confirmation of *HCH1* deletion
2959-DL-Cpr6-pRS-f	CTTTCCCTCCCCTCTTCTCATCCATTCGCTTC ATTTATGCAGATTGTACTGAGAGTGC AC	Deletion of *CPR6*
2960-DL-Cpr6-pRS-r	CGTCTCTTGGTGCAGACCAGTTTAACTTGGG AGCCACTGCCTGTGCGGTATTTCACA CCG	Deletion of *CPR6*; Confirmation of *CPR6* deletion
2961-DL-Cpr6 KO chk-f	TAAAGTAATCATACCTAGATAAAT C	Confirmation of *CPR6* deletion
2631-DL-Cpr7-pRS-f	TCTGAAAGGTGTTCGGCAGCAACAACCTAC ATCCAACGCGAGATTGTACTGAGAGT GCAC	Deletion of *CPR7*
2632-DL-Cpr7-pRS-r	GGGTTATTTAATCTCAAATTTCAGCCTTACA AGTAACTAACTGTGCGGTATTTCACA CCG	Deletion of *CPR7*; Confirmation of *CPR7* deletion
2780-DL-Cpr7 KO chk-f	ATATTTTTCTGTTTTTGTAGGTG	Confirmation of *CPR7* deletion
2953-DL-Sba1-pRS-f	GAGACAAAGAGGAAGTTAAAGAAAGTTCAT TTGTGACCTCAGATTGTACTGAGAGT GCAC	Deletion of *SBA1*
2954-DL-Sba1-pRS-r	CCCTACGATGGCCATTTAAGCGACACGTGG GCCTTAGGTGCTGTGCGGTATTTCACA CCG	Deletion of *SBA1*; Confirmation of *SBA1* deletion
2955-DL-Sba1 KO chk-f	TAACTCATTTTAAATATTCACACG	Confirmation of *SBA1* deletion
2947-DL-Sti1-pRS-f	GGGCGAGTTGCTGTGGAGTTTTTCGATGATC AGGGCGATGAGATTGTACTGAGAGTG CAC	Deletion of *STI1*
2948-DL-Sti1-pRS-r	GGATGCAACCCCCCTTCTCCAAAGAAAATT GATGCCTGTGCGGTATTTCACACCG	Deletion of *STI1*; Confirmation of *STI1* deletion

2949-DL-Sti1 KO chk-f	TAACTTCCAAGCTTTGACGAACA	Confirmation of *STI1* deletion
3704-DL-Tah1-pRS-f	CCTCGAAGGGGTCTGTGGGAATGTCACTCTG CTGGACCGGAGATTGTACTGAGAGTG CAC	Deletion of *TAH1*
3705-DL-Tah1-pRS-r	TGTATAGTTTCGTACTATGAAAATCGAAGTT TTAAGCGGCCTGTGCGGTATTTCACA CCG	Deletion of *TAH1*; Confirmation of *TAH1* deletion
3706-DL-Tah1 KO chk-f	TAAAAGAACTCCCGTCGCATGTG	Confirmation of *TAH1* deletion
2593-DL-Sse1-pRS-f	TCGATAGCCATAAGCAAAAAGTACATTGAC AAACAACATTTCTTTAAAAGAGATTGTA CTGAGAGTGCA	Deletion of *SSE1*
2594-DL-Sse1-pRS-r	GCATGTCCCCATTCATGCATACATATATTCG TAAACATACACATATTCATCTGTGCGGT ATTTCACACCG	Deletion of *SSE1*; Confirmation of *SSE1* deletion
2761-DL-Sse1 KO chk-f	AACAAATTGGCTCATCCACT	Confirmation of *SSE1* deletion
2629-DL-Sse2-pRS-f	TTTTTTACCTGTAACAGACGTAACCAAAGGA TATAATATAAGATTGTACTGAGAGTG CAC	Deletion of *SSE2*
2630-DL-Sse2-pRS-r	AGAATAAAGAGGGAACAATCCAAATAGACA AAAATTCCGACTGTGCGGTATTTCACA CCG	Deletion of *SSE2*; Confirmation of *SSE2* deletion
2779-DL-Sse2 KO chk-f	GGCATCCTAATGTAAGCAAG	Confirmation of *SSE2* deletion
2944-DL-Ssa2-pRS-f	CCCATCTATCCCACCATTCGTCAAAAGAGCT TATAATGCAAGATTGTACTGAGAGTG CAC	Deletion of *SSA2*
4063-DL-Ssa2-pRS-r	AAAATACAGAGGAAAGCAAAAGTAAA ACTTTTCGGATATTTTACAGGGCGATC GCTAAGCCTGTGCGGTATTTCACAC GCC	Deletion of *SSA2*; Confirmation of *SSA2* deletion
4064-DL-Ssa2 KO chk-f	TTCTGGTTGTTCACTCCAAG	Confirmation of *SSA2* deletion
2625-DL-Ssa3-pRS-f	ACTAAACGGATAGAATAGGTACTAAACGCT ACAAAGAAAAAGATTGTACTGAGAGT GCAC	Deletion of *SSA3*
2626-DL-Ssa3-pRS-r	AACATAAAAAGTAGCTAAATAGAACACTAT AGAAGAATAACTGTGCGGTATTTCAC ACCG	Deletion of *SSA3*; Confirmation of *SSA3* deletion

2777-DL-Ssa3 KO chk-f	GTACAATCTTACCGAGTTTGTG	Confirmation of *SSA3* deletion
2950-DL-Ydj1-pRS-f	GGGGAAGAGAGTGCAGAGTTTCTAAAAGCACTTGAAAACGAGATTGTACTGAGAGTGCAC	Deletion of *YDJ1*
2951-DL-Ydj1-pRS-r	GCGATGACTGTAGGTGGTACTTTTACATTTTTATGTGCGCCTGTGCGGTATTTCACACCG	Deletion of *YDJ1*; Confirmation of *YDJ1* deletion
2952-DL-Ydj1 KO chk-f	TAATATGCAGTGGTATAGTATGC	Confirmation of *YDJ1* deletion

[a] Regions designed for homologous recombination are in SMALL FONT.
[b] Regions specific to the *HIS3* cassette are in underlined.

2.8 Protein manipulations and analysis

2.8.1 Purification of protein from yeast whole cell lysates

When protein was required in a non-denatured state, yeast lysates were prepared by disruption with glass beads (Needleman and Tzagoloff, 1975). Cell cultures were harvested by centrifugation at 2,000 × *g* for 5 minutes at 4°C, washed twice with 10 ml ddH_2O, and resuspended in 2 ml of ice-cold native lysis buffer (Table 2-7). 200 µl of ice-cold acid-washed glass beads were added to the cell suspension and the mixture was vortexed twice for 15 minutes at 4°C, with a 10 minute break between vortexes. The glass beads and unbroken cells were pelleted by centrifugation at 600 × *g* for 1 minute at 4°C. The supernatant was recovered and the remaining cellular debris was cleared by centrifugation at 10,000 × *g* for 5 minutes at 4°C. The supernatant was stored at -80°C.

Alternatively, when native protein was not required, yeast lysates were prepared by denaturation with alkaline and reducing agents. Cells harvested by centrifugation at 2,000 × *g* for 5 minutes, transferred to a microcentrifuge tube, and resuspended in 240 µl of 1.85 M NaOH and 7.4% β-mercaptoethanol. The cell suspension was incubated on ice for 5 minutes and then mixed with an equal volume of 50% trichloroacetic acid. After

another 5 minutes of incubation on ice, the mixture was centrifuged at 16,000 × *g* for 10 minutes at 4°C. The supernatant was discarded and the pellet washed once in water before being resuspended in 70 µl of Magic A (1 M unbuffered Tris•HCl, 13% SDS detergent). 70 µl of Magic B (30% w/v glycerol, 200 mM DTT, 0.25% bromophenol blue) was added to the suspension and the mixture was incubated at 65°C for 15 minutes. Debris was cleared by centrifugation at 16,000 × *g* for 1 minute and the supernatant was stored at -80°C.

2.8.2 Purification of protein from *E. coli*

HIS-tagged *S. cerevisiae* protein was produced and purified from *E. coli* following a protocol adapted from Alberti *et al.* (2009). First, 500 ml cultures of BL21 *E. coli* carrying pJC45 vectors to express 10×HIS tagged yeast proteins were grown to a concentration of OD_{600} ~0.4 and then induced by the addition of IPTG to 1 mM concentration. After 3-4 hours of induction, the cells were pelleted by centrifugation and resuspended in 5-10 ml lysis buffer (7 M GuHCl; 100mM K_2HPO_4, pH 8.0; 5mM imidazole; 300 mM NaCl; 5 mM 2-mercaptoethanol) for 1 hour at room temperature. Lysates were then cleared by centrifugation at 20,000 rcf at 4°C for 20 minutes. The HIS-tagged protein was then purified from the cleared lysate using TALON Superflow Metal Affinity Resin following the manufacturer's instructions (Clontech). Protein was recovered from the resin with 1-2 ml of elution buffer (8 M urea; 100 mM NaOAc/HOAc, pH 4.0; 5 mM 2-mercaptoethanol) and precipitated in 5 volumes of methanol. The precipitated protein was resuspended in 10-50 µl of resuspension buffer (7M GuHCl; 100 mM K_2HPO_4, pH 5.0; 300 mM NaCl, 5 mM EDTA, 5mM TCEP) and protein concentrations were measured optically as described in Section 2.8.3.

2.8.3 Determination of protein concentration

The protein concentration was measured by the protocol developed by Bradford (1976). A standard curve was prepared by adding 900 µl of fresh Bio-Rad Protein Dye to 100 µl aliquots of ddH_2O containing 0.0, 0.02, 0.04, 0.06, 0.08 and 0.1 µg/µl Bovine Serum Albumin (BSA). Samples were incubated for 5 minutes at room temperature, and absorbance at 595nm was measured using a Beckman DU640 spectrophotometer. Absorbance values were plotted against the BSA concentrations to generate the standard curve. Absorbance of a protein sample was measured in the same manner as for the BSA standards, with the protein concentration being estimated by comparing the absorbance values of two dilutions of the sample that fall within the linear range of the standard curve. Alternatively, protein concentrations were determined optically by measuring absorption at 280 nm using calculated extinction coefficients (Stoscheck, 1990).

2.8.4 Separation of proteins by SDS-polyacrylamide gel electrophoresis

Proteins were separated by sodium dodecyl sulfate-poluacrylamide gel electrophoresis (SDS-PAGE) (Shapiro et al., 1967). Protein samples were mixed 5:1 with 6 × sample buffer (Table 2-7), denatured by boiling for 10 minutes, and separated by electrophoresis on discontinuous slab gels. Stacking gels contained 3% acrylamide mixture (30:0.08 acrylamide:*N*,*N*′-methylen-*bis*-acrylamide), 60mM Tris•HCl, pH 6.8, 0.1% SDS, 0.1% v/v TEMED, and 0.1% ammonium persulfate. Resolving gels were composed of 10% acrylamide mixture (as above), 370mM Tris• HCl, pH 8.8, 0.1% SDS, 0.1% v/v TEMED, and 0.043% ammonium persulfate. Electrophoresis was conducted in 1 × SDS-PAGE running buffer (Table 2-7) at 50-120 V using a Bio-Rad Mini Protean Tetra gel system.

2.8.5 Detection of protein by gel staining

Proteins in a polyacrylamide gel were visualized by staining with 0.1% Coomassie Brilliant Blue R-250, 10% v/v acetic acid, 35% v/v methanol for ~ 1 h while being gently agitated. Coomassie dye not bound to protein was removed by multiple washes in 10% v/v acetic acid, 35% v/v methanol. Kimwipes (Kimberly-Clark Professional) were placed in the washing container to adsorb washed dye during agitation. Gels were analyzed using a GS-800 Calibrated Densitometer (Bio-Rad).

2.8.6 Semi-denaturing detergent-agarose gel electrophoresis (SDD-AGE)

One method employed in the biochemical analysis of amyloid proteins *ex vivo* is SDD-AGE (Kryndushkin et al., 2003). Non-denatured protein samples were mixed 3:1 with 4 × loading buffer (2x TAE, 20% glycerol, 8% SDS, Bromophenol blue to desired pigmentation). If the sample was to serve as a marker for denatured protein of interest, it was boiled for 10 minutes, otherwise it was kept at room temperature until loaded into the SDD-AGE gel as outlined by Halfmann and Lindquist (2008). Briefly, the samples were loaded in a 1.5% agarose, 0.1% SDS gel and subjected to electrophoresis (3V/cm gel length) in 1xTAE (0.1% SDS) until the bromophenol marker had migrated the desired distance. The protein was then detected by immunoblotting as described in Section 2.8.7.

2.8.7 Detection of protein by immunoblotting

Proteins separated by SDS-PAGE were transferred to nitrocellulose membrane (Bio-Rad) in 1 × transfer buffer (Table 2-7) at 400 mA for 2 hours at room temperature using an ET-20 semi-dry electrophoretic transfer system (Tyler Research Instruments). Proteins separated by SDD-AGE were transferred to nitrocellulose membrane by capillary transfer overnight using 1 × TBS (20mM Tris•HCl, pH 7.4, 150mM NaCl).

Briefly, the gel was placed upon a wick of 1 × TBS soaked filter paper, with a similarly soaked nitrocellulose membrane cut to match the gel placed on top of the gel. Two soaked and cut filter papers are placed on top of the membrane with a thick layer of paper towels on top to provide the capillary to take up the 1xTBS buffer. Care was taken to prevent buffer transfer through any other point than the gel by flanking the gel with parafilm (Pechiney Plastic Packaging). Transfer of protein to the membrane was visually confirmed by staining with Ponceau stain (Table 2-7) for 10 minutes followed by destaining with ddH_2O. The membrane was then incubated in blocking solution (5% skim milk powder w/v in TBST (Table 2-7)) with gentle agitation at room temperature for at least 1 hour to coat the nitrocellulose membrane and prevent non-specific binding of antibodies during the later steps of this protocol. Specific proteins were detected by incubating the pre-blocked membrane with primary antibody diluted in blocking buffer for 1 hour at room temperature with gentle agitation. Unbound primary antibody was washed from the membrane by 5 sequential 5-minute washes in blocking buffer and then it was incubated in the presence of HRP-conjugated secondary antibody diluted in blocking buffer for 1 hour at room temperature with gentle agitation. Unbound secondary antibody was washed from the membrane with 2 5-minute washes in blocking buffer followed by 2, 5 minute washes in 1 × TBST. Antigen-antibody complexes were detected using ECL (enhance chemiluminescence) Western Blotting Detection Kit according to the manufacturer's instruction (Amersham Biosciences) and exposing the nitrocellulose membrane to X-Omat BT film (Kodak), which was then developed using an X-Omat 2000A Processor (Kodak).

2.8.8 Stripping of nitrocellulose membrane

Used nitrocellulose membranes employed in immunoblotting as described in Section 2.8.7 were subjected to incubation with 1 × Re-Blot Plus reagent (Millipore) for 30 minutes at room temperature with gentle agitation. This disrupted antigen-antibody complexes and, after subsequent washes with 1 × TBST, prepared the membrane for another immunoblotting experiment with fresh primary antibody.

2.8.9 Prion sedimentation assay

The sedimentation assay distinguished [*prion*$^-$] and [*PRION*$^+$] cells by separating soluble prion protein from aggregated prion protein by centrifugation (Sondheimer and Lindquist, 2000; Bradley et al., 2002). Non-denatured protein samples were prepared as described in 2.8.1 and 500 µl of the sample were subjected to a 30 minute centrifugation at 73,000 rpm in a TLA-120.2 Beckman rotor (~260,000 × *g*) at 4°C in an Optima TLX Ultracentrifuge (Beckman). The supernatant was transferred to a fresh microcentrifuge tube and the pelleted protein was resuspended in 500 µl of native lysis buffer (Table 2-7). Total protein samples, along with 260,000 × *g* pellet and supernatant samples were analyzed by polyacrylamide gel electrophoresis and immunoblotting as described in Sections 2.6.4-8.

2.8.10 Thioflavin T amyloid assembly assay

Protein purified as described in 2.8.2 was heated for 5 minutes at 95°C then diluted to 20 µM in assembly buffer (5 mM K_2HPO_4, pH 6.6; 150 mM NaCl; 5 mM EDTA; 2 mM TCEP; 0.5 mM ThT) (Alberti et al., 2009). 100 µl of assembly reaction was transferred per well of a black non-binding 96-well glass bottom plate (Griener Bio-One). The plate was agitated at 200 rpm at 30°C. Fluorescence measurements (450 nm

excitation, 482 nm emission) were made with a Microplate Spectrophotometer (BioTek). In order to minimize variation arising from sporadic sampling of very large fluorescent aggregates, values for each time point represent the averages of 10 readings taken over a 5-minute period.

2.9 Microscopy

2.9.1 Fluorescence microscopy

Micrographs were captured at room temperature on an Olympus IX81 Inverted Microscope equipped with either 60 × 1.35 UPlan-Apo or 100 × 1.4 UPlan-Apo objectives (Carl Zeiss). Fluorophores were excited by an X-cite 120PC Fluorescence Illumination System (EXFO) with signal filtered by Brightline zero pixel shift filter cubes (Olympus). Z-stacks were acquired as 21 optical sections, spaced 0.261 μm apart and subsequently deconvoluted using algorithms provided by Huygens Professional software (Scientific Volume Imaging BV, The Netherlands). Specifically, 3D data sets were processed to remove noise and reassign blur through an interative Classic Maximum Likelihood Estimation (CMLE) algorithm and a theoretical point spread function. Post-processing operations such as 3D reconstruction were performed using Imaris 7.0 software (Bitplane, Zurich, Switzerland). Imaris 7.0 was also used to process the transmission bright-field images. The levels were modified so as to display only the outline of the cell, artificial blue colour was applied, and its edges were smoothed using a Gaussian filter. Fluorescence images form each stack were projected as maximum intensity projections (MIP). Adobe Photoshop CS4 (Adobe Systems) was used to combine MIPs and bright-field images.

2.9.1.1 Quantification of cytologically detectable candidate prion aggregates

Candidate prion genes were tagged with GFP and expressed on the galactose driven plasmid pYES.20 as described in Section 2.6.1. Primary cultures were grown in CSM-URA 2% glucose overnight, then inoculated into CSM-URA 2% galactose and incubated for 48 hours. 0.5 ml of culture was transferred to a microcentrifuge tube. Cells were pelleted by centrifugation then treated with Trypan Blue to determine cell viability (Freshney, 1983). This was done by resuspending the cell pellet in 1 ml ddH_2O, adding 1 µl of Trypan Blue solution (Gibco), allowing 5 minutes for dye uptake, and then washing the cells twice in 1 ml ddH_2O. The pellet was then resuspended in 70 µl ddH_2O, 1-2 µl of this suspension was then placed onto a clear glass microscope slide (Fisher Scientific), and covered with a microscope cover glass (Fisher Scientific). Ten single slice micrographs (~500 cells) were acquired for each trial at 60 × magnification and Z-stacks were acquired at 100 × magnification. As Trypan Blue is negatively charged, it cannot be taken up by the cell unless the membrane is damaged, thereby staining all damaged cells and leaving viable cells unstained (Maniatis et al., 1982; Freshney, 1983). Cells and cytologically detectable candidate protein-GFP foci were quantified using Image J (Abramoff et al., 2004). The foci frequency was calculated as a percentage of all viable cells that contain foci.

2.9.1.2 Quantification of the pattern of Rnq1-GFP aggregate localization

Strains carrying pYES2.0-Rnq1-GFP and expressing GFP-tagged Rnq1p were grown up and prepared in the same manner described in Section 2.9.2.1 only varying in that the strains were only incubated in CSM-URA 2% galactose for 24 hours instead of 48. In addition to quantifying the overall frequency of foci containing cells as a

percentage of all viable cells, foci containing cells were scored based on the number of foci observed within the cell. They were classified as either single-focus cells, containing only one focus, or multi-foci cells, containing multiple foci per cell. These were then expressed as a percentage of all viable foci containing cells.

2.9.1.3 Quantification of SUP35NM-GFP aggregate morphology

Strains carrying pYES2.0-Sup35NM-GFP and expressing GFP-tagged Sup35NM were grown up and prepared in the same manner described in Section 2.9.2.1. In addition to quantifying the overall frequency of foci containing cells as a percentage of all viable cells, foci morphology was also scored. They were classified as either punctate or filamentous and then expressed as a percentage of all viable foci containing cells.

2.9.2 Staining of yeast vacuoles with FM 4-64

The lipophilic styryl dye, N-(3-triethylammoniumpropyl)-4-(p-diethylamino-phenyl-hexatrienyl) pyridinium dibromide (FM 4-64), is a vital stain used to follow bulk membrane-internalization and transport to the vacuole in yeast (Vida and Emr, 1995). It does not permeate the cell membrane but, instead intercalates into the plasma membrane and is then taken into the cells by endocytosis, finally localizing to the vacuole membrane (Maniatis et al., 1982; Vida and Emr, 1995). As FM 4-64 is a vital dye, cells cannot be fixed then stained, nor stained then fixed. Cells must be living at the time of staining and observation. Vacuole staining was accomplished following the protocol outlined by Vida and Emr (Maniatis et al., 1982; Vida and Emr, 1995). Briefly, strains were grown as described in Section 2.9.2 and then sub-culturing in YEP + 2% galactose at 30°C for 3 hours to an OD600 ~0.8-1.6. Then 0.2 ml of culture was transferred to a sterile microcentrifuge tube, mixed by vortexing with 1 µl of FM 4-64 stock solution (16 µM in

DMSO), and incubated for 30 minutes at 30°C. 0.8 ml of fresh media was added, the cells were pelleted by microcentrifugation at low speed, and the media was aspirated. The cells were incubated in 1 ml of fresh media for 2 hours at 30°C to allow the dye time to be taken up by endocytosis and localize to the vacuole membrane. Cells were then observed on an Olympus IX81 fluorescent microscope using a Texas Red filter.

2.10 Polyclonal antibody production

Elena Savidov performed antibody preparations. Antibodies were raised in guinea pigs against Sup35p and Riq1p as follows: DNA fragments were cloned into pJC45 downstream and in-frame to the ORF of 10 × His residues and an Xa cleavage site as described in Section 2.6. pJC45-Sup35 and pJC45-Riq1 were then transformed into chemically competent *E. coli BL21*. Proteins were then purified following the procedure outlined in Section 2.8.2. Proteins were further purified by gel electrophoresis according to Harlow and Lane (1988). Gels were stained with 0.05% Coomassie Brilliant Blue R-250 in water for 10-15 minutes and destained in water. Gel fragments containing the protein of interest were excised and placed into dialysis tubing. Elution buffer (0.2 M Tris-acetate, pH 7.4, 1% SDS, 10 mM DTT) was added to the tubing at a concentration of 10 ml per g of wet gel. Proteins were eluted from the gel by electrophoresis at 50 V overnight at 4°C in 50 mM Tris-HCl, pH 7.4, 0.1% SDS. The eluate was placed into 2 to 3 new dialysis tubes and dialyzed against 4 L of 50 mM ammonium bicarbonate once at room temperature and three times at 4°C. The protein solution was then frozen at -80°C and dried by lyophilization. Lyophilized protein was resuspending in a minimal volume of water, and the protein concentration was measured as described in Section 2.8.3.

Animals were immunized according to Harlow and Lane (1988). Proteins were adjusted to a concentration of 500 μg/ml and mixed in equal volume of Freund's complete or incomplete adjuvant for primary and subsequent injections, respectively. Guinea pigs were injected with 0.4 ml of antigen suspension containing 80 μg of protein at several sites subcutaneously every 6 weeks. Bleeds were taken 10 days after each injection. Serum was separated from cells in clotted blood by centrifugation at 2000 × *g* for 15 minutes at room temperature. Serum was stored at -20°C in aliquots. The presence of specific antibodies in serum was determined by immunoblotting.

2.11 Yeast two-hybrid analysis

Yeast two-hybrid analysis was performed using the Matchmaker Two-Hybrid System according to the manufacturer's instructions (Clontech) with modifications. Plasmid pairs, constructed as described in Section 2.6 and listed in Table 2-12, encoding activation domain (AD) and binding domain (BD) fusion proteins were transformed into *S. cerevisae* strain HF7c as described in Section 2.3.2. Transformants were grown on the appropriate medium to maintain selective pressure for the plasmids. Possible interactions between AD and BD fusion proteins were detected by streaking colonies on selective medium lacking histidine, with selective medium including histidine as a growth control.

2.12 Computer aided DNA and protein sequence analysis

DNA sequences were analyzed using Vector NTI Software (Invitrogen) and the NCBI BLASTn suite (http://blast.ncbi.nlm.nih.gov/Blast.cgi?CMD=Web&PAGE_TYPE=BlastHome). Protein sequences were analyzed using the *Saccharomyces* Genome Database (http://www.yeastgenome.org). Prion candidate proteins were selected from the *S. cerevisiae* proteome based upon the results of a PERL scripted search with the

parameters that likely candidates would have at least 30% N or Q content over at least 100 amino acid residues. C. Melissa Dobson composed the PERL script and candidates were ranked by N/Q content.

CHAPTER THREE:

RIQ1p, A POTENTIAL PRION PROTEIN

Overview

Previous work performed by Susan Lindquist's lab has suggested that while prion proteins have been found to be rich in asparagine (N) and glutamine (Q), the two amino acid residues promote the formation of amyloids with different qualities. Specifically, N promotes the formation of "benign self-templating amyloids", and Q leads to the formation of "toxic non-amyloid conformers" (Alberti et al., 2009; Halfmann et al., 2011). Prior to the publication of these findings, I hypothesized that novel prion candidates might be identified through an *in silico* screen for proteins rich N and/or Q. In this chapter I report the results of this screen and document the prion-like behavior of a Q-rich protein encoded by the previously uncharacterized open reading frame, *YLR177w*, which I have named Riq1p (**R**ich **I**n **Q**). I demonstrate that Riq1p forms aggregates both *in vivo* and *in vitro* and can rescue the prion capabilities of Sup35p if its complete amino acid sequence is used to replace the Sup35p's prion determining domain (PrD). As Riq1p is particularly rich in Q, my findings demonstrate a potential exception to the theories proposed concerning the effects of Q upon prion amyloid and suggest that non-Q-rich domains in amyloid forming proteins may mitigate Q-linked cytotoxicity.

3.1 Screening *Saccharomyces cerevisiae* proteome for novel prion proteins

3.1.1 *In silico* selection of prion candidates

N and Q residues are important for the formation of the amyloid core of the prion aggregate (Michelitsch and Weissman, 2000). They have been found in high concentrations in prions and prion-like proteins (Wickner, 1994; Sondheimer and Lindquist, 2000; Du et al., 2008; Alberti et al., 2009). As such, Dr. Melissa Dobson and I selected proteins to be screened for prion characteristics based upon the proportion of N

and Q in their primary amino acid sequence. We searched the *S. cerevisiae* proteome with a PERL script designed to return all proteins containing at least 30% N and/or Q over 100 amino acid residues. The search returned 118 candidates, including all of the then characterized prions (Table 3-1).

Alberti and colleagues published a similar screen for novel prions that was based upon a hidden Markov Model (HMM) approach that used the PrDs of the then identified prion and prion-like *S. cerevisiae* proteins (Sup35p, Ure2p, Rnq1p, and New1p) as positive training examples to scan the proteome for other potential PrDs. Both the HMM approach and that of this study are biased in that they discount potential prions that may not be enriched in N or Q. Acknowledging that shortcoming, I compared the candidates selected by my criteria against theirs and found that ~50% of my candidates were also screened by Alberti and colleagues (Alberti et al., 2009). My list of candidates and their disposition in relation to the Alberti screen are summarized in Table 3-1 and Table 3-2.

Table 3-1. Prion candidates found in both this study and the Alberti et al. 2009 study and their localization to detectable foci in *S. cerevisiae*

Gene name/designation	Determined to a prion-like protein by Alberti *et al.* (Y/N)	Cytologically detectable GFP foci (This study)
DEF1 / YKL054c	N	Foci observed
ENT2 / YLR206w	N	Foci observed
IXR1 / YKL032c	N	Foci observed
MOT3 / YMR070w	Y	Foci observed
NEW1 / YPL226w	Y	Foci observed
PCF11 / YDR228c	N	Foci observed
PSP2 / YML017w	N	Foci observed
RNQ1 / YCL028c	Y	Foci observed
SIN3 / YOL004w	N	Foci observed
SUP35 / YDR172w	Y	Foci observed
TAF12 / YDR145w	N	Foci observed
URE2 / YNL229c	Y	Foci observed
YLR177w	N	Foci observed
GFP	N	No foci observed
AKL1 / YBR059c	N	No foci observed

CYC8 / YBR112c	Y	No foci observed
DDR48 / YMR173w	N	No foci observed
ENT1 / YDL161w	N	No foci observed
JSN1 / YJR091c	N	No foci observed
KSP1 / YHR082c	Y	No foci observed
LSM4 / YER112w	Y	No foci observed
MCM1 / YMR043w	N	No foci observed
MED2 / YDL005c	N	No foci observed
PDC2 / YDR081c	N	No foci observed
PDR1 / YGL013c	Y	No foci observed
POP2 / YNR052c	N	No foci observed
PUB1 / YNL016w	Y	No foci observed
SNF2 / YOR290c	N	No foci observed
SWI1 / YPL016w	Y	No foci observed
YAP1801 / YHR161c	N	No foci observed
YBR016w	N	No foci observed
YDL012c	N	No foci observed
YPR022c	Y	No foci observed
AZF1 / YOR113w	N	Not tested
CBK1 / YNL161w	Y	Not tested
CCR4 / YAL021c	N	Not tested
EPL1 / YFL024c	N	Not tested
GAL11 / YOL051w	N	Not tested
HRR25 / YPL204w	N	Not tested
MCA1 / YOR197w	N	Not tested
MSS11 / YMR164c	N	Not tested
NAB3 / YPL190c	N	Not tested
NGR1 / YBR212w	Y	Not tested
NUP100 / YKL068w	N	Not tested
NUP116 / YMR047c	N	Not tested
NUP49 / YGL172w	N	Not tested
NUP57 / YGR119c	N	Not tested
PAN1 / YIR006c	N	Not tested
PSP1 / YDR505c	N	Not tested
PUF4 / YGL014w	N	Not tested
RAT1 / YOR048c	N	Not tested
RLM1 / YPL089c	Y	Not tested
SAP30 / YMR263w	Y	Not tested
SCD5 / YOR329c	N	Not tested
SGF73 / YGL066w	N	Not tested
SLA2 / YNL243w	N	Not tested
SLM1 / YIL105c	N	Not tested
SNF5 / YBR289w	N	Not tested
TIF4631 / YGR1623w	N	Not tested
TIF4632 / YGL049c	N	Not tested
UPC2 / YDR213w	N	Not tested
YCK1 / YHR135c	N	Not tested

Table 3-2. Prion candidates and their localization to detectable foci in *S. cerevisiae*

Gene name/designation	Cytologically detectable GFP foci (This study)
ATG13 / YPR185w	Foci observed
CDC7 / YDL017w	Foci observed
ESL2 / YKR096w	Foci observed
PHO81 / YGR233c	Foci observed
YLR278c	Foci observed
GFP	No foci observed
ARP1 / YHR129c	No foci observed
CDC39 / YCR093w	No foci observed
DBP1 / YPL119c	No foci observed
MUD2 / YKL074c	No foci observed
RPI1 / YIL119c	No foci observed
RSP0a / YGR214w	No foci observed
SEC61 / YLR378c	No foci observed
SEN1 / YLR430w	No foci observed
SLF1 / YDR515w	No foci observed
SPT10 / YJL127c	No foci observed
SPT20 / YOL148c	No foci observed
SWI4 / YER111c	No foci observed
TBS1 / YBR150c	No foci observed
TPA1 / YER049w	No foci observed
VHR1 / YIL056w	No foci observed
AIM21 / YIR003w	Not tested
ANP1 / YEL036c	Not tested
ASG1 / YIL130w	Not tested
BCS1 / YDR375c	Not tested
BUB1 / YGR188c	Not tested
CDC27 / YBL084c	Not tested
CRZ1 / YNL027w	Not tested
DAL81 / YIR023w	Not tested
FAB1 / YFR019w	Not tested
FAR11 / YNL127w	Not tested
FKS1 / YLR342w	Not tested
HOT1 / YMR172w	Not tested
ITC1 / YGL133w	Not tested
MAD1 / YGL086w	Not tested
MIT1 / YEL007w	Not tested
MPT5 / YGL178w	Not tested
MSS116 / YDR194c	Not tested
NHP6A / YPR052c	Not tested
NPR1 / YGL183c	Not tested
PIN4 / YBL051c	Not tested
PUF3 / YLL013c	Not tested
RIM15 / YFL033c	Not tested
RMD8 / YFR048w	Not tested
SCH9 / YHR205w	Not tested
SET1 / YHR119w	Not tested
SFP1 / YLR403w	Not tested
SIZ1 / YDR409w	Not tested
SKS1 / YPL026c	Not tested
SKY1 / YMR216c	Not tested

STE18 / YJR086w	Not tested
UME6 / YDR207c	Not tested
VID22 / YLR373c	Not tested
YCK2 / YNL154c	Not tested
YBL029w	Not tested
YBR238c	Not tested
YDR210w	Not tested
YML053c	Not tested

Since the Alberti et al.'s publication in *Cell* (2009) and our own screen of the yeast proteome, several different programs have been introduced that attempt to predict amyloidogenic proteins based on a variety of different criteria (reviewed in Hamodrakas, 2011). Some of the more prominent software used to predict amyloid formation based upon the primary sequence of the protein are TANGO (Fernandez-Escamilla et al., 2004), PASTA (Trovato et al., 2006), AGGRESCAN (Conchillo-Solé et al., 2007), AMYLPRED (Frousios at al., 2009), NETCSSP (Kim et al., 2009), FOLDAMYLOID (Garbuzynskiy et al., 2010), WALTZ (Maurer-Stroh et al., 2010), and PAPA (Toombs et al., 2010). These programs use a variety of criteria to predict a given peptide sequence's propensity to form amyloid. For example, PASTA scanned for regions able to pair and form β-sheets and AGGRESCAN predicts aggregation "hot-spots" based upon a series of *in vivo* experiments to measure the relative aggregation potential of individual amino acid residues and calculations that provide an aggregation value based on a sliding-window averaging technique of the primary sequence. None of these methods are unduly biased to select Q/N rich protein regions as potential prion determining domains. Future analysis of *S. cerevisiae'*s proteome for potential amyloidogenic proteins would likely be more efficient and informative if they use one of these methods or a combination of several.

3.1.2 Screen of novel prion candidates for aggregation *in vivo*

Other prions have been shown to localize to bright foci when tagged with GFP and overproduced in a [*PRION*$^{+}$] background. I used this characteristic as my primary assay to test prion candidates for aggregate formation. I used PCR to amplify sequences encoding C-terminally GFP-tagged prion candidates from the GFP library strains (Huh et al., 2003) and ligated that sequence into a galactose driven expression vector, pYES2.0 (Invitrogen). As it has been shown that some proteins adopt their prion conformation more readily in the presence of other prions (Derkatch et al., 2001), I overexpressed my GFP-tagged candidates in the wild type GT17 [*PSI*$^{+}$][*PIN*$^{+}$] strain for 48 hours and observed the cells for the appearance of cytologically detectable fluorescent foci *in vivo*, using fluorescence microscopy. Of the 118 candidates, I tested 52 and found that 18 of these contained fluorescent foci (Table 3-1; Fig. 3-1). This was a sufficient number of positive hits for me to move forward with the next steps of testing. I intend to test the untested candidates at a later date. Among the positive hits were Sup35p, Ure2p, Rnq1p, and New1p, which at the time were known or suspected to be prions (Wickner, 1994; Tanaka, 2005; Sondheimer and Lindquist, 2000). Mot3p, which has since been confirmed as a prion, was also a positive hit (Alberti et al., 2009).

The remaining candidates to display fluorescent foci had not previously been implicated as prion proteins. They included, Atg13p, Cdc7p, Def1p, Ent2p, Esl2p, Ixrp, Pcf11p, Pho81p, Psp2p, Sin2p, Taf12p, Yl2177wp, and Ylr278cp. Most of these formed single or multiple punctate GFP foci. Two of these stood out as unique in the pattern of their putative aggregation. First, Ent2-GFP, normally involved in actin patch assembly (Wendland et al., 1999), formed long filamentous rings. This was interesting as similar

Figure 3-1. Prion candidates identified by screen for aggregation *in vivo*. (A) Formation of aggregate-like foci by GFP-tagged prion and prion candidate proteins as shown in maximum intensity projections of cells. Mot3p has since been characterized as prion protein by Alberti and colleagues (2009). (B) Localization of Taf12-GFP to the nucleus as demonstrated by maximum intensity projection of cells expressing Taf12-GFP and stained with DNA-specific Hoechst dye. All constructs were expressed in wildtype BY4742 cells. Bar, 5 μm.

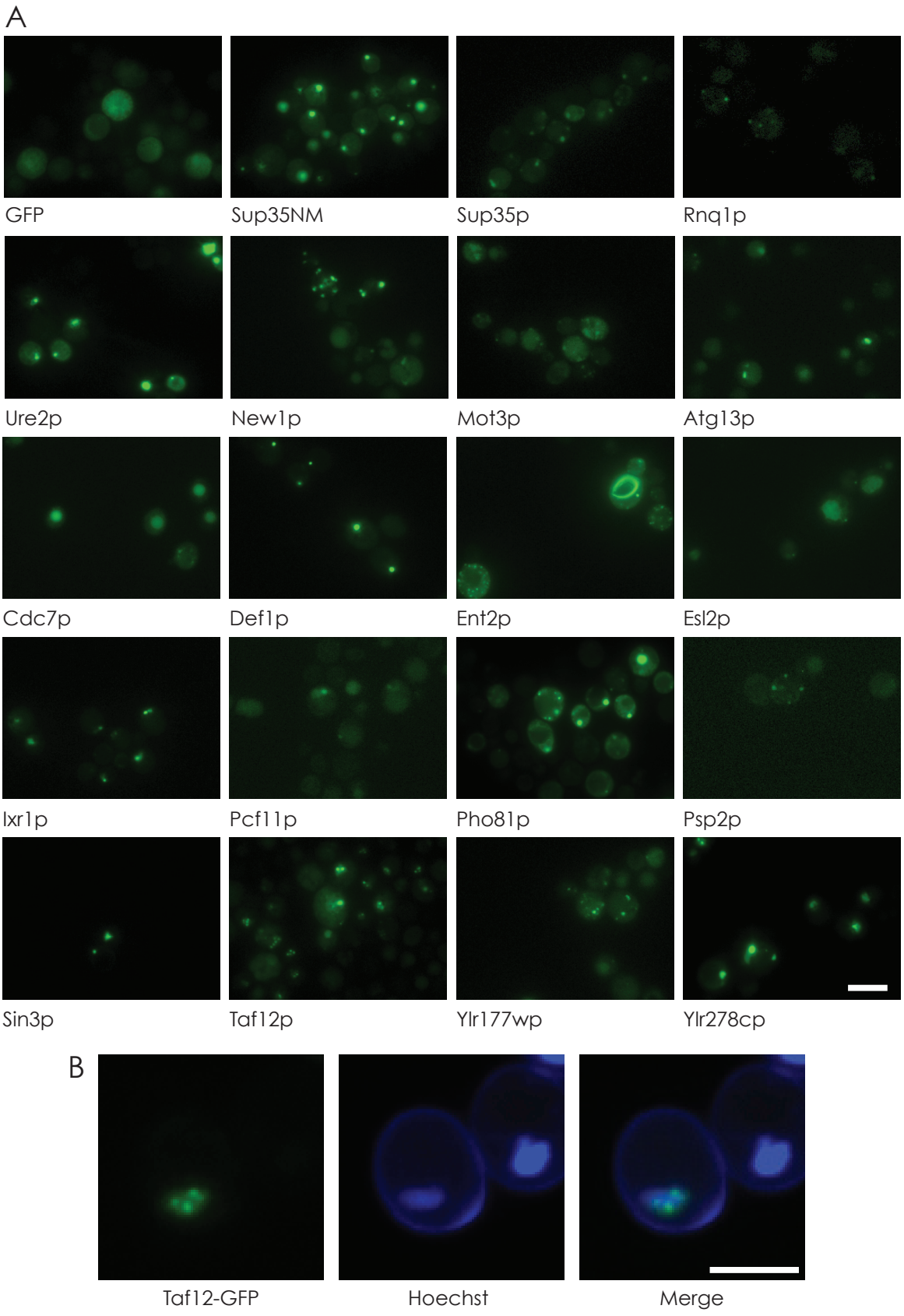
A
GFP
Sup35NM
Sup35p
Rnq1p
Ure2p
New1p
Mot3p
Atg13p
Cdc7p
Def1p
Ent2p
Esl2p
Ixr1p
Pcf11p
Pho81p
Psp2p
Sin3p
Taf12p
Ylr177wp
Ylr278cp
B
Taf12-GFP
Hoechst
Merge

rings are frequently observed in Sup35-GFP expressing cells that are induced to become [*PSI*$^+$] (Zhou et al., 2001). Second, Taf12-GFP foci were localized to the nucleus (Fig. 3-1B), although this is not surprising as Taf12p is a member of the TFIID transcription factor required to initiate RNA polymerase II transcription (Sanders et al., 2002).

At this point, I delayed further screening of the rest of the candidates in order to investigate these proteins.

3.1.3 Replacing Sup35p's PrD with prion candidate amino acid sequences

Sup35p requires its N-terminal PrD (aa 1-123) to maintain its prion characteristics (Ter-Avanesyan et al., 1993; 1994). When I deleted this region, the remaining truncation (Sup35MC, aa 124-685) gives the cell a dominant, anti-nonsense-suppression phenotype. It has been demonstrated that replacing the lost PrD with the amino acid sequence of another prion can restore reversibly curable, [*PSI*$^+$]-like nonsense suppression (Sondheimer and Lindquist, 2000). I took advantage of this and replaced Sup35p's PrD with the complete amino acid sequences of a number of my candidate prions. I chose to use the entire protein to replace Sup35p's PrD as opposed to only a predicted PrD of my candidate because I did not want to unintentionally exclude a potential positive hit that may require regions outside of its Q/N-rich domain(s) to adopt an amyloid conformation (Fig. 3-2A). Using wild type GT17 [*PSI*$^+$][*PIN*$^+$] as the parental strain, I generated *SUP35MC*, *TAF12-SUP35MC*, *DEF1-SUP35MC*, *ENT2-SUP35MC*, and *YLR177w-SUP35MC* strains as described in Section 2.7.2. All of these strains contain the *ADE1-14 UGA* nonsense mutation and so they can only grow on medium lacking adenine if they have a nonsense-suppression phenotype. Additionally, nonsense-suppressor strain

Figure 3-2. Replacing Sup35p PrD with prion candidate amino acid sequences. (A) Schematic of the replacement of Sup35p's Q/N-rich PrD with the complete amino acid sequence of prion candidate proteins. (B) Growth of chimeric strains on CSM-ADE demonstrates rescue of nonsense suppression that was lost with deletion of the sequence encoding Sup35p's PrD. (C) After incubation with the prion curing agent guanidine hydrochloride (GuHCl, 5 mM) in liquid culture for 48h, chimeric strains were plated on rich plates (YEPD) to gauge pigment change associated with loss of nonsense suppression.

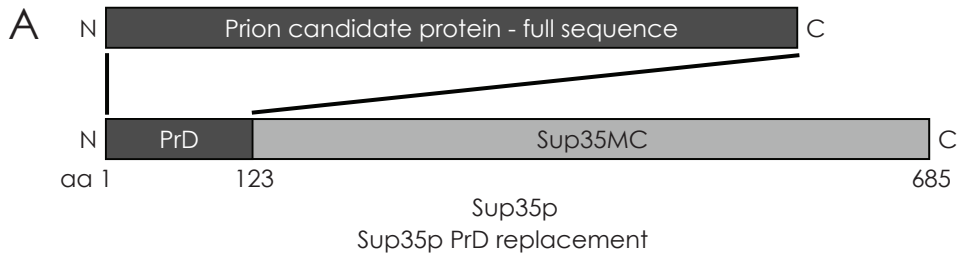
A
N
Prion candidate protein - full sequence
C
N
PrD
Sup35MC
C
aa 1
123
685
Sup35p
Sup35p PrD replacement

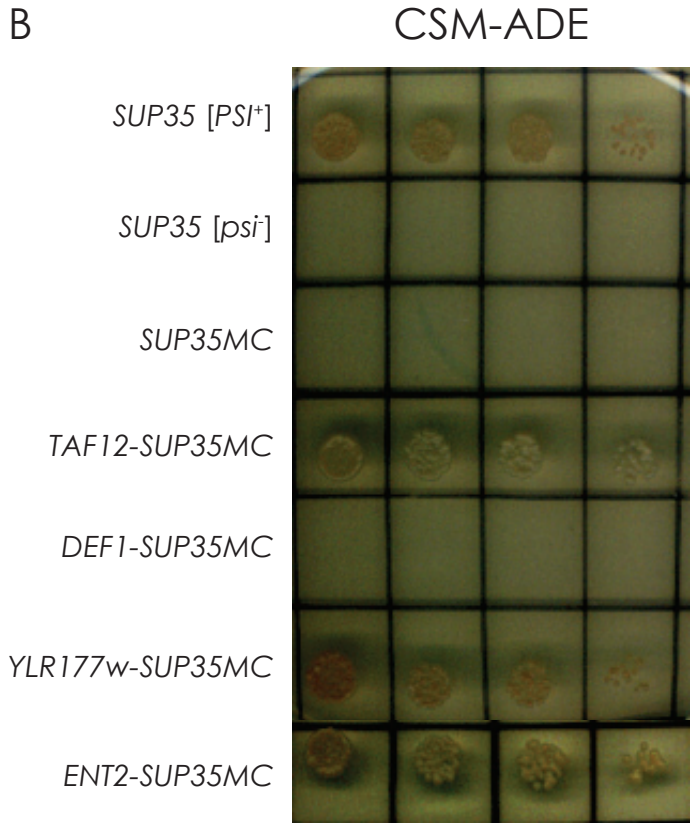
B
CSM-ADE
SUP35 [PSI+]
SUP35 [psi-]
SUP35MC
TAF12-SUP35MC
DEF1-SUP35MC
YLR177w-SUP35MC
ENT2-SUP35MC

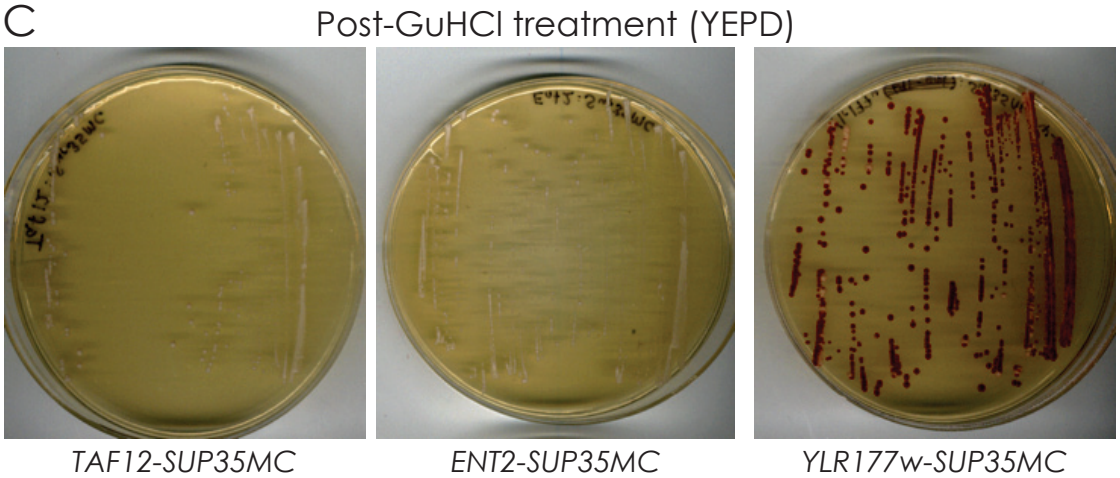
C
Post-GuHCl treatment (YEPD)
TAF12-SUP35MC
ENT2-SUP35MC
YLR177w-SUP35MC

colonies will appear paler, while non-suppressors will appear red due to a secondary metabolite normally consumed in adenine biosynthesis.

I plated my chimeric strains on CSM-ADE plates (Fig. 3-2B) and found that replacing Sup35p's PrD with Taf12p, Ent2p, or Ylr177wp led to a nonsense-suppression phenotype, while using Def1p did not. When I attempted to cure the nonsense-suppressor strains with treatment with 5 mM GuHCl as described in Section 2.2.7, pigment change suggested that of these candidates only the *YLR177w-SUP35MC* strains could be cured (Fig. 3-2C). This is not surprising as both Taf12p and Ent2p normally localize to the nucleus and actin patches, respectively, and so their chimera could easily localize there as well and be unable to contribute to translation termination regardless of their putative prion state.

Having identified a protein, Ylr177wp, whose sequence could rescue nonsense-suppression and could be cured, I decided to focus my efforts towards its characterization.

3.2 Aggregation of Riq1p

3.2.1 Aggregation of Riq1-GFP *in vivo* as detected by fluorescence microscopy

The ORF *YLR177w* had not been linked to a specific function in the cell. The protein it encodes is not essential for viability, localizes to the cytosol, and is phosphorylated by Dnf2p-Mob1p *in vitro*, but beyond this, its function is unknown (Huh et al., 2003; Posteraro et al., 2005; Mah et al., 2005). An examination of its amino acid sequence revealed that it is especially rich in Q, with a 14 residue repeat region from residue 156 to 169. This being the case, I dubbed it *RIQ1* (Rich In Q).

In an attempt to determine the specific regions responsible for its putative prion characteristics, I inserted sequences encoding the following GFP-tagged truncations into the galactose driven plasmid pYES2.0: Riq1p (full-length protein), RiqQ (the region with the highest NQ content, aa 100-230), RiqNQ (the N-terminus including the NQ-rich region), and RiqC (the C-terminus lacking the NQ-rich region) (Fig. 3-3A). I found that only Riq1-GFP and RiqNQ-GFP formed detectable GFP foci when overexpressed, with the other constructs localizing to the cytoplasm (Fig. 3-3). I also found that deletion of *HSP104* or *RNQ1* did not inhibit formation of these fluorescent foci. This suggests that if Riq1p does prove to be a prion, it is not dependent on [*PIN*$^+$] or Hsp104p chaperone activity. Staining these cells with the vacuole-specific dye FM 4-64 showed that the foci localized at or near the vacuole. This was interesting as Daniel Kaganovich and colleagues have provided evidence for the existence an amyloid aggregate specific sub-compartment juxta-localized to the vacuole called the IPOD (Insoluble Protein Deposit) (2008).

3.2.2 Biochemical characterization of Riq1p aggregation *ex vivo*

The fluorescent foci reported in Section 3.2.1 are consistent with prion formation but may simply represent non-prion aggregates or Riq1p's normal localization made brighter through overexpression. Many proteins localize in a punctate manner without aggregation. To clarify this, I biochemically characterized Riq1p. Some of my results suggest that Riq1p does form some sort of aggregate, but they also show that these aggregates do not have the same characteristics as previously identified prion proteins. Differential centrifugation and subsequent western blot analysis (Section 2.8.9) showed that endogenous Riq1p localizes to the same insoluble pellet fraction as other known

Figure 3-3. Fluoresence microscopy detection of Riq1p aggregate formation *in vivo*. (A) Riq1p primary amino acid sequence with Q/N-rich domain in red and truncation schematic. (B) Maximum intensity projections of the GFP-tagged Riq1p and its truncations along with vacuole staining (FM 4-64). Bar, 5 μm. (C) Western Blot of GFP-tagged Rnq1p, RiqQp, RiqNQp, and RiqCp.

A

Riq1

aa1 - MELPSINSTTSISDNQELRNYYDKLLFKNNSGKSLADLPGKMADFNDNSAAAHPRSRVDFINGYIGFREDKQSLLGQKNTKRASFSAFADEGRKQSEMSI
101 - NGKSPNLSLFSFEFNGTPTQDRKPYKQDYLNVMNTSPNNILSPLNNSSQKYYPQKQQQQQQQQQQQQQQSIFDPGRRSSYISDALIHGNAATQQPQYSQP
201 - VYINNNPSLQVPYTAPSEYTQQQQYSSPFNARRNTQPVLNLHPAAAPTNDAGLAVVDGKNLTSSKELHDLYLDCGSNYFASDKVYKFIDSIKGTLRGDNV
301 - SASSSRIIEFLDFLKNCNLNYNPQSDAFISTAVSNASSTGAAKSKNSTSMHLHYKPLVLVSLKNGKLELLSKPQTATLILKRGDLVIIDGDRGKDLVLVV
401 - EPVVDINLALFINFLKKKIHFDSLITNSQQHFPNDQFIKTLVDTTNGKPVAHELNPKLYDIIELTQLIIPSKQVLRFATPWESSTNLHNKFQDELKALHI
501 - AQLKLRSLNNNNSGGGLNIKILNAEFQFDRKKLTFYYICQERNDFRDLIKELFKFYKTRIWLCAIPNNLSIDSKFYDSNKFEWEMYQDMMSHYSMDNTGI
601 - VVAPELNRLKLDDFQIGVYMELVKVLFG - 628

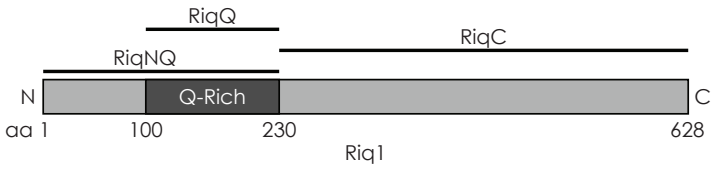

B

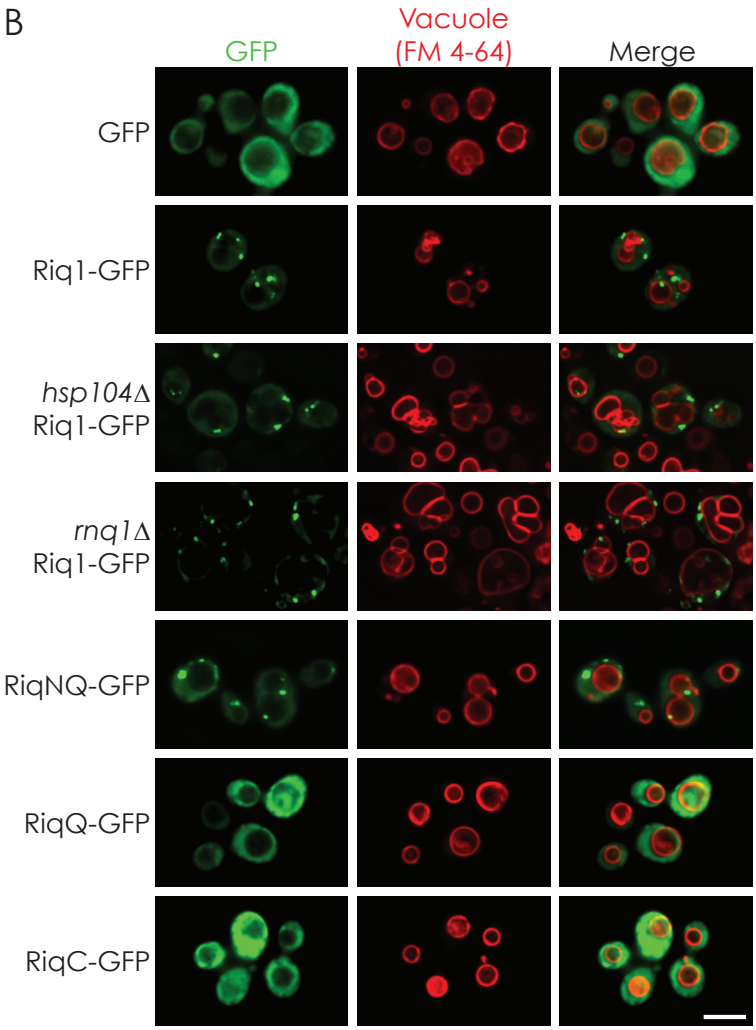

C

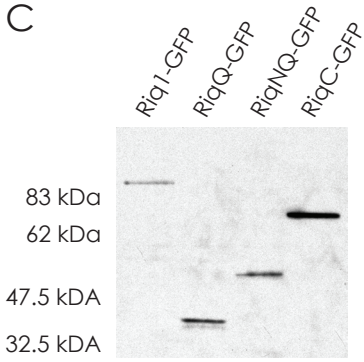

prions, suggesting it may be included in an insoluble aggregate (Fig. 3-4A). On the other hand, when I used antibody raised against Riq1p to probe an SDD-AGE blot I did not observe SDS-resistant polymers typical of prions (Fig. 3-4B). Instead, I only observed signal in the lower molecular weight region of the blot where monomeric protein is commonly detected.

Interestingly, when the protein sample was split, and one half was heated at 95ºC and the other half was kept at room temperature prior to loading on the gel, the heated sample gave a stronger signal (Fig. 3-4B). This suggested a number of possibilities. It could have been that non-heated Riq1p did not readily enter the gel, perhaps remaining completely insoluble in the well. Or, it could also have been that my anti-Riq1p antibody cannot bind native Riq1p and that heating the sample denatures it, allowing more Riq1p to be detected. To control for these possibilities, I spotted split heated and non-heated samples directly onto the nitrocellulose membrane, allowing it to dry before probing the membrane as described in Section 2.8.7 (Fig. 3-4C). This showed that heating the sample at 95ºC increased protein detection, suggesting that simply entering the gel was not the problem.

As my anti-Riq1p antibody's ability to detect non-denatured Riq1p was in question, I made vectors to express HA-tagged Riq1p truncations (pGREG535-Riq1, -RiqNQ, -RiqQ, and -RiqC) so that I could use the anti-HA antibody that I had already shown capable of detecting another prion, Rnq1p, in its prion conformation (Fig. 3-4B,D). I expressed these proteins and analyzed split heated and non-heated samples by SDD-AGE (Fig. 3-4E). I was unable to detect HA-RiqNQp or HA-RiqQp, but I did observe that both HA-Riq1p and HA-RiqCp migrated in the SDD-AGE gel in high-

Figure 3-4. Biochemical detection of Riq1p aggregation *ex vivo*. (A) Differential centrifugation of Riq1p analyzed by SDS-PAGE western blot. S, supernatant; P, pellet (B) SDD-AGE of native protein sample split; sample heated at 95°C for 10 minutes (+) non-heated sample (-). Probed for HA-Rnq1p and Riq1p. HA-Rnq1p was detected with anti-HA (F-7 Sc7392) and Riq1p was detected with anti-Riq1 (PU7-4). (C) Spot-immunoblot of sample heated at 95°C for 10 minutes and non-heated sample probed for HA-Rnq1p or Riq1p. (D) SDS-PAGE western blot of HA-Riq1p truncation constructs. (E) SDD-AGE of HA-Riq1p constructs. HA-Riq1p constructs were detected using anti-HA (F-7 Sc7392). SDD-AGE protein samples were split; heated at 95°C for 10 minutes (+) and non-heated sample (-).

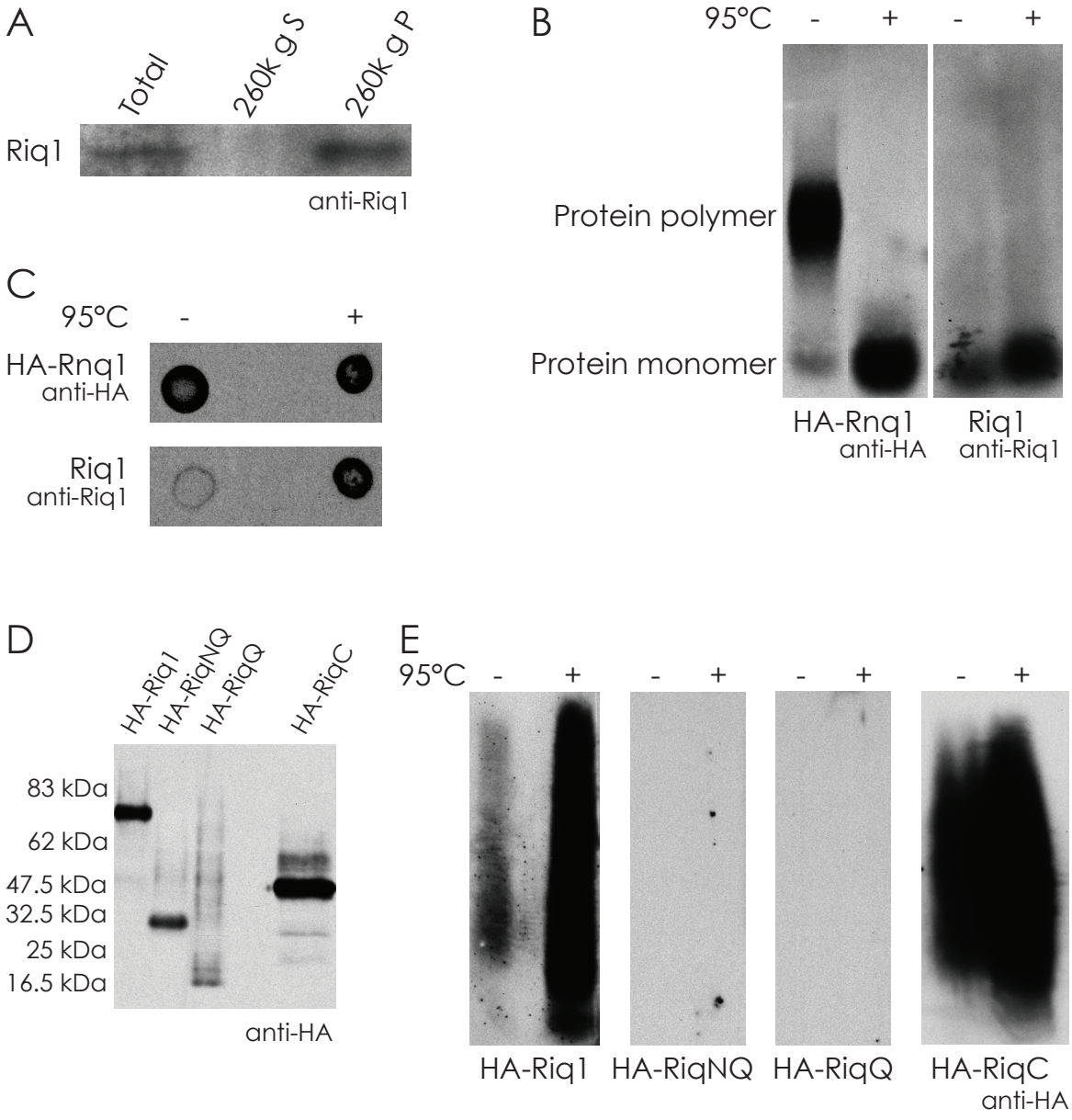
A
Total
260k g S
260k g P
Riq1
anti-Riq1
B
95°C - + - +
Protein polymer
Protein monomer
HA-Rnq1
anti-HA
Riq1
anti-Riq1
C
95°C - +
HA-Rnq1
anti-HA
Riq1
anti-Riq1
D
HA-Riq1
HA-RiqNQ
HA-RiqQ
HA-RiqC
83 kDa
62 kDa
47.5 kDa
32.5 kDa
25 kDa
16.5 kDa
anti-HA
E
95°C - + - + - + - +
HA-Riq1
HA-RiqNQ
HA-RiqQ
HA-RiqC
anti-HA

molecular weight, SDS-resistant polymers. Strangely, heating of the samples for times up to an hour did not completely denature the aggregates but, as in the case of blots probed with anti-Riq1p, increased the strength of the signal especially in the "monomer band". To my knowledge, no other yeast prion protein has been shown to have the same degree of heat resistance.

3.2.3 Riq1p aggregation *in vitro*

Thioflavin T (ThioT) is an amyloid specific dye that undergoes a shift in absorption and emission spectra when bound to amyloid (LeVine, 1993). Specifically, unbound ThioT has an absorption peak around 340nm and emits at 445nm; amyloid-bound ThioT absorbs at 440nm and has an emission peak at 480nm (Fig. 3-5A). To characterize Riq1p aggregation *in vitro* and to determine if it is amyloid, I purified HIS-tagged Sup35p and Riq1p constructs (Section 2.8.2) and performed the Thioflavin T binding assay outlined in Section 2.8.9 (Fig. 3-5C).

It is important to note that the spectrophotometer I employed lacked the excitation and emission reading filters to read at the optimal wavelengths for ThioT so I was limited to exciting the dye between 465-505nm and reading emissions between 505-555nm. As such my emission reading was at the right end of the emission spectrum.

Bearing this in mind, when I performed the assay in quadruplicate for three independent purified protein samples for each protein, I found that emissions between 505-555nm increased over time in all samples except the buffer, which lacked protein. I detected no emissions over background for protein samples incubated without ThioT (Fig. 3-5B). This may suggest Riq1p constructs are capable of forming amyloid.

Figure 3-5. Riq1p aggregation *in vitro*. (A) Fluorescence spectra of ThioT in the presence and in the absence of aggregated β(1-28) and β(1-40) amyloid peptides. Excitation spectra: 3 μM ThT in 50 mM potassium phosphate buffer, pH 6.0, in the absence (solid line) of peptide, and in the presence of equifluorescent quantities of preaggregated β(1-28), 5 μg/mL (short dashed line), or β(1-40), 10 μg/mL (long dashed line) peptide. Excitation bandpass = 5 nm; A, = 482 nm, bandpass = 10nm. There was no contribution noticeable from the peptide alone. (Adapted from Levine, 1993) (B) Quantification of ThioT fluorescence in arbitrary light emission units (505nm-555nm) for different protein constructs with no ThioT added to the sample. (C) Quantification of ThioT fluorescence in arbitrary light emission units (505nm-555nm) for different protein constructs. The microplate spectrophotometer that I employed for this assay was limited in both the specificity and ranges available for excitation and detection of emmissions. Accordingly, I was restricted to exciting the samples at 465-505nm and detecting emmissions from 505-555nm at the right end of the spectrum.

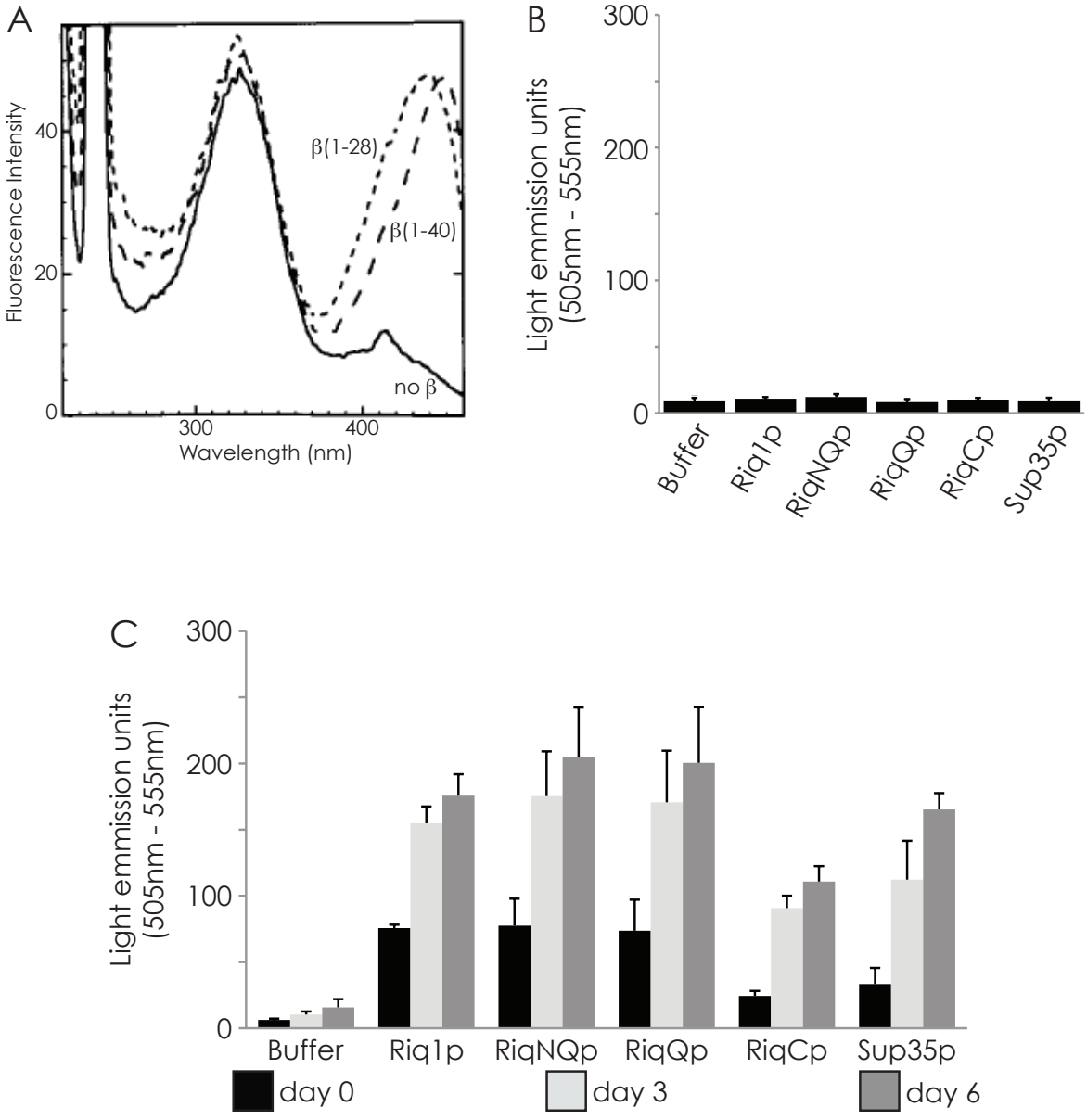
A
Fluorescence Intensity
40
20
0
300
400
Wavelength (nm)
β(1-28)
β(1-40)
no β
B
Light emmission units
(505nm - 555nm)
300
200
100
0
Buffer
Riq1p
RiqNQp
RiqQp
RiqCp
Sup35p
C
Light emmission units
(505nm - 555nm)
300
200
100
0
Buffer
Riq1p
RiqNQp
RiqQp
RiqCp
Sup35p
day 0
day 3
day 6

3.3 Prion rescue with Riq1p

3.3.1 Construction of *RIQ1-SUP35MC* strains

To more carefully examine Riq1p's ability to rescue prion behavior in strains lacking Sup35p's PrD, and to determine the specific region(s) of Riq1p that may be important to prion rescue, I made strains with different Riq1p truncations fused to the N-terminus of Sup35MC. I confirmed expression of the Riq1-Sup35MC constructs by western blot analysis, probing the membrane first with anti-Sup35p (U6) and then stripping it and reprobing with anti-Riq1p (PU7-4) (Fig. 3-6). As wild type Sup35p gave a strong signal, I diluted that protein sample by a factor of 5 leading to low endogenous Riq1p signal in second probing. Even so, some anti-Sup35p signal was not fully stripped from the membrane leading to a light Sup35p signal in the second probing. The low signal observed for full-length Riq1-Sup35MCp when probed with the anti-Sup35p antibody may be due to diminished visibility of the Sup35MC domain when in this construct.

3.3.2 Curing of *RIQ1-SUP35MC* strains

I next tested these strains for curing with 5 mM GuHCl in liquid culture as outlined in Section 2.2.6 (Fig. 3-7). Prior to curing, wild type GT17 [PSI^+][PIN^+] cells containing full-length Sup35p grew pale pink colonies as did the *RIQ1-SUP35MC* strain. *RIQNQ-* and *RIQQ-SUP35MC* colonies had a browner pigment, while both *SUP35MC* and *RIQC-SUP35MC* strains grew colonies with deep red colour. After curing, only the wild type and the *RIQ1-SUP35MC* strains gave rise to appreciably redder colonies, although when single red *RIQ1-SUP35MC* colonies were selected and restreaked, a mixture of red and pale pink colonies grew. This may suggest a high rate of spontaneous

Figure 3-6. *RIQ1-SUP35MC* construct strains. Demonstration of the expression of Rnq1-Sup35MC protein constructs in construct strains using SDS-PAGE western blot analysis. The WT sample was diluted by a factor of 5 as signal from full-length Sup35p is very strong relative to the other constructs. Sup35p-derived proteins were detected with anti-Sup35p (RU6) and Riq1p-derived proteins were detected with anti-Riq1p (PU7-4).

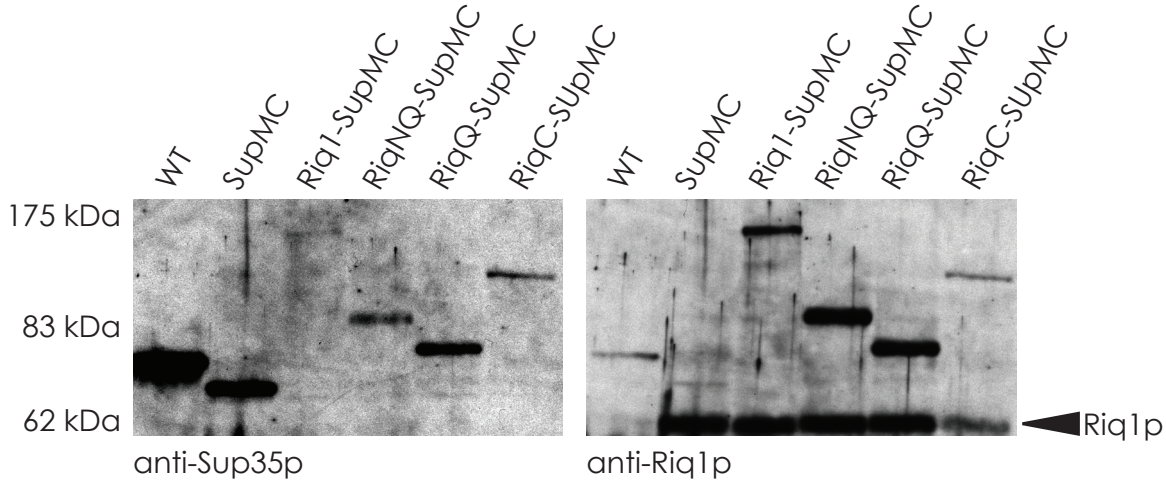
WT
SupMC
Riq1-SupMC
RiqNQ-SupMC
RiqQ-SupMC
RiqC-SUpMC
WT
SupMC
Riq1-SupMC
RiqNQ-SupMC
RiqQ-SupMC
RiqC-SUpMC
175 kDa
83 kDa
62 kDa
Riq1p
anti-Sup35p
anti-Riq1p

Figure 3-7. Curing of *RIQ1-SUP35MC* construct strains. Riq1-Sup35MC construct strains were "cured" through incubation in liquid medium containing 5 mM GuHCl. Strains were streaked out before and after "curing".

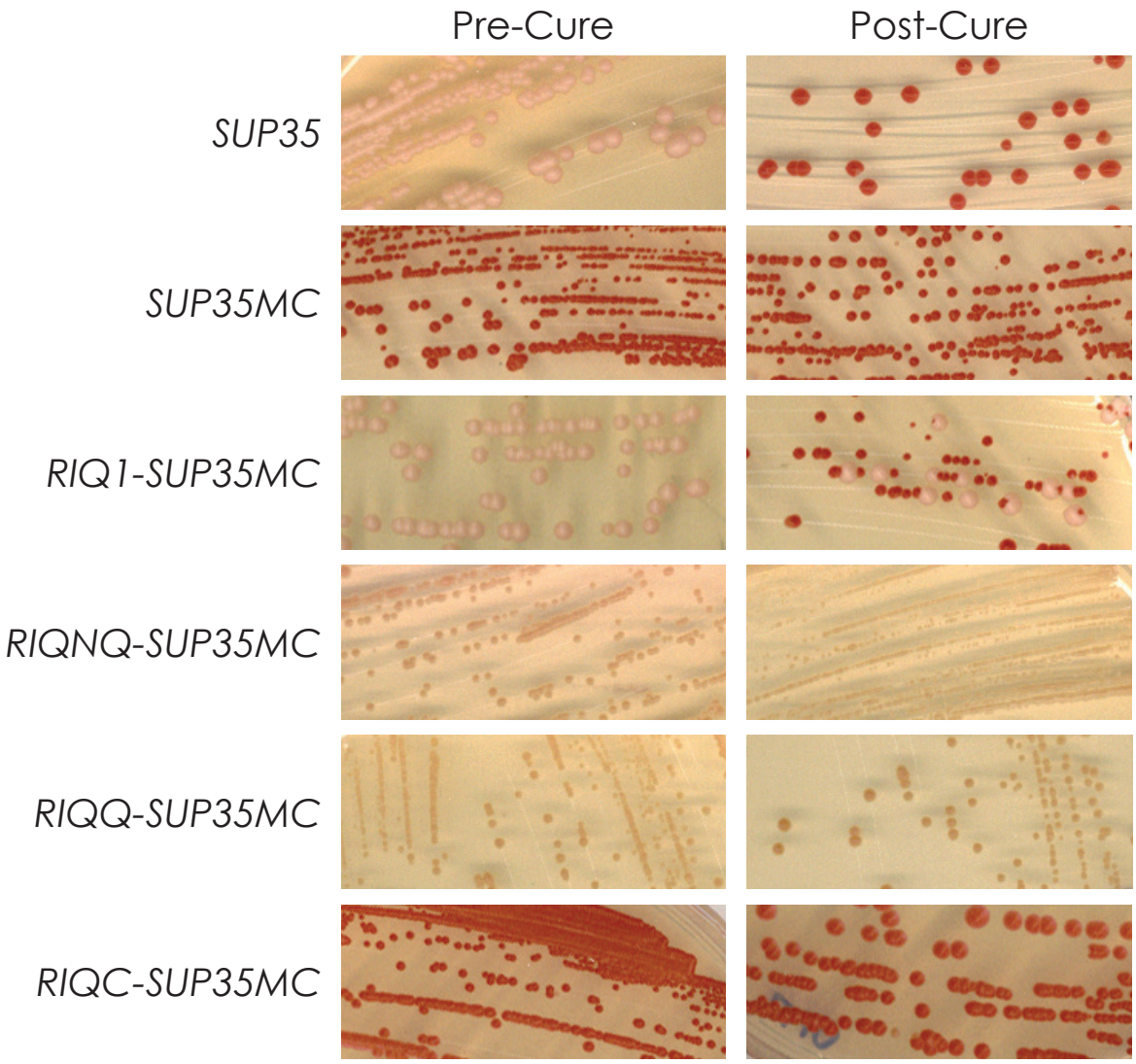
Pre-Cure
Post-Cure
SUP35
SUP35MC
RIQ1-SUP35MC
RIQNQ-SUP35MC
RIQQ-SUP35MC
RIQC-SUP35MC

reversion. Strangely, I did not observe colonies with sectored pigmentation that are typically observed in the case of unstable conformations of prion proteins. This could mean that these cells are not reverting, but my represent cells that were never actually cured. Pale pink colonies in this strain were designated [*RIQ*$^{+}$] and red colonies were designated [*riq*$^{-}$].

I then performed a nonsense-suppression assay for these strains by spotting serial dilutions of liquid culture on YEPD (growth control) and CSM-ADE plates (nonsense-suppression) (Fig. 3-8A). I found that the *RIQC-SUP35MC* strain did not grow on CSM-ADE, while [*RIQ*$^{+}$] *RIQ1-*, *RIQNQ-*, and *RIQQ-SUP35MC* strains did, although *RIQQ-SUP35MC* growth was weaker. Serial dilutions derived from single [*riq*$^{-}$] *RIQ1-SUP35MC* colonies showed significantly less growth, and that which I did observe could have been due to the spontaneous reversion or non-curing suggested earlier. These results were supported by growth curves of *RIQ1-SUP35MC* construct strains in liquid YEPD and CSM-ADE media, which showed that [*riq*$^{-}$] *RIQ1-* and *RIQQ-SUP35MC* growth was delayed in CSM-ADE (Fig. 3-8B).

3.3.3 Induction of [*RIQ*$^{+}$]

Prions can be induced through overproduction of the prion protein or just the PrD of that prion protein. To test if [*RIQ*$^{+}$] can be induced more efficiently by this method, I overproduced GFP-tagged versions of Riq1p and its truncations in the cured [*riq*$^{-}$] *RIQ1-SUP35MC* strain and measured subsequent nonsense-suppression as performed above (Fig. 3-9). [*RIQ*$^{+}$] induction efficiency was calculated as described in Section 2.2.5). Again, I observed a high rate of putative spontaneous reversion as shown in the strain expressing only GFP (~20%). Overproduction of RiqC-GFP did not induce [*RIQ*$^{+}$] any

Figure 3-8. Nonsense suppression in *RIQ1-SUP35* construct strains. (A) Nonsense suppression assay for *RIQ1-SUP35MC* construct strains. (B) Growth curves of *RIQ1-SUP35MC* construct strains over 48 hours in liquid YEPD and CSM-ADE medium. Absorbance at 600nm.

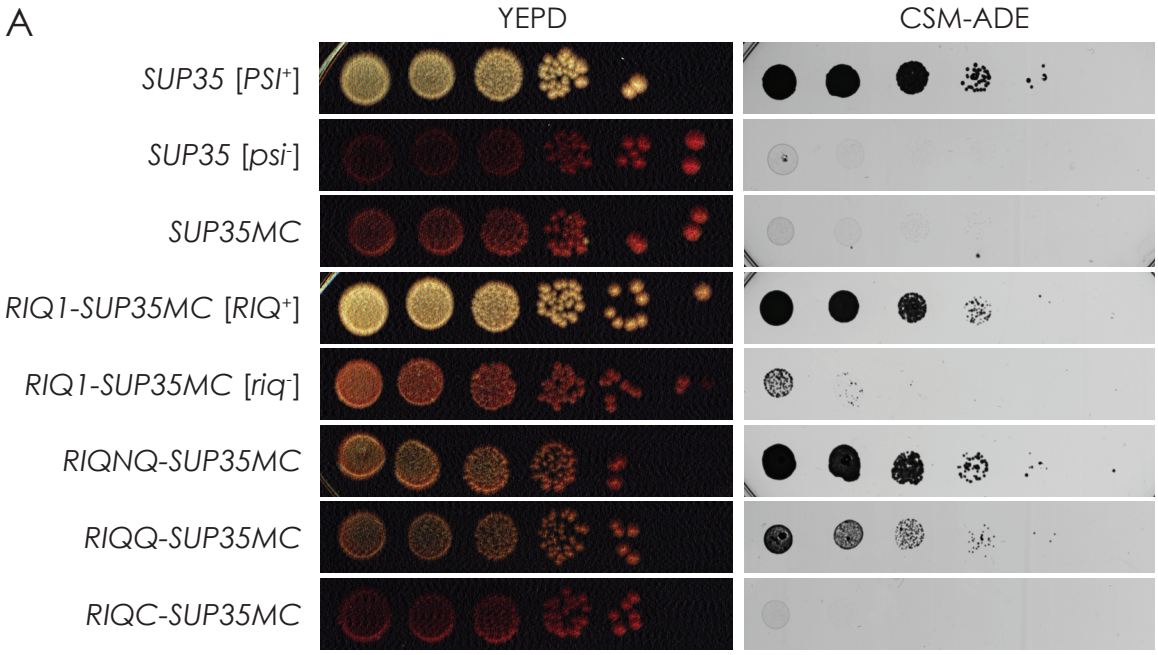
A
YEPD
CSM-ADE
SUP35 [PSI+]
SUP35 [psi-]
SUP35MC
RIQ1-SUP35MC [RIQ+]
RIQ1-SUP35MC [riq-]
RIQNQ-SUP35MC
RIQQ-SUP35MC
RIQC-SUP35MC

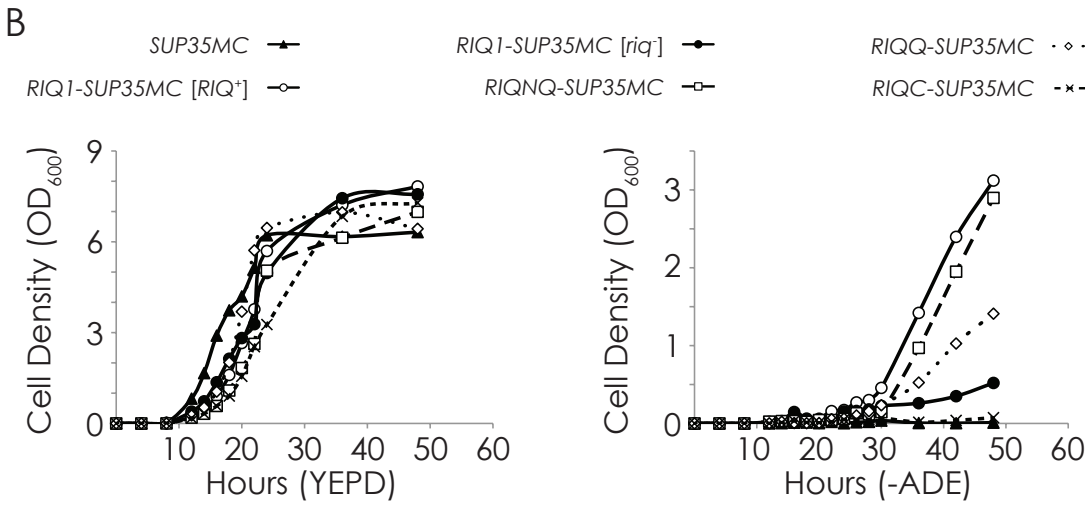
B
SUP35MC
RIQ1-SUP35MC [RIQ+]
RIQ1-SUP35MC [riq-]
RIQNQ-SUP35MC
RIQQ-SUP35MC
RIQC-SUP35MC
Cell Density (OD600)
Hours (YEPD)
Hours (-ADE)

Figure 3-9. Induction of [*RIQ*$^+$] by different Riq1p truncations. The [*riq*$^-$] strain derived from curing the [*RIQ*$^+$] *RIQ1-SUP35MC* strain were induced to become [*RIQ*$^+$] through overproduction of GFP-tagged Riq1p truncation constructs. Induction was measured by growth on CSM-ADE medium. Induction was calculated as [(cfu-ADE)/(cfu-YEPD)] × 100. Error bars represent standard error of the mean. *P< 0.05, **P< 0.01.

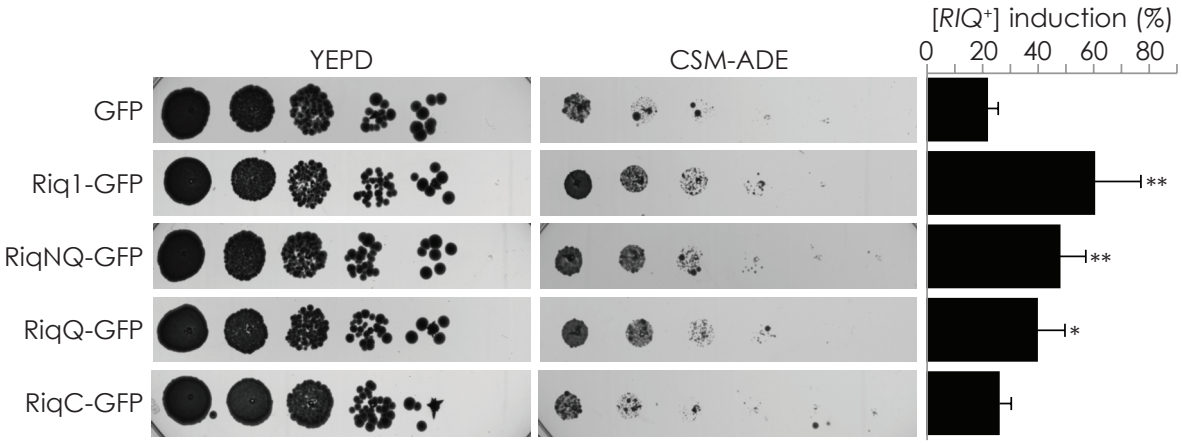
YEPD
CSM-ADE
[RIQ+] induction (%)
0 20 40 60 80
GFP
Riq1-GFP
RiqNQ-GFP
RiqQ-GFP
RiqC-GFP
**
**
*

more efficiently than GFP alone. On the other hand, full-length Riq1p, and the other truncations showed a higher rate of induction, although RiqQ-GFP overproduction did so with the lowest degree of statistical certainty.

3.4 [*RIQ*$^{+}$] and non-Mendelian inheritance

If [*RIQ*$^{+}$] is indeed a prion-linked phenotype, I would expect it to be inherited in a non-Mendelian manner. In order to investigate this, I generated *MATa* versions of my [*RIQ*$^{+}$] and [*riq*$^{-}$] strains as well as wild type [*PSI*$^{+}$] and [*psi*$^{-}$] strains. The original *MAT*α strains were transformed with empty pYES2.0, and the new *MATa* strains were transformed with empty pGREG505 prior to mating so that diploids could be auxotrophically selected for on CSM-LEU-URA medium.

Strangely, unlike wild type strains, *RIQ1-SUP35MC* strains could not be sporulated by classical methods (Fig. 3-10). The reasons for this are unclear but the morphology of *RIQ1-SUP35MC* diploids is dramatically different than that observed in wild type diploids. Haploid growth did not appear to be affected.

3.5 Discussion

At this point in its characterization the results of several experiments suggest that Riq1p may constitute a novel prion protein in *S. cerevisiae*. It localizes to punctate foci when tagged with GFP. It fractionates to the insoluble 200,000 × *g* pellet fraction and forms large SDS-resistant aggregates detectable by SDD-AGE. Most compelling, Riq1p's amino acid sequence can be used to replace Sup35p's PrD and rescue the reversibly curable nonsense-suppression phenotype normally associated with [*PSI*$^{+}$].

Not all of Riq1p's characteristics conformed to that of typical prions. While some prion variants, such as [*PIN*$^{+}$]^{low} and [*PIN*$^{+}$]$^{med.}$, are resistant to moderate levels of heat

Figure 3-10. Diploids derived from mating *RIQ1-SUP35* construct strains cannot be sporulated by normal methods. (A) Light microscopy images of alpha-factor treated wildtype and *RIQ1-SUP35* construct cells as well as *MAT*α cells generated and selected as described in Section 2.3.5. (B) Light microscopy images of diploid strains selected for growth on CSM-HIS-LYS. (C) Light microscopy images of diploid strains after subjected to the sporulation protocol outlined in Section 2.2.3.

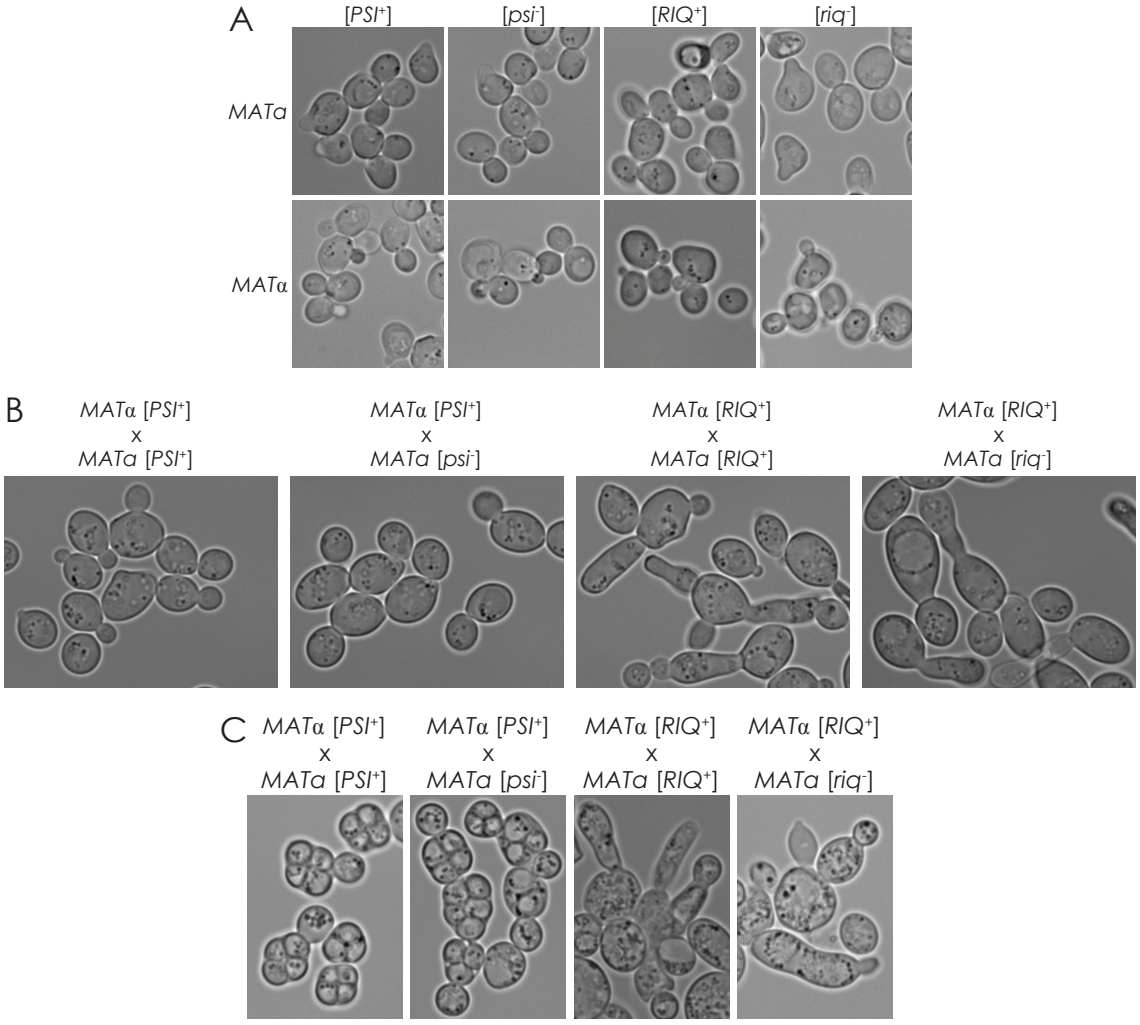
A
[PSI+]
[psi-]
[RIQ+]
[riq-]
MATa
MATα
B
MATα [PSI+] x MATa [PSI+]
MATα [PSI+] x MATa [psi-]
MATα [RIQ+] x MATa [RIQ+]
MATα [RIQ+] x MATa [riq-]
C
MATα [PSI+] x MATa [PSI+]
MATα [PSI+] x MATa [psi-]
MATα [RIQ+] x MATa [RIQ+]
MATα [RIQ+] x MATa [riq-]

(50-60°C) (Liebman et al., 2006), SDS-resistant Riq1p aggregates proved to be stable even after prolonged exposure to 95ºC temperatures (> 1h). This might indicate an extremely strong amyloid core if Riq1p proves to form amyloid or it might be that Riq1p aggregates have a unique, non-amyloid stable structure. My ThioT experiment showed that all regions of Riq1p could form amyloid *in vitro*, but this does not confirm that amyloid is formed *in vivo.* To investigate if Riq1p forms amyloid like aggregates *in vivo* I could use fast-freezing electron microscopy methods described by Kawai-Noma and colleagues to directly visualize them (2010).

How Riq1p prion might propagate efficiently is uncertain. Deletion of *HSP104* seemed to have no effect, suggesting that if it requires fragmentation by chaperones to form prion seeds, Hsp104p is not essential to the process. This also suggests that GuHCl has another mechanism to cure prions that is not mediated by Hsp104p inhibition, agreeing with the finding that [*ISP*$^+$] could be cured by GuHCl and not deletion of *HSP104* (Volkov et al., 2002; Rogoza et al., 2010). I also observed that after curing with GuHCl putative [*riq*$^-$] colonies had a very high reversion rate to [*RIQ*$^+$] of up to 20%, which is orders of magnitude higher than the spontaneous formation of prions such as [*PSI*$^+$]. It could be that its putative hyper-stable aggregate configuration contributes to the high reversion rate by being the most favorable configuration. But, as this was observed without the multi-coloured sectoring of colonies that is normally observed in colonies with unstable prions, it seems unlikely that what we observed is simple reversion. It could also be that putative cured cells are not fully cured. As it is only necessary for sufficient Sup35MC domains to be free to act in translation termination to eliminate the nonsense-suppression phenotype, it may be that GuHCl treatment somehow liberates Riq1-

Sup35MCp from, or prevents the inclusion of newly translated Riq1-Sup35MCp into, the aggregate, leaving only a slow growing, extremely stable seed. This could contribute the high number of colonies that regain the [*RIQ*$^{+}$] phenotype as a function of age. Older cells revert, while the younger cells accumulate pigment, keeping the first colony red. Then, when they are streaked out, older colonies that have reverted give rise to [*RIQ*$^{+}$] daughter cells.

Table 3-3 Summary of Riq1p prion characteristics

	Forms GFP foci	SDS-resistant particles	Binds ThioT	Rescues nonsense-suppression	Reversibly curable	Can induce [*RIQ*$^{+}$]
Riq1p (aa 1-628)	+	+++	++	++	+	++
RiqNQ (aa 1-230)	+	NA	++	++	-	++
RiqQ (aa 100-230)	-	NA	++	+	-	+
RiqC (aa 231-628)	-	+++	+	-	NA	-
Ylr177w cPrD[a] (aa 124-230)	-	+	-	+	NA	-

[a](Alberti et al., 2009)

Attempts to dissect Rnq1p to isolate its putative PrD were inconclusive overall, with only the full-length protein providing positive results for the prion criteria that I assayed (Table 3-3). Nevertheless, my results, while not lending themselves to easy interpretation, do raise some interesting questions.

First, GFP-foci formation suggests that RiqNQ is necessary and sufficient for aggregate formation *in vitro* while RiqQp alone was not. I also found [*RIQ*$^{+}$] induction is most increased by Riq1p and RiqNQp overproduction with RiqQp overproduction's

effect less statistically certain. This is interesting, as the Lindquist group showed that the amino acid sequence from 124 to 230, which includes most of RiqQp, did not have strong prion-like characteristics on its own (Alberti et al., 2009). Together, this suggests that Riq1p's prion-like characteristics are not solely dependent upon the N/Q-rich domain localized in Riq1Qp and calls into question the approach taken by Alberti *et al*.'s prion screen. It could be that good prion protein candidates were discounted because the predicted PrD's tested in the screen did not contain all the sequence necessary for prion formation. That being said, while it did form GFP foci, RiqNQp alone could not rescue [*PSI*$^{+}$] prion behavior in the *RIQNQ-SUP35MC* strain. It did cause nonsense-suppression, as did RiqQp, but this phenotype was not curable. It could be that it generated a variant not sensitive to GuHCl curing, a hypothesis that could be tested through genetic analysis of this strain back-crossed with cured [*riq*$^{-}$] *RIQ1-SUP35MC* strain to determine if the nonsense-suppression was inherited in a non-Mendelian manner. A simpler explanation is that RiqNQ- and RiqQ-Sup35MCp misfolded in a non-prion manner that did not allow Sup35MC to act in translation termination. Overall, my data suggests that RiqNQp is not sufficient to form a prion. Future characterization of Riq1p will require a number of additional truncations and mutations to find the minimal required PrD.

Another interesting question to arise from study of Riq1p truncation constructs is what is the nature of the SDS/heat-resistant aggregates observed for Riq1p and RiqCp by SDD-AGE? While, Riq1p's aggregates could have been explained as especially stable prion aggregates, the fact that RiqCp does not display any other prion-like characteristics does not fit that theory. While heating improves detection of both constructs, RiqCp is easily detectable prior to heating while Riq1p is not. Perhaps full-length Riq1p is folded

in such a manner as to conceal the epitope normally detected by the primary antibody and heating denatures the Riq1p aggregate sufficiently to expose the epitope. Meanwhile, RiqCp may not efficiently conceal the epitope. Epitope concealment may only be incidental to the large aggregates. Testing other detergents and protein denaturants may allow me to determine if this is a prion specific characteristic or if it is intrinsic to Riq1p's normal structure.

Taking all of my results into consideration, I have enough positive data to suggest that Riq1p may be a novel self-propagating amyloid. Future experiments, such as genetic analysis for prion-like inheritance patterns and *in vitro* studies for protein-only infection, are required to support this conclusion. Recently, a large scale screen showed *RIQ1* mutants have decreased starvation resistance (Davey et al., 2012). If the [*RIQ*$^{+}$] phenotype resembles a *riq1*Δ phenotype, this may serve as a tool for genetic analysis as wild type cells lacking a *RIQ1-SUP35MC* construct can be sporulated normally. If Riq1p proves to be a prion, it will call into question the effectiveness of screening for prions based only on predicted PrDs. It will also demand a reexamination of the hypothesis proposed by Halfmann and colleagues (2011), that N-rich proteins are more likely to form prions than Q-rich proteins. Methods for further Riq1p characterization will be discussed in Chapter five.

CHAPTER FOUR:

CHAPERONES AND [*PIN*$^+$] VARIANT DETERMINATION

A version of this chapter has been published.
Lancaster, D.L., C.M. Dobson, and R.A. Rachubinski. 2013. Chaperone proteins select and maintain [*PIN*$^+$] prion conformations in *Saccharomyces cerevisiae*. *JBC*. 228:1266-76.

Overview

If prions have a positive adaptive role in yeast that is situation-dependent, then the cell may have mechanisms in place to regulate the prion's role for greatest advantage. In this chapter, I report the identification of several chaperone genes that may have a role in such a mechanism and could act by giving rise to stable shifts in [*PIN*$^+$] variant when disrupted in the budding yeast *S. cerevisiae*.

The results of a genetic screen suggest that deletion of genes encoding chaperones affects Sup35p aggregation upon *de novo* formation of [*PSI*$^+$]. Further investigation reveals that it also leads to changes in a number of [*PIN*$^+$] variant-linked phenotypes. These phenotypes include [*PSI*$^+$] induction efficiency, the pattern of Rnq1-GFP localization *in vivo*, and Rnq1p aggregate size. I go on to demonstrate that these deletion-induced phenotypic changes persist upon reintroduction of the wild type chaperone gene and can be stably inherited in a non-Mendelian manner. Together, my findings are consistent with a deletion-induced shift in [*PIN*$^+$] variant. This suggests that these chaperones, several of which are primarily identified with Hsp90 activity, have a role in determining the [*PIN*$^+$] variant carried by the cell.

4.1 Screening for factors affecting aggregate morphology upon [*PSI*$^+$] induction

Although this study demonstrates a role for chaperones in prion variant determination, my initial intent was to identify genes that affect Sup35p unique aggregate morphology upon induction of [*PSI*$^+$]. When Sup35p's PrD and middle domain (Sup35NM) are tagged with GFP and overexpressed *in vivo*, their pattern of localization is dependent upon the [*PSI*$^+$] and [*PIN*$^+$] state of the cell (Zhou et al., 2001). In [*psi*$^-$][*pin*$^-$] cells Sup35NM-GFP localizes diffusely to the cytoplasm. In [*PSI*$^+$] cells it forms bright, punctate foci, and in [*psi*$^-$][*PIN*$^+$] cells they are often found to form long, filamentous

Sup35NM-GFP aggregates. These filamentous aggregates can present as rings or linear structures. Daughter cells of mothers with filamentous aggregates are frequently [*PSI*$^+$] and do not inherit the filamentous aggregates, instead displaying punctate foci (Mathur et al., 2010). Why filamentous aggregates only occur in freshly induced cells remains unclear. To identify factors that may be involved in this process, I screened for gene deletions that affected the frequency of filamentous Sup35NM-GFP aggregates.

First, Dr. Melissa Dobson generated a list of 175 candidates through a literature survey for all genes implicated in any type of amyloidosis. She also included potential interacting partners based upon the Biomolecule Interaction Network Database (BIND) and synthetic lethal interactions (Alfarano et al., 2005; Issel-Tarver et al., 2002). Strains deleted for these genes were selected from a single gene disruption library available in my lab (Giaever et al., 2002). The [*PSI*$^+$]/[*PIN*$^+$] states of these strains were determined by subjecting whole cell lysates to differential centrifugation as described in Section 2.8.9 (Fig. 4-1). The relative solubility of Sup35p and Rnq1p suggested that most strains were [*psi*$^-$][*PIN*$^+$] with the exception of *hsp104*Δ and *rnq1*Δ, which were [*psi*$^-$][*pin*$^-$]. This fundamentally agreed with other findings showing that the majority of the strains in this particular deletion library are [*PIN*$^+$] (Manogaran et al., 2009). It also meant that while these strains were [*psi*$^-$], they were ready to be induced to become [*PSI*$^+$] through overproduction of Sup35p's PrD, which made them acceptable for examining the frequency of filamentous aggregates upon *de novo* formation of [*PSI*$^+$].

I next transformed my strains with pYES2.0-Sup35NM-GFP and quantified the pattern of Sup35NM-GFP aggregation according to the protocol in Section 2.9.1.3. This was done for between 5,000-10,000 cells for each strain. The results, including aggregate

Figure 4-1. Sedimentation of Rnq1p and Sup35p in deletion strain library. Whole protein preparations were subjected to a 200,000 × g centrifugation. Upon removal of the supernatant, the pellet was resuspended in an equal volume of protein buffer. The soluble protein in the supernatant (Sol.) and the insoluble protein in the pellet (Pel.) were compared by SDS-PAGE and Western blot using antibodies against Sup35p (R25) and Rnq1p (Sondheimer and Lindquist, 2000). Results organized by GO ontology.

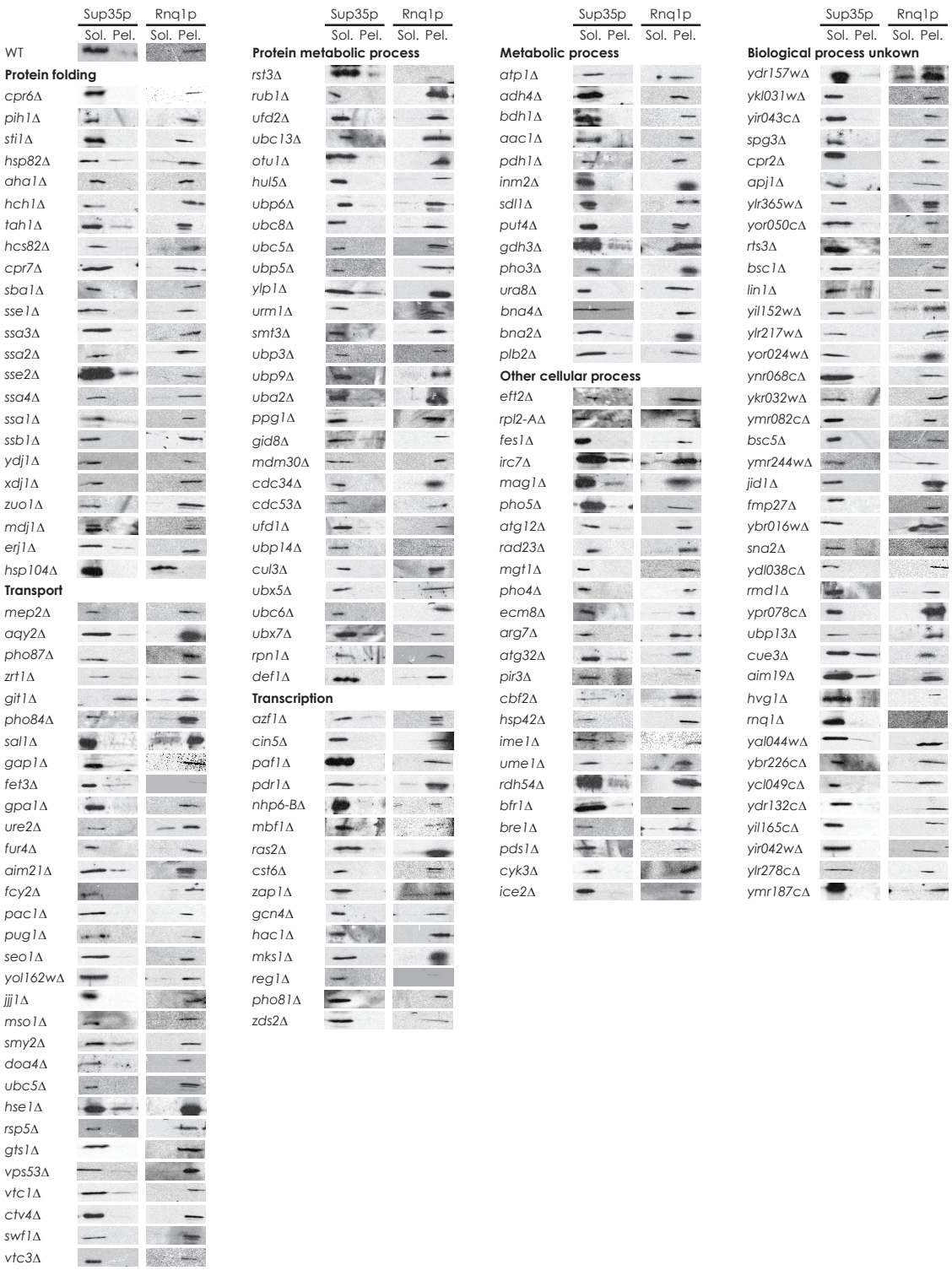
Sup35p
Rnq1p
Sol. Pel.
Sol. Pel.
WT
Protein folding
cpr6Δ
pih1Δ
sti1Δ
hsp82Δ
aha1Δ
hch1Δ
tah1Δ
hcs82Δ
cpr7Δ
sba1Δ
sse1Δ
ssa3Δ
ssa2Δ
sse2Δ
ssa4Δ
ssa1Δ
ssb1Δ
ydj1Δ
xdj1Δ
zuo1Δ
mdj1Δ
erj1Δ
hsp104Δ
Transport
mep2Δ
aqy2Δ
pho87Δ
zrt1Δ
git1Δ
pho84Δ
sal1Δ
gap1Δ
fet3Δ
gpa1Δ
ure2Δ
fur4Δ
aim21Δ
fcy2Δ
pac1Δ
pug1Δ
seo1Δ
yol162wΔ
jjj1Δ
mso1Δ
smy2Δ
doa4Δ
ubc5Δ
hse1Δ
rsp5Δ
gts1Δ
vps53Δ
vtc1Δ
ctv4Δ
swf1Δ
vtc3Δ
Protein metabolic process
rst3Δ
rub1Δ
ufd2Δ
ubc13Δ
otu1Δ
hul5Δ
ubp6Δ
ubc8Δ
ubc5Δ
ubp5Δ
ylp1Δ
urm1Δ
smt3Δ
ubp3Δ
ubp9Δ
uba2Δ
ppg1Δ
gid8Δ
mdm30Δ
cdc34Δ
cdc53Δ
ufd1Δ
ubp14Δ
cul3Δ
ubx5Δ
ubc6Δ
ubx7Δ
rpn1Δ
def1Δ
Transcription
azf1Δ
cin5Δ
paf1Δ
pdr1Δ
nhp6-BΔ
mbf1Δ
ras2Δ
cst6Δ
zap1Δ
gcn4Δ
hac1Δ
mks1Δ
reg1Δ
pho81Δ
zds2Δ
Metabolic process
atp1Δ
adh4Δ
bdh1Δ
aac1Δ
pdh1Δ
inm2Δ
sdl1Δ
put4Δ
gdh3Δ
pho3Δ
ura8Δ
bna4Δ
bna2Δ
plb2Δ
Other cellular process
eft2Δ
rpl2-AΔ
fes1Δ
irc7Δ
mag1Δ
pho5Δ
atg12Δ
rad23Δ
mgt1Δ
pho4Δ
ecm8Δ
arg7Δ
atg32Δ
pir3Δ
cbf2Δ
hsp42Δ
ime1Δ
ume1Δ
rdh54Δ
bfr1Δ
bre1Δ
pds1Δ
cyk3Δ
ice2Δ
Biological process unkown
ydr157wΔ
ykl031wΔ
yir043cΔ
spg3Δ
cpr2Δ
apj1Δ
ylr365wΔ
yor050cΔ
rts3Δ
bsc1Δ
lin1Δ
yil152wΔ
ylr217wΔ
yor024wΔ
ynr068cΔ
ykr032wΔ
ymr082cΔ
bsc5Δ
ymr244wΔ
jid1Δ
fmp27Δ
ybr016wΔ
sna2Δ
ydl038cΔ
rmd1Δ
ypr078cΔ
ubp13Δ
cue3Δ
aim19Δ
hvg1Δ
rnq1Δ
yal044wΔ
ybr226cΔ
ycl049cΔ
ydr132cΔ
yil165cΔ
yir042wΔ
ylr278cΔ
ymr187cΔ

frequency as a percentage of total cells and filamentous aggregate frequency as a percentage of total aggregate containing cells, are summarized in Table 4-1 and Fig. 4-2.

Table 4-1. Results of Sup35NM-GFP aggregation screen

Gene Ontology and p-value determined by GO Slim Mapper (p value vs. the rest of the genome)	Deleted Gene	Total foci frequency (% of viable cells containing foci)	Filamentous foci frequency (% of foci containing cells containing filamentous foci)
BY4742 (wildtype)	NA	0.454	19.8
Protein folding p value = 3.66e-44			
Hsp90 family	*CPR6*	0.089	100
	PIH1	0.344	86.8
	STI1	0.148	86.8
	HSP82	0.161	86.7
	AHA1	0.123	85
	HCH1	0.687	82
	TAH1	0.355	81.9
	HSC82	0.299	80
	CPR7	1.189	70
	SBA1	0.193	17.9
Hsp70 family	*SSE1*	1.586	95.2
	SSA3	0.953	91.1
	SSA2	0.133	85.2
	SSE2	0.317	75
	SSA4	0.229	33.3
	SSA1	0.133	0
	SSB1	0.28	0
Hsp40 family	*YDJ1*	0.069	100
	XDJ1	0.172	60
	ZUO1	0.268	41.7
	MDJ1	0.189	0
Others	*ERJ1*	0.399	0
	HSP104	< 0.01	0
Cellular protein metabolic process p value = 4.62e-19			
Post-translational protein modification	*RST3*	0.102	40
	RUB1	0.49	20

P value = 1.18e-20	*UFD2*	0.447	17.2
	UBC13	0.392	17
	OTU1	0.556	16.3
	HUL5	0.532	15.4
	UBP6	0.418	13.4
	UBC8	0.451	11.3
	UBC5	0.512	8.8
	UBP5	0.494	8.8
	YLP1	0.25	4.5
	URM1	0.563	3.9
	SMT3	0.563	3.8
	UBP3	0.449	2.5
	UBP9	0.489	2.1
	UBA2	0.58	2.0
	PPG1	0.162	0
Ubiquitin-dependent protein catabolic process p value = 1.92e-19	*GID8*	0.08	66.7
	MDM30	0.206	66.7
	CDC34	0.463	21.4
	CDC53	0.472	16.8
	UFD1	0.389	13.9
	UBP14	0.533	13.6
	CUL3	0.357	10.9
	UBX5	0.53	10.4
	UBC6	0.473	5.5
	UBX7	0.406	5.5
	RPN1	0.444	3.2
	DEF1	<0.01	0
Transcription (DNA-dependent) p value = 4.40e-13			
	AZF1	0.179	100
	CIN5	0.058	100
	PAF1	0.021	100
	PDR1	1.74	69.4
	NHP6-B	0.129	50
	MBF1	0.123	42.9
	RAS2	0.336	37.5
	CST6	0.176	33.3
	ZAP1	0.106	28.6
	GCN4	0.522	21
	HAC1	0.478	14.5
	MKS1	1.613	3.1
	REG1	0.296	0

	PHO81	< 0.01	0
	ZDS2	< 0.01	0
Transport **p value = 1.53e-21**			
Transport *p value – 2.14e-14*	*MEP2*	0.256	100
	AQY2	0.976	95.8
	PHO87	0.181	80
	ZRT1	0.418	75
	GIT1	0.439	60
	PHO84	0.735	41.2
	SAL1	0.263	33.3
	GAP1	0.074	33.3
	FET3	0.397	28.6
	GPA1	0.355	21.9
(*Known prion protein*)	*URE2*	0.309	20
	FUR4	0.451	5.6
	AIM21	0.365	3.6
	FCY2	0.308	0
	PAC1	0.077	0
	PUG1	< 0.01	0
	SEO1	0.299	0
	YOL162w	0.043	0
Vesicle-mediated transport *p value = 1.53e-10*	*JJJ1*	0.093	100
	MSO1	0.152	42.9
	SMY2	0.065	25
	DOA4	0.468	13.2
	UBC5	0.512	8.8
	HSE1	0.387	8.4
	RSP5	0.563	3.1
	GTS1	0.029	0
	VPS53	< 0.01	0
Vacuole fusion *p value = 7.87e-9*	*VTC1*	0.059	100
	CTV4	0.235	97.1
	SWF1	1.117	90
	VTC3	0.676	84.2
Metabolic process **p value = 0.00449**			
Generation of precursor metabolites and energy	*ATP1*	2.207	81.3
	ADH4	0.134	60

p value = 0.00025	*BDH1*	0.209	35.4
	AAC1	0.303	25
	PDH1	0.297	16.7
Cellular carbohydrate metabolic process	*INM2*	0.299	32.4
Cellular amino acid and	*SDL1*	1.796	81
derivative metabolic process	*PUT4*	0.666	60
p value = 0.00044	*GDH3*	0.231	21.6
Cellular aromatic compound	*PHO3*	0.53	77.8
metabolic process	*URA8*	0.618	64
Vitamin metabolic process	*BNA4*	0.008	100
	BNA2	1.046	64.7
Cellular lipid metabolic process	*PLB2*	0.213	0
Other cellular process **p value = 0.00663**			
Translation	*EFT2*	0.168	66.7
	RPL21-A	0.025	54.2
	FES1	0.067	0
Cellular homeostasis	*IRC7*	0.189	80
Response to stress	*MAG1*	0.244	42.9
p value = 2.94e-7	*PHO5*	0.259	16.7
	ATG12	0.444	6.7
	RAD23	0.511	6.5
	MGT1	<0.01	0
	PHO4	0.08	0
Cell wall organization	*ECM8*	0.583	65.6
p value = 1.90e-6	*ARG7*	0.207	33.3
	ATG32	0.291	24.4
	PIR3	0.019	0
Cytoskeleton organization	*CBF2*	0.478	0
	HSP42	0.16	0
Meiosis	*IME1*	0.043	100
p value = 4.63e-9	*UME1*	0.202	80
	RDH54	0.269	50.1
	BFR1	0.15	20
	BRE1	0.484	14.6
	PDS1	0.363	7.1
Cytokinesis	*CYK3*	0.116	100

ER inheritance	*ICE2*	2.759	91.7
Biological Process Unknown p value = N/A			
	YDR157w	0.134	100
	YKL031w	0.587	100
	YIR043c	1.227	94.7
	SPG3	0.296	87.5
	CPR2	0.4	86.7
	APJ1	0.795	81.8
	YLR365w	0.615	80
	YOR050c	2.071	72.4
	RTS3	0.189	70
	BSC1	0.324	66.7
	LIN1	0.159	66.7
	YIL152w	0.43	66.7
	YLR217w	1.246	65
	YOR024w	0.934	64.2
	YNR068c	0.927	63.3
	YKR032w	0.184	50
	YMR082c	0.166	50
	BSC5	0.895	49
	YMR244w	0.209	45.7
	JID1	0.726	41.2
	FMP27	0.098	37.5
	YBR016w	1.042	37.5
	SNA2	0.174	34.6
	YDL038c	0.192	33.3
	RMD1	0.394	15.6
	YPR078c	0.726	7.1
	UBP13	0.379	2
	CUE3	0.356	0
	AIM19	0.306	0
	HVG1	< 0.01	0
(*Known prion protein*)	*RNQ1*	< 0.01	0
	YAL044w-A	0.047	0
	YBR226c	< 0.01	0
	YCL049c	< 0.01	0
	YDR132c	0.056	0
	YIL165c	0.064	0
	YIR042c	0.05	0
	YLR278c	< 0.01	0
	YMR187c	0.051	0

Figure 4-2. Summary of genetic screen for factors affecting prion aggregation. (A) Maximum intensity projections of typical cytologically detectable localization of Sup35NM-GFP. Localization patterns depend upon prion background. Bar, 5 μm. (B) Gene deletions affecting Sup35NM-GFP aggregate frequency arranged by GO ontology. (C) Gene deletions affecting filamentous Sup35NM-GFP aggregate frequency arranged by GO ontology. (D) Chaperone gene deletions affecting filamentous Sup35NM-GFP aggregate frequency arranged by chaperone family. Numbers indicate the number of gene deletions assigned to each category based on results listed in Table 4-1.

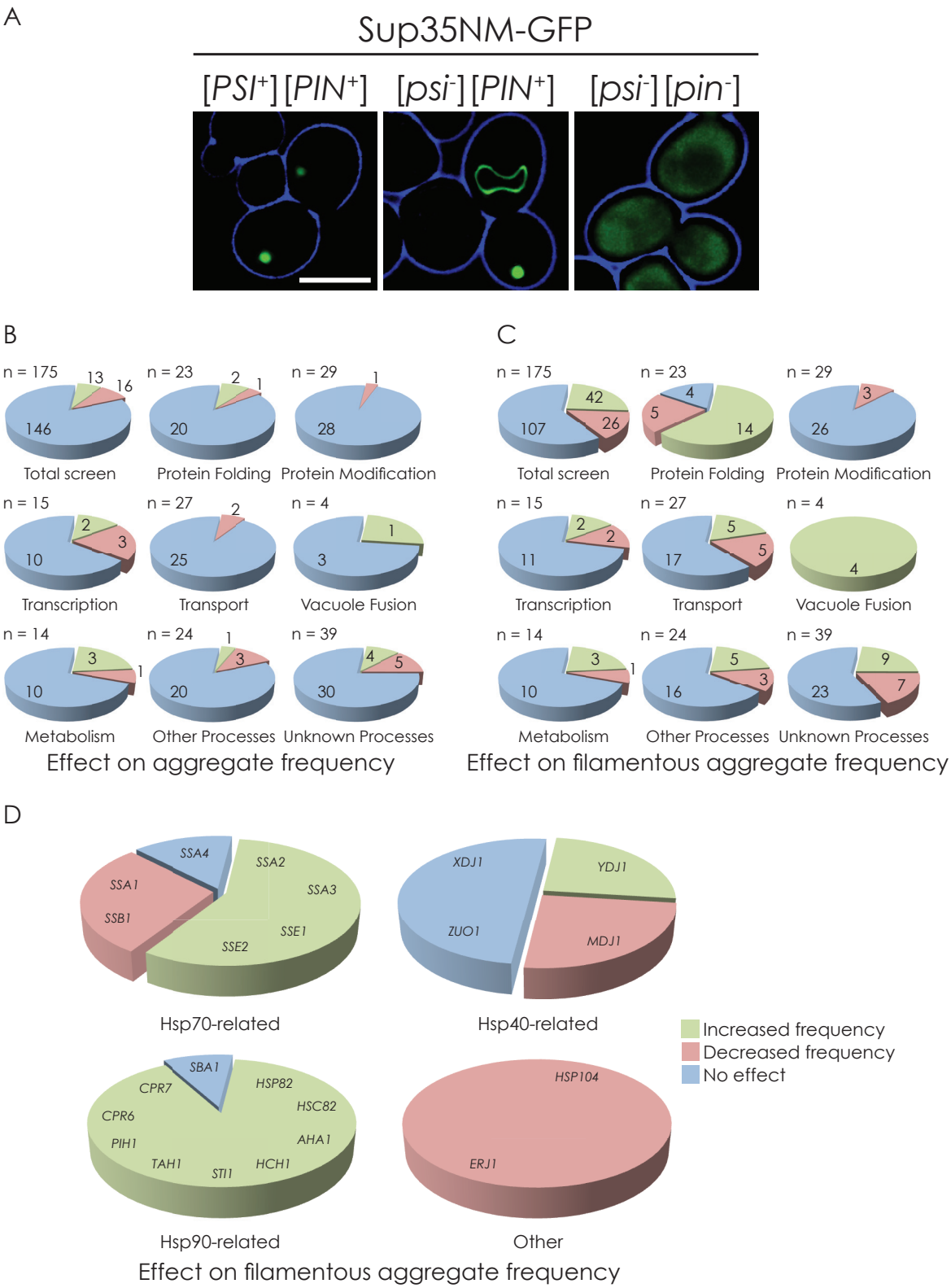
A
Sup35NM-GFP
[PSI+] [PIN+]
[psi-] [PIN+]
[psi-] [pin-]
B
n = 175
146
13
16
Total screen
n = 23
20
2
1
Protein Folding
n = 29
28
1
Protein Modification
n = 15
10
2
3
Transcription
n = 27
25
2
Transport
n = 4
3
1
Vacuole Fusion
n = 14
10
3
1
Metabolism
n = 24
20
1
3
Other Processes
n = 39
30
4
5
Unknown Processes
Effect on aggregate frequency
C
n = 175
107
42
26
Total screen
n = 23
5
4
14
Protein Folding
n = 29
26
3
Protein Modification
n = 15
11
2
2
Transcription
n = 27
17
5
5
Transport
n = 4
4
Vacuole Fusion
n = 14
10
3
1
Metabolism
n = 24
16
5
3
Other Processes
n = 39
23
9
7
Unknown Processes
Effect on filamentous aggregate frequency
D
SSA4
SSA2
SSA3
SSA1
SSB1
SSE1
SSE2
Hsp70-related
XDJ1
YDJ1
ZUO1
MDJ1
Hsp40-related
Increased frequency
Decreased frequency
No effect
SBA1
CPR7
HSP82
HSC82
CPR6
AHA1
PIH1
TAH1
HCH1
STI1
Hsp90-related
HSP104
ERJ1
Other
Effect on filamentous aggregate frequency

These results show that few deletions significantly altered the frequency of aggregation overall (Fig 4-2B) but a higher proportion altered the frequency of filamentous aggregates (Fig. 4-2C). Around 61% of gene deletions had no effect upon filamentous aggregate frequency, while ~25% increased it above 70% and ~14% decreased it below 2.0%. Wild type, BY4742 had a filamentous aggregate frequency of 19.8% ± 8.6%. When I categorized each deletion strain by GO ontology using the GO Slim mapper tool provided by the *Saccharomyces cerevisiae* genome database (Issel-Tarver et al., 2002), I observed some noteworthy trends. First, each of the four genes linked to vacuole fusion included in this screen (*VTC1*, *VTC3*, *CTV4*, and *SWF1*) gave rise to increased filamentous aggregate frequency. Next, a high proportion of genes encoding chaperone proteins increased filamentous foci frequency when deleted (65%) as opposed to the proportion of all deletions (25%). And finally, when the chaperone encoding genes were further divided into the chaperone sub-families Hsp40, Hsp70, and Hsp90, I saw that Hsp90-related gene deletions in particular had a strong effect, with 9 of 10 deletions increasing filamentous frequency, the only exception being *sba1*Δ (Fig. 4-2D). Although many chaperones are known to act upon prion proteins, little evidence has been provided directly implicating Hsp90. For this reason, I chose to focus my investigation upon the effects of Hsp90-related deletions.

4.2 Chaperone gene deletions affect [*PSI*$^+$] induction efficiency

As filamentous Sup35NM-GFP aggregates are linked to *de novo* formation of [*PSI*$^+$], I thought that my chaperone gene deletions might have an effect on [*PSI*$^+$] induction efficiency. Unfortunately, the gene deletion library that I employed for my primary screen did not have an effective [*PSI*$^+$] reporter. I therefore regenerated my

deletion strains of interest in the following strains: L1943 (WT [*PIN*$^{+}$]^{low}), L1945 (WT [*PIN*$^{+}$]$^{med.}$), L1749 (WT [*PIN*$^{+}$]^{high}), and GT17 (WT [*pin*$^{-}$]) (Table 2-10). Each of these strains were confirmed to be [*psi*$^{-}$] and carried a nonsense-suppression reporting mutation (*ADE1-14* UGA). Using theses strains, I was able to detect [*PSI*$^{+}$] colonies by growth on medium lacking adenine and by the depletion of a red pigment normally consumed in adenine biosynthesis (Fig. 1-5). Also, by testing my deletions in backgrounds containing different [*PIN*$^{+}$] variants, I was able to investigate the possibility that my deletions may have [*PIN*$^{+}$]-dependent effects.

These strains were subjected to the nonsense-suppression assay outlined in Section 2.2.5 (Fig. 4-3). In brief, I overproduced Sup35NM-GFP using the galactose driven expression vector pYES2.0-Sup35NM-GFP and quantified colony-forming units (cfu) on CSM-ADE medium plates relative to cfu on CSM medium plates. From this I calculated [*PSI*$^{+}$] induction efficiency as [cfu (CSM-ADE)/cfu (CSM)] × 100. The relative strength of the induced [*PSI*$^{+}$] variants was not factored into my calculations of [*PSI*$^{+}$] induction efficiency. Only the number of colonies, not their size or pigmentation, was considered. ADE-competent colonies were confirmed to be prion-linked by the prion curing assay described in Section 2.2.6, which showed them to lose ADE-competence after treatment with GuHCl (Fig. 4-4). Deletion strains generated in a WT [*pin*$^{-}$] parental strain showed no growth on CSM-ADE medium but had normal growth on CSM medium. This suggested that they were could not be induced to become [*PSI*$^{+}$]. From this I could conclude that none of my deletion strains eliminated [*PSI*$^{+}$] dependence on [*PIN*$^{+}$] for efficient induction.

Figure 4-3. The effect of chaperone gene deletion upon [*PSI*$^{+}$] induction efficiency in relation to [*PIN*$^{+}$] variants. (A) Nonsense suppression assay. Chaperone gene deletions were generated in [*psi*$^{-}$][*PIN*$^{+}$]$^{low/med./high}$ strains, which were then induced to become [*PSI*$^{+}$] by overproduction of Sup35NM-GFP. Normal growth is shown on CSM medium and [*PSI*$^{+}$]-dependent growth is shown on -ADE medium. (B) [*PSI*$^{+}$] induction efficiency as determined by quantification of the nonsense suppression assay, expressing average -ADE cfu as a percentage of average CSM cfu. Error bars represent standard error of the mean. Student's t-tests were performed to compare [*PSI*$^{+}$] induction efficiency of deletion strains with that of their parental wildtype strain, *P< 0.05, **P< 0.01, ***P<0.001.

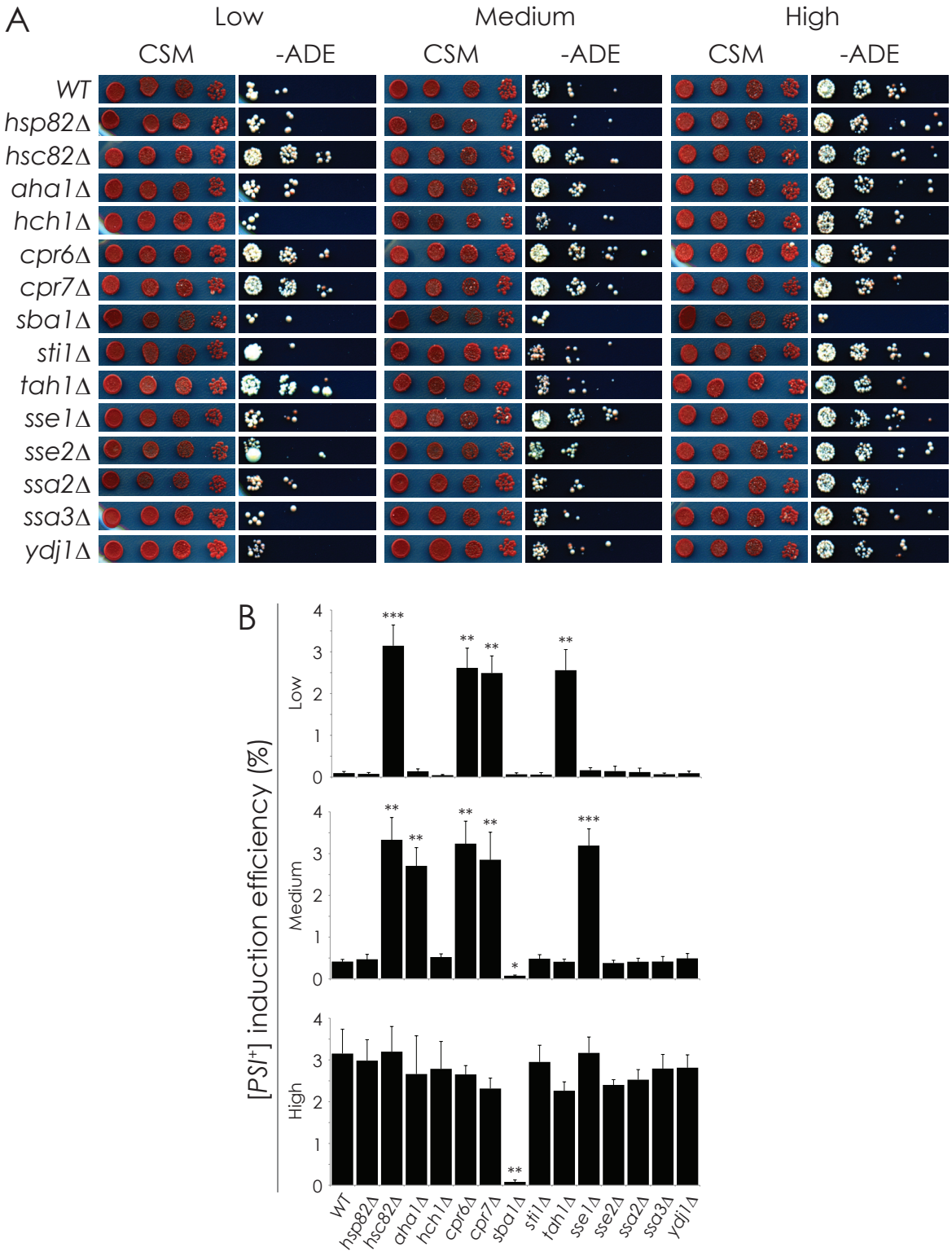
A
Low
Medium
High
CSM
-ADE
WT
hsp82Δ
hsc82Δ
aha1Δ
hch1Δ
cpr6Δ
cpr7Δ
sba1Δ
sti1Δ
tah1Δ
sse1Δ
sse2Δ
ssa2Δ
ssa3Δ
ydj1Δ
B
[PSI+] induction efficiency (%)
Low
Medium
High
0
1
2
3
4
*
**
***
WT
hsp82Δ
hsc82Δ
aha1Δ
hch1Δ
cpr6Δ
cpr7Δ
sba1Δ
sti1Δ
tah1Δ
sse1Δ
sse2Δ
ssa2Δ
ssa3Δ
ydj1Δ

Figure 4-4. Confirmation of [*PSI*$^+$] induction in haploid deletion strains. Putative [*PSI*$^+$] colonies from Fig. 4-3 were streaked on YEPD medium containing 3 mM GuHCl and then re-streaked out on CSM and CSM-ADE media to confirm effective prion curing. Red pigment on CSM and lack of growth on CSM-ADE suggests [*PSI*$^+$] was effectively cured, signifying that growth of induced colonies on CSM-ADE medium observed in Fig. 4-3 was prion related and suggesting that they were [*PSI*$^+$].

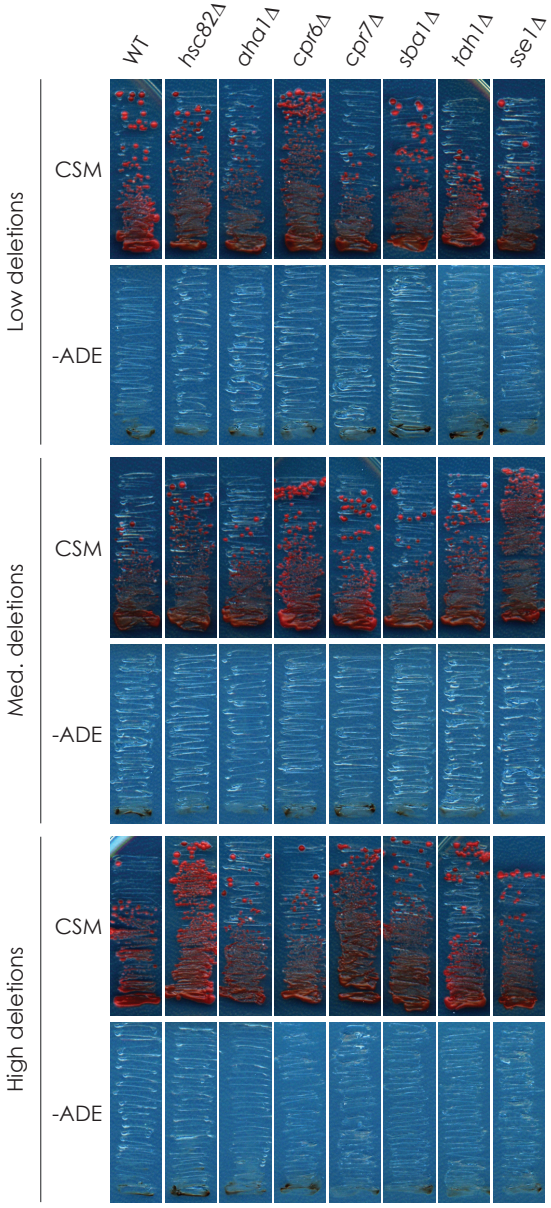
WT
hsc82Δ
aha1Δ
cpr6Δ
cpr7Δ
sba1Δ
tah1Δ
sse1Δ
Low deletions
CSM
-ADE
Med. deletions
CSM
-ADE
High deletions
CSM
-ADE

WT [*PIN*$^+$]^{low}, WT [*PIN*$^+$]$^{med.}$, and WT [*PIN*$^+$]^{high} were found to form [*PSI*$^+$] at relative low, medium, and high efficiencies as expected (Bradley et al., 2002). Interestingly, several of my deletion strains generated in these backgrounds had significantly different [*PSI*$^+$] induction efficiencies. Deletion of *HSC82*, *CPR6, CPR7*, and *TAH1* from WT [*PIN*$^+$]^{low} as well as *HSC82*, *AHA1*, *CPR6, CPR7*, and *SSE1* in WT [*PIN*$^+$]^{medium} strains increased growth on CSM-ADE medium to levels significantly higher than WT [*PIN*$^+$]^{low} and WT [*PIN*$^+$]^{medium} but not significantly different from WT [*PIN*$^+$]^{high}. Deletion of these same genes from WT [*PIN*$^+$]^{high} did not affect [*PSI*$^+$] induction efficiency. Conversely, deletion of *SBA1* in WT [*PIN*$^+$]^{medium} and WT [*PIN*$^+$]^{high} backgrounds decreased the efficiency of [*PSI*$^+$] induction to levels matching WT [*PIN*$^+$]^{low}, but did not significantly decrease the efficiency of [*PSI*$^+$] induction when deleted in WT [*PIN*$^+$]^{low}.

It was possible that changes in [*PSI*$^+$] induction efficiency were due to a plasmid-dependent nonsense-suppression effect. I controlled for this in two ways. First, by repeating the nonsense-suppression assay for all strains, only overproducing GFP alone using pYES2.0-GFP. This was ineffective at inducing [*PSI*$^+$], leading to no colonies on CSM-ADE medium, suggesting that the GFP tag and the pYES2.0 plasmid backbone were not responsible for altering [*PSI*$^+$] induction efficiency. Second, I performed a plasmid retention assay for all strains, as well as for ADE+ colonies for all strains, as described in Section 2.3.4. If a strain were to have lost the plasmid at a higher rate than others, then that could have reduced [*PSI*$^+$] induction efficiency. Conversely, higher than average plasmid retention could have led to greater [*PSI*$^+$] induction. I found that both wild type and deletion strains retained plasmid at levels between 90-95% and that this

rate of retention remained consistent even when examining exclusively ADE-competent colonies. Together these results confirmed that the ADE-competent colonies were prion-linked.

Nearly all strains gave rise to [*PSI*$^+$] colonies with varied levels of red pigment, ranging from pink to almost white (Fig. 4-3A). This implied that a mixture of [*PSI*$^+$] variants was induced. The only exception was the [*PIN*$^+$]^{low} strain deleted for *TAH1* whose colonies were almost entirely white in color after induction, suggesting that its induced [*PSI*$^+$] colonies may all carry a stronger [*PSI*$^+$] variant.

The most interesting aspect of these results is that my chaperone gene deletions altered [*PSI*$^+$] induction efficiencies in a [*PIN*$^+$]-variant dependent manner. These levels were consistent with [*PIN*$^+$] variants other than the one originally present in the parental wild type strain. This led me to suspect that chaperone deletions may affect [*PSI*$^+$] induction efficiency by altering [*PIN*$^+$] variant.

4.3 Chaperone gene deletions affect the pattern of Rnq1-GFP localization *in vivo*

If the [*PIN*$^+$] variant carried by my strains had been altered by chaperone gene deletion, then it was likely that other variant-specific phenotypes would have also been affected. One of these phenotypes is the localization pattern of overproduced Rnq1-GFP in the cell. [*PIN*$^+$]^{high} strains form multiple Rnq1-GFP foci per cell, while [*PIN*$^+$]^{medium} and [*PIN*$^+$]^{low} strains mostly form only a single Rnq1-GFP focus (Bradley and Liebman, 2003). I overexpressed Rnq1-GFP using pYES2.0-Rnq1-GFP and found that, for the most part, the number of foci per foci containing cell observed in my strains correlated with their [*PSI*$^+$] induction efficiency levels (Fig. 4-5). Specifically, *hsc82*Δ, *cpr6*Δ, *cpr7*Δ, and *tah1*Δ deletion strains in [*PIN*$^+$]^{low}; and *hsc82*Δ, *aha1*Δ, *cpr6*Δ, *cpr7*Δ, and

Figure 4-5. The effect of chaperone gene deletion upon the pattern of Rnq1-GFP localization in relation to [*PIN*$^+$] variants. (A) Typical patterns of Rnq1-GFP localization in different [*PIN*$^+$] variant backgrounds. (B) Rnq1-GFP was overproduced in deletion strains of interest and the frequency of multiple Rnq1-GFP foci in foci-containing cells was calculated as a percentage. Error bars represent standard error of the mean. Student's t-tests were performed to compare multiple Rnq1-GFP foci frequency of each deletion strain with that of its parental wildtype strain. For example the [*PIN*$^+$]^{low} strain deleted for *HSC82* was compared to wildtype [*PIN*$^+$]^{low}, **P< 0.01, ***P< 0.001.

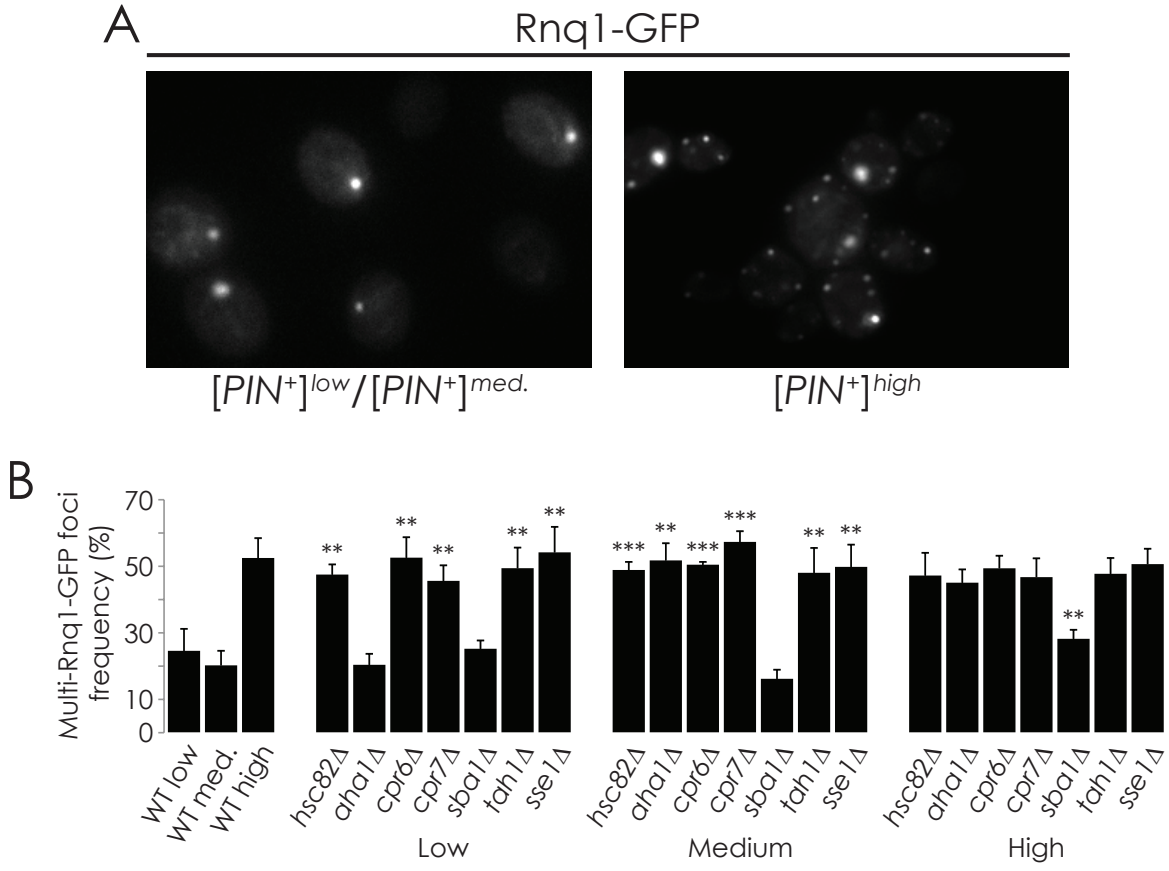
A
Rnq1-GFP
[PIN+]low/[PIN+]med.
[PIN+]high
B
Multi-Rnq1-GFP foci frequency (%)
70
50
30
10
0
WT low
WT med.
WT high
hsc82Δ
aha1Δ
cpr6Δ
cpr7Δ
sba1Δ
tah1Δ
sse1Δ
Low
Medium
High

*sse1*Δ in [*PIN*$^+$]$^{med.}$ all showed a higher frequency of multiple Rnq1-GFP foci (~50%) compared to the wild type strains in which they were generated (~25%). *Sba1*Δ in [*PIN*$^+$]^{high} decreased the frequency of multiple Rnq1-GFP foci per cell to [*PIN*$^+$]$^{low/med.}$ levels. Exceptions to the trend were deletion of *TAH1* in [*PIN*$^+$]$^{med.}$ and *SSE1* in [*PIN*$^+$]^{low}, both of which increased multiple Rnq1p-GFP foci frequency to [*PIN*$^+$]^{high} levels although they did not display any changes in [*PSI*$^+$] induction efficiency.

4.4 Chaperone inhibition affects the pattern of Rnq1-GFP localization *in vivo*

As several of the proteins encoded by these genes have been implicated in Hsp90 chaperone activity, I tested the effect of inhibiting Hsp90 ATPase activity with geldanamycin (GA) or NVP-AUY-922 (NVP) upon RNQ1-GFP aggregate morphology (Whitesell et al., 1994; Brough et al., 2008) (Fig. 4-6). I found that when cultured in CSM-URA liquid medium with 10 μM GA or 200 μM NVP, WT [*PIN*$^+$]^{low} and WT [*PIN*$^+$]^{medium} displayed an increased frequency of multiple Rnq1-GFP foci relative to the DMSO control treatment. Multiple Rnq1-GFP foci in treated WT [*PIN*$^+$]^{high} only increased by the same amount seen in DMSO treated cells. Upon transfer to a medium lacking chemical inhibitors, the relative change in frequency persisted for GA-treated cells, but not for NVP treated cells.

Cyclosporin A (CsA) is a chemical inhibitor of Cpr6p and Cpr7p peptidyl-prolyl isomerase activity (Dolinski et al., 1997). Treatment cultures in CSM-URA liquid medium with 20 μM CsA had similar effects as GA treatment, with [*PIN*$^+$]^{low} and [*PIN*$^+$]^{medium} cells increasing multiple RNQ1-GFP foci frequency relative to DMSO treatment, and with the increase persisting after removal of CsA (Fig. 4-6). These results specifically implicate peptidyl-prolyl isomerase activity.

Figure 4-6. The effect of chaperone inhibition upon the pattern of Rnq1-GFP localization in relation to [*PIN*$^+$] variants. Rnq1-GFP was overproduced in the presence of Hsp90 inhibitors Geldanamycin (GA) and NVP-AUY-922 (NVP) or Cyclosporin A (CsA), an inhibitor of Cpr6p/Cpr7p peptidyl-prolyl isomerase activity. The frequency of multiple Rnq1-GFP foci in foci-containing cells was calculated as a percentage for cells during treatment (A) and after treatment (B). Error bars represent standard error of the mean. Student's t-tests were performed to compare inhibitor-treated strains to DMSO-treated control strains, **P< 0.01, ***P< 0.001.

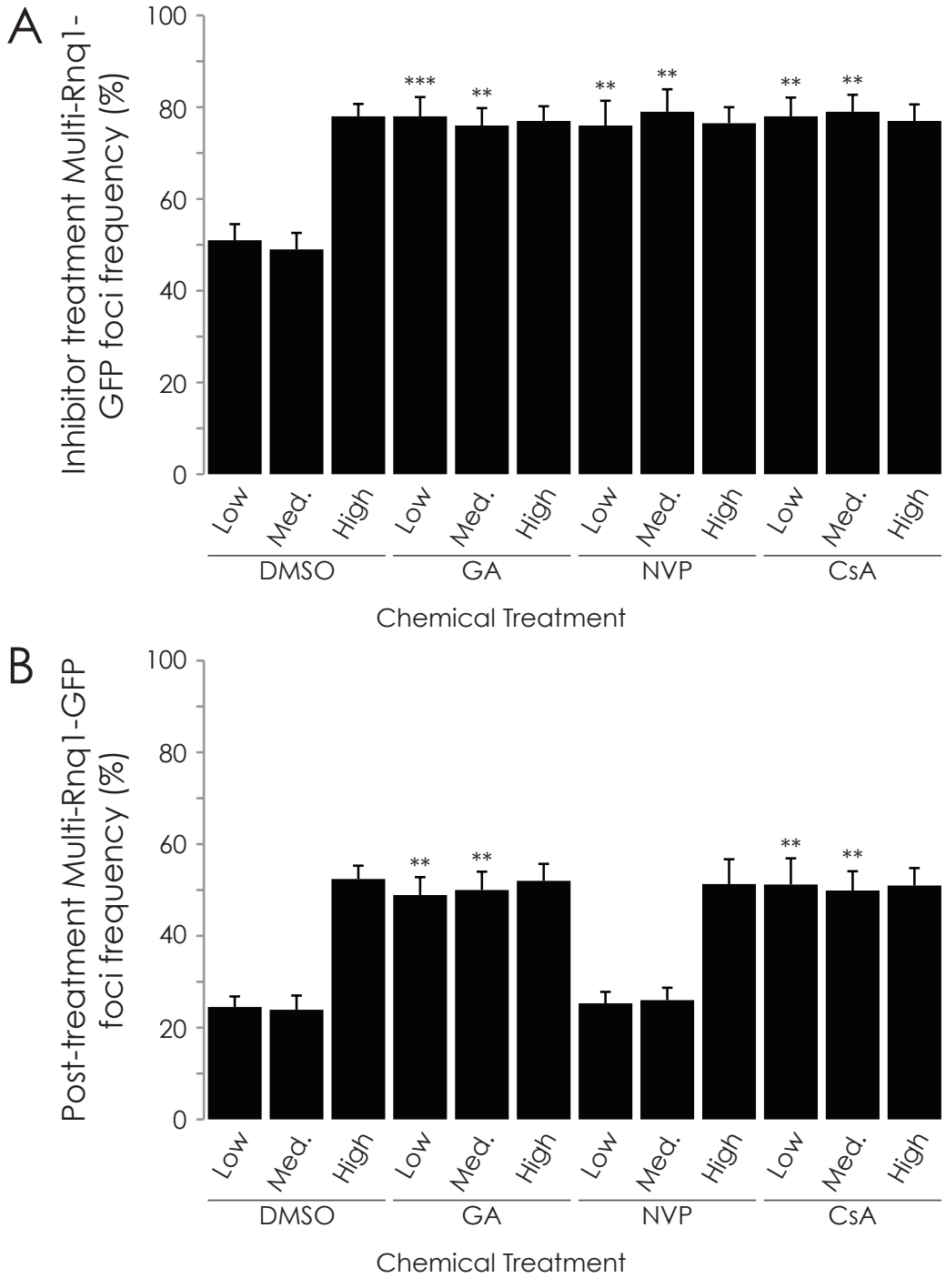
A
Inhibitor treatment Multi-Rnq1-GFP foci frequency (%)
100
80
60
40
20
0
***
**
**
**
**
**
Low
Med.
High
DMSO
GA
NVP
CsA
Chemical Treatment
B
Post-treatment Multi-Rnq1-GFP foci frequency (%)
100
80
60
40
20
0
**
**
**
**
Low
Med.
High
DMSO
GA
NVP
CsA
Chemical Treatment

4.5 Chaperone gene deletions affect HA-Rnq1p aggregate size

Another [*PIN*$^+$] variant-linked phenotype that I investigated was the size of Rnq1p prion amyloid aggregates. Using SDD-AGE (outlined in Section 2.8.6), it has been shown that [*PIN*$^+$] variants containing predominately a single Rnq1-GFP focus, such as [*PIN*$^+$]^{low} or [*PIN*$^+$]$^{med.}$, display aggregates that migrate in a relatively narrow range of high molecular weights. Strains such as [*PIN*$^+$]^{high}, which contains more cells with multiple Rnq1-GFP foci, display a broader range of Rnq1p aggregate sizes (Bradley et al., 2002; Bagriantsev and Liebman, 2004; Liebman et al., 2006). [*PIN*$^+$]^{high} aggregates have also been shown to more readily degrade when heated compared to the other variants. Accordingly, I expressed HA-tagged Rnq1p in my wild type and deletion strains, using pGREG535-Rnq1, and then prepared protein samples enriched for HA-Rnq1p in the prion state by differential centrifugation. I treated my samples at either room temperature or 55°C to measure temperature sensitivity and compared the size of the purified HA-Rnq1p amyloid aggregates using SDD-AGE (Fig. 4-7). I found that deleting *SBA1* in the WT [*PIN*$^+$]^{high} strain eliminated small HA-Rnq1p amyloid aggregates, leaving a narrower range of larger aggregates, consistent with wild type [*PIN*$^+$]^{low} or [*PIN*$^+$]^{medium}. I also observed that *hsc82*Δ, *aha1*Δ, *cpr6*Δ, *cpr7*Δ, and *sse1*Δ strains, which increased [*PSI*$^+$] induction efficiency in WT [*PIN*$^+$]^{low} and/or [*PIN*$^+$]^{medium} backgrounds up to WT [*PIN*$^+$]^{high} levels, had amyloid aggregates of a broader range of sizes consistent with WT [*PIN*$^+$]^{high}. Also, like WT [*PIN*$^+$]^{high}, these aggregates were temperature sensitive, partially degrading to a monomer when treated at 55°C. It is important to note that the pattern of protein migration displayed by these partially degraded protein aggregates is easily distinguished from that of the WT [*pin*$^-$] control

Figure 4-7. The effect of chaperone gene deletion upon HA-Rnq1p aggregate size in relation to [*PIN*$^+$] variants. Rnq1p aggregate size in deletion strains of interest was compared by SDD-AGE. Non-denatured protein samples were incubated at room-temperature (top) or at 55°C (bottom) prior to loading. HA-tagged Rnq1p was detected using HA antibody (F-7 Sc7392).

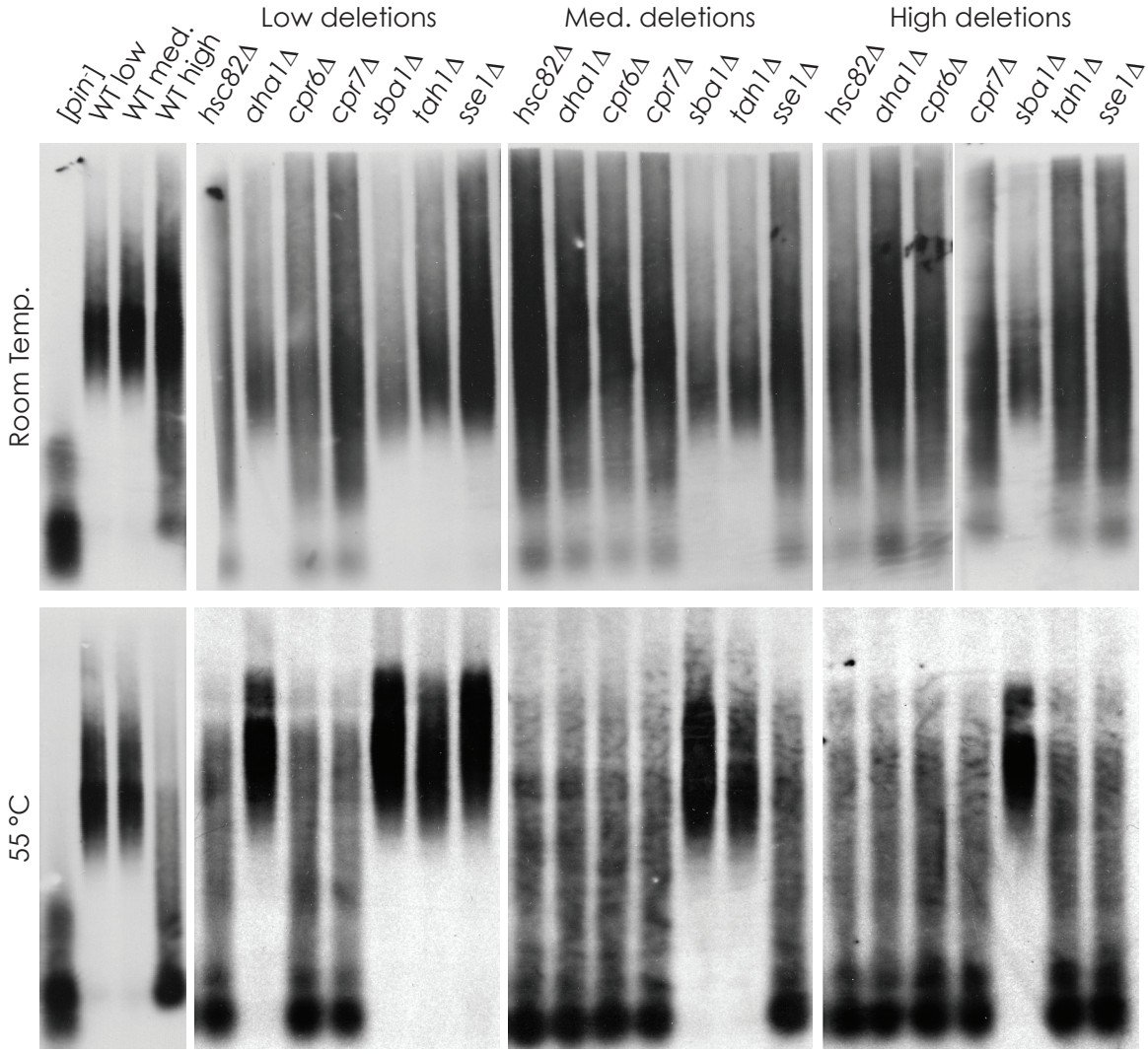
Low deletions
Med. deletions
High deletions
[pin-]
WT low
WT med.
WT high
hsc82Δ
aha1Δ
cpr6Δ
cpr7Δ
sba1Δ
tah1Δ
sse1Δ
Room Temp.
55 °C

sample. WT [*pin*$^-$] protein localized to the monomer and another low molecular weight band, while partially degraded aggregates still displayed aggregates of higher molecular weight. This suggested that my chaperone gene deletions lead to changes in the prion amyloid's physical properties, affecting the size distribution of aggregate subparticles and their heat sensitivity.

These results show general correlation between aggregate size and the other changes observed in [*PIN*$^+$]-linked phenotypes. Two exceptions were again the *tah1*Δ and *sse1*Δ strains generated in the [*PIN*$^+$]^{low} background, whose aggregates migrated in a narrow range even though their cells were shown to contain a higher proportion multiple Rnq1-GFP foci in previous experiments.

4.6 Deletion-induced phenotypes are inherited in a non-Mendelian manner

The changes in [*PIN*$^+$] variant-dependent phenotypes were consistent with a change in [*PIN*$^+$] variant. Still, other explanations were possible. It could have been that the [*PIN*$^+$] variant was not physically altered, but that the activity of these particular chaperones was simply involved in determining their phenotypes. Another possibility was that I was disrupting the cell's chaperone network by depleting these chaperones from the cell. As the chaperone network is classically responsible for correctly folding protein, disrupting that activity may have impaired the cells ability to deal with overexpressed proteins such as HA-Rnq1p or Rnq1-GFP. If these proteins were not folded correctly, it is plausible that they may have aggregated to a non-prion state. These non-prion aggregates could have been mistaken for small prion aggregates, such as the multiple Rnq1-GFP foci observed *in vivo* and the small HA-Rnq1p aggregates typical of WT [*PIN*$^+$]^{high}.

To control for deletion-specific genetic effects, I backcrossed my deletion strains to WT [*pin*$^-$] that had been switched to *MAT*α as described in Sections 2.2.3 and 2.3.5. By reintroducing the deleted chaperone genes in this way, I expected to reverse any phenotypic changes dependent upon an impaired chaperone network. I chose to use a WT [*pin*$^-$] strain for the backcross so as to avoid any convolution of my results due to variant dominance (Bradley et al., 2002). I characterized [*PSI*$^+$] induction efficiency, the pattern of Rnq1-GFP aggregate localization, and HA-Rnq1p aggregate size for each of these diploid strains (Fig. 4-8). I found that the majority of the deletion-induced phenotypes remained stable in the diploid strains. Only the increased frequency of multiple Rnq1-GFP foci induced by deletion of *SSE1* in WT [*PIN*$^+$]^{low} or deletion of *TAH1* in WT [*PIN*$^+$]$^{med.}$ was lost upon restoration of *SSE1* and *TAH1* respectively, suggesting that these phenotypic changes were not due to stable physical changes in the [*PIN*$^+$] variant. Strangely, diploids generated from WT [*PIN*$^+$]^{low} and WT [*PIN*$^+$]$^{med.}$ were not distinguishable by [*PSI*$^+$] induction efficiency or any other [*PIN*$^+$]-linked phenotype. Why this was the case remains uncertain, but for the purpose of categorizing the observed phenotypes as consistent with previously characterized [*PIN*$^+$] variants, I could only designate them as consistent with [*PIN*$^+$]^{high} or [*PIN*$^+$]$^{low/med.}$ (Fig. 4-8D). Together, these results suggest that deletion of *HSC82*, *AHA1*, *CPR6*, *CPR7*, or *SSE1* can induce a switch in prion variant consistent with [*PIN*$^+$]^{high} depending on the original [*PIN*$^+$] variant carried by the strain. Similarly, deletion of *SBA1* shifts WT [*PIN*$^+$]^{high} cell variant to one similar to [*PIN*$^+$]$^{low/med.}$. Deletion of *SSE1* in WT [*PIN*$^+$]^{low} or deletion of *TAH1* in WT [*PIN*$^+$]$^{med.}$ gave rise to stable phenotypic changes that did not correlate to any currently characterized [*PIN*$^+$] variant.

Figure 4-8. The maintenance of chaperone gene deletion-induced changes in [*PIN*$^+$] variant-dependent phenotypes. Chaperone deletion strains were mated with a wildtype [*psi*$^-$][*pin*$^-$] strain and the resulting diploids were analyzed for (A) [*PSI*$^+$] induction efficiency, (B) frequency of multiple Rnq1-GFP foci in foci-containing cells, and (C) HA-Rnq1p aggregate size (at 55°C). (D) These phenotypes were then categorized as either [*PIN*$^+$]$^{low/med.}$ or [*PIN*$^+$]^{high}. Student's t-tests were performed to compare quantification of deletion strains with that of their parental wildtype strain, *P< 0.05, **P< 0.01, ***P< 0.001. HA-tagged Rnq1p was detected using HA antibody (F-7 Sc7392).

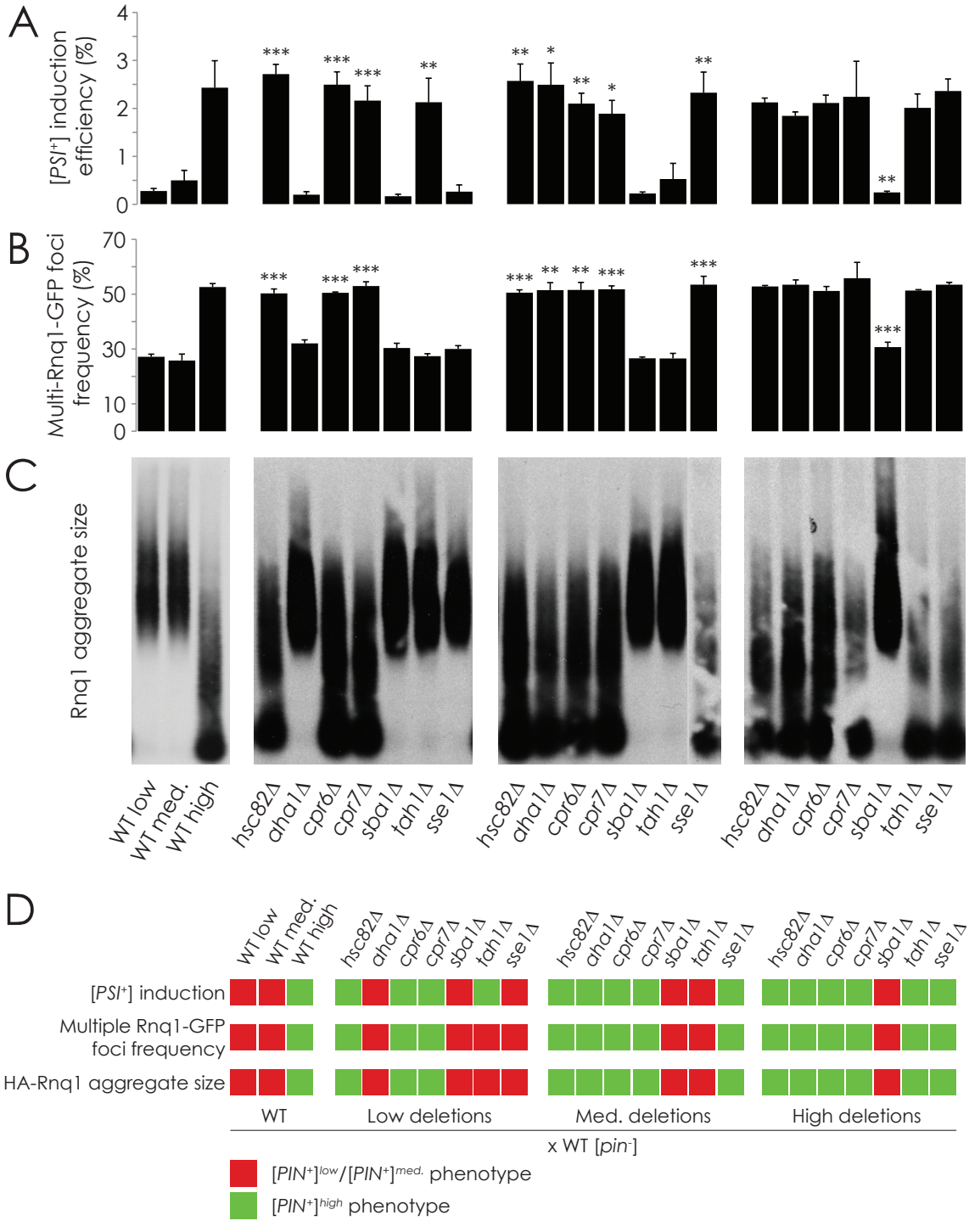
A
[PSI+] induction efficiency (%)
B
Multi-Rnq1-GFP foci frequency (%)
C
Rnq1 aggregate size
WT low
WT med.
WT high
hsc82Δ
hsh1Δ
cpr6Δ
cpr7Δ
sba1Δ
tah1Δ
sse1Δ
D
[PSI+] induction
Multiple Rnq1-GFP foci frequency
HA-Rnq1 aggregate size
WT
Low deletions
Med. deletions
High deletions
x WT [pin-]
[PIN+]low/[PIN+]med. phenotype
[PIN+]high phenotype

It is still possible that the chaperone networks of the heterozygous diploids I made by mating my original deletion strains with WT [*pin*$^-$] were not functioning as effectively as in homozygous wild type cells. Or, it could have been that my original deletion strains had accrued spurious mutations with a Mendelian dominant effect upon [*PIN*$^+$]-linked phenotypes. To control for this I sporulated my diploids, dissected the resulting tetrads, and characterized their [*PSI*$^+$] induction efficiency and HA-Rnq1p aggregate size (Fig. 4-9, 4-10). If the phenotypes were due to factors inherited in a Mendelian manner, then only half of the haploid progeny should maintain the phenotypic changes, with the other half reverting to the wild type phenotype of the strain in which the deletion was generated. Deletion-carrying and wild type progeny were distinguished by the presence of the *HIS3* cassette used to disrupt the chaperone encoding genes, which was determined by growth of haploids on CSM-HIS plates. The genetic specificity of this experiment was demonstrated by mating wild type strains carrying different [*PIN*$^+$] variants with a strain deleted for *HSP104*, which is required for both [*PSI*$^+$] and [*PIN*$^+$] propagation (Chernoff et al., 1995; Derkatch et al., 1997). I found that phenotypes observed in the original deletion strains and the diploid strains were inherited in a non-Mendelian manner, remaining stable in all progeny regardless of whether the chaperone gene of interest was deleted. This ruled out Mendelian factors and confirmed that deletion of specific chaperone genes can give rise to stable shifts in [*PIN*$^+$] variant.

4.7 Putative variants conform to classical patterns of [*PIN*$^+$] variant dominance

Another characteristic of prion variants is that one is often dominant over another. In the case of [*PIN*$^+$] variants, [*PIN*$^+$]^{high} is dominant over [*PIN*$^+$]^{med} which is then dominant over [*PIN*$^+$]^{low} (Bradley et al., 2002). Most of my deletion-induced variants'

Figure 4-9. Non-Mendelian inheritance of chaperone gene deletion-induced changes in [*PIN*$^+$] variant-dependent phenotypes. The diploids from mating deletion strains with wildtype [*psi*$^-$][*pin*$^-$] were sporulated and the resulting tetrads were dissected. Depicted here are wildtype (+) and deletion carrying (-) haploid progeny. Haploid progeny were analyzed for (A) [*PSI*$^+$] induction efficiency and (B) HA-Rnq1p aggregate size (at 55°C). Wildtype strains were mated with *hsp104*Δ strains to demonstrate genetic specificity for this experiment. The hsp104Δ samples had a greater exposure on a continuous SDD-AGE gel with the wildtype controls. Haploids not depicted in (B) followed the same pattern of HA-Rnq1 migration in SDD-AGE as the wildtype strains from which they were originally derived. 24 tetrads were analyzed per diploid. HA-tagged Rnq1p was detected using HA antibody (F-7 Sc7392).

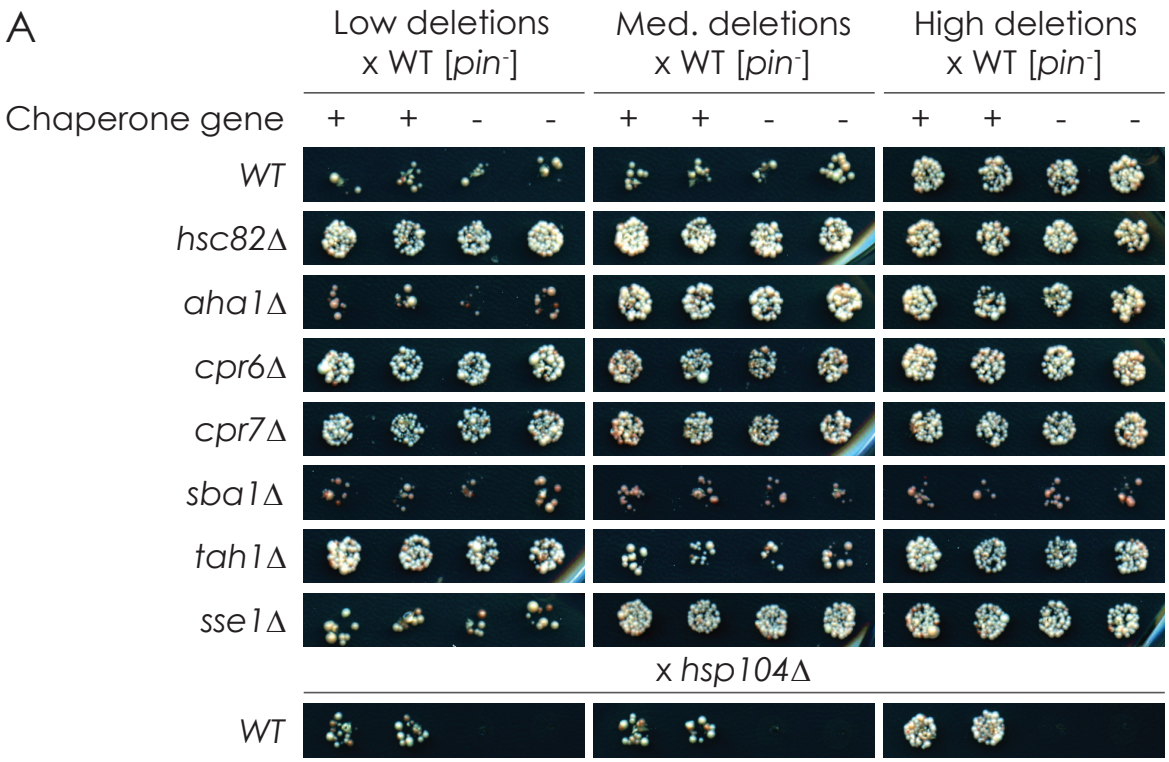
A
Low deletions x WT [pin-]
Med. deletions x WT [pin-]
High deletions x WT [pin-]
Chaperone gene
+ + - - + + - - + + - -
WT
hsc82Δ
aha1Δ
cpr6Δ
cpr7Δ
sba1Δ
tah1Δ
sse1Δ
x hsp104Δ
WT

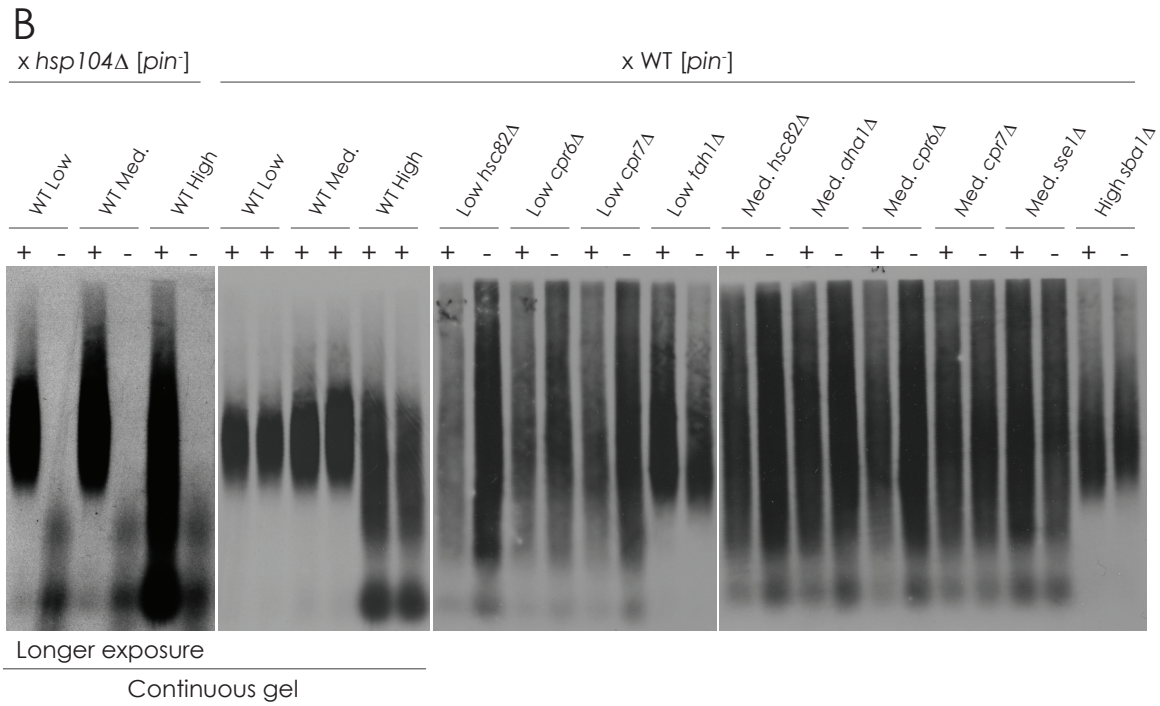
B
x hsp104Δ [pin-]
x WT [pin-]
WT Low
WT Med.
WT High
WT Low
WT Med.
WT High
Low hsc82Δ
Low cpr6Δ
Low cpr7Δ
Low tah1Δ
Med. hsc82Δ
Med. aha1Δ
Med. cpr6Δ
Med. cpr7Δ
Med. sse1Δ
High sba1Δ
+ - + - + - + + + + + + + - + - + - + - + - + - + - + - + -
Longer exposure
Continuous gel

Figure 4-10. Confirmation of [*PSI*$^+$] induction in haploid progeny. Putative [*PSI*$^+$] colonies from wildtype (+) and mutant (-) haploid progeny (Fig. 4-9) were streaked on YEPD medium containing 3 mM GuHCl and then re-streaked out on CSM and CSM-ADE media to confirm effective prion curing. Red pigment on CSM and lack of growth on CSM-ADE suggests [*PSI*$^+$] was effectively cured, signifying that growth of induced colonies on CSM-ADE medium observed in Fig. 4-9 was prion related and suggesting that they were [*PSI*$^+$].

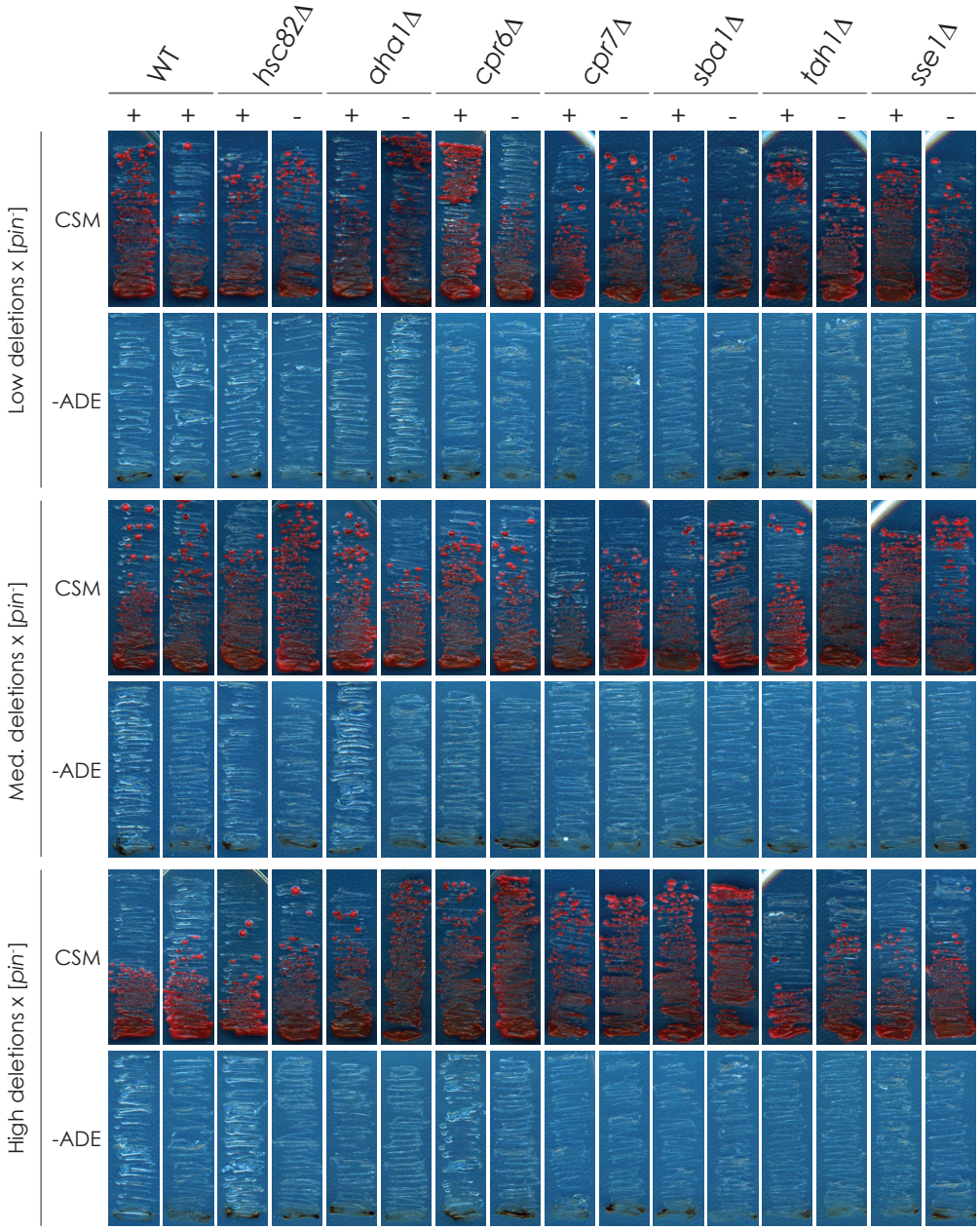
WT
hsc82Δ
aha1Δ
cpr6Δ
cpr7Δ
sba1Δ
tah1Δ
sse1Δ
+ + + - + - + - + - + - + - + -
Low deletions x [pin-]
CSM
-ADE
Med. deletions x [pin-]
CSM
-ADE
High deletions x [pin-]
CSM
-ADE

phenotypes matched that of WT [*PIN*$^+$]^{high} with the exceptions of *sba1*Δ, which resembled [*PIN*$^+$]$^{low/med.}$, and *tah1*Δ and *sse1*Δ, which did not correlate precisely to any [*PIN*$^+$] variant. It remained unclear if these variants were actually [*PIN*$^+$]^{high}, [*PIN*$^+$]$^{low/med}$, or novel, previously uncharacterized variants. If they were not novel, then they would be expected to follow the same hierarchy of variant dominance in relation to other [*PIN*$^+$] variants. To determine the hierarchy of the induced variants, I crossed deletions to isogenic *MATα* wild type strains generated from the same wild type strains in which the original deletions were created. I then characterized the resulting diploid strains in the same manner as in Section 4.6. [*PSI*$^+$] induction efficiency is shown in Fig. 4-11, Rnq1-GFP localization pattern in Fig. 4-12, and HA-Rnq1p aggregate size in Fig. 4-13. The classification of phenotypes is summarized in Fig. 4-14. I observed that putative [*PIN*$^+$]^{high} phenotypes were dominant over WT [*PIN*$^+$]^{low} and WT [*PIN*$^+$]$^{med.}$ phenotypes, with the exception of the increased frequency of multiple Rnq1-GFP foci seen in *tah1*Δ and *sse1*Δ which reverted to [*PIN*$^+$]$^{low/med.}$ levels. Also, the presumed [*PIN*$^+$]$^{low/med.}$ variant induced by the deletion of *SBA1* was shown to be eliminated by the introduction of the more dominant [*PIN*$^+$]^{high}.

In all, these findings demonstrated my deletion-induced variants to be consistent with previously characterized variants, but did not rule out the possibility that they may have distinct physical structures while displaying very similar phenotypes.

4.8 Physical interaction between Hsp90-related chaperone proteins and Rnq1p

I performed a yeast two-hybrid analysis to investigate possible physical interactions between chaperones of interest and Rnq1p (Fig. 4-15A). With growth on CSM-HIS media as a reporter of interaction, I detected a previously documented

Figure 4-11. Dominance of [*PSI*$^{+}$] induction efficiency. Chaperone deletion strains were mated with wildtype [*psi*$^{-}$][*PIN*$^{+}$]$^{low/med./high}$ strains and the resulting diploids were analyzed for [*PSI*$^{+}$] induction efficiency. Student's t-tests were performed to compare quantification of deletion based diploid strains with that of diploids based on parental wildtype strains, *P< 0.05, **P< 0.01.

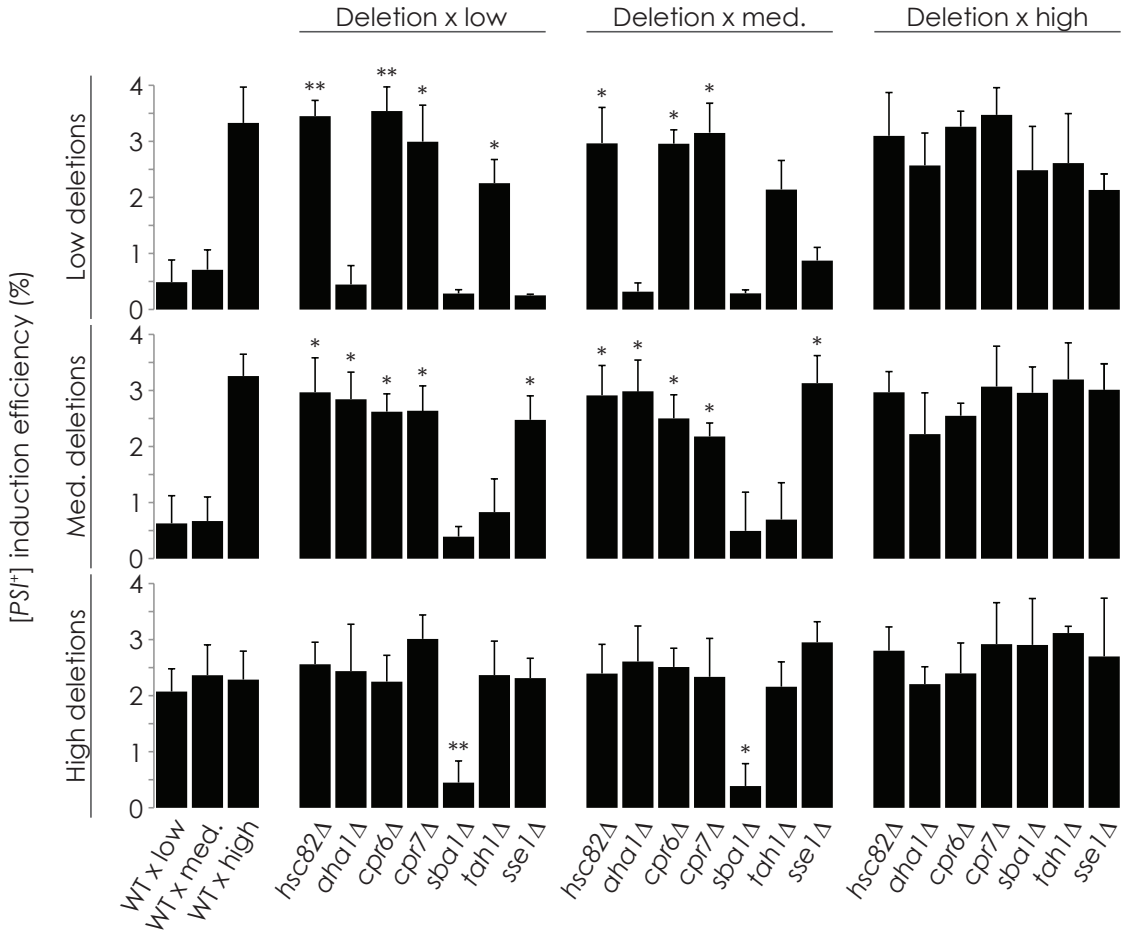
Deletion x low
Deletion x med.
Deletion x high
[PSI+] induction efficiency (%)
Low deletions
Med. deletions
High deletions
0
1
2
3
4
WT x low
WT x med.
WT x high
hsc82Δ
aha1Δ
cpr6Δ
cpr7Δ
sba1Δ
tah1Δ
sse1Δ

Figure 4-12. Dominance of patterns of Rnq1-GFP aggregation. Chaperone deletion strains were mated with wildtype [*psi*$^{-}$][*PIN*$^{+}$]$^{low/med./high}$ strains and the resulting diploids were analyzed for multiple Rnq1-GFP foci frequency. Student's t-tests were performed to compare quantification of deletion based diploid strains with that of diploids based on parental wildtype strains, **P< 0.01, ***P< 0.001.

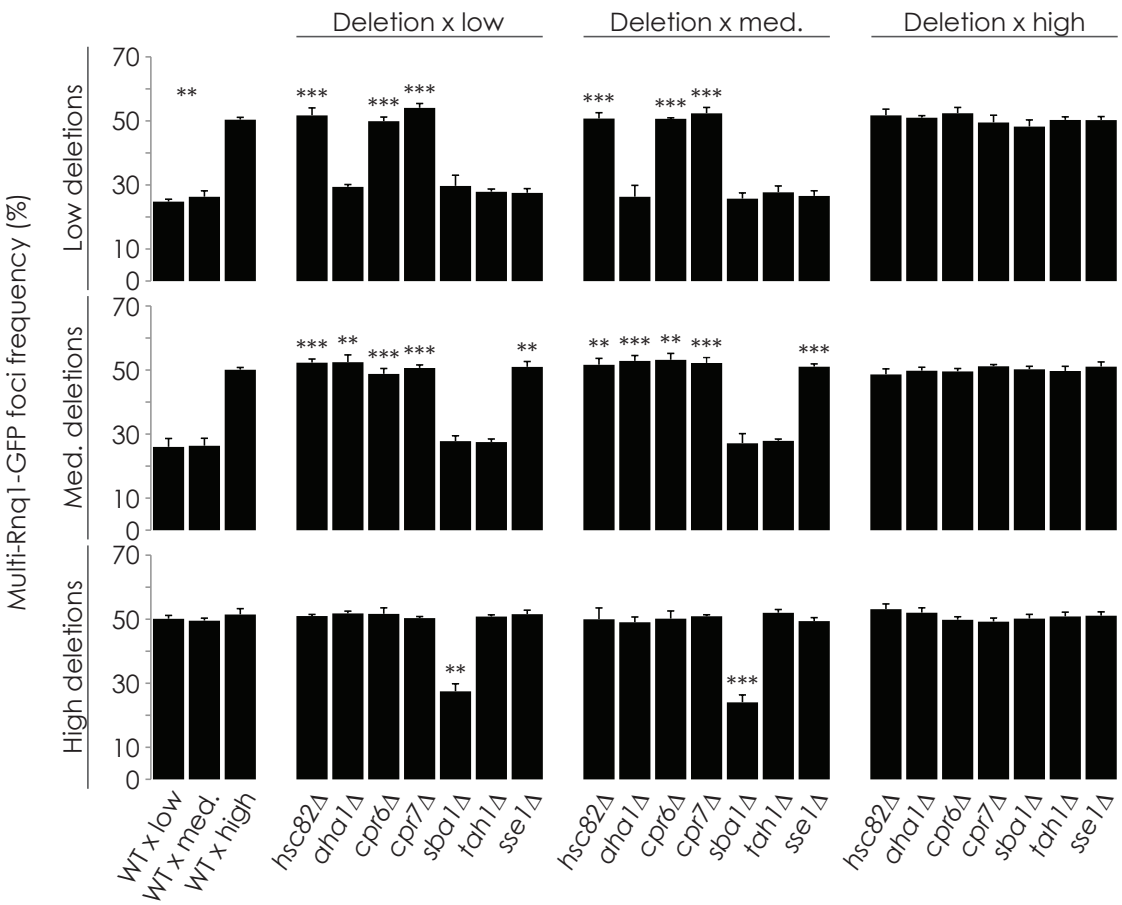
Deletion x low
Deletion x med.
Deletion x high
Multi-Rnq1-GFP foci frequency (%)
Low deletions
Med. deletions
High deletions
70
50
30
10
0
**
***
***
***
***
***
***
**
***
**
***
***
**
**
***
**
***
***
**
***
WT x low
WT x med.
WT x high
hsc82Δ
aha1Δ
cpr6Δ
cpr7Δ
sba1Δ
tah1Δ
sse1Δ

Figure 4-13. Dominance of HA-Rnq1p aggregate size. Chaperone deletion strains were mated with wildtype [*psi*$^-$][*PIN*$^+$]$^{low/med./high}$ strains and the resulting diploids were analyzed for HA-Rnq1p aggregate size (at 55°C) by SDD-AGE. HA-tagged Rnq1p was detected using HA antibody (F-7 Sc7392).

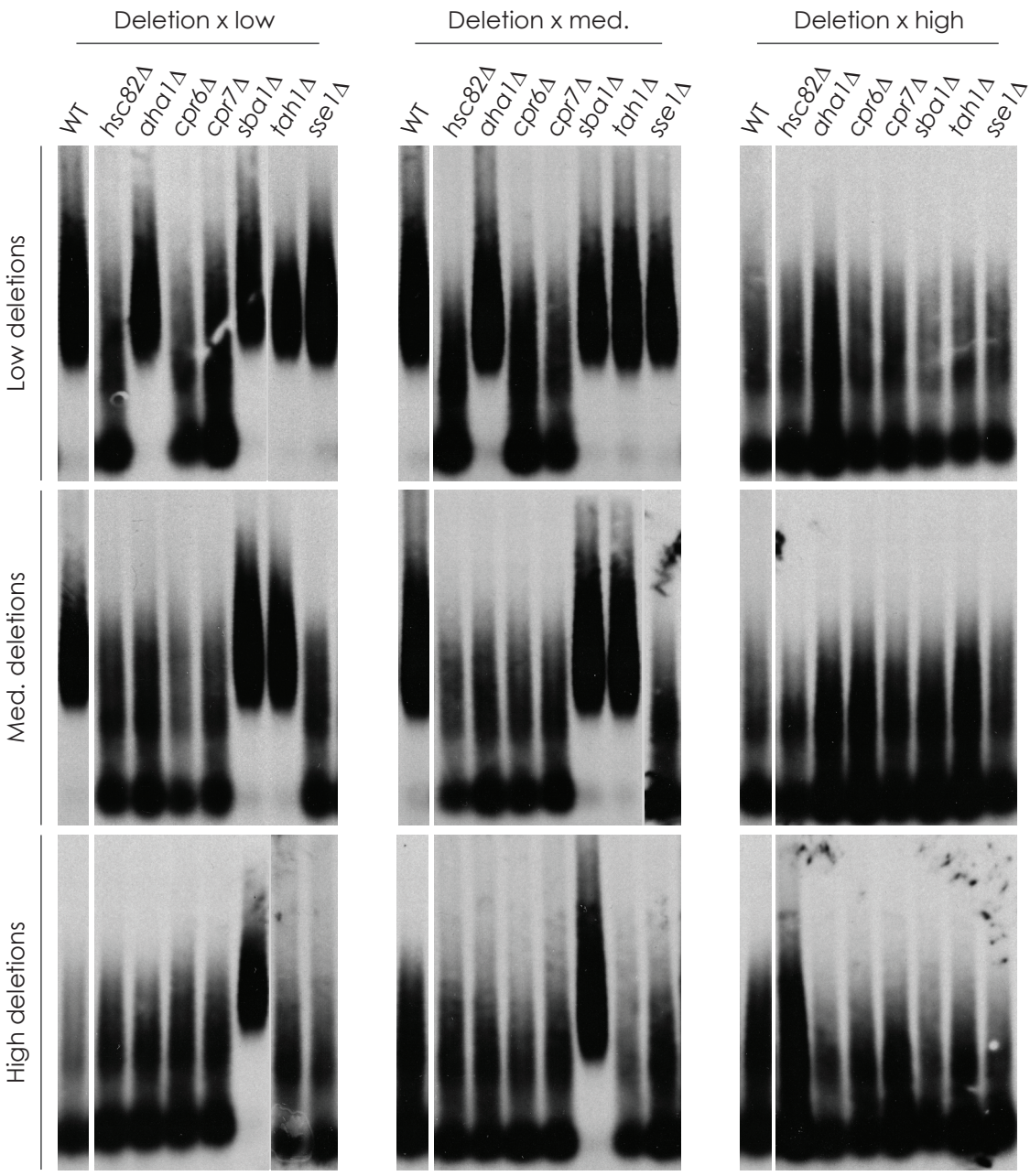
Deletion x low
Deletion x med.
Deletion x high
WT
hsc82Δ
hsp82Δ
aha1Δ
cpr6Δ
cpr7Δ
sba1Δ
tah1Δ
sse1Δ
Low deletions
Med. deletions
High deletions

Figure 4-14. Summary of deletion-induced [*PIN*$^+$]-linked phenotype dominance patterns. Chaperone deletion strains were mated with wildtype [*psi*$^-$][*PIN*$^+$]$^{low/med./high}$ strains and the resulting diploids were analyzed for [*PSI*$^+$] induction efficiency, multiple Rnq1-GFP foci frequency, and HA-Rnq1p aggregate size. These phenotypes were then categorized as either [*PIN*$^+$]$^{low/med.}$ or [*PIN*$^+$]^{high}.


Deletion x low
Deletion x med.
Deletion x high
WT
hsc82Δ
aha1Δ
cpr6Δ
cpr7Δ
sba1Δ
tah1Δ
sse1Δ
[PSI+] induction
[PIN+]low deletions
[PIN+]med. deletions
[PIN+]high deletions
Multiple Rnq1-GFP foci frequency
[PIN+]low deletions
[PIN+]med. deletions
[PIN+]high deletions
HA-Rnq1 aggregate size
[PIN+]low deletions
[PIN+]med. deletions
[PIN+]high deletions
[PIN+]low/[PIN+]med. phenotype
[PIN+]high phenotype

Figure 4-15. Yeast two-hybrid analysis of Rnq1p and chaperone proteins. (A) Cpr7p, Sba1p, and Tah1p are found to physically interact with Rnq1p based upon growth on CSM-HIS medium. Total growth of strains (top) and growth arising from protein interaction (bottom) are shown. The pattern presented is representative of four independent experiments. AD, activation domain; BD, binding domain. (B) Rnq1-GFP in HF7c localizes in a diffuse manner without visible puncta. (C) SDD-AGE of HA-Rnq1p purified from [*pin*$^-$], [*PIN*$^+$]^{low}, [*PIN*$^+$]$^{med.}$, [*PIN*$^+$]^{high}, and HF7c. HF7c HA-Rnq1p migrates in the same manner as the [*pin*$^-$] control. HA-tagged Rnq1p was detected using HA antibody (F-7 Sc7392).

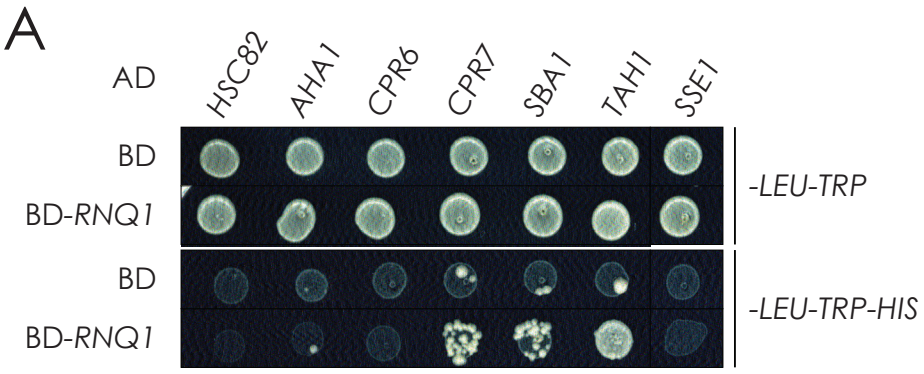
A
AD
HSC82
AHA1
CPR6
CPR7
SBA1
TAH1
SSE1
BD
BD-RNQ1
-LEU-TRP
BD
BD-RNQ1
-LEU-TRP-HIS

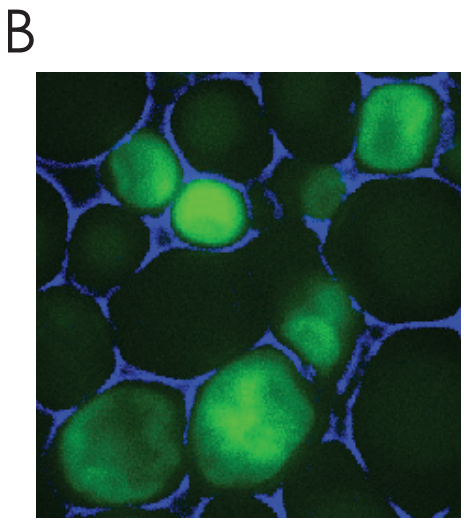
B

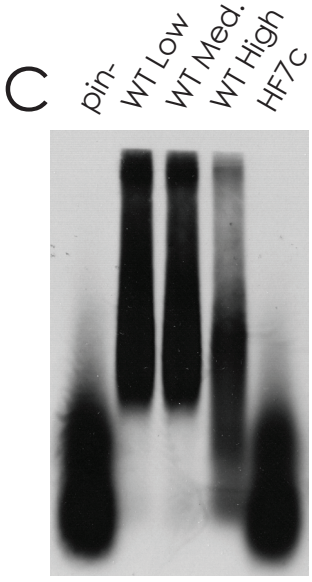
C
pin-
WT Low
WT Med.
WT High
HF7c

interaction between Rnq1p and Tah1p (Yu et al., 2008). I also identified two novel interactions: Cpr7p and Sba1p with Rnq1p. No interaction was detected between the remaining chaperones and Rnq1p. When I characterized the [*PIN*$^+$] variant of my yeast two-hybrid strain (HF7c) by SDD-AGE and localization of Rnq1-GFP (Fig. 4-15B-C), I found it to be [*pin*$^-$], suggesting that the interactions I detected occur when Rnq1p is in its non-prion conformation.

4.9 Discussion

4.9.1 Chaperones have a role in [*PIN*$^+$] variant determination

Although recombinant *S. cerevisiae* prion proteins do not require any cofactors in order to misfold into multiple infectious variants *in vitro*, they need the activity of a variety of different chaperone proteins to stably propagate *in vivo*. Most prominent among these are Hsp104p, Sis1p and members of the Ssa subfamily (reviewed in Masison et al., 2009; Romanova and Chernoff, 2009; Summers et al., 2009a). Together these chaperones facilitate the fragmentation of growing amyloid fibrils, thereby exposing more growing ends and generating more infectious prion seeds. It is believed that the conformational differences between variants alter their susceptibility to fragmentation and their rate of fibril growth, and that equilibrium between these determines the stability of prion propagation and the strength of the prion phenotype (Tanaka et al., 2006; Sindi and Serio, 2009; Derdowski et al., 2010). For example, [*PSI*$^+$]^{strong} has a smaller amyloid core that fragments more easily, allowing the generation of more growing ends and a higher rate of Sup35p incorporation into a greater number of prion seeds. This in turn leads to increased nonsense suppression and more stable propagation.

Chaperones have also been implicated in variant determination, with alteration of Hsf1p or Sse1p activity affecting [*PSI*$^{+}$] variant at *de novo* induction and truncation of Sis1p leading to stable changes in established [*PIN*$^{+}$] variant (Sondheimer et al., 2001; Park et al., 2006; Fan et al., 2007). The findings of my study provide further evidence that chaperones are important to selection of prion variants. Deletion of *AHA1* in a [*PIN*$^{+}$]$^{med.}$ background or deletion of *HSC82*, *CPR6*, or *CPR7* in either [*PIN*$^{+}$]^{low} or [*PIN*$^{+}$]$^{med.}$ backgrounds increases [*PSI*$^{+}$] induction efficiency to levels comparable to wild type [*PIN*$^{+}$]^{high}. Conversely, deletion of *SBA1* from [*PIN*$^{+}$]^{high} decreases [*PSI*$^{+}$] induction to wild type [*PIN*$^{+}$]$^{low/med.}$ levels. These deletion induced variants may yet prove to be distinct from classical [*PIN*$^{+}$] variants but, for the purpose of discussion, I will refer to them as [*PIN*$^{+}$]^{high} and [*PIN*$^{+}$]$^{low/med.}$ respectively.

Similar to the other chaperone gene deletions, deletion of *TAH1* or *SSE1* in [*PIN*$^{+}$]^{low} or [*PIN*$^{+}$]$^{med.}$ backgrounds gives rise to changes in [*PIN*$^{+}$] variant-dependent phenotypes. Unlike the others, not all of the tested phenotypes were altered and of those that were, not all were maintained after the wild type gene was restored. This suggests that at least some of the observed changes are not from [*PIN*$^{+}$] variant shifts and that any putative shift that may have occurred does not correspond to previously characterized variants (Bradley et al., 2002; Bradley and Liebman, 2003). It should be noted that, contrary to my own findings, Fan and colleagues found that the deletion of *SSE1* impaired [*PSI*$^{+}$] induction efficiency (2007). This may be due to a difference in background variant as the precise [*PIN*$^{+}$] variant carried by their deletion strain in their study was uncharacterized.

[*PIN*$^+$]^{high} phenotypes were easily identified but [*PIN*$^+$]^{low} and [*PIN*$^+$]$^{med.}$ were difficult to distinguish. Their [*PSI*$^+$] induction efficiencies did not vary greatly and properties of their aggregates were identical using my methods. As such, it is interesting that deletion of *AHA1*, *TAH1*, or *SSE1* had specific effects depending upon whether they were deleted in [*PIN*$^+$]^{low} or [*PIN*$^+$]$^{med.}$. This reinforces that [*PIN*$^+$]^{low} and [*PIN*$^+$]$^{med.}$ are unique from one another and may serve as a genetic fingerprint to experimentally differentiate the two in future studies.

It could be that deleting these genes has a [*PIN*$^+$]-independent effect, with its [*PIN*$^+$] variant-specific effects explained by different chaperone requirements for *de novo* formation of [*PSI*$^+$] in the presence of different [*PIN*$^+$] variants. Different chaperone requirement for different [*PSI*$^+$] variant propagation is not without precedent as it has been shown that a [*PSI*$^+$] variant with exceptionally large aggregates requires increased Hsp104p levels in order to stably propagate (Borchsenius et al., 2006). Still, I think this unlikely, as the observed changes are accompanied by alterations to the size and localization pattern of Rnq1p, consistent with a shift in [*PIN*$^+$] variant. Additionally, these phenotypic shifts persist when I reintroduce the deleted chaperone gene, even after subsequent sporulation into wild type and deletion-carrying haploid progeny. Taken together, my results suggest stable shifts in [*PIN*$^+$] variant lie behind the deletion-induced phenotypes, which implicates chaperone proteins as potential regulators of prion variants.

4.9.2 Potential mechanisms to mediate [*PIN*$^+$] variant switch

My results do not clarify by what mechanism the deletion of chaperone genes might mediate variant changes, but what is currently understood about the activity of these chaperones suggests a number of possibilities.

Rnq1p may be a client of the Hsp90 complex. Hsp90 has not previously been directly linked to prions, but my primary screen showed a higher proportion of Hsp90-related deletions to increase Sup35NM-GFP filamentous aggregate frequency than any other chaperone family. *HSC82* encodes the constitutively expressed isomer of Hsp90 and *AHA1*, *CPR6*, and *CPR7* encode cofactors that positively affect Hsp90 ATPase activity (Borkovich et al., 1989; Prodromou et al., 1999; Panaretou et al., 2002). Deletion of these genes shifted [*PIN*$^+$] variant to [*PIN*$^+$]^{high}. Interestingly, depletion of Sba1p, the p23 homologue that decreases Hsp90 ATPase activity by stabilizing the Hsp90-client complex in a closed conformation, had the opposite effect. It lead to a switch from [*PIN*$^+$]^{high} to [*PIN*$^+$]$^{low/med.}$ (Fang et al., 1998; Young and Hartl, 2000; Freeman et al., 2000). Also, chemical inhibition of Hsp90 ATPase activity increased the number of Rnq1-GFP foci per cell consistent with [*PIN*$^+$]^{high}. Together, these data suggest that Hsp90 dynamics could be important in maintaining [*PIN*$^+$] variants.

Some data reported in the literature further supports the idea that Hsp90 may act in prion variant determination. Park *et al*. reported that the C-terminal Hsf1p truncation strain predisposed to form unstable [*PSI*$^+$] also had markedly decreased Hsp90 levels (2006). Ochel and colleagues reported that inhibiting Hsp90 with geldanamycin or other chemical inhibitors affected the electrophoretic migration of mammalian PrP^C (2003). Their findings suggest that inhibition of Hsp90 gives rise to physical changes in PrP^C. As electrophoretic behavior is commonly used to distinguish variants of PrP^{Sc}, [*PSI*$^+$], and other prions (Collinge et al., 1996; Tanaka et al., 2006), it is conceivable that the physical changes in PrP^C mediated by Hsp90 could translate into different PrP^{Sc} variants.

It could also be that these chaperones have Hsp90-independent effects. I detected physical interactions with Rnq1p for Cpr7p, Sba1p, and Tah1p, but not for the other chaperones. This suggests that these chaperones may act directly upon Rnq1p independent of Hsp90. Cpr7p, for example has intrinsic proline isomerase activity (Duina et al., 1996a; Mayr et al., 2000). Rnq1p contains three proline residues: one in the N-terminal region (P34), a region shown to affect prion propagation (Kurahashi et al., 2008), and two more in a putative loop region between β-sheets of the amyloid core (P358, P372) (Wickner et al., 2008a). As a side note, P358 and P372 are part of a repeated amino acid sequence (GQQQA/SNEYGR**P**Q) the significance of which is currently unknown. Isomerization of any of these prolines could potentially have a potent effect on Rnq1p's conformation. This is further supported the observed increase in multiple Rnq1-GFP foci in [*PIN*$^+$]^{low} and [*PIN*$^+$]$^{med.}$ strains when treated with cyclosporin A .

As numerous physical interactions between these chaperones and other chaperone complexes have been documented, changes in their levels may affect how Hsp40s, Hsp70s and/or Hsp104p interact with Rnq1p, resulting in a variant change. Cpr7p, for one, has been shown to interact with Hsp104p in a manner not essential to its thermotolerance activity (Abbas-Terki et al., 2001; Mackay et al., 2008). Additionally, inhibition of Hsp90 ATPase activity has been shown to increase both Hsp104p and Hsp70 levels (Reidy and Masison, 2010). Hsp70s are further implicated by [*PIN*$^+$] variant-specific shifts observed upon deletion of *SSE1*, which encodes an important Hsp70 nucleotide exchange factor (Shaner et al., 2006). Fan *et al*. found that manipulation of Sse1p levels affected [*PSI*$^+$] variant (2007). Another point of interest is

that mutations in Sis1p caused the same increase in Rnq1-GFP foci that I observed in several of my deletion strains (Sondheimer et al., 2001). It may be that my gene deletions indirectly impaired Sis1p activity and/or its association with Rnq1p.

It could also be that disruption of the chaperone network affects the activity of another, as yet unidentified variant regulating factor. None of these possibilities are mutually exclusive. Overall, an investigation of how the loss of specific chaperones alters the levels and/or activities of other chaperones, in addition to their interaction with Rnq1p, would serve to clarify what mechanisms may lay behind the observed variant changes.

Chaperones could mediate [*PIN*$^+$] variant changes by altering the conformation of Rnq1p. They may regulate the folding of monomeric Rnq1p such that it is predisposed to adopt a specific variant upon *de novo* formation or encountering prion seeds. More likely as I documented changes to established variants, these chaperones may work together to affect the conformation of existing amyloid polymers. For this to be effective only the growing ends need be remodeled. For example, their stability when treated with SDS suggests that Rnq1p in the [*PIN*$^+$]$^{low/med.}$ configuration forms an amyloid that is more stable and likely has a larger region incorporated into its amyloid core as compared to [*PIN*$^+$]^{high}. If chaperone activity could refold the Rnq1p at the growing end so as to hide or reveal more prion determining domains that could lead newly incorporated Rnq1p molecules to form an amyloid core that includes only those prion determining domains in its amyloid core. Alternatively, if multiple or unstable variants are present in the cell simultaneously, as has been shown to occur for [*PSI*$^+$] (Sharma and Liebman, 2012), the changes in the chaperone environment could alter fragmentation and/or prion seed

generation rates in a variant-specific manner. In this way one variant could be selected over others.

In all I have demonstrated that altering the chaperone complement of the cell can alter existing variants without the introduction of exogenous prion material. By modulating existing prion variants, the cell can maintain prion seeds within the cell while mitigating potential negative effects of stronger prion phenotypes, and, when environmental pressures demand, the existing variant could be quickly altered to provide a more advantageous phenotype. In light of recent findings that demonstrate the prevalence of prions in wild strains of yeast as well as the apparent survival advantages that they bestow (Halfmann et al., 2012), prion variant regulation represents a powerful mechanism for adaptability and evolution.

CHAPTER FIVE: PERSPECTIVES

5.1 Synopsis

This thesis describes the characterization of a possible prion protein, Riq1p, demonstrating that it forms aggregates and is sufficient to maintain a phenotype that is reversibly curable with GuHCl treatment. Additionally, I report the results of a screen for genes affecting the aggregation pattern of Sup35-GFP upon *de novo* induction of [*PSI*$^{+}$]. Further investigation of chaperone gene deletions implicated from this screen showed that they lead to the stable shift of pre-existing [*PIN*$^{+}$] variants to new variants. This finding suggests a role for chaperone proteins in regulating prion variants *in vivo*.

5.2 Future directions in studies on novel prion candidates

The systematic survey of the *S. cerevisiae* proteome for novel prions performed by the Lindquist research group provided an impressive set of results, identifying several likely prion candidates with diverse roles in the cell (Alberti et al., 2009). Their screen, which limited investigation to predicted PrDs as opposed to full-length proteins, found little evidence to suggest that their predicted Riq1p PrD was sufficient to act as a prion. My results, which show that full-length Riq1p does have characteristics consistent with a prion, suggest that domains outside of currently accepted PrDs could be required for prion behavior. Further investigation of my prion candidate proteins and future screens for novel prions in this and other model systems should consider this and examine whole proteins whenever practical. This could serve to reduce the number of overlooked prion candidates and provide a more complete list of prion proteins.

5.3 Future directions for studies on Riq1p

Although I have provided compelling evidence to suggest that Riq1p is a novel prion, a number of additional experiments will be required to conclude this with

certainty. Electron microscopy to visualize Riq1p aggregates and polarized light microscopy with Congo red dye to detect amyloid-like green birefringence would serve to determine Riq1p's aggregation capabilities *in vitro*. The nature of the GFP-tagged aggregated observed *in vivo* could also be investigated using techniques employed to demonstrate that the cytologically detectable Sup35-GFP aggregates are composed of ordered fibril-like shapes (Kawai-Noma et al., 2010).

Effective testing of non-Mendelian [*RIQ*$^+$] inheritance was prevented by technical difficulties in sporulation of *RIQ1-SUP35MC* diploid strains. One solution is to determine if there is a detectable [*RIQ*$^+$] phenotype independent of fusion with *SUP35MC*. As wild type cells did not display sporulation defects, genetic analysis of such a phenotype could prove more feasible, and would also provide context to understand what role [*RIQ*$^+$] may play in the cell. A large-scale study found that *riq1*Δ strains are less viable under starvation conditions (Davey et al., 2012). As [*PRION*$^+$] phenotypes are often similar to null phenotypes, one may be able to detect [*RIQ*$^+$] inheritance by decreased survival when starved. Alternatively, as this phenotype does not lend itself to easy visual identification, it may be that testing of a broader assortment of *RIQ1-SUP35MC* truncation constructs could identify a [*RIQ*$^+$]-competent domain that does not impair sporulation. This would have the added benefit of identifying Riq1p's minimal PrD.

The unique physical characteristics of Riq1p aggregates detected by SDD-AGE and their Hsp104p-independent propagation raise questions surrounding the mechanism of [*RIQ*$^+$] inheritance from mother to daughter. Investigation of Riq1p using methods such as solid-state NMR, electron microscopy, and X-ray crystallography would help to

understand the structural properties underlying Riq1p's interesting physical traits. Also, a genetic screen of *S. cerevisiae* chaperone gene deletions that impair [*RIQ*$^{+}$] propagation, followed by testing Riq1p-chaperone protein interactions by yeast two-hybrid and protein pull-down assays, will identify cofactors important to generation of [*RIQ*$^{+}$] prion seeds and shed light on how the ultra-stable Riq1p aggregate(s) may be inherited.

5.4 Future directions for studies on Sup35p aggregation-affecting factors

It would be interesting to further characterize the effects of other gene deletions that I found to affect the frequency and morphology of Sup35NM-GFP aggregates. For example, each of the four vacuole fusion-related genes tested showed an increase in the frequency of filamentous Sup35pNM-GFP aggregates, which is notable as Sup35NM-GFP rings often surround the vacuole (Ganusova et al., 2006). Deletion of *ICE2*, which encodes an integral ER protein implicated in cortical ER morphology, also caused an increase in filamentous aggregate frequency as well as the greatest increase in Sup35NM-GFP aggregation overall. This suggested that ER morphology could affect early Sup35p aggregation. Investigation of vacuole and ER morphology related genes should include quantification of Sup35NM-GFP association with vacuoles, 4D microscopy of aggregate formation, and [*PSI*$^{+}$] induction efficiency. If deletions are shown to affect [*PSI*$^{+}$] induction, [*PIN*$^{+}$] variant involvement should be examined as well. It may be that the frequency of filamentous Sup35NM-GFP aggregates is a function of the background [*PIN*$^{+}$] variant. Overall, characterization of these deletion strains could contribute to the understanding of the early events in [*PSI*$^{+}$] induction *in vivo*.

5.5 Future directions for studies on [*PIN*$^+$] variants

Why some [*PIN*$^+$] variants are more effective in facilitating *de novo* [*PSI*$^+$] formation is not yet known. My findings suggest a possible explanation. I did not expect my screen for factors affecting the frequency of filamentous Sup35p-GFP aggregates to eventually show a role for chaperones in [*PIN*$^+$] variant determination. The correlation of these two effects suggests that they may be linked and may suggest a mechanism by which [*PIN*$^+$] variants affect [*PIN*$^+$] induction efficiency. Sup35p aggregates have been shown to have a cytotoxic effect (Zhou et al., 2001; Ganusova et al., 2006). It could be that different [*PIN*$^+$] variants can ameliorate Sup35p aggregate toxicity at different levels. A cell carrying aggregates with mitigated cytotoxicity would survive to give rise to more [*PSI*$^+$] daughter cells, thereby increasing [*PSI*$^+$] induction efficiency. According to this model, a first generation [*PSI*$^+$] cell arising in a [*PIN*$^+$]^{high} background would give rise to more viable [*PSI*$^+$] daughter cells than [*PIN*$^+$]$^{low/med.}$. To test this, one could micromanipulate filamentous aggregate containing cells generated in different [*PIN*$^+$] variant backgrounds to test their viability. One could also dissect the micro-colonies arising from these cells to gauge their viability and [*PSI*$^+$] state as well. If [*PIN*$^+$]^{high} reduces Sup35p aggregate toxicity, then those cells should have statistically higher viability and should give rise to more viable [*PSI*$^+$] daughter cells.

Another important avenue of research to pursue is characterizing the structural differences that exist between the [*PIN*$^+$] variants. Using methods such as protease digestion and solid-state NMR could provide insight into the composition of each variant's amyloid core region and may provide insight into how processing by chaperone or other variant determining factors may contribute to the observed variant shifts.

5.6 Future directions for studies on [*PIN*$^+$] variant determination

The question remains of how deleting specific chaperone genes alters [*PIN*$^+$] variant. There are several avenues of inquiry that could contribute to understanding the mechanism behind this phenomenon. First of all, any study of [*PIN*$^+$] variants would benefit from the characterization of the physical and structural differences that exist between variants similar to the work that has already been done for [*PSI*$^+$] variants (Tanaka et al., 2006; Toyama et al., 2007). Understanding how the variants differ structurally could suggest amino acid residues in Rnq1p that may prove important in variant determination. Some such residues could be the three proline residues that were implicated by my *CPR6/CPR7* deletion strains and cyclophilins inhibition experiments. To investigate this, the prolines should be mutated singly and in series and the resulting alterations in [*PIN*$^+$] variant observed. Proline analogues resistant to *cis/trans* isomerization , such as (S)-oxazolidine-4-carboxylic acid (Kern et al., 1997), could also be introduced to control for proline-specific effects independent of cyclophilins.

In Section 4.9.2, I suggested that the effects of my gene deletions might be mediated by altering the levels of other chaperones. To investigate this I suggest analyzing the levels for various chaperones for patterns that correlate with [*PIN*$^+$] variant shifts using western immunoblot methods. The levels of Sis1p will be of particular interest as it is already implicated in [*PIN*$^+$] variant changes (Sondheimer et al., 2001), but those of Hsp104p, Hsp70s, and Hsp90s may also be suggestive. Furthermore, the strength of interaction of these chaperones with specific [*PIN*$^+$] variants in wild type and deletion strains should also be determined. Control [*PIN*$^+$] variants could be introduced into yeast two-hybrid strains with a β-galactosidase reporter gene by transfection and the

strength of any interactions quantified by spectrophotometer. This would have the added benefit of facilitating the detection of any [*PIN*$^{+}$]-specific Rnq1p-chaperone interactions. Protein interactions could be confirmed through other methods such as protein pull-down experiments.

My data does not confirm that Rnq1p is an Hsp90 client but provides indirect evidence that it might be. That deletion of *SBA1*, which normally acts to stabilize Hsp90-client complexes and slows Hsp90 ATPase activity, had the opposite effect to deletion of genes encoding Hsp90 ATPase promoting genes is intriguing. Also, expanding the work that I have done with chemical chaperone inhibitors to determine if stable [*PIN*$^{+}$] variant shifts are induced could provide more support for Hsp90's role. Future protein interaction experiments proposed above could also provide evidence that Rnq1p is an Hsp90 client. If so, I propose a model for [*PIN*$^{+}$] variant determination that depends upon the stability of interaction between Hsp90. According to this model, Rnq1p is an Hsp90 client and remodeling by Hsp90 under normal conditions allows Rnq1p aggregates to adopt any of the three prion variants examined in this study. But, when the Hsp90-client complex is made more transient, for example by deletion of *SBA1*, Rnq1p aggregates may be partially processed and therefore cannot become [*PIN*$^{+}$]^{high} and are more likely to become [*PIN*$^{+}$]$^{low/med.}$. Or if overall Hsp90 activity is diminished, for example through deletion of *AHA1*, then Rnq1p may not be processed at all and therefore be predisposed to become [*PIN*$^{+}$]^{high}. If an Rnq1p-Hsp90 interaction can be detected, one could test this model by measuring the strength Hsp90-Rnq1p interaction in my deletion strains, and also by examining the effects of Hsp90 mutations with increased and decreased Hsp90 ATPase activity (Zurawska et al., 2010).

Finally, if changes in the chaperone complement of the cell induce [*PIN*$^+$] variant shifts, it is possible that specific environmental circumstances could simulate that effect. To this end, wild type strains with different [*PIN*$^+$] variants could be subjected to different stress conditions (e.g. heat/cold-shock, starvation, pH imbalance) and [*PIN*$^+$] variants measured. If this proved to be the case, it would support the concept that chaperone-mediated variant regulation can be an adaptive advantage.

5.4 Concluding remarks

When first proposed, the concepts of protein-only infection and inheritance met with considerable resistance. It has only been through ingenious and rigorous research preformed by many outstanding scientists that the prion hypothesis has come to be generally accepted. The perception of prions has evolved from disease vectors, to agents of epigenetic inheritance, to possible actors in the formation of memories. Still, many aspects of prion biology remain poorly understood. What function do prions perform in the cell, what events occur early in *de novo* prion formation, and how are prions regulated are among the unanswered questions surrounding prions. By focusing their efforts on elucidating these points, researchers will not only contribute to the basic understanding of cellular mechanisms, but also provide essential knowledge required to devise effective diagnostic tests and treatments for prion and amyloid-linked diseases.

CHAPTER SIX: REFERENCES

Abbas-Terki, T., O. Donzé, P.A. Briand, and D. Picard. 2001. Hsp104 interacts with Hsp90 cochaperones in respiring yeast. *Mol Cell Biol*. 21:7569–7575.

Abramoff, M.D., P.J. Magelhaes, and S.J. Ram. 2004. Image Processing with ImageJ. *Biophotonics international*. 11:36–42.

Aguzzi, A. and L. Rajendran. 2009. The transcellular spread of cytosolic amyloids, prions and prionoids. *Neuron*. 64:783-790.

Alberti, S., R. Halfmann, O. King, A. Kapila, and S. Lindquist. 2009. A systematic survey identifies prions and illuminates sequence features of prionogenic proteins. *Cell*. 137:146–158.

Alfarano, C., C.E. Andrade, K. Anthony, N. Bahroos, M. Bajec, K. Bantoft, D. Betel, B. Bobechko, K. Boutilier, E. Burgess, K. Buzadzija, R. Cavero, C. D'Abreo, I. Donaldson, D. Dorairajoo, M.J. Dumontier, M.R. Dumontier, V. Earles, R. Farrall, H. Feldman, E. Garderman, Y. Gong, R. Gonzaga, V. Grytsan, E. Gryz, V. Gu, E. Haldorsen, A. Halupa, R. Haw, A. Hrvojic, L. Hurrell, R. Isserlin, F. Jack, F. Juma, A. Khan, T. Kon, S. Konopinsky, V. Le, E. Lee, S. Ling, M. Magidin, J. Moniakis, J. Montojo, S. Moore, B. Muskat, I. Ng, J.P. Paraiso, B. Parker, G. Pintilie, R. Pirone, J.J. Salama, S. Sgro, T. Shan, Y. Shu, J. Siew, D. Skinner, K. Snyder, R. Stasiuk, D. Strumpf, B. Tuekam, S. Tao, Z. Wang, M. White, R. Willis, C. Wolting, S. Wong, A. Wrong, C. Xin, R. Yao, B. Yates, S. Zhang, K. Zheng, T. Pawson, B.F.F. Ouellette, and C.W.V. Hogue. 2005. The Biomolecular Interaction Network Database and related tools 2005 update. *Nucleic Acids Res*. 33:D418–24.

Allen, K.D., R.D. Wegrzyn, T.A. Chernova, S. Müller, G.P. Newnam, P.A. Winslett, K.B. Wittich, K.D. Wilkinson, and Y.O. Chernoff. 2005. Hsp70 chaperones as modulators of prion life cycle: novel effects of Ssa and Ssb on the Saccharomyces cerevisiae prion [PSI+]. *Genetics*. 169:1227–1242.

Alper, T., D.A. Haig, and M.C. Clarke. 1966. The exceptionally small size of the scrapie agent. *Biochem Biophys Res Commun*. 22:278–284.

Alper, T., W.A. Cramp, D.A. Haig, and M.C. Clarke. 1967. Does the agent of scrapie replicate without nucleic acid? *Nature*. 214:764–766.

Altschul, S.F., T.L. Madden, A.A. Schäffer, J. Zhang, Z. Zhang, W. Miller, and D.J. Lipman. 1997. Gapped BLAST and PSI-BLAST: a new generation of protein database search programs. *Nucleic Acids Res*. 25:3389–3402.

Altschul, S.F., W. Gish, W. Miller, E.W. Myers, and D.J. Lipman. 1990. Basic local alignment search tool. *J Mol Biol*. 215:403–410.

Andrewes, C.H. 1964. Viruses of vertebrates. Baillière, Tindall, and Cox, London, UK.

Anfinsen, C.B. 1973. Principles that govern the folding of protein chains. *Science*. 181:223–230.

Antonyuk, S.V., C.R. Trevitt, R.W. Strange, G.S. Jackson, D. Sangar, M. Batchelor, S. Cooper, C. Fraser, S. Jones, T. Georgiou, A. Khalili-Shirazi, A.R. Clarke, S.S. Hasnain, and J. Collinge. 2009. Crystal structure of human prion protein bound to a therapeutic antibody. *Proc Natl Acad Sci USA*. 106:2554–2558.

Ausubel, F.M., R. Brent, R.E. Kingston, D.D. Moore, J. Seidman, and J.A. Smith. 1993. Current Protocols in Molecular Biology. Green Publishing Associates, New York, NY.

Avery, O.T., C.M. Macleod, and M. McCarty. 1944. Studies on the chemical nature of the substance inducing transformation of pneumococcal types. *J. Exp. Med.* 79:137–158.

Bagriantsev, S., and S.W. Liebman. 2004. Specificity of prion assembly in vivo. [PSI+] and [PIN+] form separate structures in yeast. *J Biol Chem*. 279:51042–51048.

Bagriantsev, S.N., E.O. Gracheva, J.E. Richmond, and S.W. Liebman. 2008. Variant-specific [PSI+] infection is transmitted by Sup35 polymers within [PSI+] aggregates with heterogeneous protein composition. *Mol Biol Cell*. 19:2433–2443.

Bai, M., J.-M. Zhou, and S. Perrett. 2004. The yeast prion protein Ure2 shows glutathione peroxidase activity in both native and fibrillar forms. *J Biol Chem*. 279:50025–50030.

Bailleul, P.A., G.P. Newnam, J.N. Steenbergen, and Y.O. Chernoff. 1999. Genetic study of interactions between the cytoskeletal assembly protein sla1 and prion-forming domain of the release factor Sup35 (eRF3) in Saccharomyces cerevisiae. *Genetics*. 153:81–94.

Bardill, J.P., and H.L. True. 2009. Heterologous prion interactions are altered by mutations in the prion protein Rnq1p. *J Mol Biol*. 388:583–596.

Bardill, J.P., J.E. Dulle, J.R. Fisher, and H.L. True. 2009. Requirements of Hsp104p activity and Sis1p binding for propagation of the [RNQ+] prion. *Prion*. 3:151–160.

Barry, R.A., S.B. Kent, M.P. McKinley, R.K. Meyer, S.J. DeArmond, L.E. Hood, and S.B. Prusiner. 1986. Scrapie and cellular prion proteins share polypeptide epitopes. *J. Infect. Dis.* 153:848–854.

Basler, K., B. Oesch, M. Scott, D. Westaway, M. Wälchli, D.F. Groth, M.P. McKinley, S.B. Prusiner, and C. Weissmann. 1986. Scrapie and cellular PrP isoforms are encoded by the same chromosomal gene. *Cell*. 46:417–428.

Baxa, U., K.L. Taylor, J.S. Wall, M.N. Simon, N. Cheng, R.B. Wickner, and A.C. Steven. 2003. Architecture of Ure2p prion filaments: the N-terminal domains form a central core fiber. *J Biol Chem*. 278:43717–43727.

Baxa, U., N. Cheng, D.C. Winkler, T.K. Chiu, D.R. Davies, D. Sharma, H. Inouye, D.A. Kirschner, R.B. Wickner, and A.C. Steven. 2005. Filaments of the Ure2p prion protein have a cross-beta core structure. *J Struct Biol*. 150:170–179.

Baxa, U., P.D. Ross, R.B. Wickner, and A.C. Steven. 2004. The N-terminal prion domain of Ure2p converts from an unfolded to a thermally resistant conformation upon filament formation. *J Mol Biol*. 339:259–264.

Baxa, U., P.W. Keller, N. Cheng, J.S. Wall, and A.C. Steven. 2011. In Sup35p filaments (the [PSI+] prion), the globular C-terminal domains are widely offset from the amyloid fibril backbone. *Mol Microbiol*. 79:523–532.

Baxa, U., R.B. Wickner, A.C. Steven, D.E. Anderson, L.N. Marekov, W.-M. Yau, and R. Tycko. 2007. Characterization of beta-sheet structure in Ure2p1-89 yeast prion fibrils by solid-state nuclear magnetic resonance. *Biochemistry*. 46:13149–13162.

Bendheim, P.E., R.A. Barry, S.J. DeArmond, D.P. Stites, and S.B. Prusiner. 1984. Antibodies to a scrapie prion protein. *Nature*. 310:418–421.

Bernstein, F.C., T.F. Koetzle, G.J. Williams, E.F. Meyer, M.D. Brice, J.R. Rodgers, O. Kennard, T. Shimanouchi, and M. Tasumi. 1977. The Protein Data Bank: a computer-based archival file for macromolecular structures. *J Mol Biol*. 112:535–542.

Bessen, R.A., and R.F. Marsh. 1992. Biochemical and physical properties of the prion protein from two strains of the transmissible mink encephalopathy agent. *J Virol*. 66:2096–2101.

Blond-Elguindi, S., S.E. Cwirla, W.J. Dower, R.J. Lipshutz, S.R. Sprang, J.F. Sambrook, and M.J. Gething. 1993. Affinity panning of a library of peptides displayed on bacteriophages reveals the binding specificity of BiP. *Cell*. 75:717–728.

Boeke, J.D., J. Trueheart, G. Natsoulis, and G.R. Fink. 1987. 5-Fluoroorotic acid as a selective agent in yeast molecular genetics. *Meth Enzymol*. 154:164–175.

Borchsenius, A.S., R.D. Wegrzyn, G.P. Newnam, S.G. Inge-Vechtomov, and Y.O. Chernoff. 2001. Yeast prion protein derivative defective in aggregate shearing and production of new 'seeds'. *EMBO J*. 20:6683–6691.

Borchsenius, A.S., S. Müller, G.P. Newnam, S.G. Inge-Vechtomov, and Y.O. Chernoff. 2006. Prion variant maintained only at high levels of the Hsp104 disaggregase. *Curr Genet*. 49:21–29.

Borkovich, K.A., F.W. Farrelly, D.B. Finkelstein, J. Taulien, and S. Lindquist. 1989. hsp82 is an essential protein that is required in higher concentrations for growth of cells at higher temperatures. *Mol Cell Biol*. 9:3919–3930.

Brachmann, C.B., A. Davies, G.J. Cost, E. Caputo, J. Li, P. Hieter, and J.D. Boeke. 1998. Designer deletion strains derived from Saccharomyces cerevisiae S288C: a useful set of strains and plasmids for PCR-mediated gene disruption and other applications. *Yeast*. 14:115–132.

Bradford, M.M. 1976. A rapid and sensitive method for the quantitation of microgram quantities of protein utilizing the principle of protein-dye binding. *Anal Biochem*. 72:248–254.

Bradley, M.E., and S.W. Liebman. 2003. Destabilizing interactions among [PSI(+)] and [PIN(+)] yeast prion variants. *Genetics*. 165:1675–1685.

Bradley, M.E., H.K. Edskes, J.Y. Hong, R.B. Wickner, and S.W. Liebman. 2002. Interactions among prions and prion "strains" in yeast. *Proc Natl Acad Sci USA*. 99 Suppl 4:16392–16399.

Bradley, M.E., S. Bagriantsev, N. Vishveshwara, and S.W. Liebman. 2003. Guanidine reduces stop codon read-through caused by missense mutations in SUP35 or SUP45. *Yeast*. 20:625–632.

Brough, P.A., W. Aherne, X. Barril, J. Borgognoni, K. Boxall, J.E. Cansfield, K.-M.J. Cheung, I. Collins, N.G.M. Davies, M.J. Drysdale, B. Dymock, S.A. Eccles, H. Finch, A. Fink, A. Hayes, R. Howes, R.E. Hubbard, K. James, A.M. Jordan, A. Lockie, V. Martins, A. Massey, T.P. Matthews, E. McDonald, C.J. Northfield, L.H. Pearl, C. Prodromou, S. Ray, F.I. Raynaud, S.D. Roughley, S.Y. Sharp, A. Surgenor, D.L. Walmsley, P. Webb, M. Wood, P. Workman, and L. Wright. 2008. 4,5-diarylisoxazole Hsp90 chaperone inhibitors: potential therapeutic agents for the treatment of cancer. *J. Med. Chem.* 51:196–218.

Brzobohatý, B., and L. Kovác. 1986. Factors enhancing genetic transformation of intact yeast cells modify cell wall porosity. *J Gen Microbiol*. 132:3089–3093.

Burnette, N. 1981. "Western Blotting": Electrophoretic transfer of proteins from sodium dodecyl sulfate-polyacrylamide gels to unmodified nitrocellulose and radiographic detection with antibody and radioiodinated protein A. *Anal Biochem*. 112:195–203.

Burnie, J.P., T.L. Carter, S.J. Hodgetts, and R.C. Matthews. 2006. Fungal heat-shock proteins in human disease. *FEMS Microbiol. Rev.* 30:53–88.

Büeler, H., A. Aguzzi, A. Sailer, R.A. Greiner, P. Autenried, M. Aguet, and C. Weissmann. 1993. Mice devoid of PrP are resistant to scrapie. *Cell*. 73:1339–1347.

Büeler, H., A. Raeber, A. Sailer, M. Fischer, A. Aguzzi, and C. Weissmann. 1994. High prion and PrPSc levels but delayed onset of disease in scrapie-inoculated mice heterozygous for a disrupted PrP gene. *Mol. Med.* 1:19–30.

Büeler, H., M. Fischer, Y. Lang, H. Bluethmann, H.P. Lipp, S.J. DeArmond, S.B. Prusiner, M. Aguet, and C. Weissmann. 1992. Normal development and behaviour of mice lacking the neuronal cell-surface PrP protein. *Nature*. 356:577–582.

Byrne, L.J., B.S. Cox, D.J. Cole, M.S. Ridout, B.J.T. Morgan, and M.F. Tuite. 2007. Cell division is essential for elimination of the yeast [PSI+] prion by guanidine hydrochloride. *Proc Natl Acad Sci USA*. 104:11688–11693.

Byrne, L.J., D.J. Cole, B.S. Cox, M.S. Ridout, B.J.T. Morgan, and M.F. Tuite. 2009. The number and transmission of [PSI] prion seeds (Propagons) in the yeast Saccharomyces cerevisiae. *PLoS ONE*. 4:e4670.

Calzolai, L., D.A. Lysek, D.R. Pérez, P. Güntert, and K. Wüthrich. 2005. Prion protein NMR structures of chickens, turtles, and frogs. *Proc Natl Acad Sci USA*. 102:651–655.

Caplan, A.J., and M.G. Douglas. 1991. Characterization of YDJ1: a yeast homologue of the bacterial dnaJ protein. *J Cell Biol*. 114:609–621.

Cashikar, A.G., M. Duennwald, and S.L. Lindquist. 2005. A chaperone pathway in protein disaggregation. Hsp26 alters the nature of protein aggregates to facilitate reactivation by Hsp104. *J Biol Chem*. 280:23869–23875.

Castilla, J., P. Saá, C. Hetz, and C. Soto. 2005. In vitro generation of infectious scrapie prions. *Cell*. 121:195–206.

Caughey, B. 2001. Interactions between prion protein isoforms: the kiss of death? *Trends Biochem Sci*. 26:235–242.

Caughey, B.W., A. Dong, K.S. Bhat, D. Ernst, S.F. Hayes, and W.S. Caughey. 1991. Secondary structure analysis of the scrapie-associated protein PrP 27-30 in water by infrared spectroscopy. *Biochemistry*. 30:7672–7680.

Chacinska, A., B. Szczesniak, N.V. Kochneva-Pervukhova, V.V. Kushnirov, M.D. Ter-Avanesyan, and M. Boguta. 2001. Ssb1 chaperone is a [PSI+] prion-curing factor. *Curr Genet*. 39:62–67.

Chan, J.C.C., N.A. Oyler, W.-M. Yau, and R. Tycko. 2005. Parallel beta-sheets and polar zippers in amyloid fibrils formed by residues 10-39 of the yeast prion protein Ure2p. *Biochemistry*. 44:10669–10680.

Chandler, R.L. 1961. Encephalopathy in mice produced by inoculation with scrapie brain material. *Lancet*. 1:1378–1379.

Chen, B., K.R. Thurber, F. Shewmaker, R.B. Wickner, and R. Tycko. 2009. Measurement of amyloid fibril mass-per-length by tilted-beam transmission electron microscopy. *Proc Natl Acad Sci USA*. 106:14339–14344.

Chen, P., H.-H. Liu, R. Cui, Z.-L. Zhang, D.-W. Pang, Z.-X. Xie, H.-Z. Zheng, Z.-X. Lu, and H. Tong. 2008. Visualized investigation of yeast transformation induced with Li+ and polyethylene glycol. *Talanta*. 77:262–268.

Chernoff, Y.O., G.P. Newnam, J. Kumar, K. Allen, and A.D. Zink. 1999. Evidence for a protein mutator in yeast: role of the Hsp70-related chaperone ssb in formation, stability, and toxicity of the [PSI] prion. *Mol Cell Biol*. 19:8103–8112.

Chernoff, Y.O., I.L. Derkach, and S.G. Inge-Vechtomov. 1993. Multicopy SUP35 gene induces de-novo appearance of psi-like factors in the yeast Saccharomyces cerevisiae. *Curr Genet*. 24:268–270.

Chernoff, Y.O., I.L. Derkatch, V.L. Tikhomirova, A.R. Dagkesamanskaya, M.D. Ter-Avanesyan, and S.G. Inge-Vechtomov. 1988. Nonsense-suppression by amplification of translation protein factor gene. *Doklady Akademii Nauk SSSR (Biol. Sci.)*. 1227–1229.

Chernoff, Y.O., S.L. Lindquist, B. Ono, S.G. Inge-Vechtomov, and S.W. Liebman. 1995. Role of the chaperone protein Hsp104 in propagation of the yeast prion-like factor [psi+]. *Science*. 268:880–884.

Chesebro, B. 1998. BSE and prions: uncertainties about the agent. *Science*. 279:42–43.

Chesebro, B., R. Race, K. Wehrly, J. Nishio, M. Bloom, D. Lechner, S. Bergstrom, K. Robbins, L. Mayer, and J.M. Keith. 1985. Identification of scrapie prion protein-specific mRNA in scrapie-infected and uninfected brain. *Nature*. 315:331–333.

Chiti, F., and C.M. Dobson. 2006. Protein misfolding, functional amyloid, and human disease. *Annu. Rev. Biochem.* 75:333–366.

Cho, H.J. 1976. Is the scrapie agent a virus? *Nature*. 262:411–412.

Choe, Y.-J., Y. Ryu, H.-J. Kim, and Y.-J. Seok. 2009. Increased [PSI+] appearance by fusion of Rnq1 with the prion domain of Sup35 in Saccharomyces cerevisiae. *Eukaryotic Cell*. 8:968–976.

Cintron, N.S., and D. Toft. 2006. Defining the requirements for Hsp40 and Hsp70 in the Hsp90 chaperone pathway. *J Biol Chem*. 281:26235–26244.

Clos, J., and S. Brandau. 1994. pJC20 and pJC40--two high-copy-number vectors for T7 RNA polymerase-dependent expression of recombinant genes in Escherichia coli. *Protein Expr Purif*. 5:133–137.

Cohen, F.E., and S.B. Prusiner. 1998. Pathologic conformations of prion proteins. *Annu. Rev. Biochem.* 67:793–819.

Collinge, J. 2001. Prion diseases of humans and animals: their causes and molecular basis. *Annu Rev Neurosci*. 24:519–550.

Collinge, J., K.C. Sidle, J. Meads, J. Ironside, and A.F. Hill. 1996. Molecular analysis of prion strain variation and the aetiology of “new variant” CJD. *Nature*. 383:685–690.

Collins, S.R., A. Douglass, R.D. Vale, and J.S. Weissman. 2004. Mechanism of prion propagation: amyloid growth occurs by monomer addition. *PLoS Biol*. 2:e321.

Come, J.H., P.E. Fraser, and P.T. Lansbury. 1993. A kinetic model for amyloid formation in the prion diseases: importance of seeding. *Proc Natl Acad Sci USA*. 90:5959–5963.

Conchillo-Solé, O., N.S. de Groot, F.X. Aviles, J. Vendrell, X., Daura, and S. Ventura. 2007. AGGRESCAN: a server for the prediction and evaluation of "hot spots" of aggregation in polypeptides. *BCM Bioinformatics*. 8:65-81.

Cottrelle, P., M. Cool, P. Thuriaux, V.L. Price, D. Thiele, J.M. Buhler, and P. Fromageot. 1985. Either one of the two yeast EF-1 alpha genes is required for cell viability. *Curr Genet*. 9:693–697.

Coustou, V., C. Deleu, S. Saupe, and J. Begueret. 1997. The protein product of the het-s heterokaryon incompatibility gene of the fungus Podospora anserina behaves as a prion analog. *Proc Natl Acad Sci USA*. 94:9773–9778.

Cox, B. 1965. PSI, a cytoplasmic suppressor of super-suppressor in yeast. *Heredity (Edinb)*. 20:505–521.

Cox, B., F. Ness, and M. Tuite. 2003. Analysis of the generation and segregation of propagons: entities that propagate the [PSI+] prion in yeast. *Genetics*. 165:23–33.

Cox, B.S., L.J. Byrne, and M.F. Tuite. 2007. Prion stability. *Prion*. 1:170–178.

Crow, E.T., and L. Li. 2011. Newly identified prions in budding yeast, and their possible functions. *Seminars in cell & developmental biology*. 22:452–459.

Csermely, P., J. Kajtár, M. Hollósi, G. Jalsovszky, S. Holly, C.R. Kahn, P. Gergely, C. Söti, K. Mihály, and J. Somogyi. 1993. ATP induces a conformational change of the 90-kDa heat shock protein (hsp90). *J Biol Chem*. 268:1901–1907.

Cullie, J., and P.L. Chelle. 1939. Experimental transmission of trembling to the goat. *Comptes Rendus des Seances de l'Academie des Sciences*. 1058–1160.

Cunningham, C.N., K.A. Krukenberg, and D.A. Agard. 2008. Intra- and intermonomer interactions are required to synergistically facilitate ATP hydrolysis in Hsp90. *J Biol Chem*. 283:21170–21178.

Cyr, D.M., X. Lu, and M.G. Douglas. 1992. Regulation of Hsp70 function by a eukaryotic DnaJ homolog. *J Biol Chem*. 267:20927–20931.

D'Andrea, L.D., and L. Regan. 2003. TPR proteins: the versatile helix. *Trends Biochem Sci*. 28:655–662.

Davey, H.M., E.J.M. Cross, C.L. Davey, K. Gkargkas, D. Delneri, D.C. Hoyle, S.G. Oliver, D.B. Kell, and G.W. Griffith. 2012. Genome-wide analysis of longevity in nutrient-deprived Saccharomyces cerevisiae reveals importance of recycling in maintaining cell viability. *Environ. Microbiol.* 14:1249–1260.

De Fea, K.A., D.H. Nakahara, M.C. Calayag, C.S. Yost, L.F. Mirels, S.B. Prusiner, and V.R. Lingappa. 1994. Determinants of carboxyl-terminal domain translocation during prion protein biogenesis. *J Biol Chem*. 269:16810–16820.

DeArmond, S.J., M.P. McKinley, R.A. Barry, M.B. Braunfeld, J.R. McColloch, and S.B. Prusiner. 1985. Identification of prion amyloid filaments in scrapie-infected brain. *Cell*. 41:221–235.

DePace, A.H., A. Santoso, P. Hillner, and J.S. Weissman. 1998. A critical role for amino-terminal glutamine/asparagine repeats in the formation and propagation of a yeast prion. *Cell*. 93:1241–1252.

Derdowski, A., S.S. Sindi, C.L. Klaips, S. DiSalvo, and T.R. Serio. 2010. A size threshold limits prion transmission and establishes phenotypic diversity. *Science*. 330:680–683.

Derkatch, I.L., M.E. Bradley, J.Y. Hong, and S.W. Liebman. 2001. Prions affect the appearance of other prions: the story of [PIN(+)]. *Cell*. 106:171–182.

Derkatch, I.L., M.E. Bradley, P. Zhou, and S.W. Liebman. 1999. The PNM2 mutation in the prion protein domain of SUP35 has distinct effects on different variants of the [PSI+] prion in yeast. *Curr Genet*. 35:59–67.

Derkatch, I.L., M.E. Bradley, P. Zhou, Y.O. Chernoff, and S.W. Liebman. 1997. Genetic and environmental factors affecting the de novo appearance of the [PSI+] prion in Saccharomyces cerevisiae. *Genetics*. 147:507–519.

Derkatch, I.L., M.E. Bradley, S.V. Masse, S.P. Zadorsky, G.V. Polozkov, S.G. Inge-Vechtomov, and S.W. Liebman. 2000. Dependence and independence of [PSI(+)] and [PIN(+)]: a two-prion system in yeast? *EMBO J*. 19:1942–1952.

Derkatch, I.L., S.M. Uptain, T.F. Outeiro, R. Krishnan, S.L. Lindquist, and S.W. Liebman. 2004. Effects of Q/N-rich, polyQ, and non-polyQ amyloids on the de novo formation of the [PSI+] prion in yeast and aggregation of Sup35 in vitro. *Proc Natl Acad Sci USA*. 101:12934–12939.

Derkatch, I.L., Y.O. Chernoff, V.V. Kushnirov, S.G. Inge-Vechtomov, and S.W. Liebman. 1996. Genesis and variability of [PSI] prion factors in Saccharomyces cerevisiae. *Genetics*. 144:1375–1386.

Diamant, S., and P. Goloubinoff. 1998. Temperature-controlled activity of DnaK-DnaJ-GrpE chaperones: protein-folding arrest and recovery during and after heat shock depends on the substrate protein and the GrpE concentration. *Biochemistry*. 37:9688–9694.

Diaz-Avalos, R., C.-Y. King, J. Wall, M. Simon, and D.L.D. Caspar. 2005. Strain-specific morphologies of yeast prion amyloid fibrils. *Proc Natl Acad Sci USA*. 102:10165–10170.

Dickinson, A.G., and V.M. Meikle. 1969. A comparison of some biological characteristics of the mouse-passaged scrapie agents, 22A and ME7. *Genet. Res.* 13:213–225.

Didichenko, S.A., M.D. Ter-Avanesyan, and V.N. Smirnov. 1991. Ribosome-bound EF-1 alpha-like protein of yeast Saccharomyces cerevisiae. *Eur J Biochem*. 198:705–711.

DiSalvo, S., A. Derdowski, J.A. Pezza, and T.R. Serio. 2011. Dominant prion mutants induce curing through pathways that promote chaperone-mediated disaggregation. *Nat Struct Mol Biol*. 18:486–492.

Dolinski, K., S. Muir, M. Cardenas, and J. Heitman. 1997. All cyclophilins and FK506 binding proteins are, individually and collectively, dispensable for viability in Saccharomyces cerevisiae. *Proc Natl Acad Sci USA*. 94:13093–13098.

Douglas, P.M., S. Treusch, H.-Y. Ren, R. Halfmann, M.L. Duennwald, S. Lindquist, and D.M. Cyr. 2008. Chaperone-dependent amyloid assembly protects cells from prion toxicity. *Proc Natl Acad Sci USA*. 105:7206–7211.

Doyle, S.M., J. Shorter, M. Zolkiewski, J.R. Hoskins, S. Lindquist, and S. Wickner. 2007. Asymmetric deceleration of ClpB or Hsp104 ATPase activity unleashes protein-remodeling activity. *Nat Struct Mol Biol*. 14:114–122.

Dragovic, Z., S.A. Broadley, Y. Shomura, A. Bracher, and F.U. Hartl. 2006. Molecular chaperones of the Hsp110 family act as nucleotide exchange factors of Hsp70s. *EMBO J*. 25:2519–2528.

Du, Z., K.-W. Park, H. Yu, Q. Fan, and L. Li. 2008. Newly identified prion linked to the chromatin-remodeling factor Swi1 in Saccharomyces cerevisiae. *Nat Genet*. 40:460–465.

Duina, A.A., H.C. Chang, J.A. Marsh, S. Lindquist, and R.F. Gaber. 1996a. A cyclophilin function in Hsp90-dependent signal transduction. *Science*. 274:1713–1715.

Duina, A.A., J.A. Marsh, and R.F. Gaber. 1996b. Identification of two CyP-40-like cyclophilins in Saccharomyces cerevisiae, one of which is required for normal growth. *Yeast*. 12:943–952.

Eaglestone, S.S., L.W. Ruddock, B.S. Cox, and M.F. Tuite. 2000. Guanidine hydrochloride blocks a critical step in the propagation of the prion-like determinant [PSI+] of Saccharomyces cerevisiae. *Proc Natl Acad Sci USA*. 97:240–244.

Easton, D.P., Y. Kaneko, and J.R. Subjeck. 2000. The hsp110 and Grp1 70 stress proteins: newly recognized relatives of the Hsp70s. *Cell Stress Chaperones*. 5:276–290.

Eckert, K., J.-M. Saliou, L. Monlezun, A. Vigouroux, N. Atmane, C. Caillat, S. Quevillon-Chéruel, K. Madiona, M. Nicaise, S. Lazereg, A. Van Dorsselaer, S. Sanglier-Cianférani, P. Meyer, and S. Moréra. 2010. The Pih1-Tah1 cochaperone complex inhibits Hsp90 molecular chaperone ATPase activity. *J Biol Chem*. 285:31304–31312.

Edskes, H.K., V.T. Gray, and R.B. Wickner. 1999. The [URE3] prion is an aggregated form of Ure2p that can be cured by overexpression of Ure2p fragments. *Proc Natl Acad Sci USA*. 96:1498–1503.

Eigen, M. 1996. Prionics or the kinetic basis of prion diseases. *Biophys. Chem.* 63:A1–18.

Erhardt, M., R.D. Wegrzyn, and E. Deuerling. 2010. Extra N-terminal residues have a profound effect on the aggregation properties of the potential yeast prion protein Mca1. *PLoS ONE*. 5:e9929.

Fan, C.-Y., H.-Y. Ren, P. Lee, A.J. Caplan, and D.M. Cyr. 2005. The type I Hsp40 zinc finger-like region is required for Hsp70 to capture non-native polypeptides from Ydj1. *J Biol Chem*. 280:695–702.

Fan, Q., K.-W. Park, Z. Du, K.A. Morano, and L. Li. 2007. The role of Sse1 in the de novo formation and variant determination of the [PSI+] prion. *Genetics*. 177:1583–1593.

Fang, Y., A.E. Fliss, J. Rao, and A.J. Caplan. 1998. SBA1 encodes a yeast hsp90 cochaperone that is homologous to vertebrate p23 proteins. *Mol Cell Biol*. 18:3727–3734.

Fay, N., Y. Inoue, L. Bousset, H. Taguchi, and R. Melki. 2003. Assembly of the yeast prion Ure2p into protein fibrils. Thermodynamic and kinetic characterization. *J Biol Chem*. 278:30199–30205.

Fayard, B., N. Fay, G. David, J. Doucet, and R. Melki. 2006. Packing of the prion Ure2p in protein fibrils probed by fluorescence X-ray near-edge structure spectroscopy at sulfur K-edge. *J Mol Biol*. 356:843–849.

Fernandez-Escamilla, A.M., F. Rousseaux, J. Schymkowitz, and L. Serrano. 2004. Prediction of sequence-dependent and mutational effects on the aggregation of peptides and proteins. *Nat. Biotechnol.* 22:1302-1306.

Ferreira, P.C., F. Ness, S.R. Edwards, B.S. Cox, and M.F. Tuite. 2001. The elimination of the yeast [PSI+] prion by guanidine hydrochloride is the result of Hsp104 inactivation. *Mol Microbiol*. 40:1357–1369.

Flynn, G.C., J. Pohl, M.T. Flocco, and J.E. Rothman. 1991. Peptide-binding specificity of the molecular chaperone BiP. *Nature*. 353:726–730.

Fraser, H., and A.G. Dickinson. 1973. Scrapie in mice. Agent-strain differences in the distribution and intensity of grey matter vacuolation. *J. Comp. Pathol.* 83:29–40.

Freeman, B.C., S.J. Felts, D.O. Toft, and K.R. Yamamoto. 2000. The p23 molecular chaperones act at a late step in intracellular receptor action to differentially affect ligand efficacies. *Genes Dev*. 14:422–434.

Freshney, I. 1983. Culture of Animal Cells: A Manual of Basic Technique. *interscience.wiley.com*.

Frolova, L., X. Le Goff, H.H. Rasmussen, S. Cheperegin, G. Drugeon, M. Kress, I. Arman, A.L. Haenni, J.E. Celis, and M. Philippe. 1994. A highly conserved eukaryotic protein family possessing properties of polypeptide chain release factor. *Nature*. 372:701–703.

Frousios, K.K., V.A. Iconomidou, C.M. Karletidi, and S.J. Hamodrakas. 2009. Amyloidogenic determinants are usually not buried. *BMC Struct. Biol.* 9:44.

Frydman, J. 2001. Folding of newly translated proteins in vivo: the role of molecular chaperones. *Annu. Rev. Biochem.* 70:603–647.

Gajdusek, D.C., C.J. Gibbs, and M. Alpers. 1966. Experimental transmission of a Kuru-like syndrome to chimpanzees. *Nature*. 209:794–796.

Ganusova, E.E., L.N. Ozolins, S. Bhagat, G.P. Newnam, R.D. Wegrzyn, M.Y. Sherman, and Y.O. Chernoff. 2006. Modulation of prion formation, aggregation, and toxicity by the actin cytoskeleton in yeast. *Mol Cell Biol*. 26:617–629.

Garbuzynskiy, S.O., M.Y. Lobanov, and O.V. Galzitskaya. 2010. FoldAmyloid: a method of prediction of amyloidogenic regions from protein sequence. *Bioinformatics*. 26:326-332.

Gasset, M., M.A. Baldwin, R.J. Fletterick, and S.B. Prusiner. 1993. Perturbation of the secondary structure of the scrapie prion protein under conditions that alter infectivity. *Proc Natl Acad Sci USA*. 90:1–5.

Gautschi, M., A. Mun, S. Ross, and S. Rospert. 2002. A functional chaperone triad on the yeast ribosome. *Proc Natl Acad Sci USA*. 99:4209–4214.

Giaever, G., A.M. Chu, L. Ni, C. Connelly, L. Riles, S. Véronneau, S. Dow, A. Lucau-Danila, K. Anderson, B. André, A.P. Arkin, A. Astromoff, M. El-Bakkoury, R. Bangham, R. Benito, S. Brachat, S. Campanaro, M. Curtiss, K. Davis, A. Deutschbauer, K.-D. Entian, P. Flaherty, F. Foury, D.J. Garfinkel, M. Gerstein, D. Gotte, U. Güldener, J.H. Hegemann, S. Hempel, Z. Herman, D.F. Jaramillo, D.E. Kelly, S.L. Kelly, P. Kötter, D. LaBonte, D.C. Lamb, N. Lan, H. Liang, H. Liao, L. Liu, C. Luo, M. Lussier, R. Mao, P. Menard, S.L. Ooi, J.L. Revuelta, C.J. Roberts, M. Rose, P. Ross-Macdonald, B. Scherens, G. Schimmack, B. Shafer, D.D. Shoemaker, S. Sookhai-Mahadeo, R.K. Storms, J.N. Strathern, G. Valle, M. Voet, G. Volckaert, C.-Y. Wang, T.R. Ward, J. Wilhelmy, E.A. Winzeler, Y. Yang, G. Yen, E. Youngman, K. Yu, H. Bussey, J.D. Boeke, M. Snyder, P. Philippsen, R.W. Davis, and M. Johnston. 2002. Functional profiling of the Saccharomyces cerevisiae genome. *Nature*. 418:387–391.

Gibbs, C.J., D.C. Gajdusek, D.M. Asher, M.P. Alpers, E. Beck, P.M. Daniel, and W.B. Matthews. 1968. Creutzfeldt-Jakob disease (spongiform encephalopathy): transmission to the chimpanzee. *Science*. 161:388–389.

Gietz, R.D., and A. Sugino. 1988. New yeast-Escherichia coli shuttle vectors constructed with in vitro mutagenized yeast genes lacking six-base pair restriction sites. *Gene*. 74:527–534.

Gietz, R.D., and R.A. Woods. 2002. Transformation of yeast by lithium acetate/single-stranded carrier DNA/polyethylene glycol method. *Meth Enzymol*. 350:87–96.

Gisler, S.M., E.V. Pierpaoli, and P. Christen. 1998. Catapult mechanism renders the chaperone action of Hsp70 unidirectional. *J Mol Biol*. 279:833–840.

Ghetti, B., P. Piccardo, B. Frangione, O. Bugiani, G. Giaccone, K. Young, F. Prelli, M.R. Farlow, S.R. Dlougy, and F. Tagliavini. 1996. Prion protein amyloidosis. *Brain Pathol.* 5:61-75.

Glenner, G.G., E.D. Eanes, H.A. Bladen, R.P. Linke, and J.D. Termine. 1974. Beta-pleated sheet fibrils. A comparison of native amyloid with synthetic protein fibrils. *J. Histochem. Cytochem.* 22:1141–1158.

Glover, D.M., and B.D. Hames. 1995. DNA cloning : a practical approach. 2nd ed. Oxford University Press, New York.

Glover, J.R., A.S. Kowal, E.C. Schirmer, M.M. Patino, J.J. Liu, and S. Lindquist. 1997. Self-seeded fibers formed by Sup35, the protein determinant of [PSI+], a heritable prion-like factor of S. cerevisiae. *Cell*. 89:811–819.

Glover, J.R., and S. Lindquist. 1998. Hsp104, Hsp70, and Hsp40: a novel chaperone system that rescues previously aggregated proteins. *Cell*. 94:73–82.

Gokhale, K.C., G.P. Newnam, M.Y. Sherman, and Y.O. Chernoff. 2005. Modulation of prion-dependent polyglutamine aggregation and toxicity by chaperone proteins in the yeast model. *J Biol Chem*. 280:22809–22818.

Gordon, W.S. 1946. Advances in veterinary research. *Vet. Rec.* 58:516–525.

Gossert, A.D., S. Bonjour, D.A. Lysek, F. Fiorito, and K. Wüthrich. 2005. Prion protein NMR structures of elk and of mouse/elk hybrids. *Proc Natl Acad Sci USA*. 102:646–650.

Govaerts, C., H. Wille, S.B. Prusiner, and F.E. Cohen. 2004. Evidence for assembly of prions with left-handed beta-helices into trimers. *Proc Natl Acad Sci USA*. 101:8342–8347.

Graf, C., M. Stankiewicz, G. Kramer, and M.P. Mayer. 2009. Spatially and kinetically resolved changes in the conformational dynamics of the Hsp90 chaperone machine. *EMBO J*. 28:602–613.

Grenert, J.P., W.P. Sullivan, P. Fadden, T.A. Haystead, J. Clark, E. Mimnaugh, H. Krutzsch, H.J. Ochel, T.W. Schulte, E. Sausville, L.M. Neckers, and D.O. Toft. 1997. The amino-terminal domain of heat shock protein 90 (hsp90) that binds geldanamycin is an ATP/ADP switch domain that regulates hsp90 conformation. *J Biol Chem*. 272:23843–23850.

Griffith, F. 1928. The Significance of Pneumococcal Types. *J Hyg (Lond)*. 27:113–159.

Griffith, J.S. 1967. Self-replication and scrapie. *Nature*. 215:1043–1044.

Grimminger, V., K. Richter, A. Imhof, J. Buchner, and S. Walter. 2004. The prion curing agent guanidinium chloride specifically inhibits ATP hydrolysis by Hsp104. *J Biol Chem*. 279:7378–7383.

Hainzl, O., M.C. Lapina, J. Buchner, and K. Richter. 2009. The charged linker region is an important regulator of Hsp90 function. *J Biol Chem*. 284:22559–22567.

Halfmann, R., and S. Lindquist. 2008. Screening for amyloid aggregation by Semi-Denaturing Detergent-Agarose Gel Electrophoresis.

Halfmann, R., and S. Lindquist. 2010. Epigenetics in the extreme: prions and the inheritance of environmentally acquired traits. *Science*. 330:629–632.

Halfmann, R., D.F. Jarosz, S.K. Jones, A. Chang, A.K. Lancaster, and S. Lindquist. 2012. Prions are a common mechanism for phenotypic inheritance in wild yeasts. *Nature*. 482:363–368.

Halfmann, R., S. Alberti, and S. Lindquist. 2010. Prions, protein homeostasis, and phenotypic diversity. *Trends in cell biology*.

Halfmann, R., S. Alberti, R. Krishnan, N. Lyle, C.W. O'Donnell, O.D. King, B. Berger, R.V. Pappu, and S. Lindquist. 2011. Opposing effects of glutamine and asparagine govern prion formation by intrinsically disordered proteins. *Mol Cell*. 43:72–84.

Hamodrakas, S.J. 2011. Protein aggregation and amyloid formation prediction software from primary sequence: towards controlling the formation of bacterial inclusion bodies. *FEBS Journal*. 278:2428-2435.

Hanahan, D. 1983. Studies on transformation of Escherichia coli with plasmids. *J Mol Biol*. 166:557–580.

Harlow, E., and D. Lane. 1988. Antibodies: a laboratory manual. *books.google.com*.

Harris, D.A. 2003. Trafficking, turnover and membrane topology of PrP. *Br Med Bull*. 66:71–85.

Harris, S.F., A.K. Shiau, and D.A. Agard. 2004. The crystal structure of the carboxy-terminal dimerization domain of htpG, the Escherichia coli Hsp90, reveals a potential substrate binding site. *Structure*. 12:1087–1097.

Harst, A., H. Lin, and W.M.J. Obermann. 2005. Aha1 competes with Hop, p50 and p23 for binding to the molecular chaperone Hsp90 and contributes to kinase and hormone receptor activation. *Biochem J*. 387:789–796.

Haslbeck, M., A. Miess, T. Stromer, S. Walter, and J. Buchner. 2005. Disassembling protein aggregates in the yeast cytosol. The cooperation of Hsp26 with Ssa1 and Hsp104. *J Biol Chem*. 280:23861–23868.

Helsen, C.W., and J.R. Glover. 2012. Insight into molecular basis of curing of [PSI+] prion by overexpression of 104-kDa heat shock protein (Hsp104). *J Biol Chem*. 287:542–556.

Hershey, A., and M. Chase. 1952. Independent functions of viral protein and nucleic acid in growth of bacteriophage. *J. Gen. Physiol.* 36:39–56.

Herskowitz, I., and R.E. Jensen. 1991. Putting the HO gene to work: practical uses for mating-type switching. *Meth Enzymol*. 194:132–146.

Hessling, M., K. Richter, and J. Buchner. 2009. Dissection of the ATP-induced conformational cycle of the molecular chaperone Hsp90. *Nat Struct Mol Biol*. 16:287–293.

Hettema, E.H., C.C. Ruigrok, M.G. Koerkamp, M. van den Berg, H.F. Tabak, B. Distel, and I. Braakman. 1998. The cytosolic DnaJ-like protein djp1p is involved specifically in peroxisomal protein import. *J Cell Biol*. 142:421–434.

Higurashi, T., J.K. Hines, C. Sahi, R. Aron, and E.A. Craig. 2008. Specificity of the J-protein Sis1 in the propagation of 3 yeast prions. *Proc Natl Acad Sci USA*. 105:16596–16601.

Hines, J.K., X. Li, Z. Du, T. Higurashi, L. Li, and E.A. Craig. 2011. [SWI], the prion formed by the chromatin remodeling factor Swi1, is highly sensitive to alterations in Hsp70 chaperone system activity. *PLoS Genet*. 7:e1001309.

Holstein, S.E., H. Ungewickell, and E. Ungewickell. 1996. Mechanism of clathrin basket dissociation: separate functions of protein domains of the DnaJ homologue auxilin. *J Cell Biol*. 135:925–937.

Horiuchi, M., S.A. Priola, J. Chabry, and B. Caughey. 2000. Interactions between heterologous forms of prion protein: binding, inhibition of conversion, and species barriers. *Proc Natl Acad Sci USA*. 97:5836–5841.

Horton, R.M., H.D. Hunt, S.N. Ho, J.K. Pullen, and L.R. Pease. 1989. Engineering hybrid genes without the use of restriction enzymes: gene splicing by overlap extension. *Gene*. 77:61–68.

Hosoda, N., T. Kobayashi, N. Uchida, Y. Funakoshi, Y. Kikuchi, S. Hoshino, and T. Katada. 2003. Translation termination factor eRF3 mediates mRNA decay through the regulation of deadenylation. *J Biol Chem*. 278:38287–38291.

Hsiao, K.K., D. Groth, M. Scott, S.L. Yang, H. Serban, D. Rapp, D. Foster, M. Torchia, S.J. DeArmond, and S.B. Prusiner. 1994. Serial transmission in rodents of neurodegeneration from transgenic mice expressing mutant prion protein. *Proc Natl Acad Sci USA*. 91:9126–9130.

Hsiao, K.K., M. Scott, D. Foster, D.F. Groth, S.J. DeArmond, and S.B. Prusiner. 1990. Spontaneous neurodegeneration in transgenic mice with mutant prion protein. *Science*. 250:1587–1590.

Huang, T.Y., L.S. Minamide, J.R. Bamburg, and G.M. Bokoch. 2008. Chronophin mediates an ATP-sensing mechanism for cofilin dephosphorylation and neuronal cofilin-actin rod formation. *Dev Cell*. 15:691–703.

Huh, W.-K., J.V. Falvo, L.C. Gerke, A.S. Carroll, R.W. Howson, J.S. Weissman, and E.K. O'Shea. 2003. Global analysis of protein localization in budding yeast. *Nature*. 425:686–691.

Hundley, H., H. Eisenman, W. Walter, T. Evans, Y. Hotokezaka, M. Wiedmann, and E. Craig. 2002. The in vivo function of the ribosome-associated Hsp70, Ssz1, does not require its putative peptide-binding domain. *Proc Natl Acad Sci USA*. 99:4203–4208.

Hung, G.-C., and D.C. Masison. 2006. N-terminal domain of yeast Hsp104 chaperone is dispensable for thermotolerance and prion propagation but necessary for curing prions by Hsp104 overexpression. *Genetics*. 173:611–620.

Innis, M.A., and D.H. Gelfland. 1990. PCR protocols: a guide to methods and applications. M.A. Innis, D.H. Gelfland, J.J. Sninsky, and T.J. White, editors. Academic Press, Waltham, MA.

Inoue, Y., A. Kishimoto, J. Hirao, M. Yoshida, and H. Taguchi. 2001. Strong growth polarity of yeast prion fiber revealed by single fiber imaging. *J Biol Chem*. 276:35227–35230.

Issel-Tarver, L., K.R. Christie, K. Dolinski, R. Andrada, R. Balakrishnan, C.A. Ball, G. Binkley, S. Dong, S.S. Dwight, D.G. Fisk, M. Harris, M. Schroeder, A. Sethuraman, K. Tse, S. Weng, D. Botstein, and J.M. Cherry. 2002. Saccharomyces Genome Database. *Meth Enzymol*. 350:329–346.

Jakob, U., I. Meyer, H. Bügl, S. André, J.C. Bardwell, and J. Buchner. 1995. Structural organization of procaryotic and eucaryotic Hsp90. Influence of divalent cations on structure and function. *J Biol Chem*. 270:14412–14419.

Jansen, G., C. Wu, B. Schade, D.Y. Thomas, and M. Whiteway. 2005. Drag&Drop cloning in yeast. *Gene*. 344:43–51.

Jiang, J., K. Prasad, E.M. Lafer, and R. Sousa. 2005. Structural basis of interdomain communication in the Hsc70 chaperone. *Mol Cell*. 20:513–524.

Jones, G., Y. Song, S. Chung, and D.C. Masison. 2004. Propagation of Saccharomyces cerevisiae [PSI+] prion is impaired by factors that regulate Hsp70 substrate binding. *Mol Cell Biol*. 24:3928–3937.

Jung, G., and D.C. Masison. 2001. Guanidine hydrochloride inhibits Hsp104 activity in vivo: a possible explanation for its effect in curing yeast prions. *Curr. Microbiol.* 43:7–10.

Jung, G., G. Jones, R.D. Wegrzyn, and D.C. Masison. 2000. A role for cytosolic hsp70 in yeast [PSI(+)] prion propagation and [PSI(+)] as a cellular stress. *Genetics*. 156:559–570.

Kabani, M., J.-M. Beckerich, and J.L. Brodsky. 2002. Nucleotide exchange factor for the yeast Hsp70 molecular chaperone Ssa1p. *Mol Cell Biol*. 22:4677–4689.

Kadnar, M.L., G. Articov, and I.L. Derkatch. 2010. Distinct type of transmission barrier revealed by study of multiple prion determinants of Rnq1. *PLoS Genet*. 6:e1000824.

Kaganovich, D., R. Kopito, and J. Frydman. 2008. Misfolded proteins partition between two distinct quality control compartments. *Nature*. 454:1088–1095.

Kakihara, Y., and W.A. Houry. 2012. The R2TP complex: discovery and functions. *Biochim Biophys Acta*. 1823:101–107.

Kalastavadi, T., and H.L. True. 2010. Analysis of the [RNQ+] prion reveals stability of amyloid fibers as the key determinant of yeast prion variant propagation.

Kampinga, H.H., and E.A. Craig. 2010. The HSP70 chaperone machinery: J proteins as drivers of functional specificity. *Nat Rev Mol Cell Biol*. 11:579–592.

Kawai-Noma, S., C.-G. Pack, T. Kojidani, H. Asakawa, Y. Hiraoka, M. Kinjo, T. Haraguchi, H. Taguchi, and A. Hirata. 2010. In vivo evidence for the fibrillar structures of Sup35 prions in yeast cells. *J Cell Biol*.

Kern, D., M. Schutkowski, and D. Torbjorn. 1997. Rotational Barriers of cis/trans isomerization of proline analogues and their catalysis by cyclophilin. *J. Am. Chem. Soc.* 8403–8408.

Kim, S., J. Choi, S.J. Lee, W.J. Welsh, and S. Yoon. 2009. NetCSSP: web application for predicting chameleon sequences and amyloid fibril formation. *Nucl. Acids Res.* 37:W469-W473.

Kimberlin, R.H. 1982. Scrapie agent: prions or virinos? *Nature*. 297:107–108.

King, C.-Y., and R. Diaz-Avalos. 2004. Protein-only transmission of three yeast prion strains. *Nature*. 428:319–323.

King, C.Y. 2001. Supporting the structural basis of prion strains: induction and identification of [PSI] variants. *J Mol Biol*. 307:1247–1260.

King, C.Y., P. Tittmann, H. Gross, R. Gebert, M. Aebi, and K. Wüthrich. 1997. Prion-inducing domain 2-114 of yeast Sup35 protein transforms in vitro into amyloid-like filaments. *Proc Natl Acad Sci USA*. 94:6618–6622.

Kirkland, P.A., M. Reidy, and D.C. Masison. 2011. Functions of yeast Hsp40 chaperone Sis1p dispensable for prion propagation but important for prion curing and protection from prion toxicity. *Genetics*. 188:565–577.

Kishimoto, A., K. Hasegawa, H. Suzuki, H. Taguchi, K. Namba, and M. Yoshida. 2004. beta-Helix is a likely core structure of yeast prion Sup35 amyloid fibers. *Biochem Biophys Res Commun*. 315:739–745.

Kitamoto, T., J. Tateishi, T. Tashima, I. Takeshita, R.A. Barry, S.J. DeArmond, and S.B. Prusiner. 1986. Amyloid plaques in Creutzfeldt-Jakob disease stain with prion protein antibodies. *Ann. Neurol.* 20:204–208.

Kochneva-Pervukhova, N.V., M.B. Chechenova, I.A. Valouev, V.V. Kushnirov, V.N. Smirnov, and M.D. Ter-Avanesyan. 2001. [Psi(+)] prion generation in yeast: characterization of the "strain" difference. *Yeast*. 18:489–497.

Kocisko, D.A., J.H. Come, S.A. Priola, B. Chesebro, G.J. Raymond, P.T. Lansbury, and B. Caughey. 1994. Cell-free formation of protease-resistant prion protein. *Nature*. 370:471–474.

Kocisko, D.A., S.A. Priola, G.J. Raymond, B. Chesebro, P.T. Lansbury, and B. Caughey. 1995. Species specificity in the cell-free conversion of prion protein to protease-resistant forms: a model for the scrapie species barrier. *Proc Natl Acad Sci USA*. 92:3923–3927.

Krishnan, R., and S.L. Lindquist. 2005. Structural insights into a yeast prion illuminate nucleation and strain diversity. *Nature*. 435:765–772.

Krukenberg, K.A., T.O. Street, L.A. Lavery, and D.A. Agard. 2011. Conformational dynamics of the molecular chaperone Hsp90. *Q. Rev. Biophys.* 44:229–255.

Kryndushkin, D., and R.B. Wickner. 2007. Nucleotide exchange factors for Hsp70s are required for [URE3] prion propagation in Saccharomyces cerevisiae. *Mol Biol Cell*. 18:2149–2154.

Kryndushkin, D.S., I.M. Alexandrov, M.D. Ter-Avanesyan, and V.V. Kushnirov. 2003. Yeast [PSI+] prion aggregates are formed by small Sup35 polymers fragmented by Hsp104. *J Biol Chem*. 278:49636–49643.

Kryndushkin, D.S., R.B. Wickner, and R. Tycko. 2011. The core of Ure2p prion fibrils is formed by the N-terminal segment in a parallel cross-β structure: evidence from solid-state NMR. *J Mol Biol*. 409:263–277.

Kryndushkin, D.S., V.N. Smirnov, M.D. Ter-Avanesyan, and V.V. Kushnirov. 2002. Increased expression of Hsp40 chaperones, transcriptional factors, and ribosomal protein Rpp0 can cure yeast prions. *J Biol Chem*. 277:23702–23708.

Krzewska, J., M. Tanaka, S.G. Burston, and R. Melki. 2007. Biochemical and functional analysis of the assembly of full-length Sup35p and its prion-forming domain. *J Biol Chem*. 282:1679–1686.

Kurahashi, H., C.-G. Pack, S. Shibata, K. Oishi, Y. Sako, and Y. Nakamura. 2011. [PSI(+)] aggregate enlargement in rnq1 nonprion domain mutants, leading to a loss of prion in yeast. *Genes Cells*. 16:576–589.

Kurahashi, H., M. Ishiwata, S. Shibata, and Y. Nakamura. 2008. A regulatory role of the Rnq1 nonprion domain for prion propagation and polyglutamine aggregates. *Mol Cell Biol*. 28:3313–3323.

Kurahashi, H., S. Shibata, M. Ishiwata, and Y. Nakamura. 2009. Selfish prion of Rnq1 mutant in yeast. *Genes Cells*. 14:659–668.

Kushnirov, V.V., and M.D. Ter-Avanesyan. 1998. Structure and replication of yeast prions. *Cell*. 94:13–16.

Kushnirov, V.V., D.S. Kryndushkin, M. Boguta, V.N. Smirnov, and M.D. Ter-Avanesyan. 2000. Chaperones that cure yeast artificial [PSI+] and their prion-specific effects. *Curr. Biol.* 10:1443–1446.

Lacroute, F. 1971. Non-Mendelian mutation allowing ureidosuccinic acid uptake in yeast. *J Bacteriol*. 106:519–522.

Lancaster, A.K., J.P. Bardill, H.L. True, and J. Masel. 2010. The spontaneous appearance rate of the yeast prion [PSI+] and its implications for the evolution of the evolvability properties of the [PSI+] system. *Genetics*. 184:393–400.

Lancaster, D.L., C.M. Dobson, and R.A. Rachubinksi. 2013. Chaperone proteins select and maintain [*PIN*$^{+}$] prion conformations in *Saccharomyces cerevisiae*. *JBC*. 288:1266-1276.

Laufen, T., M.P. Mayer, C. Beisel, D. Klostermeier, A. Mogk, J. Reinstein, and B. Bukau. 1999. Mechanism of regulation of hsp70 chaperones by DnaJ cochaperones. *Proc Natl Acad Sci USA*. 96:5452–5457.

Legname, G., I.V. Baskakov, H.-O.B. Nguyen, D. Riesner, F.E. Cohen, S.J. DeArmond, and S.B. Prusiner. 2004. Synthetic mammalian prions. *Science*. 305:673–676.

Leibowitz, M.J., and R.B. Wickner. 1978. Pet18: a chromosomal gene required for cell growth and for the maintenance of mitochondrial DNA and the killer plasmid of yeast. *Mol. Gen. Genet.* 165:115–121.

LeVine, H. 1993. Thioflavine T interaction with synthetic Alzheimer's disease beta-amyloid peptides: detection of amyloid aggregation in solution. *Protein Sci*. 2:404–410.

Li, J., K. Richter, and J. Buchner. 2011. Mixed Hsp90-cochaperone complexes are important for the progression of the reaction cycle. *Nat Struct Mol Biol*. 18:61–66.

Li, J., Y. Wu, X. Qian, and B. Sha. 2006. Crystal structure of yeast Sis1 peptide-binding fragment and Hsp70 Ssa1 C-terminal complex. *Biochem J*. 398:353–360.

Li, J., K. Richter, J. Reinstein, and J. Buchner. 2013. Integration of the accelerator Aha1 in the Hsp90 co-chaperone cycle. *Nat. Struct. Mol. Biol.* 10.1038.nsmb.20502.

Lian, H.-Y., H. Zhang, Z.-R. Zhang, H.M. Loovers, G.W. Jones, P.J.E. Rowling, L.S. Itzhaki, J.-M. Zhou, and S. Perrett. 2007. Hsp40 interacts directly with the native state of the yeast prion protein Ure2 and inhibits formation of amyloid-like fibrils. *J Biol Chem*. 282:11931–11940.

Liebman, S.W., and M. Cavenagh. 1980. An antisuppressor that acts on omnipotent suppressors in yeast. *Genetics*. 95:49–61.

Liebman, S.W., and Y.O. Chernoff. 2012. Prions in Yeast. *Genetics*. 191:1041–1072.

Liebman, S.W., S.N. Bagriantsev, and I.L. Derkatch. 2006. Biochemical and genetic methods for characterization of [PIN+] prions in yeast. *Methods*. 39:23–34.

Liu, J.-J., N. Sondheimer, and S.L. Lindquist. 2002. Changes in the middle region of Sup35 profoundly alter the nature of epigenetic inheritance for the yeast prion [PSI+]. *Proc Natl Acad Sci USA*. 99 Suppl 4:16446–16453.

Lopez, N., R. Aron, and E.A. Craig. 2003. Specificity of class II Hsp40 Sis1 in maintenance of yeast prion [RNQ+]. *Mol Biol Cell*. 14:1172–1181.

López García, F., R. Zahn, R. Riek, and K. Wüthrich. 2000. NMR structure of the bovine prion protein. *Proc Natl Acad Sci USA*. 97:8334–8339.

Lu, Z., and D.M. Cyr. 1998a. The conserved carboxyl terminus and zinc finger-like domain of the co-chaperone Ydj1 assist Hsp70 in protein folding. *J Biol Chem*. 273:5970–5978.

Lu, Z., and D.M. Cyr. 1998b. Protein folding activity of Hsp70 is modified differentially by the hsp40 co-chaperones Sis1 and Ydj1. *J Biol Chem*. 273:27824–27830.

Luke, M.M., A. Sutton, and K.T. Arndt. 1991. Characterization of SIS1, a Saccharomyces cerevisiae homologue of bacterial dnaJ proteins. *J Cell Biol*. 114:623–638.

Lysek, D.A., C. Schorn, L.G. Nivon, V. Esteve-Moya, B. Christen, L. Calzolai, C. von Schroetter, F. Fiorito, T. Herrmann, P. Güntert, and K. Wüthrich. 2005. Prion protein NMR structures of cats, dogs, pigs, and sheep. *Proc Natl Acad Sci USA*. 102:640–645.

Mackay, R.G., C.W. Helsen, J.M. Tkach, and J.R. Glover. 2008. The C-terminal extension of Saccharomyces cerevisiae Hsp104 plays a role in oligomer assembly. *Biochemistry*. 47:1918–1927.

Maddelein, M.-L., S. Dos Reis, S. Duvezin-Caubet, B. Coulary-Salin, and S.J. Saupe. 2002. Amyloid aggregates of the HET-s prion protein are infectious. *Proc Natl Acad Sci USA*. 99:7402–7407.

Mah, A.S., A.E.H. Elia, G. Devgan, J. Ptacek, M. Schutkowski, M. Snyder, M.B. Yaffe, and R.J. Deshaies. 2005. Substrate specificity analysis of protein kinase complex Dbf2-Mob1 by peptide library and proteome array screening. *BMC Biochem.* 6:22.

Majumdar, A., W.C. Cesario, E. White-Grindley, H. Jiang, F. Ren, M.R. Khan, L. Li, E.M.-L. Choi, K. Kannan, F. Guo, J. Unruh, B. Slaughter, and K. Si. 2012. Critical Role of Amyloid-like Oligomers of Drosophila Orb2 in the Persistence of Memory. *Cell*.

Maniatis, T., J. Sambrook, and E. Fritsch. 1982. Molecular cloning: a laboratory manual. Cold Spring Harbor Laboratory, Cold Spring Harbor, N.Y.

Manogaran, A.L., V.M. Fajardo, R.J.D. Reid, R. Rothstein, and S.W. Liebman. 2009. Most, but not all, yeast strains in the deletion library contain the [PIN(+)] prion. *Yeast*.

Marsh, J.A., H.M. Kalton, and R.F. Gaber. 1998. Cns1 is an essential protein associated with the hsp90 chaperone complex in Saccharomyces cerevisiae that can restore cyclophilin 40-dependent functions in cpr7Delta cells. *Mol Cell Biol*. 18:7353–7359.

Masison, D.C., and R.B. Wickner. 1995. Prion-Inducing Domain of Yeast Ure2p and Protease Resistance of Ure2p in Prion-Containing Cells. *Science*. 270:93–95.

Masison, D.C., P.A. Kirkland, and D. Sharma. 2009. Influence of Hsp70s and their regulators on yeast prion propagation. *Prion*. 3:65–73.

Mastrianni, J.A., and K. Brown. 2010. The Prion Diseases. *Journal of geriatric psychiatry and neurology*. 23:277–298.

Mastushita-Sakai, T., E. White-Grindley, J. Samuelson, C. Seidel, and K. Si. 2010. Drosophila Orb2 targets genes involved in neuronal growth, synapse formation, and protein turnover. *Proc Natl Acad Sci USA*. 107:11987–11992.

Mathur, V., V. Taneja, Y. Sun, and S.W. Liebman. 2010. Analyzing the Birth and Propagation of Two Distinct Prions in Yeast. *Mol Biol Cell*.

Maurer-Stroh, S., M. Debulpaep, N. Kuemmerer, M. Lopez de la Paz, I.C. Martins, J. Reumers, K.L. Morris, A. Copland, L. Serpell, L. Serrano, et al. 2010. Exploring the sequence determinants of amyloid structure using position-specific scoring matrices. *Nat. Methods*. 7:237-245.

Mayer, M.P., H. Schröder, S. Rüdiger, K. Paal, T. Laufen, and B. Bukau. 2000. Multistep mechanism of substrate binding determines chaperone activity of Hsp70. *Nat. Struct. Biol.* 7:586–593.

Mayr, C., K. Richter, H. Lilie, and J. Buchner. 2000. Cpr6 and Cpr7, two closely related Hsp90-associated immunophilins from Saccharomyces cerevisiae, differ in their functional properties. *J Biol Chem*. 275:34140–34146.

McCarty, J.S., A. Buchberger, J. Reinstein, and B. Bukau. 1995. The role of ATP in the functional cycle of the DnaK chaperone system. *J Mol Biol*. 249:126–137.

McGlinchey, R.P., D. Kryndushkin, and R.B. Wickner. 2011. Suicidal [PSI+] is a lethal yeast prion. *Proc Natl Acad Sci USA*. 108:5337–5341.

McGowan, J. 1922. Scrapie in sheep. *Scottish Journal of Agriculture*. 365–375.

McKinley, M.P., D.C. Bolton, and S.B. Prusiner. 1983. A protease-resistant protein is a structural component of the scrapie prion. *Cell*. 35:57–62.

McLaughlin, S.H., F. Sobott, Z.-P. Yao, W. Zhang, P.R. Nielsen, J.G. Grossmann, E.D. Laue, C.V. Robinson, and S.E. Jackson. 2006. The co-chaperone p23 arrests the Hsp90 ATPase cycle to trap client proteins. *J Mol Biol*. 356:746–758.

Mestel, R. 1996. Putting prions to the test. *Science*. 273:184–189.

Meyer, P., C. Prodromou, C. Liao, B. Hu, S. Mark Roe, C.K. Vaughan, I. Vlasic, B. Panaretou, P.W. Piper, and L.H. Pearl. 2004. Structural basis for recruitment of the ATPase activator Aha1 to the Hsp90 chaperone machinery. *EMBO J*. 23:1402–1410.

Meyer, R.K., M.P. McKinley, K.A. Bowman, M.B. Braunfeld, R.A. Barry, and S.B. Prusiner. 1986. Separation and properties of cellular and scrapie prion proteins. *Proc Natl Acad Sci USA*. 83:2310–2314.

Michelitsch, M.D., and J.S. Weissman. 2000. A census of glutamine/asparagine-rich regions: implications for their conserved function and the prediction of novel prions. *Proc Natl Acad Sci USA*. 97:11910–11915.

Millson, S.H., C.K. Vaughan, C. Zhai, M.M.U. Ali, B. Panaretou, P.W. Piper, L.H. Pearl, and C. Prodromou. 2008. Chaperone ligand-discrimination by the TPR-domain protein Tah1. *Biochem J*. 413:261–268.

Minami, Y., Y. Kimura, H. Kawasaki, K. Suzuki, and I. Yahara. 1994. The carboxy-terminal region of mammalian HSP90 is required for its dimerization and function in vivo. *Mol Cell Biol*. 14:1459–1464.

Moosavi, B., J. Wongwigkarn, and M.F. Tuite. 2010. Hsp70/Hsp90 co-chaperones are required for efficient Hsp104-mediated elimination of the yeast [PSI(+)] prion but not for prion propagation. *Yeast*. 27:167–179.

Morano, K.A., C.M. Grant, and W.S. Moye-Rowley. 2012. The response to heat shock and oxidative stress in Saccharomyces cerevisiae. *Genetics*. 190:1157–1195.

Moriyama, H., H.K. Edskes, and R.B. Wickner. 2000. [URE3] prion propagation in Saccharomyces cerevisiae: requirement for chaperone Hsp104 and curing by overexpressed chaperone Ydj1p. *Mol Cell Biol*. 20:8916–8922.

Mukai, H., T. Kuno, H. Tanaka, D. Hirata, T. Miyakawa, and C. Tanaka. 1993. Isolation and characterization of SSE1 and SSE2, new members of the yeast HSP70 multigene family. *Gene*. 132:57–66.

Nadeau, K., A. Das, and C.T. Walsh. 1993. Hsp90 chaperonins possess ATPase activity and bind heat shock transcription factors and peptidyl prolyl isomerases. *J Biol Chem*. 268:1479–1487.

Nakayashiki, T., C.P. Kurtzman, H.K. Edskes, and R.B. Wickner. 2005. Yeast prions [URE3] and [PSI+] are diseases. *Proc Natl Acad Sci USA*. 102:10575–10580.

Narang, H. 2002. A critical review of the nature of the spongiform encephalopathy agent: protein theory versus virus theory. *Exp. Biol. Med. (Maywood)*. 227:4–19.

Nathan, D.F., M.H. Vos, and S. Lindquist. 1999. Identification of SSF1, CNS1, and HCH1 as multicopy suppressors of a Saccharomyces cerevisiae Hsp90 loss-of-function mutation. *Proc Natl Acad Sci USA*. 96:1409–1414.

Needleman, R.B., and A. Tzagoloff. 1975. Breakage of yeast: a method for processing multiple samples. *Anal Biochem*. 64:545–549.

Nelson, R.J., T. Ziegelhoffer, C. Nicolet, M. Werner-Washburne, and E.A. Craig. 1992. The translation machinery and 70 kd heat shock protein cooperate in protein synthesis. *Cell*. 71:97–105.

Nemecek, J., T. Nakayashiki, and R.B. Wickner. 2009. A prion of yeast metacaspase homolog (Mca1p) detected by a genetic screen. *Proc Natl Acad Sci USA*. 106:1892–1896.

Ness, F., P. Ferreira, B.S. Cox, and M.F. Tuite. 2002. Guanidine hydrochloride inhibits the generation of prion "seeds" but not prion protein aggregation in yeast. *Mol Cell Biol*. 22:5593–5605.

Newnam, G.P., R.D. Wegrzyn, S.L. Lindquist, and Y.O. Chernoff. 1999. Antagonistic interactions between yeast chaperones Hsp104 and Hsp70 in prion curing. *Mol Cell Biol*. 19:1325–1333.

Ngo, S., V. Chiang, and Z. Guo. 2012. Quantitative analysis of spin exchange interactions to identify β strand and turn regions in Ure2 prion domain fibrils with site-directed spin labeling. *J Struct Biol*.

Ochel, H.J., G. Gademann, J. Trepel, and L. Neckers. 2003. Modulation of prion protein structural integrity by geldanamycin. *Glycobiology*. 13:655–660.

Oesch, B., D. Westaway, M. Wälchli, M.P. McKinley, S.B. Kent, R. Aebersold, R.A. Barry, P. Tempst, D.B. Teplow, and L.E. Hood. 1985. A cellular gene encodes scrapie PrP 27-30 protein. *Cell*. 40:735–746.

Ogden, R.C., and D.A. Adams. 1987. Electrophoresis in agarose and acrylamide gels. *Meth Enzymol*. 152:61–87.

Oh, H.J., X. Chen, and J.R. Subjeck. 1997. Hsp110 protects heat-denatured proteins and confers cellular thermoresistance. *J Biol Chem*. 272:31636–31640.

Osherovich, L.Z., and J.S. Weissman. 2001. Multiple Gln/Asn-rich prion domains confer susceptibility to induction of the yeast [PSI(+)] prion. *Cell*. 106:183–194.

Osherovich, L.Z., and J.S. Weissman. 2002. The utility of prions. *Dev Cell*. 2:143–151.

Osipiuk, J., M.A. Walsh, B.C. Freeman, R.I. Morimoto, and A. Joachimiak. 1999. Structure of a new crystal form of human Hsp70 ATPase domain. *Acta Crystallogr. D Biol. Crystallogr.* 55:1105–1107.

Owens-Grillo, J.K., K. Hoffmann, K.A. Hutchison, A.W. Yem, M.R. Deibel, R.E. Handschumacher, and W.B. Pratt. 1995. The cyclosporin A-binding immunophilin CyP-40 and the FK506-binding immunophilin hsp56 bind to a common site on hsp90 and exist in independent cytosolic heterocomplexes with the untransformed glucocorticoid receptor. *J Biol Chem*. 270:20479–20484.

Palmer, K.J., M.S. Ridout, and B.J.T. Morgan. 2011. Kinetic models of guanidine hydrochloride-induced curing of the yeast [PSI+] prion. *J. Theor. Biol.* 274:1–11.

Pan, K.M., M. Baldwin, J. Nguyen, M. Gasset, A. Serban, D. Groth, I. Mehlhorn, Z. Huang, R.J. Fletterick, and F.E. Cohen. 1993. Conversion of alpha-helices into beta-sheets features in the formation of the scrapie prion proteins. *Proc Natl Acad Sci USA*. 90:10962–10966.

Panaretou, B., G. Siligardi, P. Meyer, A. Maloney, J.K. Sullivan, S. Singh, S.H. Millson, P.A. Clarke, S. Naaby-Hansen, R. Stein, R. Cramer, M. Mollapour, P. Workman, P.W. Piper, L.H. Pearl, and C. Prodromou. 2002. Activation of the ATPase activity of hsp90 by the stress-regulated cochaperone aha1. *Mol Cell*. 10:1307–1318.

Park, K.-W., J.-S. Hahn, Q. Fan, D.J. Thiele, and L. Li. 2006. De novo appearance and "strain" formation of yeast prion [PSI+] are regulated by the heat-shock transcription factor. *Genetics*. 173:35–47.

Parsell, D.A., A.S. Kowal, M.A. Singer, and S. Lindquist. 1994. Protein disaggregation mediated by heat-shock protein Hsp104. *Nature*. 372:475–478.

Patel, B.K., and S.W. Liebman. 2007. "Prion-proof" for [PIN+]: infection with in vitro-made amyloid aggregates of Rnq1p-(132-405) induces [PIN+]. *J Mol Biol*. 365:773–782.

Patel, B.K., J. Gavin-Smyth, and S.W. Liebman. 2009. The yeast global transcriptional co-repressor protein Cyc8 can propagate as a prion. *Nat Cell Biol*. 11:344–349.

Patino, M.M., J.J. Liu, J.R. Glover, and S. Lindquist. 1996. Support for the prion hypothesis for inheritance of a phenotypic trait in yeast. *Science*. 273:622–626.

Paushkin, S.V., V.V. Kushnirov, V.N. Smirnov, and M.D. Ter-Avanesyan. 1996. Propagation of the yeast prion-like [psi+] determinant is mediated by oligomerization of the SUP35-encoded polypeptide chain release factor. *EMBO J*. 15:3127–3134.

Paushkin, S.V., V.V. Kushnirov, V.N. Smirnov, and M.D. Ter-Avanesyan. 1997. In vitro propagation of the prion-like state of yeast Sup35 protein. *Science*. 277:381–383.

Pellecchia, M., T. Szyperski, D. Wall, C. Georgopoulos, and K. Wüthrich. 1996. NMR structure of the J-domain and the Gly/Phe-rich region of the Escherichia coli DnaJ chaperone. *J Mol Biol*. 260:236–250.

Peretz, D., M.R. Scott, D. Groth, R.A. Williamson, D.R. Burton, F.E. Cohen, and S.B. Prusiner. 2001. Strain-specified relative conformational stability of the scrapie prion protein. *Protein Sci*. 10:854–863.

Peretz, D., R.A. Williamson, Y. Matsunaga, H. Serban, C. Pinilla, R.B. Bastidas, R. Rozenshteyn, T.L. James, R.A. Houghten, F.E. Cohen, S.B. Prusiner, and D.R. Burton. 1997. A conformational transition at the N terminus of the prion protein features in formation of the scrapie isoform. *J Mol Biol*. 273:614–622.

Phillips, J.J., Z.-P. Yao, W. Zhang, S. McLaughlin, E.D. Laue, C.V. Robinson, and S.E. Jackson. 2007. Conformational dynamics of the molecular chaperone Hsp90 in complexes with a co-chaperone and anticancer drugs. *J Mol Biol*. 372:1189–1203.

Picard, D. 2002. Heat-shock protein 90, a chaperone for folding and regulation. *Cell. Mol. Life Sci.* 59:1640–1648.

Pishvaee, B., G. Costaguta, B.G. Yeung, S. Ryazantsev, T. Greener, L.E. Greene, E. Eisenberg, J.M. McCaffery, and G.S. Payne. 2000. A yeast DNA J protein required for uncoating of clathrin-coated vesicles in vivo. *Nat Cell Biol*. 2:958–963.

Polier, S., Z. Dragovic, F.U. Hartl, and A. Bracher. 2008. Structural basis for the cooperation of Hsp70 and Hsp110 chaperones in protein folding. *Cell*. 133:1068–1079.

Posteraro, B., M. Sanguinetti, L. Romano, R. Torelli, L. Novarese, and G. Fadda. 2005. Molecular tools for differentiating probiotic and clinical strains of Saccharomyces cerevisiae. *Int. J. Food Microbiol.* 103:295–304.

Prodromou, C., B. Panaretou, S. Chohan, G. Siligardi, R. O'Brien, J.E. Ladbury, S.M. Roe, P.W. Piper, and L.H. Pearl. 2000. The ATPase cycle of Hsp90 drives a molecular "clamp" via transient dimerization of the N-terminal domains. *EMBO J*. 19:4383–4392.

Prodromou, C., G. Siligardi, R. O'Brien, D.N. Woolfson, L. Regan, B. Panaretou, J.E. Ladbury, P.W. Piper, and L.H. Pearl. 1999. Regulation of Hsp90 ATPase activity by tetratricopeptide repeat (TPR)-domain co-chaperones. *EMBO J*. 18:754–762.

Prodromou, C., S.M. Roe, P.W. Piper, and L.H. Pearl. 1997a. A molecular clamp in the crystal structure of the N-terminal domain of the yeast Hsp90 chaperone. *Nat. Struct. Biol.* 4:477–482.

Prodromou, C., S.M. Roe, R. O'Brien, J.E. Ladbury, P.W. Piper, and L.H. Pearl. 1997b. Identification and structural characterization of the ATP/ADP-binding site in the Hsp90 molecular chaperone. *Cell*. 90:65–75.

Prusiner, S. 1982. Novel proteinaceous infectious particles cause scrapie. *Science*. 216:136–144.

Prusiner, S.B. 1998. Prions. *Proceedings of the National Academy of Sciences*. 95:13363–13383.

Prusiner, S.B., D.C. Bolton, D.F. Groth, K.A. Bowman, S.P. Cochran, and M.P. McKinley. 1982. Further purification and characterization of scrapie prions. *Biochemistry*. 21:6942–6950.

Prusiner, S.B., D.F. Groth, D.C. Bolton, S.B. Kent, and L.E. Hood. 1984. Purification and structural studies of a major scrapie prion protein. *Cell*. 38:127–134.

Prusiner, S.B., M. Scott, D. Foster, K.M. Pan, D. Groth, C. Mirenda, M. Torchia, S.L. Yang, D. Serban, and G.A. Carlson. 1990. Transgenetic studies implicate interactions between homologous PrP isoforms in scrapie prion replication. *Cell*. 63:673–686.

Prusiner, S.B., M.P. McKinley, K.A. Bowman, D.C. Bolton, P.E. Bendheim, D.F. Groth, and G.G. Glenner. 1983. Scrapie prions aggregate to form amyloid-like birefringent rods. *Cell*. 35:349–358.

Qiu, X.-B., Y.-M. Shao, S. Miao, and L. Wang. 2006. The diversity of the DnaJ/Hsp40 family, the crucial partners for Hsp70 chaperones. *Cell. Mol. Life Sci.* 63:2560–2570.

Ramos, C.H.I., C.L.P. Oliveira, C.-Y. Fan, I.L. Torriani, and D.M. Cyr. 2008. Conserved central domains control the quaternary structure of type I and type II Hsp40 molecular chaperones. *J Mol Biol*. 383:155–166.

Raviol, H., H. Sadlish, F. Rodriguez, M.P. Mayer, and B. Bukau. 2006. Chaperone network in the yeast cytosol: Hsp110 is revealed as an Hsp70 nucleotide exchange factor. *EMBO J*. 25:2510–2518.

Reidy, M., and D.C. Masison. 2010. Sti1 regulation of Hsp70 and Hsp90 is critical for curing of Saccharomyces cerevisiae [PSI+] prions by Hsp104. *Mol Cell Biol*. 30:3542–3552.

Resende, C.G., T.F. Outeiro, L. Sands, S. Lindquist, and M.F. Tuite. 2003. Prion protein gene polymorphisms in Saccharomyces cerevisiae. *Mol Microbiol*. 49:1005–1017.

Retzlaff, M., F. Hagn, L. Mitschke, M. Hessling, F. Gugel, H. Kessler, K. Richter, and J. Buchner. 2010. Asymmetric activation of the hsp90 dimer by its cochaperone aha1. *Mol Cell*. 37:344–354.

Richter, K., and J. Buchner. 2011. Closing in on the Hsp90 chaperone-client relationship. *Structure*. 19:445–446.

Richter, K., P. Muschler, O. Hainzl, J. Reinstein, and J. Buchner. 2003. Sti1 is a non-competitive inhibitor of the Hsp90 ATPase. Binding prevents the N-terminal dimerization reaction during the atpase cycle. *J Biol Chem*. 278:10328–10333.

Riek, R., S. Hornemann, G. Wider, M. Billeter, R. Glockshuber, and K. Wüthrich. 1996. NMR structure of the mouse prion protein domain PrP(121-231). *Nature*. 382:180–182.

Rine, J., R. Jensen, D. Hagen, L. Blair, and I. Herskowitz. 1981. Pattern of switching and fate of the replaced cassette in yeast mating-type interconversion. *Cold Spring Harb Symp Quant Biol*. 45 Pt 2:951–960.

Rogoza, T., A. Goginashvili, S. Rodionova, M. Ivanov, O. Viktorovskaya, A. Rubel, K. Volkov, and L. Mironova. 2010. Non-Mendelian determinant [ISP+] in yeast is a nuclear-residing prion form of the global transcriptional regulator Sfp1. *Proc Natl Acad Sci USA*. 107:10573–10577.

Romanova, N.V., and Y.O. Chernoff. 2009. Hsp104 and prion propagation. *Protein Pept Lett*. 16:598–605.

Rose, M.D., F.M. Winston, and P. Heiter. 1990. Methods in yeast genetics: a laboratory course manual. Cold Spring Harbor Laboratory Press, Cold Spring Harbor, N.Y.

Ross, E.D., H.K. Edskes, M.J. Terry, and R.B. Wickner. 2005. Primary sequence independence for prion formation. *Proc Natl Acad Sci USA*. 102:12825–12830.

Ross, E.D., U. Baxa, and R.B. Wickner. 2004. Scrambled prion domains form prions and amyloid. *Mol Cell Biol*. 24:7206–7213.

Rothstein, R. 1991. Targeting, disruption, replacement, and allele rescue: integrative DNA transformation in yeast. *Meth Enzymol*. 194:281–301.

Rüdiger, S., L. Germeroth, J. Schneider-Mergener, and B. Bukau. 1997. Substrate specificity of the DnaK chaperone determined by screening cellulose-bound peptide libraries. *EMBO J*. 16:1501–1507.

Sadlish, H., H. Rampelt, J. Shorter, R.D. Wegrzyn, C. Andréasson, S. Lindquist, and B. Bukau. 2008. Hsp110 chaperones regulate prion formation and propagation in S. cerevisiae by two discrete activities. *PLoS ONE*. 3:e1763.

Sahi, C., and E.A. Craig. 2007. Network of general and specialty J protein chaperones of the yeast cytosol. *Proc Natl Acad Sci USA*. 104:7163–7168.

Saifitdinova, A.F., A.A. Nizhnikov, A.G. Lada, A.A. Rubel, Z.M. Magomedova, V.V. Ignatova, S.G. Inge-Vechtomov, and A.P. Galkin. 2010. [NSI (+)]: a novel non-Mendelian nonsense suppressor determinant in Saccharomyces cerevisiae. *Curr Genet*.

Saiki, R.K., D.H. Gelfand, S. Stoffel, S.J. Scharf, R. Higuchi, G.T. Horn, K.B. Mullis, and H.A. Erlich. 1988. Primer-directed enzymatic amplification of DNA with a thermostable DNA polymerase. *Science*. 239:487–491.

Sanchez, Y., and S.L. Lindquist. 1990. HSP104 required for induced thermotolerance. *Science*. 248:1112–1115.

Sanchez, Y., J. Taulien, K.A. Borkovich, and S. Lindquist. 1992. Hsp104 is required for tolerance to many forms of stress. *EMBO J*. 11:2357–2364.

Sanders, S.L., K.A. Garbett, and P.A. Weil. 2002. Molecular characterization of Saccharomyces cerevisiae TFIID. *Mol Cell Biol*. 22:6000–6013.

Sanger, F., S. Nicklen, and A.R. Coulson. 1977. DNA sequencing with chain-terminating inhibitors. *Proc Natl Acad Sci USA*. 74:5463–5467.

Santoso, A., P. Chien, L.Z. Osherovich, and J.S. Weissman. 2000. Molecular basis of a yeast prion species barrier. *Cell*. 100:277–288.

Satpute-Krishnan, P., and T.R. Serio. 2005. Prion protein remodelling confers an immediate phenotypic switch. *Nature*. 437:262–265.

Satpute-Krishnan, P., S.X. Langseth, and T.R. Serio. 2007. Hsp104-dependent remodeling of prion complexes mediates protein-only inheritance. *PLoS Biol*. 5:e24.

Savistchenko, J., J. Krzewska, N. Fay, and R. Melki. 2008. Molecular chaperones and the assembly of the prion Ure2p in vitro. *J Biol Chem*. 283:15732–15739.

Schaffner, F.J. ed. 1968. Planet of the Apes. 20th Century Fox, 20th Centruy Fox. USA.

Schlumpberger, M., H. Wille, M.A. Baldwin, D.A. Butler, I. Herskowitz, and S.B. Prusiner. 2000. The prion domain of yeast Ure2p induces autocatalytic formation of amyloid fibers by a recombinant fusion protein. *Protein Sci*. 9:440–451.

Schlumpberger, M., S.B. Prusiner, and I. Herskowitz. 2001. Induction of distinct [URE3] yeast prion strains. *Mol Cell Biol*. 21:7035–7046.

Schmid, D., A. Baici, H. Gehring, and P. Christen. 1994. Kinetics of molecular chaperone action. *Science*. 263:971–973.

Schwarz, E., B. Westermann, A.J. Caplan, G. Ludwig, and W. Neupert. 1994. XDJ1, a gene encoding a novel non-essential DnaJ homologue from Saccharomyces cerevisiae. *Gene*. 145:121–124.

Schwimmer, C., and D.C. Masison. 2002. Antagonistic interactions between yeast [PSI(+)] and [URE3] prions and curing of [URE3] by Hsp70 protein chaperone Ssa1p but not by Ssa2p. *Mol Cell Biol*. 22:3590–3598.

SGD-Project. PDB Homolog: HSP104/YLL026W. *yeastgenome.org*.

Shaner, L., and K.A. Morano. 2007. All in the family: atypical Hsp70 chaperones are conserved modulators of Hsp70 activity. *Cell Stress Chaperones*. 12:1–8.

Shaner, L., R. Sousa, and K.A. Morano. 2006. Characterization of Hsp70 binding and nucleotide exchange by the yeast Hsp110 chaperone Sse1. *Biochemistry*. 45:15075–15084.

Shapiro, A.L., E. Viñuela, and J.V. Maizel. 1967. Molecular weight estimation of polypeptide chains by electrophoresis in SDS-polyacrylamide gels. *Biochem Biophys Res Commun*. 28:815–820.

Sharma, D., R.F. Stanley, and D.C. Masison. 2009. Curing of yeast [URE3] prion by the Hsp40 cochaperone Ydj1p is mediated by Hsp70. *Genetics*. 181:129–137.

Sharma, J., and S.W. Liebman. 2012. [PSI(+)] prion variant establishment in yeast. *Mol Microbiol*.

Shewmaker, F., D. Kryndushkin, B. Chen, R. Tycko, and R.B. Wickner. 2009. Two prion variants of Sup35p have in-register parallel beta-sheet structures, independent of hydration. *Biochemistry*. 48:5074–5082.

Shewmaker, F., E.D. Ross, R. Tycko, and R.B. Wickner. 2008. Amyloids of shuffled prion domains that form prions have a parallel in-register beta-sheet structure. *Biochemistry*. 47:4000–4007.

Shewmaker, F., R.P. McGlinchey, and R.B. Wickner. 2011. Structural insights into functional and pathological amyloid. *J Biol Chem*. 286:16533–16540.

Shibata, S., H. Kurahashi, and Y. Nakamura. 2009. Localization of prion-destabilizing mutations in the N-terminal non-prion domain of Rnq1 in Saccharomyces cerevisiae. *Prion*. 3:250–258.

Shorter, J. 2010. Emergence and natural selection of drug-resistant prions. *Molecular bioSystems*. 1–20.

Shorter, J., and S. Lindquist. 2006. Destruction or potentiation of different prions catalyzed by similar Hsp104 remodeling activities. *Mol Cell*. 23:425–438.

Shorter, J., and S. Lindquist. 2008. Hsp104, Hsp70 and Hsp40 interplay regulates formation, growth and elimination of Sup35 prions. *EMBO J*. 27:2712–2724.

Si, K., S. Lindquist, and E.R. Kandel. 2003. A neuronal isoform of the aplysia CPEB has prion-like properties. *Cell*. 115:879–891.

Si, K., Y.-B. Choi, E. White-Grindley, A. Majumdar, and E.R. Kandel. 2010. Aplysia CPEB can form prion-like multimers in sensory neurons that contribute to long-term facilitation. *Cell*. 140:421–435.

Siligardi, G., B. Hu, B. Panaretou, P.W. Piper, L.H. Pearl, and C. Prodromou. 2004. Co-chaperone regulation of conformational switching in the Hsp90 ATPase cycle. *J Biol Chem*. 279:51989–51998.

Sindi, S.S., and T.R. Serio. 2009. Prion dynamics and the quest for the genetic determinant in protein-only inheritance. *Curr. Opin. Microbiol.* 12:623–630.

Sipe, J.D., and A.S. Cohen. 2000. Review: history of the amyloid fibril. *J Struct Biol*. 130:88–98.

Smith, D.F., W.P. Sullivan, T.N. Marion, K. Zaitsu, B. Madden, D.J. McCormick, and D.O. Toft. 1993. Identification of a 60-kilodalton stress-related protein, p60, which interacts with hsp90 and hsp70. *Mol Cell Biol*. 13:869–876.

Sondheimer, N., and S. Lindquist. 2000. Rnq1: an epigenetic modifier of protein function in yeast. *Mol Cell*. 5:163–172.

Sondheimer, N., N. Lopez, E.A. Craig, and S. Lindquist. 2001. The role of Sis1 in the maintenance of the [RNQ+] prion. *EMBO J*. 20:2435–2442.

Soto, D.C. 2006. Prions. CRC Press, Boca Raton, FL.

Southworth, D.R., and D.A. Agard. 2008. Species-dependent ensembles of conserved conformational states define the Hsp90 chaperone ATPase cycle. *Mol Cell*. 32:631–640.

Sparrer, H.E., A. Santoso, F.C. Szoka, and J.S. Weissman. 2000. Evidence for the prion hypothesis: induction of the yeast [PSI+] factor by in vitro- converted Sup35 protein. *Science*. 289:595–599.

Stahl, N., M.A. Baldwin, A.L. Burlingame, and S.B. Prusiner. 1990. Identification of glycoinositol phospholipid linked and truncated forms of the scrapie prion protein. *Biochemistry*. 29:8879–8884.

Stahl, N., M.A. Baldwin, D.B. Teplow, L. Hood, B.W. Gibson, A.L. Burlingame, and S.B. Prusiner. 1993. Structural studies of the scrapie prion protein using mass spectrometry and amino acid sequencing. *Biochemistry*. 32:1991–2002.

Stansfield, I., K.M. Jones, V.V. Kushnirov, A.R. Dagkesamanskaya, A.I. Poznyakovski, S.V. Paushkin, C.R. Nierras, B.S. Cox, M.D. Ter-Avanesyan, and M.F. Tuite. 1995. The products of the SUP45 (eRF1) and SUP35 genes interact to mediate translation termination in Saccharomyces cerevisiae. *EMBO J*. 14:4365–4373.

Stoscheck, C.M. 1990. Quantitation of protein. *Meth Enzymol*. 182:50–68.

Street, T.O., L.A. Lavery, and D.A. Agard. 2011. Substrate binding drives large-scale conformational changes in the Hsp90 molecular chaperone. *Mol Cell*. 42:96–105.

Sullivan, W., B. Stensgard, G. Caucutt, B. Bartha, N. McMahon, E.S. Alnemri, G. Litwack, and D. Toft. 1997. Nucleotides and two functional states of hsp90. *J Biol Chem*. 272:8007–8012.

Summers, D.W., P.M. Douglas, and D.M. Cyr. 2009a. Prion propagation by Hsp40 molecular chaperones. *Prion*. 3:59–64.

Summers, D.W., P.M. Douglas, H.-Y. Ren, and D.M. Cyr. 2009b. The type I Hsp40 Ydj1 utilizes a farnesyl moiety and zinc finger-like region to suppress prion toxicity. *J Biol Chem*. 284:3628–3639.

Suzuki, G., N. Shimazu, and M. Tanaka. 2012. A yeast prion, Mod5, promotes acquired drug resistance and cell survival under environmental stress. *Science*. 336:355–359.

Sweeny, E.A., and J. Shorter. 2008. Prion proteostasis: Hsp104 meets its supporting cast. *Prion*. 2:135–140.

Szabo, A., T. Langer, H. Schröder, J. Flanagan, B. Bukau, and F.U. Hartl. 1994. The ATP hydrolysis-dependent reaction cycle of the Escherichia coli Hsp70 system DnaK, DnaJ, and GrpE. *Proc Natl Acad Sci USA*. 91:10345–10349.

Szilard, R.K., and R.A. Rachubinski. 2000. Tetratricopeptide repeat domain of Yarrowia lipolytica Pex5p is essential for recognition of the type 1 peroxisomal targeting signal but does not confer full biological activity on Pex5p. *Biochem J*. 346 Pt 1:177–184.

Taipale, M., D.F. Jarosz, and S. Lindquist. 2010. HSP90 at the hub of protein homeostasis: emerging mechanistic insights. *Nat Rev Mol Cell Biol*. 11:515–528.

Tanaka, M. 2005. [Final proof of "prion hypothesis" in the yeast prion [PSI+] system]. *Tanpakushitsu Kakusan Koso*. 50:207–214.

Tanaka, M., P. Chien, K. Yonekura, and J.S. Weissman. 2005. Mechanism of cross-species prion transmission: an infectious conformation compatible with two highly divergent yeast prion proteins. *Cell*. 121:49–62.

Tanaka, M., P. Chien, N. Naber, R. Cooke, and J.S. Weissman. 2004. Conformational variations in an infectious protein determine prion strain differences. *Nature*. 428:323–328.

Tanaka, M., S.R. Collins, B.H. Toyama, and J.S. Weissman. 2006. The physical basis of how prion conformations determine strain phenotypes. *Nature*. 442:585–589.

Taneja, V., M.-L. Maddelein, N. Talarek, S.J. Saupe, and S.W. Liebman. 2007. A non-Q/N-rich prion domain of a foreign prion, [Het-s], can propagate as a prion in yeast. *Mol Cell*. 27:67–77.

Telling, G.C., M. Scott, J. Mastrianni, R. Gabizon, M. Torchia, F.E. Cohen, S.J. DeArmond, and S.B. Prusiner. 1995. Prion propagation in mice expressing human and chimeric PrP transgenes implicates the interaction of cellular PrP with another protein. *Cell*. 83:79–90.

Telling, G.C., M. Scott, K.K. Hsiao, D. Foster, S.L. Yang, M. Torchia, K.C. Sidle, J. Collinge, S.J. DeArmond, and S.B. Prusiner. 1994. Transmission of Creutzfeldt-Jakob disease from humans to transgenic mice expressing chimeric human-mouse prion protein. *Proc Natl Acad Sci USA*. 91:9936–9940.

Telling, G.C., P. Parchi, S.J. DeArmond, P. Cortelli, P. Montagna, R. Gabizon, J. Mastrianni, E. Lugaresi, P. Gambetti, and S.B. Prusiner. 1996. Evidence for the conformation of the pathologic isoform of the prion protein enciphering and propagating prion diversity. *Science*. 274:2079–2082.

Ter-Avanesyan, M.D., A.R. Dagkesamanskaya, V.V. Kushnirov, and V.N. Smirnov. 1994. The SUP35 omnipotent suppressor gene is involved in the maintenance of the non-Mendelian determinant [psi+] in the yeast Saccharomyces cerevisiae. *Genetics*. 137:671–676.

Ter-Avanesyan, M.D., V.V. Kushnirov, A.R. Dagkesamanskaya, S.A. Didichenko, Y.O. Chernoff, S.G. Inge-Vechtomov, and V.N. Smirnov. 1993. Deletion analysis of the SUP35 gene of the yeast Saccharomyces cerevisiae reveals two non-overlapping functional regions in the encoded protein. *Mol Microbiol*. 7:683–692.

Thompson, J.R., E. Register, J. Curotto, M. Kurtz, and R. Kelly. 1998. An improved protocol for the preparation of yeast cells for transformation by electroporation. *Yeast*. 14:565–571.

Tipton, K.A., K.J. Verges, and J.S. Weissman. 2008. In vivo monitoring of the prion replication cycle reveals a critical role for Sis1 in delivering substrates to Hsp104. *Mol Cell*. 32:584–591.

Toombs, J.A., B.R. McCarty, and E.D. Ross. 2010. Compositional determinants of prion formation in yeast. *Mol Cell Biol*. 30:319–332.

Towbin, H., T. Staehelin, and J. Gordon. 1979. Electrophoretic transfer of proteins from polyacrylamide gels to nitrocellulose sheets: procedure and some applications. *Proc Natl Acad Sci USA*. 76:4350–4354.

Toyama, B.H., M.J.S. Kelly, J.D. Gross, and J.S. Weissman. 2007. The structural basis of yeast prion strain variants. *Nature*. 449:233–237.

Trovato, A., F. Chiti, A. Maritan, and F. Seno. 2006. Insight into the structure of amyloid fibrils from the analysis of globular proteins. *PLOS Comp. Biol.* 2:1608-1618.

True, H.L., and S.L. Lindquist. 2000. A yeast prion provides a mechanism for genetic variation and phenotypic diversity. *Nature*. 407:477–483.

Tsutsumi, S., M. Mollapour, C. Graf, C.-T. Lee, B.T. Scroggins, W. Xu, L. Haslerova, M. Hessling, A.A. Konstantinova, J.B. Trepel, B. Panaretou, J. Buchner, M.P. Mayer, C. Prodromou, and L. Neckers. 2009. Hsp90 charged-linker truncation reverses the functional consequences of weakened hydrophobic contacts in the N domain. *Nat Struct Mol Biol*. 16:1141–1147.

Tuite, M.F., C.R. Mundy, and B.S. Cox. 1981. Agents that cause a high frequency of genetic change from [psi+] to [psi-] in Saccharomyces cerevisiae. *Genetics*. 98:691–711.

Tuite, M.F., P.M. Lund, A.B. Futcher, M.J. Dobson, B.S. Cox, and C.S. McLaughlin. 1982. Relationship of the [psi] factor with other plasmids of Saccharomyces cerevisiae. *Plasmid*. 8:103–111.

Tyedmers, J., M.L. Madariaga, and S. Lindquist. 2008. Prion switching in response to environmental stress. *PLoS Biol*. 6:e294.

Tyedmers, J., S. Treusch, J. Dong, J.M. McCaffery, B. Bevis, and S. Lindquist. 2010. Prion induction involves an ancient system for the sequestration of aggregated proteins and heritable changes in prion fragmentation. *Proc Natl Acad Sci USA*. 107:8633–8638.

Uptain, S.M., G.J. Sawicki, B. Caughey, and S. Lindquist. 2001. Strains of [PSI(+)] are distinguished by their efficiencies of prion-mediated conformational conversion. *EMBO J*. 20:6236–6245.

Vaughan, C.K., U. Gohlke, F. Sobott, V.M. Good, M.M.U. Ali, C. Prodromou, C.V. Robinson, H.R. Saibil, and L.H. Pearl. 2006. Structure of an Hsp90-Cdc37-Cdk4 complex. *Mol Cell*. 23:697–707.

Verges, K.J., M.H. Smith, B.H. Toyama, and J.S. Weissman. 2011. Strain conformation, primary structure and the propagation of the yeast prion [PSI+]. *Nat Struct Mol Biol*. 18:493–499.

Vida, T.A., and S.D. Emr. 1995. A new vital stain for visualizing vacuolar membrane dynamics and endocytosis in yeast. *J Cell Biol*. 128:779–792.

Vitrenko, Y.A., E.O. Gracheva, J.E. Richmond, and S.W. Liebman. 2007a. Visualization of aggregation of the Rnq1 prion domain and cross-seeding interactions with Sup35NM. *J Biol Chem*. 282:1779–1787.

Vitrenko, Y.A., M.E. Pavon, S.I. Stone, and S.W. Liebman. 2007b. Propagation of the [PIN+] prion by fragments of Rnq1 fused to GFP. *Curr Genet*. 51:309–319.

Vogel, M., B. Bukau, and M.P. Mayer. 2006a. Allosteric regulation of Hsp70 chaperones by a proline switch. *Mol Cell*. 21:359–367.

Vogel, M., M.P. Mayer, and B. Bukau. 2006b. Allosteric regulation of Hsp70 chaperones involves a conserved interdomain linker. *J Biol Chem*. 281:38705–38711.

Volkov, K.V., A.Y. Aksenova, M.J. Soom, K.V. Osipov, A.V. Svitin, C. Kurischko, I.S. Shkundina, M.D. Ter-Avanesyan, S.G. Inge-Vechtomov, and L.N. Mironova. 2002. Novel non-Mendelian determinant involved in the control of translation accuracy in Saccharomyces cerevisiae. *Genetics*. 160:25–36.

Walsh, P., D. Bursać, Y.C. Law, D. Cyr, and T. Lithgow. 2004. The J-protein family: modulating protein assembly, disassembly and translocation. *EMBO Rep.* 5:567–571.

Wandinger, S.K., K. Richter, and J. Buchner. 2008. The Hsp90 chaperone machinery. *J Biol Chem*. 283:18473–18477.

Wegele, H., M. Haslbeck, J. Reinstein, and J. Buchner. 2003. Sti1 is a novel activator of the Ssa proteins. *J Biol Chem*. 278:25970–25976.

Wegrzyn, R.D., K. Bapat, G.P. Newnam, A.D. Zink, and Y.O. Chernoff. 2001. Mechanism of prion loss after Hsp104 inactivation in yeast. *Mol Cell Biol*. 21:4656–4669.

Wendland, B., K.E. Steece, and S.D. Emr. 1999. Yeast epsins contain an essential N-terminal ENTH domain, bind clathrin and are required for endocytosis. *EMBO J*. 18:4383–4393.

Wendler, P., and H.R. Saibil. 2010. Cryo electron microscopy structures of Hsp100 proteins: crowbars in or out? *Biochem Cell Biol*. 88:89–96.

Wendler, P., J. Shorter, C. Plisson, A.G. Cashikar, S. Lindquist, and H.R. Saibil. 2007. Atypical AAA+ subunit packing creates an expanded cavity for disaggregation by the protein-remodeling factor Hsp104. *Cell*. 131:1366–1377.

Wendler, P., J. Shorter, D. Snead, C. Plisson, D.K. Clare, S. Lindquist, and H.R. Saibil. 2009. Motor mechanism for protein threading through Hsp104. *Mol Cell*. 34:81–92.

Werner-Washburne, M., D.E. Stone, and E.A. Craig. 1987. Complex interactions among members of an essential subfamily of hsp70 genes in Saccharomyces cerevisiae. *Mol Cell Biol*. 7:2568–2577.

Westaway, D., P.A. Goodman, C.A. Mirenda, M.P. McKinley, G.A. Carlson, and S.B. Prusiner. 1987. Distinct prion proteins in short and long scrapie incubation period mice. *Cell*. 51:651–662.

Whitesell, L., E.G. Mimnaugh, B. De Costa, C.E. Myers, and L.M. Neckers. 1994. Inhibition of heat shock protein HSP90-pp60v-src heteroprotein complex formation by benzoquinone ansamycins: essential role for stress proteins in oncogenic transformation. *Proc Natl Acad Sci USA*. 91:8324–8328.

Wickner, R.B. 1994. [URE3] as an altered URE2 protein: evidence for a prion analog in Saccharomyces cerevisiae. *Science*. 264:566–569.

Wickner, R.B., F. Dyda, and R. Tycko. 2008a. Amyloid of Rnq1p, the basis of the [PIN+] prion, has a parallel in-register beta-sheet structure. *Proc Natl Acad Sci USA*. 105:2403–2408.

Wickner, R.B., F. Shewmaker, D. Kryndushkin, and H.K. Edskes. 2008b. Protein inheritance (prions) based on parallel in-register beta-sheet amyloid structures. *Bioessays*. 30:955–964.

Wickner, R.B., H.K. Edskes, D. Kryndushkin, R. McGlinchey, D. Bateman, and A. Kelly. 2011. Prion Diseases of Yeast: Amyloid Structure and Biology. *Seminars in cell & developmental biology*.

Wickner, R.B., H.K. Edskes, M.L. Maddelein, K.L. Taylor, and H. Moriyama. 1999. Prions of yeast and fungi. Proteins as genetic material. *J Biol Chem*. 274:555–558.

Wille, H., M.D. Michelitsch, V. Guenebaut, S. Supattapone, A. Serban, F.E. Cohen, D.A. Agard, and S.B. Prusiner. 2002. Structural studies of the scrapie prion protein by electron crystallography. *Proc Natl Acad Sci USA*. 99:3563–3568.

Wille, H., W. Bian, M. McDonald, A. Kendall, D.W. Colby, L. Bloch, J. Ollesch, A.L. Borovinskiy, F.E. Cohen, S.B. Prusiner, and G. Stubbs. 2009. Natural and synthetic prion structure from X-ray fiber diffraction. *Proc Natl Acad Sci USA*. 106:16990–16995.

Wilson, P.G., and M.R. Culbertson. 1988. SUF12 suppressor protein of yeast. A fusion protein related to the EF-1 family of elongation factors. *J Mol Biol*. 199:559–573.

Yan, W., B. Schilke, C. Pfund, W. Walter, S. Kim, and E.A. Craig. 1998. Zuotin, a ribosome-associated DnaJ molecular chaperone. *EMBO J*. 17:4809–4817.

Young, C.S., and B.S. Cox. 1972. Extrachromosomal elements in a super-suppression system of yeast. II. Relations with other extrachromosomal elements. *Heredity (Edinb)*. 28:189–199.

Young, J.C., and F.U. Hartl. 2000. Polypeptide release by Hsp90 involves ATP hydrolysis and is enhanced by the co-chaperone p23. *EMBO J*. 19:5930–5940.

Yu, H., P. Braun, M.A. Yildirim, I. Lemmens, K. Venkatesan, J. Sahalie, T. Hirozane-Kishikawa, F. Gebreab, N. Li, N. Simonis, T. Hao, J.-F. Rual, A. Dricot, A. Vazquez, R.R. Murray, C. Simon, L. Tardivo, S. Tam, N. Svrzikapa, C. Fan, A.-S. de Smet, A. Motyl, M.E. Hudson, J. Park, X. Xin, M.E. Cusick, T. Moore, C. Boone, M. Snyder, F.P. Roth, A.-L. Barabási, J. Tavernier, D.E. Hill, and M. Vidal. 2008. High-quality binary protein interaction map of the yeast interactome network. *Science*. 322:104–110.

Yu, H., X. Liu, K. Neupane, A.N. Gupta, A.M. Brigley, A. Solanki, I. Sosova, and M.T. Woodside. 2012. Direct observation of multiple misfolding pathways in a single prion protein molecule. *Proc Natl Acad Sci USA*. 109:5283–5288.

Zahn, R., A. Liu, T. Lührs, R. Riek, C. von Schroetter, F. López García, M. Billeter, L. Calzolai, G. Wider, and K. Wüthrich. 2000. NMR solution structure of the human prion protein. *Proc Natl Acad Sci USA*. 97:145–150.

Zhou, P., I.L. Derkatch, and S.W. Liebman. 2001. The relationship between visible intracellular aggregates that appear after overexpression of Sup35 and the yeast prion-like elements [PSI(+)] and [PIN(+)]. *Mol Microbiol*. 39:37–46.

Zhou, P., I.L. Derkatch, S.M. Uptain, M.M. Patino, S. Lindquist, and S.W. Liebman. 1999. The yeast non-Mendelian factor [ETA+] is a variant of [PSI+], a prion-like form of release factor eRF3. *EMBO J*. 18:1182–1191.

Zhu, X., X. Zhao, W.F. Burkholder, A. Gragerov, C.M. Ogata, M.E. Gottesman, and W.A. Hendrickson. 1996. Structural analysis of substrate binding by the molecular chaperone DnaK. *Science*. 272:1606–1614.

Zuehlke, A.D., and J.L. Johnson. 2012. Chaperoning the Chaperone: A Role for the Co-chaperone Cpr7 in Modulating Hsp90 Function in Saccharomyces cerevisiae. *Genetics*. 191:805–814.

Zurawska, A., J. Urbanski, J. Matuliene, J. Baraniak, M.P. Klejman, S. Filipek, D. Matulis, and P. Bieganowski. 2010. Mutations that increase both Hsp90 ATPase activity in vitro and Hsp90 drug resistance in vivo. *Biochim Biophys Acta*. 1803:575–583.